ABSTRACT

PERFORMANCE-BASED SEISMIC ENGINEERING OF LOW AND MEDIUM-RISE STEEL FRAMES

by
Saeid Rashidi

The performance level of low and medium-rise steel frames designed according to the common force/strength approach of the UBC or NEHRP is determined. Several combinations of soil profile type, lateral-force-resisting system, and frame-member proportioning are included in the designs.

To evaluate the expected damage, nonlinear models of the designed frames are subjected to a number of actual and simulated ground motion accelerograms and appropriate structural response parameters such as, interstory drift, ductility demand, and dissipated hysteretic energy are obtained. In addition, a modified form of Park-Ang damage index is calculated for moment-resisting frames. The seismic performance of the steel frames is assessed in accordance with the acceptance criteria of the *NEHRP Guidelines for the Seismic Rehabilitation of Buildings* (FEMA-273) which sets forth plastic rotation and deformation limits to define the performance levels for various structural and nonstructural components.

The effect of vertical component of ground motion, geometric nonlinearity, participation of nonstructural elements, and damping representation on the seismic response of steel frames is investigated. Based on the results of the dynamic nonlinear analyses, a simple procedure is proposed which uses the pushover analysis method to estimate the average maximum interstory drift. The method defines a damage index which, after being calibrated, can directly be used for performance evaluation.

PERFORMANCE-BASED SEISMIC ENGINEERING OF LOW AND MEDIUM-RISE STEEL FRAMES

by
Saeid Rashidi

A Dissertation
Submitted to the Faculty of
New Jersey Institute of Technology
in Partial Fulfillment of the Requirements for the Degree of
Doctor of Philosophy in Civil Engineering

Department of Civil and Environmental Engineering

January 2000

APPROVAL PAGE

PERFORMANCE-BASED SEISMIC ENGINEERING OF LOW AND MEDIUM-RISE STEEL FRAMES

Saeid Rashidi

M. Ala Saadeghvaziri, Dissertation Advisor — Date
Associate Professor of Civil and Environmental Engineering
New Jersey Institute of Technology

Edward G. Dauenheimer, Committee Member — Date
Professor of Civil and Environmental Engineering
New Jersey Institute of Technology

George Deodatis, Committee Member — Date
Associate Professor of Civil Engineering and Operations Research
Princeton University

C. T Thomas Hsu, Committee Member — Date
Professor of Civil and Environmental Engineering
New Jersey Institute of Technology

William R. Spillers, Committee Member — Date
Distinguished Professor of Civil and Environmental Engineering
New Jersey Institute of Technology

BIOGRAPHICAL SKETCH

Author: Saeid Rashidi

Degree: Doctor of Philosophy in Civil Engineering

Date: January 2000

Undergraduate and Graduate Education:

- Doctor of Philosophy in Civil Engineering,
  New Jersey Institute of Technology, Newark, NJ, 2000

- Master of Science in Civil Engineering,
  Sharif University of Technology, Tehran, Iran, 1992

- Bachelor of Science in Civil Engineering,
  Sharif University of Technology, Tehran, Iran, 1989

Major: Civil Engineering

Presentations and Publications:

Ali R. Khaloo, and Saeid Rashidi, "Seismic Strengthening of R/C columns by External FGS," *Proceedings of the 10th European Conference on Earthquake Engineering*, Austria, 1994.

Saeid Rashidi, and M. Ala Saadeghvaziri, "Seismic Modeling of Multi-Span Simply-Supported Bridges Using ADINA," *Computers and Structures*, Vol. 64, No. 5/6, 1997, pp. 1025-1039.

William R. Spillers, and Saeid Rashidi, "Member Stiffness for Three-Dimensional Beam-Columns," *Journal of Structural Engineering*, ASCE, Vol. 123, No. 7, July 1997, pp. 971-972.

M. Ala Saadeghvaziri, and Saeid Rashidi, "Seismic Design and Retrofit Issues for Bridges in New Jersey," *Transportation Research Record 1594*, TRB, National Research Council, Washington, D.C., 1997, pp. 94-104.

M. Ala Saadeghvaziri, and Saeid Rashidi, "Effect of Steel Bearings on Seismic Response of Bridges in Eastern United States," *Proceedings of the 6th U.S. National Conference on Earthquake Engineering*, Seattle, WA, 1998.

M. Ala Saadeghvaziri, Alireza Yazdani-Motlagh, and Saeid Rashidi, "Nonlinear Response of Multi-Span Simply Supported Bridges Subjected to Longitudinal Earthquake Ground Motion," *Proceedings of the '99 EERI Annual Meeting*, San Diego, CA, 1999.

To my beloved family

ACKNOWLEDGMENT

I would like to express my sincere gratitude to Dr. M. Ala Saadeghvaziri for his unfailing and valuable support and supervision over the years. I also deeply appreciate the guidance provided by my dissertation committee members: Professors Edward G. Dauenheimer, George Deodatis, C. T. Thomas Hsu, and William R. Spillers. Special thanks are given to Mr. Keith MacBain for his assistance and to Dr. David Perel for his instrumental cooperation.

TABLE OF CONTENTS

TABLE OF CONTENTS
(Continued)

Chapter **Page**

TABLE OF CONTENTS
(Continued)

LIST OF TABLES

LIST OF TABLES
(Continued)

LIST OF FIGURES

LIST OF FIGURES
(Continued)

LIST OF FIGURES
(Continued)

Figure **Page**

LIST OF FIGURES
(Continued)

LIST OF FIGURES
(Continued)

LIST OF FIGURES
(Continued)

Figure **Page**

CHAPTER 1

INTRODUCTION

In the past few years, there has been a growing trend towards basing the seismic engineering and design practice on a new foundation. As it was reiterated in an international workshop *on Seismic Design Methodologies for the Next Generation of Codes* (Bled 1997), performance-based engineering will be the basis of the future seismic codes. This movement has created numerous research needs in various relevant fields which are of key importance to the development of the new generation of seismic codes. This section contains general information about performance-based seismic engineering, followed by the objectives of the present study.

1.1 Performance-Based Seismic Engineering

1.1.1 Definition

Performance-based seismic engineering (PBSE) is defined as the procedure of design and construction of structures that will resist earthquakes in a predictable manner (Hamburger 1996). It is intended to make owners and designers capable of selecting alternative performance goals-or objectives-for the design of different structures. A design *performance objective* is a statement of the desired behavior of the building-called the *performance level*-should it experience an earthquake of specified severity-called the *earthquake design level*. Design performance objectives are selected based on the occupancy of the building, the importance of functions occurring within the building, economic considerations including costs related to building damage repair and business

interruption, and considerations of the potential importance of the building as a historic or cultural resource.

A performance level is an expression of the maximum desired extent of damage to a building. Structural Engineers Association of California (SEAOC), Vision 2000 Committee, defines (SEAOC 1995) four performance levels:

1. Fully Operational
2. Operational
3. Life-Safe
4. Near Collapse

Damage states corresponding to the above performance levels range from negligible to severe. In a Fully Operational performance level, essentially no damage has occurred. An Operational performance level is characterized by moderate damage to nonstructural elements and light damage to structural elements. Life-Safe performance level corresponds to a damage state in which structural and nonstructural elements undergo moderate damage. Near Collapse is defined as a damage state in which the building has substantially lost its resistance to lateral and vertical loads.

Earthquake design levels are expressed in terms of a mean recurrence interval or a probability of being exceeded. SEAOC also recommends that the earthquake design levels defined in Table 1.1 be used for the performance-based engineering of the buildings.

SEAOC recommendations for minimum design performance objectives for buildings of three different occupancies and uses (Safety Critical Facilities, Essential/Hazardous Facilities, and Basic Facilities) are shown in Figure 1.1. Safety

Critical Facilities (SCF) are those which contain large quantities of hazardous materials, the release of which would result in an unacceptable hazard to wide segments of the public. Essential Facilities (EF) are those which are critical to post-earthquake operations. Hazardous Facilities (HF) are those which contain large quantities of hazardous materials, but where the release of those materials would be contained within the boundaries of the facility. Basic Facilities (BF) are those which are not classified as any of the previous categories.

To limit the damage to acceptable levels, SEAOC recommends to control the interstory drift. The recommended maximum permissible drifts for Fully Operational, Operational, Life-Safe, and Near Collapse performance levels are 0.2%, 0.5%, 1.5%, and 2.5%, respectively.

The *NEHRP (National Earthquake Hazards Reduction Program) Guidelines for the Seismic Rehabilitation of Buildings*, issued by Federal Emergency Management Agency (FEMA) in 1997 is probably the most comprehensive and elaborate document about performance-based seismic engineering which exists at this time. According to the *Guidelines*, the four building performance levels are Collapse Prevention, Life Safety, Immediate Occupancy, and Operational. Each building performance level is a combination of a Structural Performance Level (SPL) and a nonstructural performance level (NPL). SPL describes the limiting damage state of the structural systems and NPL describes the limiting damage state of the nonstructural systems. The SPLs are the Immediate Occupancy Level (IO), Life Safety Level (LS), and Collapse Prevention Level (CP). The maximum interstory drift values associated with these performance levels for different structural systems are given in Table 1.2. Though these values are not provided

as drift limit requirements of the *Guidelines*, they seem to be the most appropriate measure of the overall performance at present.

The *Guidelines* define two levels of earthquake shaking hazard, termed Basic Safety Earthquake 1 (BSE-1) and Basic Safety Earthquake 2 (BSE-2). BSE-1 is defined as a ground shaking with a 10% probability of being exceeded in 50 years (10%/50). BSE-2 ground shaking, also called Maximum Considered Earthquake (MCE) ground shaking, has a 2% probability of being exceeded in 50 years (2%/50) in most areas of the United States. Earthquake shaking demand on buildings is characterized by acceleration response spectra for these two hazard levels.

The recommendations published by Vision 2000 Committee provide a reasonable framework for implementation of performance-based seismic engineering, but they are too general to be used as specifications. In this respect, the provisions of the *NEHRP Guidelines* are closer to a performance-based design code of practice.

1.1.2 PBSE Methodology

The PBSE methodology is illustrated in Figure 1.2. Once the performance objectives are selected and the site seismic hazards identified, the structural design will proceed with overall conceptual design followed by preliminary and final design steps. The preliminary and final design steps involve sizing and detailing the structural framing system and the nonstructural elements so that the performance objectives can be met. The performance objectives must be converted to the limiting values of the structural response parameters which reflect the expected damage states. Then, these limiting values become targets for the design. The quantification of the performance levels in terms of response

parameters that are meaningful to the engineers is one of the major challenges in PBSE. Acceptability check and design review must then verify that the selected performance objectives are being met. The final steps are quality assurance during construction and building maintenance after construction.

Before the structural design can begin, a design approach must be chosen to accomplish the specific performance objectives. Several design approaches are available:

1. *Comprehensive design approach-* Is a probabilistic limit state design approach in which optimization of life cycle costs is considered.
2. *Displacement-based design approach-* Presumes that controlling the performance of a structure is possible by controlling displacement, or drift.
3. *Energy-based design approach-* Assumes that damage is directly related to total input energy. The energy input is a function of ground motion characteristics and the interaction between the ground motion and the structure (Teran-Gilmore 1996).
4. *General force/strength approach-* Determines a minimum lateral base shear force and distributes it over the height of the building. The lateral force is adjusted by the so-called "R" factor to account for inelastic behavior. The structural members are then designed to resist the resulting member forces and detailed to exhibit sufficient ductility. The procedures also require story drifts not to exceed certain limits.
5. *Simplified force/strength approach-* Is intended for design of certain types of relatively simple buildings on favorable building sites.
6. *Prescriptive design approach-* Provides a set of specific detailing requirements that can be used, without an engineer, to design simple buildings to meet the basic performance objective.

To this date, none of the above approaches except the general force/strength approach has been adopted by design codes. The SEAOC Seismology Committee, building on the Vision 2000 initiative, is developing a displacement-based design approach for performance-based engineering in which structures are directly designed for inelastic displacements (Court and Kowalsky 1998). While the proposed guidelines are expected to provide improvements over the current U.S. design codes as tools for performance-based engineering, the most common seismic design approach in use today is general force/strength approach and is adopted by the Uniform Building Code (UBC), National Earthquake Hazard Reduction Program (NEHRP) and other codes. At this time, there is no performance-based design code for designing new buildings.

After a structural design is proposed based on a design approach, an *acceptability analysis* is required to check its adequacy. To verify that the design performance objective is satisfied by a structural design, it must be analyzed to compare the critical response parameters with the limiting values of those parameters associated with the selected performance levels. The response parameters can be correlated with damage levels, and thus with the performance objectives. Drift, displacement, stress and strain ratios, ductility demand, energy demand, and acceleration are the most important response parameters with limiting values being so far suggested for only some parameters (SEAOC 1995, FEMA-273 1997). Additional study and testing is required in this area.

Acceptability analysis procedures applicable to PBSE include elastic analysis procedure, component-based elastic analysis procedure, capacity spectrum method, drift demand spectrum method, pushover analysis procedure, and dynamic nonlinear time history analysis procedure. The description of each procedure can be found in the

document issued by Vision 2000 Committee (SEAOC 1995). The acceptability analysis methods are selected largely independent from the design approach.

The most advanced analysis procedures used in performance-based design are pushover analysis method and dynamic nonlinear time history analysis procedure.

Static pushover analysis uses incremental static loading, usually in a non-varying distribution, to monitor the behavior of structure at increasing displacement. Assuming that the maximum non-linear displacement of the structure subjected to a specified ground motion or spectral demand is approximately the same as the maximum linear displacement, the structure is considered to be acceptable if under the incremental load, it is able to reach its target displacement (elastic displacement) without first becoming unstable or exceeding its ductility capacity. In an enhanced procedure, separate spectral analyses are performed at various softened states of the structure. The methods do not consider the higher-mode or three-dimensional effects, such as torsion and cannot be used in probabilistic evaluations.

Dynamic nonlinear time history analysis (DNTHA) is the most sophisticated and powerful technique currently available for determination of building response to ground motion. The dynamic response of the structure to a selected ground motion time history is obtained by an incremental solution of its equation of motion in the time domain. Using DNTHA, it is possible to take into account some important factors which are not usually considered in the structural analysis as a result of using simple methods of analysis. But, in spite of its potential, DNTHA has not been very popular in the engineering community so far. The reluctance for the application of DNTHA stems from the difficulty of defining the input parameters, the interpretation of the results, and the result sensitivity to the input

data. Sometimes even small changes in modeling assumptions, assumed ground motion time history, or solution method used to solve the equation of motion can drastically affect the results obtained from a DNTHA. DNTHA is a quite versatile and robust procedure, but the inherent uncertainties in the structural models and the ground motion time histories make it almost impossible to define a unique set of input parameters for a particular situation. This lack of uniqueness may lead to a wide range of demands (response parameters) so that the procedure may fail to determine a unique performance level given that a specific earthquake design level affects the building. Noting that the actual seismic response is always random in nature, the ability of DNTHA to show the scatter of seismic demand must be regarded as an advantage and not a disadvantage of the method. A reliable and accurate analysis requires a careful selection of structural model and ground motion time histories.

1.2 Previous Work

In 1992, the Structural Engineers Association of California (SEAOC) formed a special committee, called Vision 2000, to develop the framework for procedures that yield structures of predictable seismic performance. The interim report prepared by Vision 2000 Committee (SEAOC 1995) defined a series of standard performance levels, reference earthquake hazard levels, and uniform design performance objectives for buildings of different occupancies and uses. It also recommended uniform engineering procedures for performance-based seismic design. The provisions contained in this report were still too general to be used in practice. The second resource document was issued by FEMA in 1997 (FEMA 1997) and took the guidelines proposed by Vision 2000 one step

closer to the practical implementation. Now, the SEAOC Seismology Committee is developing preliminary guidelines for performance-based design using a displacement design approach (Court and Kowalsky 1998). The conceptual framework developed by Vision 2000 in 1995 is the foundation of the new guidelines. The proposed approach focuses on displacement as the key response parameter for practical performance-based design and nonstructural systems are explicitly designed to accommodate the structural drift and acceleration.

It has been recognized that the successful application of the performance-based seismic design will require additional research in many areas. The basic issues which need to be addressed in order to make performance-based seismic design a useful design approach are discussed by Krawinkler (Krawinkler 1998). These issues include identification of response parameters that control performance at various levels, quantification of demands and capacities for these parameters, and a reliability-based framework in which due consideration is given to uncertainties. The response parameters are determined by an analysis procedure. There has been a great deal of activity in developing analysis procedures to be used in performance-based design. Different analysis procedures have been evaluated to assess their reliability and accuracy (Foutch et al. 1998; Whittaker et al. 1998).

Since performance levels are nothing but expressions of different extents of damage, there has been a continuous effort in defining new, as well as refining the existing damage measures. One of the earliest damage models for steel structures was proposed by Krawinkler and Zohrei (Krawinkler and Zohrei 1983). This cumulative damage model was based on the results of low-cycle fatigue tests of structural steel

components and accounted for local buckling in beam flanges and fracture at welds. Many cumulative and low-cycle fatigue models were developed later (McCabe and Hall 1989; Ballio and Castiglioni 1994; Daali and Korol 1995; Ballio et al. 1997). Maximum deformation and cumulative damage were combined in the widely used Park-Ang damage model (Park and Ang 1985). This model was slightly modified by others (Kunnath et al. 1992; Chai et al. 1995). The damage index defined by Rodriguez also used both energy and displacement (Rodriguez 1998). A general procedure was proposed by Sorace to calibrate the free coefficients contained in the expressions of Park-Ang, McCabe-Hall and low-cycle fatigue indices to evaluate the seismic damage of steel frames (Sorace 1998). Some approaches used the change in the dynamic characteristics of the structure to assess the damage (DiPasquale and Cakmak 1988; Hassiotis and Jeong 1993). In another approach, two pushover analyses were performed for a structure subjected to a ground motion; one before and one after subjecting the structure to the ground motion. The change in the stiffness before and after the earthquake was used to define a damage index (Ghobarah et al. 1999).

Seismic performance of steel structures has recently gained attention. The SAC Joint Venture was formed in 1994 by the SEAOC, the Applied Technology Council (ATC), and California Universities for Research in Earthquake Engineering (CUREe). Its goal was to investigate the damage to welded steel moment-resisting frame buildings in the 1994 Northridge earthquake and develop repair techniques and new design approaches to reduce this damage in future earthquakes. The first phase of the research program was completed in 1995 and the second phase has now begun. The information on the model buildings and ground motion sets that are used by SAC steel project was

given by Krawinkler and Gupta (Krawinkler and Gupta 1998). They provided a summary of the behavior of the model buildings and the baseline interstory drift demands. The effect of panel zones and P-Δ was also investigated in their study.

In another study (Biddah and Heidebrecht 1998), steel moment-resisting frame buildings with ductile connections were designed for different seismic hazard levels using three design philosophies, namely strong column-weak beam, weak column-strong beam, and strong column-weak panel zone. The performance of the designed frames under ground motion was then evaluated using pushover and dynamic time history analysis methods.

1.3 Objective and Scope

As mentioned in the previous section, no performance-based seismic design code currently exists. It may take some time before the first generation of these codes becomes available. In the meantime, buildings are being designed using the common force/strength approach. This raises the important question, "what is the expected seismic performance of the buildings designed according to the current design codes?"

It was also emphasized that a reliable assessment of seismic performance requires accurate modeling of the building behavior. In this respect, there has been a lack of comprehensive studies regarding damping representation in DNTHA, participation of nonstructural elements in seismic response, geometric nonlinearity, and vertical ground motion.

It is the objective of this study to:

1. Evaluate the expected performance of low and medium-rise steel frames designed according to the common force/strength design approach of the *1997 Uniform Building Code* (UBC 97) or *1994 NEHRP Recommended Provisions for Seismic Regulations for New Buildings* (NEHRP 94). This is achieved by dynamic nonlinear time history analysis of different steel frames to assess their seismic performance. Several combinations of soil profile type, lateral-force-resisting system, and frame-member proportioning are included in the designs. The performance is evaluated using the *NEHRP Guidelines* (FEMA-273) and different damage indices that exist in the literature.
2. Propose a simple procedure to estimate the average seismic demands.
3. Investigate the effect of the following factors on the seismic response and performance of steel structures:
   - Vertical component of ground motion
   - Geometric nonlinearity
   - Participation of nonstructural elements
   - Damping representation

Low-rise (2-story, 30-ft high) and medium-rise (12-story, 150-ft high) steel buildings are designed for UBC seismic zone 4 and soil profile types S_B and S_E. The lateral-force-resisting system of the 2-story building is a special moment-resisting frame. Two alternative systems are considered for the 12-story building, a special moment-resisting frame and a special concentrically braced frame. The static lateral force

procedure of Section 1630 and the provisions of Chapter 22, Divisions III and V (UBC 97) are used to design the frames.

DNTHA of the frame models is performed using ANSYS finite element computer program. The steel frame models are made up of nonlinear beam elements. The beam element formulation admits large displacements and rotations, is capable of representing the spread of plasticity within the member, and allows the interaction of axial force and bending moment to be modeled accurately regarding both strength and stiffness. Steel behavior is represented by a bilinear uniaxial stress-strain relationship with kinematic hardening. Each frame-member is modeled with at least three I-shaped nonlinear beam elements to give an accurate representation of spread of plasticity and axial force-bending moment interaction.

Once the frame model has been developed, the time history of ground motion needs to be defined. Since the ground motion hazard for a specific site is often expressed as an elastic acceleration response spectrum, ground motion time histories for that site are obtained by scaling the recorded time histories to a spectrum-related "intensity" or generating spectrum-compatible simulated ground motion time histories. Scaling of the records will reduce the number of time histories required to estimate the average response within a predefined confidence interval. In this study the recorded time histories are scaled to the 5%-damped spectral acceleration at the fundamental frequency of the structure. It has been shown (Shome et al. 1998) that this scaling procedure is the most efficient among the alternatives and does not bias the nonlinear response estimates.

A spectral-representation-based simulation algorithm is used to generate the artificial time histories (Deodatis 1996). This procedure uses an iterative scheme to

generate seismic ground motion time histories at several locations on the ground surface. These time histories are compatible with prescribed response spectra and correlated according to a given coherence function. They include the wave propagation effect, and have a specified duration of strong ground motion.

To evaluate the expected damage, appropriate structural response parameters such as interstory drift, ductility demand, and dissipated hysteretic energy are obtained. A modified form of Park-Ang damage index is also calculated for moment-resisting frames. The implications of each damage measure and the correlation between different measures is investigated. The performance of the steel frames is also assessed according to the acceptance criteria of the *NEHRP Guidelines* (FEMA-273) which sets forth plastic rotation and deformation limits to define the performance levels for various structural and nonstructural components.

CHAPTER 2

DESIGN OF STEEL FRAMES

2.1 Introduction

Steel frames of low and medium-rise buildings considered in this study are designed in accordance with the *static force procedure* of the *1997 Uniform Building Code*. The same procedure is adopted by NEHRP in *Recommended Provisions for Seismic Regulations for New Buildings*. The buildings are located in a region with high seismicity and several designs are produced to represent different combinations of soil profile type, lateral-force-resisting system, and frame-member proportioning. Frames are designed with adequate strength to withstand the earthquake-induced forces and displacements, considering the inelastic response of the structure and the inherent redundancy, overstrength and ductility of the lateral-force-resisting system. The minimum design strength is based on the design seismic forces as determined in Section 1630 of the UBC. Components are designed in accordance with the provisions of Chapter 22, Division III (AISC-ASD) and Division V (Seismic Provisions for Structural Steel Buildings for Use with Allowable Stress Design).

In the design process each building is assigned an importance factor depending on the occupancy category for that building. Building site is assigned a soil profile type based on site geology and soil properties. Seismic hazard characteristics for the site are established based on the seismic zone and proximity of the site to active seismic sources, soil profile type, and importance factor of the building.

2.2 Design Procedure

Either Load and Resistance Factor Design method or Allowable Stress Design method may be used for structural design. According to the UBC, where allowable stress design (working stress design) is used, structures and all portions thereof should be able to resist the most critical effects resulting from the following combination of loads:

$$D \tag{2.1}$$

$$D + L + (L_r \text{ or } S) \tag{2.2}$$

$$D \pm (W \text{ or } E/1.4) \tag{2.3}$$

$$0.9D \pm E/1.4 \tag{2.4}$$

$$D + 0.75[L + (L_r \text{ or } S) \pm (W \text{ or } E/1.4)] \tag{2.5}$$

where:

D = dead load.

E = earthquake load set forth in Section 1630.1.

L = live load, except roof live load.

L_r = roof live load.

S = snow load.

W = load due to wind pressure.

No increase in allowable stresses is used with these load combinations except as specifically permitted by Section 1809.2 (soil capacity).

For both allowable stress design and strength design, the following special seismic load combinations are used as specifically required:

$$1.2D + 0.5L \pm 1.0\,E_m \tag{2.6}$$

$$0.9D \pm 1.0\,E_m \tag{2.7}$$

where:

E_m= estimated maximum earthquake force that can be developed in the structure.

and the following earthquake loads are used in the above load combinations:

$$E = \rho E_h + E_v \tag{2.8}$$

$$E_m = \Omega_0 E_h \tag{2.9}$$

where:

E_h = the earthquake load due to the base shear V as set forth in Section 1630.2.

E_v = the load effect resulting from the vertical component of the earthquake ground motion and may be taken as zero for allowable stress design.

ρ = Reliability/Redundancy Factor which depends on the maximum element-story shear ratio and the ground floor area of the structure.

Ω_0= the seismic force amplification factor accounting for structural overstrength.

The static lateral force procedure of Section 1630 may be used for regular structures under 240 ft in height with lateral force resistance provided by acceptable systems. In this procedure the total design base shear in a given direction is determined from the following formula:

$$V = \frac{C_v I}{RT} W \tag{2.10}$$

The total design base shear need not exceed the following:

$$V = \frac{2.5 C_a I}{R} W \tag{2.11}$$

The total design base shear should not be less than the following:

$$V = 0.11 C_a I W \tag{2.12}$$

In addition, for Seismic Zone 4, the total base shear should also not be less than the following:

$$V = \frac{0.8ZN_v I}{R}W \tag{2.13}$$

where:

C_a = seismic coefficient (UBC Table 16-Q).

C_v = seismic coefficient (UBC Table 16-R).

I = importance coefficient (UBC Table 16-K).

N_v = near-source factor used in the determination of C_v in Seismic Zone 4.

R = numerical coefficient representative of the inherent overstrength and global ductility capacity of lateral-force-resisting systems.

T = elastic fundamental period of vibration of the structure in the direction under consideration, seconds.

V = the total design base shear.

W = the total seismic dead load.

Z = seismic zone factor (UBC Table 16-I).

The value of T may be approximated from the following formula:

$$T = C_t(h_n)^{\frac{3}{4}} \tag{2.14}$$

where:

C_t = 0.035 for steel moment-resisting frames and 0.020 for concentrically braced frames.

h_n = height above the base to level n (uppermost level in the main portion of the structure), ft.

The total force is distributed over the height of the structure in conformance with the following formula:

$$F_x = \frac{(V - F_t)w_x h_x}{\sum_{i=1}^{n} w_i h_i} \tag{2.15}$$

where:

F_x = design seismic force applied to level x.

h_x = height above the base to level x.

w_x = that portion of W located at or assigned to level x.

The concentrated force F_t at the top, which is in addition to F_n, is determined from the formula:

$$F_t = 0.07TV \tag{2.16}$$

F_t need not exceed 0.25V and may be considered as zero when T is 0.7 seconds or less.

At each level, the force F_x is applied at the center of mass of that level. The design story shear, V_x, in any story is the sum of the forces F_t and F_x above that story. Shears may increase as a result of horizontal torsion where diaphragms are not flexible. The torsional design moment at a given story is the moment resulting from eccentricities plus an accidental torsion. To determine the accidental torsion it is assumed that the mass at each level is displaced from the calculated center of mass in each direction a distance equal to 5% of the building dimension at that level perpendicular to the direction of the force under consideration.

For both allowable stress design and strength design, the Maximum Inelastic Response Displacement, Δ_M, of the structure is computed as:

$$\Delta_M = 0.7R\Delta_S \tag{2.17}$$

Δ_S is the displacement corresponding to the design seismic forces. When allowable stress design is used, Δ_S should be calculated using the load combinations of Section 1612.2 (Load Combinations Using Strength Design or Load and Resistance Factor Design).

Calculated story drifts using Δ_M should not exceed 0.025 times the story height for structures having a fundamental period of less than 0.7 seconds and 0.020 times the story height, otherwise.

2.3 Steel Frame Design

The buildings considered in this study have a square plan of 150 ft by 150 ft. The height of the first story is 18 ft and the height of upper stories is 12 ft. The plan view of the structural layout is shown in Figure 2.1. The perimeter steel frames provide the lateral-force-resisting system while the interior frames mainly carry the vertical loads. Two different lateral-force-resisting systems are designed for twelve story buildings, special moment-resisting frame (SMRF) and special concentrically braced frame (SCBF). Two story buildings only use SMRF. A SMRF is defined by the UBC as a moment-resisting frame specially detailed to provide ductile behavior and comply with the requirements given in Chapter 22 of the Code. A SCBF is a braced frame in which the members are subjected primarily to axial forces and designed in accordance with the requirements of Chapter 12 of the Code. Braced frames are generally restricted to the perimeter of the structure to satisfy the architectural requirements. Moment-resisting frames can be used as both interior and perimeter frames. Designing all of the frames in a steel structure with moment-resisting connections provides the maximum redundancy and energy dissipation capacity, but is very costly. Therefore, to reduce the number of moment-resisting

connections it is the common practice to design only the perimeter frames with moment-resisting connections. The beam-column connections of the interior frames are simple (pinned), and thus the contribution of the interior frames to the lateral-force resistance is negligible. The configuration layout of the perimeter lateral-force-resisting frames of the twelve and the two story buildings is shown in Figure 2.2.

In the design of steel frames it is assumed that ASTM A36 carbon steel is being used which has a yield stress of 36 ksi, a tensile strength of 58 ksi, and a modulus of elasticity of 30000 ksi.

2.3.1 Earthquake Design Loads

All of the buildings are assumed to have a seismic importance factor, I, equal to 1. They are located in seismic zone 4 (zone of the highest seismicity) and are therefore assigned a seismic zone factor Z of 0.4. The closest distance of the building site to a seismic source is assumed to be greater than 15 km which implies that the near-source factors, N_a and N_v, are 1.0 (N_a is the near-source factor used in the determination of C_a in seismic zone 4). Two different soil type profiles are considered, type S_B and type S_E. S_B is defined as a rock profile where the shear wave velocity is between 2500 to 5000 ft/sec. S_E is a soft soil profile characterized by a shear wave velocity less than 600 ft/sec, a standard penetration test number less than 15 blows/ft, and an undrained shear strength less than 1000 psf. It also includes any soil profile with more than 10 ft of soft clay.

The uniform design dead loads used in the weight calculations are listed in Table 2.1. The uniform design live loads for the roof and the floors are 20 and 50 psf, respectively. The design snow load is assumed to be 20 psf. In the present case, the

seismic dead load, W, is the total dead load. The story weights, w_i, are determined as the sum of the total floor (or roof) dead load and the weight of the tributary exterior walls. For the twelve story building:

$w_1 = (150)^2(0.114) + 4(150)(9 + 6)(0.0425)(0.75)$ $= 2852$ kips

$w_{2\text{-}11} = (150)^2(0.114) + 4(150)(6 + 6)(0.0425)(0.75)$ $= 2795$ kips

$w_{12} = (150)^2(0.088) + 4(150)(6)(0.0425)(0.75) + 4(150)(3)(0.0425) = 2171$ kips

$W = \Sigma w_i = 32973$ kips

where it is assumed that only 75% of the exterior wall area is solid. Similarly, for the two story building:

$w_1 = 2852$ kips

$w_2 = 2171$ kips

$W = \Sigma w_i = 5023$ kips

The base shear vertical distribution factors are a function of height and are calculated in Tables 2.2 and 2.3 for the twelve and the two story buildings, respectively.

To determine the base shear, the values of T, R, C_a, and C_v are needed. T and R depend on the type of the lateral-force-resisting system being used. C_a and C_v depend on the site seismic hazard characteristics, the site geology, and soil properties.

For the twelve story SMRFs,

$T = 0.035(150)^{3/4} = 1.5$ sec

and

$R = 8.5$

If the base shear calculated for soil profile type S_B is denoted by V_B and the base shear calculated for soil profile type S_E is denoted by V_E, then

V_B= 0.044 W = 1451 kips

V_E= 0.075 W = 2473 kips = 1.70 V_B

For the twelve story SCBFs,

$T = 0.020(150)^{3/4} = 0.9$ sec

and

R = 6.4

Thus,

V_B= 0.069 W = 2275 kips

V_E= 0.141 W = 4649 kips = 2.04 V_B

For the two story SMRFs,

$T = 0.035(30)^{3/4} = 0.4$ sec

and

R = 8.5

Thus,

V_B= 0.118 W = 593 kips

V_E= 0.106 W = 532 kips = 0.90 V_B

Note that unlike the twelve story building, the base shear calculated for soil profile type S_B is greater than the base shear calculated for soil profile type S_E. In this case, the design base shears are given by Equation (2.11) where the spectral acceleration $2.5C_a g$ is larger for soil profile type S_B.

Assuming that the diaphragms (floor and roof decks) are not flexible, the effect of the accidental torsion must be considered on the story shear distribution. Therefore, each perimeter frame in a particular direction is designed to resist 55% of the total base shear

calculated in that direction (Figure 2.3). Tables 2.4 and 2.5 list the force F_x applied at each story level to a perimeter frame in the twelve and the two story buildings, respectively.

2.3.2 Elastic Analysis of Lateral-Force-Resisting Frames

To obtain the most critical member stresses resulting from the basic and special seismic load combinations of Section 2.2, lateral-force-resisting frames are analyzed using linear static analysis procedure. The dead and live loads are calculated based on the tributary area of the floor attached to the frame. The wind design load computed in accordance with the requirements of Chapter 16, Division III of the UBC, based on a basic wind speed of 70 mph and Exposure C, is not considered in the load combinations due to the controlling effect of the earthquake design load. The elastic drifts are computed using the load combinations of Section 1612.2.1 of the UBC.

2.3.3 Seismic Provisions for Steel Frames

Design and construction of steel framing in lateral-force-resisting systems in seismic zones 3 and 4 must conform to the additional requirements of Chapter 22, Division V of the UBC. Some of the important requirements are presented in this section. These requirements are considered in the design of moment-resisting and braced frames of this study.

Section 2213.5.1 requires that in seismic zones 3 and 4, columns in frames be designed to satisfy the following conditions:

Under axial compression,

$$1.7F_aA \geq 1.0P_{DL} + 0.7P_{LL} \pm \Omega_0 P_E \quad (2.18)$$

Under axial tension,

$$F_yA \geq 0.85P_{DL} \pm \Omega_0 P_E \quad (2.19)$$

where:

A = area of cross section.

F_a = allowable axial compressive stress.

F_y = specified minimum yield strength of steel.

P_{DL} = axial dead load.

P_E = axial load on member due to earthquake.

P_{LL} = axial live load.

Ω_0 = overstrength factor, 2.8 for SMRF and 2.2 for SCBF.

SMRFs must satisfy the following requirements:

- The girder-to-column connection must be adequate to develop the strength of the girder in flexure, or the moment corresponding to development of the panel zone shear strength, whichever is smaller.
- The panel zone of the joint must be capable of resisting the shear induced by beam bending moments due to gravity loads plus 1.85 times the prescribed seismic forces, but the shear strength need not exceed that required to develop $0.8\Sigma M_s$ of the girders framing into the column flanges at the joint, where M_s is the flexural strength of a girder.
- The girder flange width-thickness ratio, $b_f/2t_f$, must not exceed $52/\sqrt{F_y}$.

- At any moment frame joint, the following relationships must be satisfied:

$$\Sigma Z_c(F_{yc} - f_a) / \Sigma M_c > 1.0 \quad (2.20)$$

or

$$\Sigma Z_c(F_{yc} - f_a) / 1.25\Sigma M_{pz} > 1.0 \quad (2.21)$$

where:

f_a = column maximum axial compressive stress.

F_{yc} = column F_y.

M_c = the moment at column centerline due to the development of plastic hinging in the beam.

M_{pz} = the sum of beam moments when panel zone shear strength is reached.

Z_c = plastic section modulus of column.

- Drift calculations may be based on column and girder centerlines when the column panel zone strength can develop $0.8\Sigma M_s$ of girders framing into the column flanges at the joint.

The requirements for SCBFs include:

- The slenderness ratio for bracing members must not exceed $1000/\sqrt{F_y}$.
- The slenderness ratio of individual elements of built-up members between the stitches that connect the elements must not exceed 0.4 times the governing slenderness ratio of the built-up member.
- Bracing connections must have the strength to resist an axial force equal to the tensile axial strength of the brace, $\Omega_0 P_E$ combined with gravity loads, and the maximum force that can be transferred to the brace by the system, whichever is smaller.

2.3.4 Twelve Story SMRF Designs

A total of four designs are considered for the twelve story SMRF. Two of them are based on the earthquake design loads obtained for soil profile type S_B and the other two are based on the earthquake design loads obtained for soil profile type S_E. One design from each set satisfies all the requirements of the code, including strength, drift, and joint strength ratio of Section 2213.7.5. This design will be referred to as the strong column-weak beam (SCWB) design. The other design, called weak column-strong beam (WCSB), satisfies all the requirements of the code except the requirement for joint strength ratio. The 1997 UBC allows the relationships of Section 2213.7.5 to be neglected under very restrictive conditions. However, according to the earlier edition of the Code columns meeting the compactness limitations given for beams, did not need to satisfy those relationships provided that their compressive stress was less than $0.4F_y$ for all applicable load combinations, or their lateral shear strength was 50% greater than that of the story above. The columns of the WCSB design satisfy the first condition, and thus the design is considered to be acceptable for the purpose of comparison with the SCWB design, at least in the context of the earlier edition of the Code. All the designs are governed by the drift and exceed the requirements for the strength. The same section is selected for all of the columns or the beams within a story. Furthermore, the beam and the column sections are not altered from one story to the next; instead, the first two stories use the same sections which are then altered at every second story and finally the upper four stories use the same sections. The designs obtained in this way provide stiffness and strength in excess of that required for some members, but they are representative of the actual design practice.

Tables 2.6 and 2.7 show the sections selected for the SCWB and the WCSB designs at a site characterized as soil profile type S_B. These designs are referred to as SCWB-B and WCSB-B, respectively. The member sections of the SCWB and the WCSB designs for soil profile type S_E (designated as SCWB-E and WCSB-E, respectively) are given in Tables 2.8 and 2.9.

2.3.5 Twelve Story SCBF Designs

One design is provided for soil profile type S_B and one design is provided for soil profile type S_E. These designs are referred to as SCBF-B and SCBF-E, respectively. As in the case of SMRFs, both designs are controlled by the drift requirement and not by the required strength. To achieve a practical design, the column and the brace sections are kept unchanged within a story and the following pattern of variation is adopted for the column and the brace sections along the height: the first two stories use the same sections which are then altered at every second story and finally the upper four stories use the same sections. Since the beams are simply connected to the columns, their size is controlled by the bending moment resulting from the gravity loads. Beams of all floors except the roof carry the same load and therefore only one section is used for all the beams in the structure. Tables 2.10 and 2.11 list the sections selected for SCBF-B and SCBF-E, respectively.

2.3.6 Two Story SMRF Design

The design earthquake forces corresponding to soil profile type S_B and soil profile type S_E for the two story building are close, and thus only one design is provided for this

building. The controlling requirement in this design is drift. The member selection for the two story SMRF is shown in Table 2.12. The same section is selected for all columns and so is for the beams.

CHAPTER 3

MODELLING AND ANALYSIS OF STEEL FRAMES

3.1 Introduction

In order to evaluate the performance of the lateral-force-resisting frames designed in Chapter 2, the dynamic nonlinear time history analysis (DNTHA) procedure is used. This procedure requires a numerical model of the frames and a representation of the ground motion. The response of the model is then processed to predict the expected seismic performance of the structure.

This chapter presents the details of the DNTHA procedure, modelling of steel frames, selecting the ground motion time histories, and expressing the performance in terms of the response parameters.

3.2 Analysis Procedure

The nonlinear dynamic response of a system is obtained by combining three procedures: incremental formulation of the equations of motion, implicit integration, and iterative solution.

The equation of motion of a multi-degree-of-freedom (MDOF) system (general finite element assemblage) is:

$$\mathbf{M}\ddot{\mathbf{U}} + \mathbf{C}\dot{\mathbf{U}} + \mathbf{K}\mathbf{U} = \mathbf{R} \tag{3.1}$$

where **M**, **C**, and **K** are the mass, damping, and stiffness matrices; **R** is the external load vector including the effects of the element body forces, the element surface forces, the

element initial stresses, and the concentrated loads; and $\mathbf{U}$, $\dot{\mathbf{U}}$, and $\ddot{\mathbf{U}}$ are the displacement, the velocity, and the acceleration vectors of the system.

In the step-by-step analysis of MDOF systems it is convenient to use an incremental formulation which allows the procedure to be applied to nonlinear as well as linear analysis. Thus taking the difference between the equations of motion defined for times t and t+Δt, one obtains the incremental equilibrium equation:

$$\mathbf{M}\Delta\ddot{\mathbf{U}} + \mathbf{C}_t\Delta\dot{\mathbf{U}} + \mathbf{K}_t\Delta\mathbf{U} = \Delta\mathbf{R} \tag{3.2}$$

where the subscript, t, denotes the value of a variable at time t and Δ denotes the change from time t to time t+Δt of the value of a quantity. In a procedure proposed by Newmark (Clough and Penzien 1993), the velocity and the displacement at time t+Δt are expressed as follows:

$$\dot{\mathbf{U}}_{t+\Delta t} = \dot{\mathbf{U}}_t + (1-\alpha)\,\Delta t\,\ddot{\mathbf{U}}_t + \alpha\,\Delta t\,\ddot{\mathbf{U}}_{t+\Delta t} \tag{3.3}$$

$$\mathbf{U}_{t+\Delta t} = \mathbf{U}_t + \Delta t\,\dot{\mathbf{U}}_t + (\frac{1}{2}-\beta)\,(\Delta t)^2\,\ddot{\mathbf{U}}_t + \beta\,(\Delta t)^2\,\ddot{\mathbf{U}}_{t+\Delta t} \tag{3.4}$$

In the above equations, the factor α provides a linearly varying weighting between the influence of the initial and the final accelerations on the change of velocity; the factor β similarly provides for weighting the contributions of these initial and final accelerations to the change of displacement. For $\alpha = 0.5$ and $\beta = 0.25$, the Newmark's formulation reduces to the so-called constant average acceleration method which is nothing but the trapezoidal rule of time integration. In this case:

$$\dot{\mathbf{U}}_{t+\Delta t} = \dot{\mathbf{U}}_t + \frac{\Delta t}{2}(\ddot{\mathbf{U}}_t + \ddot{\mathbf{U}}_{t+\Delta t}) \tag{3.5}$$

$$\mathbf{U}_{t+\Delta t} = \mathbf{U}_t + \frac{\Delta t}{2}(\dot{\mathbf{U}}_t + \dot{\mathbf{U}}_{t+\Delta t}) \tag{3.6}$$

The above formulation is implicit because the expressions yielding the new values for a given step include other values pertaining to that same step, so that the solution for a new value requires iteration. The cost of iteration within a step may be high, thus it is desirable to convert the implicit formulation to an explicit one. The explicit incremental equilibrium equations can be stated as (Clough and Penzien 1993):

$$\tilde{\mathbf{K}}\,\Delta\mathbf{U} = \Delta\tilde{\mathbf{R}} \tag{3.7}$$

The effective stiffness matrix in this equation is given by:

$$\tilde{\mathbf{K}} = \mathbf{K}_t + \frac{2}{\Delta t}\mathbf{C}_t + \frac{4}{(\Delta t)^2}\mathbf{M} \tag{3.8}$$

and the incremental effective load vector is:

$$\Delta\tilde{\mathbf{R}} = \Delta\mathbf{R} + 2\,\mathbf{C}_t\,\dot{\mathbf{U}}_t + \mathbf{M}\left(\frac{4}{\Delta t}\dot{\mathbf{U}}_t + 2\,\ddot{\mathbf{U}}_t\right) \tag{3.9}$$

In a nonlinear analysis, the effective stiffness matrix is itself a function of the unknown degree-of-freedom values or their derivatives, hence Equation (3.7) represents a nonlinear system. A widely used procedure for solving a system of nonlinear equations is the Newton-Raphson method (Bathe 1982). The equations used in this iterative process are, for i =1, 2, 3, …, n,

$$\tilde{\mathbf{K}}_{t+\Delta t}^{(i-1)}\,\Delta\mathbf{U}^{(i)} = \tilde{\mathbf{R}}_{t+\Delta t} - \tilde{\mathbf{K}}_{t+\Delta t}^{(i-1)}\;\mathbf{U}_{t+\Delta t}^{(i-1)} \tag{3.10}$$

$$\mathbf{U}_{t+\Delta t}^{i} = \mathbf{U}_{t+\Delta t}^{(i-1)} + \Delta\mathbf{U}^{(i)} \tag{3.11}$$

with the initial conditions,

$$\mathbf{U}_{t+\Delta t}^{(0)} = \mathbf{U}_t \tag{3.12}$$

$$\tilde{\mathbf{K}}_{t+\Delta t}^{(0)} = \tilde{\mathbf{K}}_t \tag{3.13}$$

The iteration is continued until the appropriate convergence criteria are satisfied. It is noted that the right-hand side of Equation (3.10) is the residual or out-of-balance load vector. The final converged solution would be in equilibrium, such that the vector of nodal point forces that are equivalent to the element stresses would equal the vector of externally applied loads (at least to within some tolerance).

When the stiffness matrix is updated every iteration, as indicated in Equation (3.10), the process is called a *full Newton-Raphson procedure*. The major computational cost per iteration results from the calculation and factorization of the stiffness matrix. Since these computations can be prohibitively expensive when large systems are considered, some modified forms of the full Newton-Raphson procedure have been considered where the stiffness matrix is updated less frequently. The most common, and probably the most efficient, modified procedure updates the stiffness matrix at the start of every time step.

To enhance the performance of the Newton-Raphson method, one of the following techniques is used in conjunction with this method:

- *Predictor* extrapolates the degree-of-freedom solution using the previous history in order to make a better guess at the start of each time step.
- *Adaptive Descent* switches to a stiffer matrix if convergence difficulties are encountered, and switches back to the tangent stiffness matrix upon the convergence of the solution.
- *Line Search* scales the incremental solution vector at each iteration, $\Delta \mathbf{U}^{(i)}$, by a scalar value called the *line search parameter*, because in some situations the use of the full $\Delta \mathbf{U}^{(i)}$ leads to solution instabilities.

3.3 Nonlinear Frame Models

DNTHA of the frame models will be performed using ANSYS finite element computer program. The SMRF models are made up of nonlinear beam elements. The beam element used (designated as BEAM23 in ANSYS computer program) is a uniaxial element with tension-compression and bending capabilities. The element has three degrees of freedom at each node: translations in the nodal x and y directions and rotation about the nodal z-axis (Figure 3.1). The element is defined by two nodes and a cross section. The general cross section option allows specifying a section height, h, and a five-location area distribution. There are three sets of integration points along the length of the element, one at each end and one at the middle. Each set consists of five integration points through the thickness which are located at positions y = -0.5h, -0.3h, 0, 0.3h, and 0.5h, The height is defined as the distance between the top and the bottom integration points and is not necessarily the distance between the outermost fibers of the cross section. Each one of these integration points has a numerical integration factor associated with it, as well as an input area. If the integration points located at y = -0.5h to y = 0.5h are numbered from 1 to 5, the input areas, A_i, are related to the effective areas, A_{ei}, corresponding to each integration point, by:

$A_{e1} = 0.0625\ A_1$

$A_{e2} = 0.28935\ A_2$

$A_{e3} = 0.29630\ A_3$

$A_{e4} = 0.28935\ A_4$

$A_{e5} = 0.0625\ A_5$

To compute the input areas for a symmetric I-shaped cross section, three criteria are satisfied:

1. Both the effective and the actual cross sections must have the same area to guarantee the identical response to axial forces for elastic and plastic behaviors.
2. Both the effective and the actual cross sections must have the same moment of inertia to respond identically to pure bending for elastic behavior.
3. Both the effective and the actual cross sections must have the same first moment of area (plastic section modulus) to ensure the same plastic moment.

Let A, I, Z, and h denote, respectively, the area, the moment of inertia, the plastic section modulus, and the depth of the I-shaped cross section. Noting that for a symmetric cross section $A_1 = A_5$ and $A_2 = A_4$, the above criteria may be written as the following equations:

$$0.12500\ A_1 + 0.57870\ A_2 + 0.29630\ A_3 = A \tag{3.14}$$

$$0.03125\ A_1 + 0.05208\ A_2 = I \tag{3.15}$$

$$0.06250\ A_1 + 0.17361\ A_2 = Z \tag{3.16}$$

Solving the above system of simultaneous equations, the input areas A_1, A_2, and A_3 are determined.

The elastic stiffness, mass, and stress (geometric) stiffness matrices are the same as those for a two-dimensional elastic beam element. The tangent stiffness matrix for plasticity, however, is formed by numerical integration. The general form of the tangent stiffness matrix for plasticity is:

$$\mathbf{K}_n = \iiint_{vol} \mathbf{B}^T \mathbf{C}_n \mathbf{B}\, dV \tag{3.17}$$

where:

$\mathbf{B}$ = strain-displacement matrix.

$\mathbf{C}_n$ = elasto-plastic stress-strain matrix.

This stiffness matrix for a general beam element can also be written symbolically as:

$$\mathbf{K}_n = \mathbf{K}^B + \mathbf{K}^S + \mathbf{K}^A + \mathbf{K}^T \quad (3.18)$$

where the terms on the right-hand side represent bending, shear, axial, and torsional contributions, respectively. Only one component of strain is used in each of these four matrices at a time.

In SCBFs, the columns are modelled using two-dimensional nonlinear beam elements and the beams and braces are modelled using two-dimensional spar element. The two-dimensional spar element (designated as LINK1 in ANSYS computer program) can be used in a variety of engineering applications to represent a truss member, a link, a spring, etc. It is a uniaxial tension-compression element with two degrees of freedom at each node: translations in the nodal x and y directions (Figure 3.2). The axial strain is uniform in the element. The element is defined by two nodes, the cross sectional area, the initial strain, and the material properties.

To represent the behavior of structural steel, a bilinear material model with kinematic strain hardening (BKIN) is used. In this model the total stress range is assumed to be equal to twice the yield stress, so that Bauschinger effect is included. This material model may be used for materials that obey von Mises yield criterion, including most metals. The material behavior is described by a bilinear total stress-strain curve starting at the origin as shown in Figure 3.3. The initial slope of the curve is equal to the elastic modulus (Young's modulus) of the material, E. At the specified initial yield stress, σ_y, the

slope drops to the tangent modulus, E_t. In an elastic-perfectly plastic model $E_t = 0$, but usually a small value of E_t is used to avoid numerical problems in the solution process. The unloading path is always a straight line with a slope equal to the elastic modulus of the material until a yield point is reached. The yield point would either be the end point of the last nonlinear path or the point located a distance $2\sigma_y$ below or above it. For the steel model used in this study, it is assumed that E is 30,000 ksi, σ_y is 36 ksi, and $E_t = 0.01E$.

Damping representation in dynamic nonlinear time history analysis will be discussed later in Section 5.5. The damping matrix, **C**, used in the analysis of the frame models is assumed to be a linear combination of the mass and the initial stiffness matrices (Rayleigh's damping). The coefficients of these matrices are determined based on a 5% modal damping ratio in the first two modes of vibration of the elastic structure.

3.4 Ground Motion Representation

Once the frame model has been developed, the time history of ground motion acceleration needs to be defined. Since the ground motion hazard for a specific site is often expressed as an elastic acceleration response spectrum, the time histories of ground motion acceleration for that site are obtained by scaling the recorded time histories to a spectrum-related "intensity" or by generating spectrum-compatible simulated accelerograms.

3.4.1 Actual Accelerograms

Earthquake ground motions are random in nature and therefore, several acceleration records which are representative of a given site, must be used in order to determine the probable seismic response of structures located at that site. Scaling of the records will reduce the number of time histories required to estimate the average response within a predefined confidence interval. Several scaling procedures have been proposed, such as the commonly used scaling to the peak ground acceleration level, scaling to the average spectral acceleration over a frequency interval, scaling to the spectral acceleration at a higher level of damping, etc.

It is observed (Shome et al. 1998) that the scaling of ground motion records to the 5%-damped spectral acceleration at the fundamental frequency of the structure is the most efficient among the alternatives and does not bias the nonlinear response estimates. Consider a set of accelerograms that are to be scaled for the analysis of a structure having a fundamental frequency f. Let ${}^{i}S_a(f)$ denote the 5%-damped and ${}^{i}S'_a(f)$ denote the design spectral acceleration at frequency f for the ith record of the set. The scale factor S_i for this record is computed as:

$$S_i = \frac{{}^{i}S'_a}{{}^{i}S_a} \tag{3.19}$$

The scale factors so obtained depend on the frequency of the structure, and thus a particular record needs to be scaled by different factors when it is used to excite structures with different frequencies.

If it is desired to use a unique scale factor over a frequency interval, a two-step procedure described by (Schiff, Hall, and Foutch 1988) may be applicable. The first step in the scaling procedure is to normalize the ground motion records to the same Housner

intensity defined as the integral of the pseudo-velocity response spectrum over the period range 0.1<T<2.5 sec (Clough and Penzien 1993):

$$SI(\xi) \equiv \int_{0.1}^{2.5} S_{pv}(\xi, T)\, dT \tag{3.20}$$

where ξ is the damping ratio. The original period range may be replaced by a range of natural periods dominating the response of the structures under consideration.

In the second step of the scaling procedure, a new spectrum is generated by averaging at each frequency the pseudo-velocities of each response spectrum scaled with the corresponding scale factor calculated in the first step. The average spectral acceleration for the new spectrum is calculated over the desired frequency range, $[f_1 f_2]$:

$$\overline{S}_a = \frac{1}{f_2 - f_1} \int_{f_1}^{f_2} S_a\, df \tag{3.21}$$

The second scale factor is the ratio of the maximum design spectral acceleration envisioned by the code and the average spectral acceleration calculated above. The final scale factor for each record is the product of the scale factors calculated in the first and the second steps of the scaling procedure.

Throughout this study, the first procedure (Equation (3.19)) is used for the scaling of the ground motion acceleration records, except in Section 5.5 where the use of a unique (frequency-independent) scale factor greatly facilitates the creation of response spectra for different damping models.

Earthquake ground motions are irregular and each is different from all others, even at a given site. Therefore, earthquake-resistant design is based on the general characteristics of certain groups of earthquakes. Earthquakes can be classified into four groups:

1. Single shocks-Motions of this type occur only at short distances from the epicenter, only on firm ground, and only for shallow earthquakes. They are almost unidirectional, stronger in one sense than the opposite. If the energy of motion is broken down in accordance with the frequencies of vibration it excites, a prevalence of short periods of vibration (of the order of 0.2 second or shorter) would be observed.
2. Moderately long, extremely irregular motion-Motions of this type are associated with moderate distances from the focus and occur only on firm ground. Over a wide range of periods of vibration there is, on the average, equipartition of energy. These motions are nearly white noise. They are ordinarily of almost equal severity in all directions.
3. Long ground motions exhibiting pronounced prevailing periods of vibration-Such motions result from the filtering of earthquakes of the preceding types through layers of soft soil within the range of linear or almost linear soil behavior and from the successive wave reflections at the interfaces of these mantles.
4. Ground motions involving large-scale, permanent deformations of the ground-This type is representative of near-source ground motions and may produce slides or soil liquefaction.

The seismic hazard in most locations is caused by the earthquakes belonging to the second and third groups. In this study, nine events from the second group and nine events from the third group are selected to represent the design earthquakes. The selected ground motions are listed in Table 3.1 where Rock refers to the second group and Soil refers to the third ground motion category.

The response spectra used to scale these ground motion records are developed in Section 3.4.4 of this chapter.

3.4.2 Simulated Accelerograms

An alternative to the scaling of an actual accelerogram by a single factor is to generate an accelerogram which is compatible with a specified design response spectrum. Spectrum-compatible accelerograms can be obtained by modifying actual accelerograms. This is done by manipulating the actual accelerograms in the frequency domain. Some believe that this process distort the records in a manner that the corresponding ground velocity and displacement are not realistic, and the energy content is also greatly exaggerated (Lew and Naeim 1996). To them, the use of spectrum-compatible accelerograms for analysis and design can lead to overestimated demands. However, it seems that these problems may be eliminated by using an appropriate procedure for generating the spectrum-compatible accelerograms.

A full description of the method adopted in this study to generate synthetic ground motions can be found in a paper by Deodatis (Deodatis 1996). In this method, a spectral-representation-based simulation algorithm is used to generate the artificial time histories. The procedure uses an iterative scheme to generate seismic ground motion time histories at several locations on the ground surface that are compatible with prescribed response spectra and are correlated according to a given coherence function. These time histories include the wave propagation effect and have a specified duration of strong ground motion.

The process may be initiated in either way:

1. The model suggested by Jennings et al. (Jennings et al. 1968) is used for the modulating functions to control the duration of strong ground motion and the power spectral density functions are set to a non-zero constant value over the entire frequency range. Although the procedure needs less effort preparing the input data compared to the other procedure, the characteristics of the generated records and the resulting structural demands may not be realistic.
2. Alternatively, the acceleration time history of an actual earthquake is used to determine the power spectral density functions and the modulating functions. This procedure requires the Fourier amplitudes and phase angles of the actual accelerogram to be computed and input to the program. It can be regarded as a procedure of scaling the "seed" accelerogram and the characteristics of the generated records are expected to be realistic.

In this study the first nine ground motion accelerograms listed in Table 3.1 (rock records) are used as seed to obtain the synthetic accelerograms. Figure (3.4) shows the acceleration response spectra of El Centro earthquake scaled to the 5%-damped design spectral acceleration at the fundamental period of mmsb (2.2 seconds) and its associated artificial earthquake.

3.4.3 Seismic Hazard

To characterize the earthquake ground motion intensity, seismic codes generally use acceleration response spectra. The UBC defines the design response spectra in terms of the seismic coefficients C_a and C_v (Figure 3.5). These spectra are the same as those

defined by the *NEHRP Guidelines* to specify the Basic Safety Earthquake 1 (BSE-1) level, which has a 10% probability of being exceeded in 50 years. The UBC does not provide any spectrum for the Basic Safety Earthquake 2 (BSE-2) level, also termed Maximum Considered Earthquake (MCE), which has a 2% probability of being exceeded in 50 years. However, the 2%/50 spectra may be constructed by using a procedure described in the *NEHRP Guidelines*. This procedure is briefly explained here.

The mapped short-period response acceleration parameter, S_S, and the mapped response acceleration at one-second period, S_1, are determined from the ground shaking hazard maps distributed with the *Guidelines*. These parameters are adjusted for the site class to give the design short-period spectral response acceleration, S_{XS}, and the design spectral response acceleration at one-second period, S_{X1}:

$$S_{XS} = F_a S_S \tag{3.22}$$

$$S_{X1} = F_v S_1 \tag{3.23}$$

where F_a and F_v are site coefficients that depend on the site class and the values of S_S and S_1. A general, horizontal response spectrum is constructed by plotting the spectral response acceleration, S_a, versus the structural period, T, according to the following functions:

$$S_a = \frac{S_{XS}}{B_S}(0.4 + 3\frac{T}{T_0}) \qquad 0 < T < 0.2T_0 \tag{3.24}$$

$$S_a = \frac{S_{X1}}{B_1 T} \qquad T > T_0 \tag{3.25}$$

where T_0 is given by the equation

$$T_0 = \frac{S_{X1} B_S}{S_{XS} B_1} \tag{3.26}$$

and B_S and B_1 are given as a function of the effective viscous damping. It is recommended that a 5%-damped response spectrum be used for most structural systems. In this case, $B_S = B_1 = 1$, and the parameters S_{XS} and S_{X1} are related to the seismic coefficients C_a and C_v as follows:

$$S_{XS} = 2.5\ C_a \tag{3.27}$$

$$S_{X1} = C_v \tag{3.28}$$

The 5%-damped acceleration response spectra corresponding to BSE-1 and BSE-2 levels that are used in this study are shown in Figure 3.6. The mapped response parameters selected for BSE-1 which is similar to the UBC-defined design earthquake, are $S_S = 1.0g$ and $S_1 = 0.4g$. The mapped response parameters selected for BSE-2 are $S_S = 2.0g$ and $S_1 = 0.8g$. These parameters define for instance, the seismic hazard in city of San Diego. As the figure shows, the ordinate of the BSE-2 spectrum at any frequency is twice the ordinate of the BSE-1 spectrum.

The vertical-acceleration response spectrum for a given site is constructed by multiplying the ordinates of the horizontal-acceleration response spectrum for that site by 2/3.

The response spectra constructed in this section are used in the procedure of scaling the actual ground motion records and also in the process of generating simulated accelerograms.

3.5 Performance Levels and Measures of Damage

The performance levels are qualitative statements of damage. To be quantitatively defined, the performance levels must be converted to the limiting values in the structural

response parameters which reflect the expected damage states. In this study, the behavior of the designed steel frames is evaluated in terms of several damage measures. The following damage measures are considered: deformation ductility, interstory drift, dissipated hysteretic energy, Park-Ang damage index, and stiffness reduction. In addition, wherever applicable, the force and deformation limits suggested in the NEHRP *Guidelines* are used to assess the performance of the frames.

3.5.1 Deformation Ductility

Let u_m denotes the maximum absolute value of a generalized deformation (e.g., strain, curvature, etc.) and u_y denotes an arbitrarily defined yield deformation. The deformation ductility, μ, is defined as

$$\mu \equiv \frac{u_m}{u_y} \tag{3.29}$$

In this study, the generalized deformation, u, for moment-resisting elements of a structure is curvature. Consider an infinitesimal element of a beam as shown in Figure 3.7. If ε_b is the total normal strain at the bottom fiber and ε_t is the total normal strain at the top fiber, then the curvature ϕ at the cross section located at a distance x from the origin is

$$\phi = \frac{d\theta}{dx} = \frac{(\varepsilon_b\, dx - \varepsilon_t\, dx)/h}{dx} = \frac{\varepsilon_b - \varepsilon_t}{h} \tag{3.30}$$

where h is the height of the cross section. Compressive strains are negative and tensile strains are positive.

The yield curvature, ϕ_y, is defined as

$$\phi_y = \frac{2\varepsilon_y}{h} \tag{3.31}$$

where ε_y denotes the yield strain of the material. For members with symmetrical cross section and only subjected to bending moment the yield curvature defined as in Equation (3.31) corresponds to the first occurrence of the yield strain in the cross section. For members subjected to simultaneous axial force and bending moment, the curvature at the onset of yielding depends on the axial force magnitude, but it will be close to ϕ_y when the axial force is not very high.

3.5.2 Interstory Drift

The interstory drift, δ, is defined as the relative horizontal displacement between the top and the bottom floor levels of a story divided by the height of that story:

$$\delta_i = \frac{\Delta_i - \Delta_{i-1}}{H_i} \qquad i = 1, 2, \ldots, n \tag{3.32}$$

where:

δ_i = interstory drift of story i.

Δ_i = horizontal displacement of floor level i.

Δ_{i-1} = horizontal displacement of floor level i-1.

H_i = height of story i.

n = number of stories.

3.5.3 Dissipated Hysteretic Energy

The dissipated hysteretic energy per unit volume, known also as the unit plastic work, at a point of an elasto-plastic body under a uniaxial state of stress is

$$w_p = \int_0^{\bar{\varepsilon}_p} \sigma \, d\varepsilon_p \tag{3.33}$$

where σ denotes the stress (as a function of plastic strain) and ε_p denotes the plastic strain at that point. w_p is the unit dissipated hysteretic energy when the plastic strain varies from zero to a value of $\bar{\varepsilon}_p$.

The total dissipated hysteretic energy in the body, W_p, is computed as

$$W_p = \iiint_{vol} w_p \, dV \tag{3.34}$$

For a prismatic beam element of length L and cross sectional area A, the total dissipated energy is given by

$$W_p = A \int_0^L w_p \, dx \tag{3.35}$$

where x defines the position along the axis of the element with respect to a chosen origin.

In this study, the total dissipated hysteretic energy for a beam element is calculated as the difference between the total strain energy,

$$W_t = \iiint_{vol} \left(\int_0^{\bar{\varepsilon}_t} \sigma \, d\varepsilon_t \right) dV \tag{3.36}$$

and the elastic strain energy,

$$W_e = \frac{EA}{2} \int_0^L \varepsilon_e^{\,2} \, dx \tag{3.37}$$

The subscripts t and e refer to the total and the elastic values, respectively. This approach is preferred over calculating W_p using Equation (3.35) because the total hysteretic energy, W_t, can readily be obtained as a standard output from ANSYS computer program. To calculate the elastic strain energy, it is assumed that the variation of the unit elastic strain energy, w_e, between the three integration points located at the same height along the length of the element, is quadratic:

$$^{i}w_e = ax^2 + bx + c \tag{3.38}$$

where the left superscript i = 1, 2, ..., 5 refers to the height of the integration points; i = 1 refers to the integration points at y = -0.5h, i = 2 refers to the integration points at y = -0.3h, and so on. The constants a, b, and c are determined in terms of w_{i1}, w_{i2}, and w_{i3}, the unit elastic strain energies at x = 0, x = L/2, and x = L, respectively. Substituting for a, b, and c in Equation (3.38), we have

$$^{i}w_e = \left(2w_{i3} - 4w_{i2} + 2w_{i1}\right)\left(\frac{x}{L}\right)^2 + \left(-w_{i3} + 4w_{i2} - 3w_{i1}\right)\left(\frac{x}{L}\right) + w_{i1} \tag{3.39}$$

The elastic strain energy stored in the volume associated with the ith layer of integration points is

$$^{i}W_e = A_i \int_0^L {}^{i}w_e \, dx = \frac{A_i L}{6}\left(w_{i3} + 4w_{i2} + w_{i1}\right) \tag{3.40}$$

where A_i is the actual area attributed to the ith layer. w_{i1}, w_{i2}, and w_{i3}, are computed from the elastic strain, $^{e}\varepsilon_{ij}$, at each integration point (j = 1, 2, 3):

$$w_{ij} = \frac{E \, {}^{e}\varepsilon_{ij}^{\,2}}{2} \tag{3.41}$$

The total strain energy stored in the element can now be calculated as

$$W_e = \sum_{i=1}^{5} {}^{i}W_e = \frac{EL}{12}\left(\sum_{i=1}^{5} A_i \sum_{j=1}^{3} {}^{e}\varepsilon_{ij}{}^{2}\right) \tag{3.42}$$

Once the elastic strain energy has been determined, the dissipated hysteretic energy is found:

$$W_p = W_t - W_e \tag{3.43}$$

3.5.4 Park-Ang Damage Index

In the model proposed by Park and Ang (Park and Ang 1985), damage is expressed as a linear function of the maximum deformation and the cumulative plastic strain energy. The Park-Ang damage index, D_{PA}, for a structural member is given by

$$D_{PA} = \frac{\delta_m}{\delta_u} + \frac{\beta}{Q_y \delta_u}\int dE \tag{3.44}$$

where:

δ_m = maximum deformation under earthquake.

δ_u = ultimate deformation under monotonic loading.

β = loading-path-independent parameter.

Q_y = calculated yield strength.

E = dissipated plastic strain energy.

Empirical expressions to determine β were provided for reinforced concrete cantilever beams with rectangular cross section and a mean value of 0.05 was obtained for β in this case. Experimental studies conducted on H-shaped steel cantilevers gave a mean value of 0.025 for this coefficient.

The suggested values for β are based on tests performed on cantilever specimens, with δ being the free-end displacement. Applying the Park-Ang damage index to a frame member where the deformation is expressed in terms of curvature requires a modified expression. The original form will be transformed into a new form where the deformation u has been replaced with the curvature ϕ. This new form, derived based on the relationship between the end-displacement and the maximum curvature in a cantilever beam, will then be assumed to represent the damage expression for a frame member with arbitrary boundary conditions.

Consider the cantilever beam shown in Figure 3.8. The free-end displacement, δ_m, is calculated using the curvature distribution diagram:

$$\delta_m = \left(\frac{\phi_y L}{2}\frac{2L}{3}\right) + (\phi_m - \phi_y)L_p(L - L_p) \tag{3.45}$$

where:

ϕ_m = maximum curvature.

ϕ_y = yield curvature calculated as in Equation (3.31).

L = length of the beam.

L_p = length of the plastic hinge zone.

An approximation for L_p may be obtained based on the properties of the I-shaped cross sections used in the designs. Let M_p denote the plastic moment and M_y denote the yield moment of an I-shaped cross section having a moment of inertia, I, and a plastic section modulus, Z. If P is the ultimate load of a cantilever beam with this cross section,

Then

$$\frac{M_p}{M_y} = \frac{Z\sigma_y}{2I\sigma_y / h} = \frac{PL}{P(L - L_p)} \tag{3.46}$$

Solving for L_p, we find

$$L_p = L\left(1 - \frac{2I}{Zh}\right) \tag{3.47}$$

Investigation of the sections used in the designs shows that for these sections I/Zh is nearly 0.4. Therefore,

$$L_p \approx 0.2L \tag{3.48}$$

Substituting for L_p into Equation (3.45) and simplifying,

$$\delta_m = L^2\left(0.180\phi_m + 0.153\phi_y\right) \tag{3.49}$$

To find the curvature equivalent of the ultimate deformation term, δ_u, the damage index at the onset of yielding is assigned a value of 0.4 which implies a moderate damage. In this case $\delta_m = L^2\phi_y/3$ and E =0, thus

$$0.4 = \frac{L^2\phi_y / 3}{\delta_u} \tag{3.50}$$

giving,

$$\delta_u = \frac{5}{6}L^2\phi_y \tag{3.51}$$

Finally, the yield strength, Q_y, will be substituted by M_y/L to obtain the modified form of the damage index, $D_{PA,m}$, in terms of curvature:

$$D_{PA,m} = \frac{6}{5\phi_y}\left(0.180\phi_m + 0.153\phi_y + \frac{\beta}{LM_y}\int dE\right) \qquad \phi_m > \phi_y \tag{3.52}$$

When the beam remains elastic ($\delta_m < \delta_y$), $\delta_m = L^2\phi_m/3$ and E =0, thus

$$D_{PA,m} = \frac{2\phi_m}{5\phi_y} \qquad \phi_m < \phi_y \tag{3.53}$$

The damage index at each end of the element is computed and the larger of the two indices is taken as the damage index for the member. The damage distribution is closely correlated with the distribution of the absorbed energy. Therefore, the damage index for the entire structure, D_T, is calculated as the weighted average of the component damage indices (Park etal 1985):

$$D_T = \sum_i \lambda_i (D_{PA,m})_i \tag{3.54}$$

λ_i is the energy weighting factor for component i, defined as

$$\lambda_i \equiv \frac{E_i^t}{\sum_j E_j^t} \tag{3.55}$$

where E_i^t is the maximum total energy absorbed by element i, including the elastic strain energy.

3.5.5 Stiffness Reduction

In this study, a new simplified procedure is proposed and compared with the DNTHA method. This procedure uses the results of a pushover analysis to evaluate a global damage index for the structure. First, a pushover curve is obtained by plotting the base shear versus the roof horizontal displacement under increasing lateral forces that are distributed with the same pattern as the design earthquake forces. Then, the average maximum roof displacement for a given ground motion level is estimated and the point associated with this displacement is located on the pushover curve. Let K denote the

slope of a line drawn from the origin to this point (secant stiffness) and K_0 denote the initial slope of the pushover curve (initial stiffness). The damage index is defined as

$$D_K = 1 - \frac{K}{K_0} \tag{3.56}$$

This damage index can then be used to obtain the average maximum interstory drift or to determine the performance level directly. The proposed procedure is explained in Section 4.5.

CHAPTER 4

EVALUATION OF SEISMIC PERFORMANCE

4.1 Introduction

To evaluate the seismic performance of the designed frames, the following dynamic response parameters and damage measures are obtained: maximum interstory drift; maximum horizontal roof displacement, maximum frame-member ductility; frame-member, story, and total dissipated hysteretic energies; frame-member and global Park-Ang damage indices; and maximum compressive force ratio for columns in the braced frames. The results of the dynamic nonlinear time history analyses (DNTHA) are processed to determine the maximum value, minimum value, mean, standard deviation, and coefficient of variation for each parameter.

A static nonlinear pushover analysis is also performed for each frame. Pushover analysis is widely used to study nonlinear response of structures. The results of the pushover are compared with those of the dynamic analyses. In addition, the pushover analysis is necessary to compute the proposed stiffness reduction damage index for each structure.

In the following sections of this chapter, the frame models are named using a simple convention. According to this convention, the name of a moment-resisting twelve story frame model begins with *mm* (standing for moment-resisting, medium-rise), followed by a letter which specifies the column-beam proportioning (*s* for the strong column-weak beam and *w* for the weak column-strong beam design). The fourth letter specifies the soil profile type and is either *b* or *e*. The fifth letter specifies the level of the

ground motion (*d* for design earthquake and *m* for maximum considered earthquake). Finally, the last letter is the ground motion record number. The records listed in Table 3.1 are numbered from 1 to 9 for each ground profile. The name of a braced twelve story frame model begins with *b*, followed by letters showing the soil profile type, the ground motion level, and the record number, respectively. The name of a two story frame model is obtained as that of a braced frame model, except that it begins with an *l* instead of a *b*.

4.2 Nonlinear Pushover Analysis of the Designed Frames

The static pushover analysis of the designed frames is carried out by application of a set of monotonically increasing lateral forces having the same distribution as the design earthquake forces. Figures 4.1 through 4.4 show the story shear force-interstory drift, and base shear force-global drift relationships for the twelve story special moment-resisting frames. Global drift is defined as the roof horizontal displacement divided by the height of the frame. The shears are normalized with respect to the weight of the building. The force-displacement curves provide some useful information regarding the general properties of each frame model. Comparing the force-displacement curves of the moment-resisting frames with strong columns and weak beams (mmsb and mmse) and those with weak columns and strong beams (mmwb and mmwe) reveals that although the initial stiffness of both designs is almost identical for a given site, the strong column-weak beam design has about a 30% higher strength. Let the ultimate base shear be arbitrarily defined as the base shear corresponding to a 50% reduction in the secant stiffness. The ratio of the ultimate and the design base shears for frames with strong columns and weak beams is more than 4.0. The nonlinear behavior of the strong column-

weak beam frames is characterized by the uniform yielding of the stories in the lower half of the structure. However, in the weak column-strong beam frames, the nonlinear behavior mainly results from the yielding of the third, sixth, and ninth stories where the member sizes have been reduced. Higher strength and more uniform distribution of yielding makes the strong column-weak beam designs more desirable.

Figure 4.5 and 4.6 show the force-displacement curves of the special concentrically braced frames on soil profile type S_B and S_E, respectively. For each site the strength of the braced frame is nearly the same as the strength of the moment resisting frame with strong columns and weak beams. However, the initial stiffness is about 50% higher and the ratio of the ultimate and the design base shears is only about 2.5. The nonlinear behavior of the braced frames is characterized by the large inelastic interstory drifts occurring in the third through seventh stories. The initiation of the nonlinear behavior of the frames is associated with a global drift of approximately 0.6% in all of the twelve story frames.

The story and the global force-displacement relationships for the two story frame is shown in Figure 4.7. Note that the same design is used for both soil profile types S_B and S_E. Like the twelve story frames, the nonlinear behavior initiates at a global drift of about 0.6% but the ultimate base shear is more than 5 times the design base shear. The fact that all frames have the same "yield" global drift but different overstrength ratios is worth noting. It seems to be a result of the designs being controlled by the interstory drift and not by the strength requirement.

4.3 Results of Dynamic Analyses and Performance Assessment

For the purpose of the performance evaluation the results of the dynamic nonlinear time history analysis of the frame models is classified as

1. story response
2. element response
3. global response

Story response consists of the maximum Park-Ang damage index of the elements of each story, the maximum curvature ductility demand of the elements of each story, the maximum compressive force ratio (for the columns in the braced frames), the maximum axial ductility demand (for tension and compression elements), the hysteretic energy dissipated by the elements of each story, and the maximum drift of each story. The response parameters in this category are statistics, such as mean and mean plus standard deviation, calculated for the ensemble of ground motions. Let x_{ij}^k denote a non-summable response parameter (for example, maximum ductility demand or damage index) of element i in story k, when the structure is subjected to ground motion record j. The story response, $\bar{x}^k$, is computed as:

$$\bar{x}^k = \frac{\sum_{j=1}^{n} \max\left\{x_{1j}^k, x_{2j}^k, \cdots, x_{mj}^k\right\}}{n} \tag{4.1}$$

where m is the number of the beams or columns in the story under consideration and n is the number of the ground motion records. Similarly, if y_{ij}^k denotes a summable response parameter (for example, the dissipated hysteretic energy), then the story response, $\bar{y}^k$, is

$$\bar{y}^k = \frac{\sum_{j=1}^{n}\sum_{i=1}^{m} y_{ij}^k}{n} \tag{4.2}$$

The element response refers to the maximum response produced by a set of ground motions. The response parameters considered are Park-Ang damage index, ductility demand, compressive force ratio, and dissipated hysteretic energy. Therefore, if x_j denotes the maximum value of a certain response parameter when the structure is subjected to ground motion *j*, then the element response x is simply

$$x = \max\{x_1, x_2, \cdots, x_n\} \tag{4.3}$$

The global response which is obtained for each ground motion includes the Park-Ang damage index calculated for the entire structure as the weighted average of the damage index of the components (Equation (3.54)), the global drift defined as the maximum roof horizontal displacement divided by the height of the structure, and the total dissipated hysteretic energy.

The story, element, and global dissipated hysteretic energies are normalized with respect to the elastic strain energy per unit volume at yield, $\frac{\sigma_y^{\ 2}}{2E}$.

4.3.1 Twelve Story (Medium-Rise) Frames

The lateral-force-resisting system of the twelve story building is either a special moment-resisting frame or a special concentrically braced frame. Because the performance of these systems is evaluated based on different acceptance criteria, they are discussed separately in the following sections.

4.3.1.1 Special Moment-Resisting Frames: The NEHRP-recommended acceptance criteria for primary elements for Immediate Occupancy (IO), Life Safety (LS), and Collapse Prevention (CP) performance levels are given in Table 4.1. Primary elements are defined as the key components of the lateral-force-resisting system which must be able to sustain earthquake-induced forces and deformations while simultaneously supporting gravity loads. In the designed frames, all components are considered to be primary elements. The curvature ductility limits given in Table 4.1 are derived from the deformation limits recommended in Table 5-3 of the NEHRB *Guidelines* by using a procedure similar to the one used in Section 3.5.4 to formulate the damage index. The given ductility limits are intended for members meeting the compactness limitations of Section 2213.7.3 of the Uniform Building Code. It is also required that the ratio of the axial force and the expected axial yield force in the columns (P/P_{ye}) be less than 0.2. The first condition is satisfied by all the components of the moment-resisting frames designed for the purpose of the present study. The second condition is true for the interior columns under either ground motion level, but the exterior columns may experience a ratio larger than 0.2 under a BSE-2 ground motion. In this case the ductility limits given in Table 4.1 will be reduced by a factor of $1.5(1-1.7P/P_{ye})$. If the ratio is greater than 0.5-a situation that does not happen in this study-columns must be treated as force-controlled components. The interstory drift limits in Table 4.1 are also taken from the NEHRP *Guidelines*. The association of the damage index with the performance is based on the commonly assumed correlation between the damage index and the observed damage state of a component. The consistency of the limits suggested for the different damage measures is yet to be determined.

The statistics of the seismic response of the twelve story moment-resisting frames are summarized in Table 4.2. The values given in this table will later be used to assess the performance level of the twelve story moment-resisting frames.

Figures 4.8 and 4.9 show the story response for the moment-resisting frame with strong columns and weak beams on soil profile type S_B when it is subjected to the ground motions scaled to BSE-1 level (mmsbd). The response parameters are separately presented for the beams and for the columns. The solid lines represent the maximum (max), the dashed lines the mean (m), and the dotted lines the mean plus standard deviation (mps) statistics. The story response of this frame exhibits extensive nonlinear behavior in the first and the eighth through the eleventh stories. The mean damage index calculated for the elements of each story ranges between 0.2 to 0.8 where most columns show values slightly less than 0.4 and most beams show values larger than 0.4 but well below 0.8. The mean beam ductility varies from 1 to 2 with most values close to 2. The mean column ductility also lies in the same range but most values are slightly below 1. The mean interstory drift ranges from 0.5% to 1.2% with a dominant value of 0.9%.

Figure 4.10 shows the scatter of the maximum element response and also the correlation between different response parameters. The column damage index exhibits the least scatter with a coefficient of variation (C.O.V.) of 0.53, while the scatter of the element dissipated hysteretic energy is the largest (C.O.V. = 2.3). The Pearson product moment coefficient of correlation, r, is a measure of the strength of the linear relationship between two response parameters. It is observed that an almost linear relationship exists between the interstory drift with the element damage index or curvature ductility.

However, the correlation between the interstory drift and the element dissipated hysteretic energy is not strong.

The correlation between global response parameters and their scatter is shown in Figure 4.11. Among the global response parameters, the global drift (normalized roof horizontal displacement) has the smallest scatter with a C.O.V. of 0.11. There is a strong linear correlation between the maximum interstory drift with the global drift or the global damage index. One may wonder whether this correlation allows translating the limiting response values for one parameter into the limiting values for another parameter. The answer is negative, because this will lead to inconsistent results. For example, the interstory drift limits of 0.007, 0.025, and 0.050 will correspond to the global damage index limits of 0.3, 1.0, and 1.9, or to the beam ductility limits of 1, 5, and 10, respectively, which are obviously different from the recommended values given in Table 4.1. Therefore, the validity of the recommended limits is questionable. Providing reliable and consistent response limits is a cornerstone of the performance-based seismic design and yet one of the most challenging issues. In this study when such inconsistencies are encountered, the interstory drift limits are assumed to prevail because the interstory drift has been the most reliable indicator of the overall performance of a structure to this time. The component response limits such as ductility demand or damage index can only serve as a sufficient but not a necessary condition for the evaluation of the overall performance.

Based on the response values listed in Table 4.2 and the previous discussion, the performance level of this frame is most probably bounded by IO and LS and is unlikely to reach CP.

The seismic response of the same frame when it is subjected to BSE-2 ground motions is shown in Figures 4.12 through 4.15. The story response follows the same pattern as the one that was observed for BSE-1 ground motions. The average demands are more or less uniform through the height of the frame. They generally exceed the limits set forth in Table 4.1 for IO performance level but do not reach the limits of LS performance level. The maximum observed response, however, is very close the CP. As Figures 4.14 and 4.15 show, there is a strong linear correlation between the maximum story drift and maximum element damage index, maximum element ductility demand, and the global damage index. The linearity of the relationships between the maximum story drift and the maximum element dissipated hysteretic energy or the total dissipated hysteretic energy has improved compared to the case of mmsbd. The average element damage index, the average element ductility demand, and the average global damage index are approximately doubled, but the average interstory and global drifts have increased by 60%. The total dissipated hysteretic energy in the case of the BSE-2 ground motion is more than five times the total dissipated hysteretic energy in the case of the BSE-1 ground motions. Although the average global damage index implies that the structure will probably reach CP, the performance evaluated based on the member ductility and interstory drift more likely still lies between IO and LS (but closer to LS) and it is unlikely to exceed the limits of CP.

The effect of the member proportioning on the seismic performance is investigated by comparing the response of the SCWB and WCSB frames. Figures 4.16 through 4.19 show the story, element, and global responses for the twelve story frame with weak columns and strong beams on soil profile type S_B when it is subjected to BSE-

1 ground motions (mmwbd). As these figures show, the demand on the beams has substantially decreased as a result of using strong beams, but the columns sustain more damage. The maximum beam damage index ranges from 0.3 to 0.6 with an average of 0.4. The maximum beam ductility is between 0.7 to 1.7 with an average of 1.0 and the beams remain completely elastic during seven earthquakes. The column ductility ranges from 2.5 to 10.8 with an average of 4.9. This is more than twice the ductility demand in the SCWB design (mmsbd). Although the mean story drift increases about 20%, the global drift is slightly smaller than that of the SCWB design. Global damage index also increases from 0.5 to 0.8. The correlation between the story drift and the beam response (damage index and ductility demand) is poor, but a very strong linear relationship exists between the interstory drift and the column ductility demand. The most probable performance of this frame also falls between IO and LS and it is unlikely to reach CP. Compared to the SCWB design, however, the probable performance level is closer to LS than to IO, and therefore more damage is expected. The WCSB design is strongly discouraged by the seismic codes. Nevertheless, it is noted that under BSE-1 ground motions, its performance in terms of damage index, ductility demand, and interstory drift is not much different from the SCWB design.

The response of the WCSB design under BSE-2 ground motions is shown in Figures 4.20 through 4.23. This response is characterized by high column demands in the first, third, sixth, and ninth stories where the size of the frame members has been reduced. This complies with the story shear force-interstory drift curves obtained from the pushover analysis of this frame. The performance of this frame based on the ductility demand and interstory drift is most probably between LS and CP. It is possible for this

structure to exceed the limits of CP and collapse. The average global damage index of 2.0, on the other hand, suggests that the structure will most probably collapse under a BSE-2 earthquake.

Comparing the performance of the WCSB and SCWB designs under BSE-2 ground motions, now a pronounced difference is observed: while the performance of the SCWB design is unlikely to reach CP, the WCSB design is very probable to collapse under a BSE-2 ground motion. We recall that an almost identical performance is expected for these two designs under a BSE-1 ground motion.

The response of the twelve story moment-resisting frames on soil profile type S_E (soft soil) is shown in Figures 4.24 through 4.27 for the SCWB design (mmsed) and in Figures 4.28 through 4.31 for the WCSB design (mmwed). The frames are subjected to a set of nine ground motions recorded on the soil and scaled to BSE-1 level. These ground motions are listed in Table 3.1. The story response of mmsed is different from that of mmsbd (SCWB design on rock) in terms of both magnitude and pattern. The uniformity of the response of mmsbd through the height of the structure is not observed for mmsed. In mmsed the first story shows the most demand. The average member damage index, member ductility demand, dissipated hysteretic energy, and the interstory drift at each story is in general higher for soil profile type S_E, especially at lower stories. The maximum element damage index exceeds 1 for all earthquakes. The element ductility demand is between 3.3 and 9.2 and the column ductility demands can be higher than beam ductility demands in spite of the strong column-weak beam design. The mean interstory drift is 0.020 which is about 50% higher than the interstory drift for soil profile type S_B. A global damage index of 1.1 suggests that the collapse is likely. One important

feature of the response parameters obtained for the soft soil is their small C.O.V that can be attributed to the narrow band of the dominant ground motion frequencies. This means that the performance of the structure may be assessed with more confidence on soft soil than on ground rock. Based on the response values given in Table 4.2, the probable performance of the structure falls between IO and LS, closer to LS, with a negligible likelihood of reaching CP.

The WCSB design (mmwed) exhibits small beam but high column demands. The mean column damage index and ductility demand have risen to 5.3 and 17.9, respectively. The mean interstory drift also has increased from 0.020 to 0.046; however, the global drift has almost remained unchanged. This behavior can be explained by comparing the interstory drift patterns shown in Figures 4.25 and 4.29. In contrast to the SCWB design, in the WCSB design high interstory drifts tend to localize in the few stories where the size of the columns has been reduced. The performance of this frame is expected to be close to CP with the possibility of collapse even under a design-level earthquake.

The correlation between the response parameters for the structures on soft soil is not so strong as that for the structures on ground rock. This seems to be caused by the nonuniform distribution of the seismic demands in the structures on soft soil. Based on the performance evaluation of the frames designed for soil profile type S_E, it is concluded that these frames are expected to sustain extensive damage under a BSE-1 ground motion and even collapse. The failure of these frames under a BSE-2 ground motion is certain, and therefore no analysis is performed for this level of ground motion.

4.3.1.2 Special Concentrically Braced Frames: The NEHRP-recommended acceptance criteria for Immediate Occupancy (IO), Life Safety (LS), and Collapse Prevention (CP) performance levels are given in Table 4.3. The NEHRP *Guidelines* considers the axial compressive force in the columns of a braced frame to be a force-controlled action. A force-controlled action is one that has an associated deformation that is not allowed to exceed the yield value. The column axial compressive force (A.C.F.) ratio, r, is defined as

$$r = \frac{P}{P_n} \tag{4.4}$$

and must be less than 1.0. In the above equation, P is the maximum axial compressive force in the column and P_n is the nominal strength of the column calculated in accordance with the provisions in Part 6 of the AISC Manual of Steel Construction (AISC 1994).

The column or brace ductility in Table 4.3 refers to the extensional ductility, defined as the ratio of the normal strain in the axial direction and the yield strain. The limits recommended for braces in compression depend on the shape of the brace cross section and the buckling plane of the brace. The values given in Table 4.3 are for double angles buckling out of plane.

The statistics of the seismic response parameters of the braced frames on soil profile types S_B and S_E, under BSE-1 and BSE-2 ground motions are listed in Table 4.4.

Figures 4.32 and 4.33 show the story response for the braced frame on soil profile type S_B when it is subjected to the ground motions scaled to BSE-1 level (bbd). The axial compressive force (A.C.F.) ratio and ductility in tension (T) for the columns, the ductility in compression (C) and tension (T) for the braces, the dissipated hysteretic energy (D.H.E.) in the elements, and the interstory drift are shown for each story in these figures.

The solid lines represent the maximum (max), the dashed lines the mean (m), and the dotted lines the mean plus standard deviation (mps) statistics. The A.C.F. ratio of the columns is high in those stories where the size of the columns has been reduced, nevertheless, it exceeds one only in a few stories. Note that due to the small amount of strain hardening the value of the A.C.F. ratio can only slightly exceed one. The average value of 1.1 in Table 4.4 indicates that it is very probable that under any earthquake of BSE-1 level at least one column develops an A.C.F. ratio of one. However, Figure 4.32 shows that the number of the columns which develop a ratio of one is indeed small. The average ductility of the columns in tension ranges from 0.1 to 0.8, but the maximum may be as high as 1.6. The average ductility of the braces in both tension and compression is between 0.4 to 1.6. The average interstory drift ranges from 0.004 to 0.010 and it increases towards the top of the structure. As Figure 4.33 shows, only about half of the stories contribute to the dissipation of the hysteretic energy while the hysteretic energy dissipated by the elements in the rest of the structure is negligible. Unlike the moment-resisting frames, a strong linear relationship between the maximum interstory drift and the maximum element or total dissipated hysteretic energy is observed (Figures 4.34 and 4.35); however, the correlation between the interstory and the global drifts is poor. Based on the foregoing discussion and the statistics of the response in Table 4.4, the performance of this structure is most probably between IO and LS performance levels, closer to IO. It is unlikely that the response exceeds the limits of LS. This classification of performance assumes that the predicted overstress in a few columns is not a dominant criterion.

The story response resulted from the BSE-2 ground motions is shown in Figures 4.36 and 4.37. The average A.C.F. ratio in half of the stories reaches 1.0. The average ductility of the columns in tension is between 0.1 to 1.2. The average ductility of the braces ranges from 0.5 to 3.9 in compression and from 0.6 to 3.4 in tension. The average story drift is between 0.008 and 0.017 and almost uniform in the middle half of the structure. The dissipation of the hysteretic energy mainly takes place in the braces in the lower half of the frame and in the columns of the first, third, sixth, and ninth stories. As Figures 4.38 and 4.39 show, the relationships between the maximum response parameters are not strongly linear. It is noted that the C.O.V. of the element and the total dissipated hysteretic energies in this case is relatively small compared to the previous case and this causes the linear relationship between the maximum interstory drift and the dissipated hysteretic energy to disappear. For this frame, due to the frequent occurrence of average A.C.F. ratios of one or greater, the structural collapse seems probable. Note that in this case the classification of the performance based on the story drift or the member ductility would suggest a more desirable performance, most likely close to LS. The inconsistency of the acceptance limits for the performance levels often necessitates the personal judgement of the designer. In the case of the braced frame subjected to the BSE-1 ground motions it was assumed that the A.C.F. ratio was not dominant. This time, however, it is considered to be the governing parameter.

The dynamic response of the braced frame on soft soil is shown in Figures 4.40 through 4.43 for BSE-1 ground motion level and in Figures 4.44 through 4.47 for BSE-2 ground motion level. The response of the braced frame on soft soil is considerably higher than the response on ground rock. The figures show a concentration of demands in the

ninth story where under the BSE-1 ground motions the average ductility demand for the braces has increased by a factor of 3 and the average ductility demand for the columns and also the average interstory drift each has increased by a factor of 2. The average ductility demands for braces in other stories range from 0.6 to 2.7 and for columns from 0.1 to 1.1. The average A.C.F. ratio for columns remains less than one for most of the stories. Excluding the ninth story, the interstory drifts are between 0.004 to 0.017. Figure 4.42 shows a strong linear relationship between the maximum interstory drift and the maximum element ductility demand. The performance of this structure is controlled by the demands develop in the ninth story and fails to meet the requirements for CP performance level.

According to Figures 4.44 and 4.45 the BSE-2 earthquakes produce large element ductility demand and interstory drift in more than half of the stories. Figures 4.46 and 4.47 show the scatter of and the correlation between the different response parameters. The frame will most probably collapse under an earthquake of BSE-2 level by suffering extensive damage in a large portion.

4.3.2 Two Story (Low-Rise) Frames

The lateral-force-resisting system of the two story building is a special moment-resisting frame. Only one design is considered for this frame, but since two sets of ground motions are used in the analyses and either set of ground motions are scaled to both BSE-1 and BSE-2 levels, a total of four frame models should be discussed. The seismic response parameters used to evaluate the performance of the two story frame models and the acceptance criteria are the same as those previously used for the twelve story moment-

resisting frames. The results of the DNTHA are also presented in the same format. Table 4.5 lists the statistics of the response of the two story frame models.

Figures 4.48 and 4.49 show the story response of the two story frame on soil profile type S_B when it is subjected to the BSE-1 ground motions (lbd). In the first story, the damage index, the ductility demand, and the dissipated hysteretic energy in the columns are greater than those of the beams. The elements of the second story remain elastic at all times. It is seen in Figures 4.50 and 4.51 that the values of the response parameters have a rather small scatter compared to the twelve story frames. This can be attributed to the dominant effect of one mode of vibration on the dynamic response of the two story frame. According to the acceptance criteria of Table 4.1, the performance of this model most probably lies between IO and LS, close to IO. It is unlikely that the limits for LS performance level be exceeded. Increasing the ground motion level to BSE-2, triggers the nonlinear response in the second story and also increases the scatter in the response parameter values (Figures 4.52 through 4.55). The probable performance falls close to LS in the range of IO to LS with a small likelihood of reaching close to CP.

The story response of the frame on soil profile type S_E is shown in Figures 4.56 and 4.57 for BSE-1 ground motions. The beams in the second story remain elastic, but the columns exhibit a mild nonlinear behavior. The average demands imposed on the elements of the first story are higher by a factor of 1.5-2 compared to those obtained for soil profile type S_B under the same ground motion level. As Figures 4.58 and 4.59 show, the scatter in the maximum response is also larger, but a strong linear relationship between the response parameters is observed. The performance of this frame is between IO and LS with a small chance of going beyond LS. The two story frame on soft soil

under the BSE-2 ground motions suffers the most damage among all of the two story frames. The ductility demand and dissipated hysteretic energy in the columns of the first story are quite large and the average interstory drift is 0.042 (Figures 4.60 and 4.61). A rather large scatter in the response parameter values is seen in Figures 4.62 and 4.63. The performance is close to CP with the possibility of the structural failure.

4.4 Simulated versus Actual Accelerograms

It was mentioned in Chapter 3 that generating spectrum-compatible accelerograms by using the method adopted in this study could be regarded as a scaling procedure to scale the "seed" accelerograms. In this section the response of the designed frames under the simulated earthquakes is compared with the response of these frames under the corresponding "seed" earthquakes. For this purpose, the nine rock records of Table 3.1 were used to obtain nine BSE-1 spectrum-compatible accelerograms which then applied to the twelve story moment-resisting frame with strong columns and weak beams, the twelve story braced frame, and the two story frame on soil profile type S_B. The frame models subjected to the artificial earthquakes are identified by a letter *a* added to the beginning of their name.

The story response of the twelve story moment-resisting frame under the simulated ground motions is shown in Figures 4.64 through 4.65. Comparing these figures with Figures 4.8 and 4.9, it is seen that the *mean* element damage index, element ductility, dissipated hysteretic energy, and interstory drift in all stories are virtually identical for both sets of the artificial and the actual ground motions. In addition, the artificial records have produced results with much less dispersion. In other words, to

estimate the mean story response with a given confidence level, a smaller sample of artificial records may be used. Figures 4.66 and 4.67 show the maximum value of each response parameter under all records. Only the global drift exhibits a relatively large scatter with a C.O.V. of 0.21 which is slightly higher than 0.11 calculated for the actual ground motions.

Comparing the average story response obtained for the braced frame under the artificial ground motions (Figures 4.68 through 4.71) and the response under actual ground motions (Figures 4.32 through 4.35), it is once again observed that the artificial records produce an unbiased estimate of the average response with less dispersion.

Figures 4.72 and 4.73 show the story response of the two story moment-resisting frame under the artificial earthquakes. The average element damage index, element ductility, and interstory drift for all stories are statistically the same as those obtained under the actual ground motions. The average dissipated hysteretic energies look different, but considering the large dispersion in the calculated values of this parameter, the difference may not be statistically significant. The scatter of the maximum values of the response parameters seen in Figures 4.74 and 4.75 is slightly higher than that observed for the actual ground motions. There is a possible explanation for this higher dispersion. The response of the two story frame is dominated by the first mode of vibration. All the actual ground motions are scaled to the same exact spectral acceleration at the frequency of the first mode, but the artificial accelerograms have slightly different spectral accelerations at that frequency. Therefore, the actual records produce less dispersion. On the other hand, in the case of the twelve story frames the effect of the higher modes is more significant and since the artificial accelerograms have a close

spectral acceleration at all frequencies, they produce less scatter than the real accelerograms.

The results of the analyses show that the artificial accelerograms may be used to estimate the mean response parameters for a wide range of structures with different frequencies. Besides producing less disperse results in most cases, the scaling is done only once. On the contrary, the scaling of ground motions to the spectral acceleration at the fundamental frequency of the structure should be carried out each time a new frequency is encountered.

4.5 Simplified Procedure to Estimate the Mean Interstory Drift

In this section a simple but efficient method is proposed to estimate the mean interstory drift of low and medium-rise steel frames. The method proves to yield acceptable estimates of the mean interstory drift by using the results of a nonlinear pushover analysis. These mean interstory drifts can then be used to evaluate the performance or to estimate other response parameters via the correlation equations.

Dashed lines in Figures 4.76 and 4.77 show the mean interstory drifts obtained from the dynamic analysis of each frame model under the BSE-1 ground motions. The solid lines represent the interstory drifts computed from a series of pushover analyses. For each frame, the roof displacement in the pushover analysis is equal to the mean roof displacement in the dynamic analyses of that frame. As these figures show, the interstory drifts computed from the pushover analyses are generally in close agreement with those obtained from the dynamic analyses. The only exception occurs at the ninth and the tenth stories of the braced frame on soil profile type S_E, where the difference between the static

and dynamic interstory drifts is not very small. Considering the intrinsic scatter in the results of dynamic nonlinear time history analysis, it is quite legitimate to say that in general the interstory drifts have been well approximated by the static pushover analysis method.

The next step is to estimate the mean roof displacement (which is the target for pushover analysis) without performing a large number of time history analyses. This is done by relating the roof displacement of a multi-story structure to the spectral displacement of a single-degree-of-freedom (SDOF) system having the same frequency:

$$\Delta_r = \frac{CS_a}{\omega^2} \tag{4.5}$$

where Δ_r denotes the roof displacement of the multi-story structure, ω is the circular frequency of the SDOF system (the same as the fundamental circular frequency of the multi-story structure), and S_a denotes the spectral acceleration at a frequency ω as obtained from the design spectrum. C is the first-mode participation factor at the roof level of the multi-story structure, defined as

$$C = \phi_1^r \frac{\boldsymbol{\varphi}_1^T \mathbf{m}\{\mathbf{1}\}}{\boldsymbol{\varphi}_1^T \mathbf{m} \boldsymbol{\varphi}_1} \tag{4.6}$$

In the above equation, ϕ_1^r is the amplitude of the first mode shape at the roof level, $\boldsymbol{\varphi}_1$ is the first mode shape vector, $\mathbf{m}$ is the structural mass matrix, and $\{\mathbf{1}\}$ is a unit column vector. An approximation for the value of C may be obtained by assuming an appropriate shape for the first mode. If it is assumed that the first mode is linear and the masses of all stories are equal, Then C will be 1.4 for a twelve story and 1.2 for a two story frame.

The values of Δ_r obtained from Equation (4.5) are compared with the mean values of the roof displacement computed from the dynamic analyses, Δ_{rd}, in Table 4.6. It is noted that the equation yields good approximations for the roof displacement.

The correlation between the mean roof displacement and the mean interstory drift is not strong. Consequently, the roof displacement cannot directly be used to estimate the interstory drift. However, the roof displacement can be used to estimate the interstory drift in either of the following ways:

1. The point corresponding to the given roof displacement is located on the pushover base shear-global drift curve and the load factor associated with that point is obtained. The same load factor is used to determine the interstory drift from each story shear-interstory drift curve and to select the maximum value.
2. The roof displacement can be used to obtain a quantity from the base shear-global drift curve which has a strong correlation with the interstory drift.

The first approach requires the story shear-interstory drift curves of all stories to be obtained. To use the second approach, we calculate the stiffness reduction K/K_0, where K_0 is the initial stiffness of the pushover curve and K is the secant stiffness equal to the slope of a line drawn from the origin to the point corresponding to the top displacement. The correlation between the stiffness reduction and the interstory drift is shown in Figure 4.78. In this figure the stiffness reduction of each model is plotted against the average maximum interstory drift of that model obtained from the results of the dynamic analyses. The two parameters have a fair linear relationship which can be expressed by the following equation:

$$\delta = (1 - \frac{K}{K_0})/14.8 \qquad (4.7)$$

The term in parentheses was previously defined as a damage index and was denoted by D_k in Section 3.5.5. To determine the limiting values of this parameter for each performance level, Equation (4.7) may be used to translate the interstory drift limits into the corresponding D_k limits. The limiting D_k values for IO, LS, and CP performance levels for moment-resisting frames are 0.1, 0.4, and 0.8, and for braced frames are 0.1, 0.2, and 0.3.

Equation 4.7 has been used to estimate the average maximum interstory drift, δ, for each frame. The results are listed in Table 4.6. The interstory drifts obtained from the dynamic analyses, δ_d, are also listed in the table for comparison. Only in two cases the difference is significant, but even this difference does not affect the classification of the performance based on the interstory drift. The values estimated by the simplified procedure lie in the "mean ± standard deviation" interval of the dynamic analysis results which implies that they are reasonable estimates. This makes the simplified procedure an attractive alternative for the dynamic analysis.

4.6 Summary

The expected performance level of the designed frames is shown in Figure 4.79. The solid symbols represent the most probable performance level and the hollow symbols represent the likely extreme damage state.

As a simple but effective alternative to the DNTHA method, one may use the procedure proposed in this study to determine the performance level of a steel structure. This procedure consists of the following steps:

1. Obtain the base shear-roof displacement curve from a pushover analysis.

2. Using Equation (4.5), estimate the average maximum roof displacement.
3. Calculate the ratio of the secant and initial stiffnesses at the point associated with the estimated roof displacement on the base shear-roof displacement curve.
4. Use Equation (4.7) to find the average maximum interstory drift or calculate the stiffness reduction damage index according to Equation (3.56).
5. Determine the performance level based on the interstory drift or the stiffness reduction damage index.

CHAPTER 5

PARAMETRIC STUDY OF THE SEISMIC RESPONSE

5.1 Introduction

In this chapter a parametric study is carried out to reveal how the seismic response of steel structures is affected by:

1. Vertical component of ground motion
2. Geometric nonlinearity (P-Δ magnification)
3. Participation of nonstructural elements
4. Damping representation

5.2 Vertical Component of Ground Motion

The combined effect of the horizontal and the vertical components of ground motion is believed to be responsible for some structural failures happened in the past (Saadeghvaziri and Foutch 1991). The potential of the vertical component of the ground motion to increase the seismic demands has also been demonstrated by the analytical study of hypothetical frames (Anderson and Bertero 1971). However, the effect of the vertical ground motion on the seismic response of real-life steel frames has not yet been clearly identified.

In this study, the horizontal and the vertical components of the selected ground motions are simultaneously applied to a frame and the seismic demands are compared with the demands resulting from the sole horizontal component. The horizontal and the vertical accelerograms used in any analysis are associated with the same event, and thus

"compatible". The horizontal accelerogram is scaled to the design acceleration spectrum at the fundamental frequency of the structure, because the fundamental mode has the largest effective modal mass in the horizontal direction. The vertical accelerogram is scaled to the 2/3-design spectrum at the frequency of the mode with largest effective modal mass in the vertical direction.

To make the results of the analysis under the combined effect of the horizontal and the vertical accelerations comparable with the results of the analysis under the horizontal acceleration only, the same Rayleigh's damping constants are used in both analyses. These constants were determined assuming a 5% modal damping ratio in the first two modes of vibration. The floor mass at each level is lumped at four equally spaced points along the beams on that level. The interior frames have a small lateral-force resistance but they show as much resistance to the vertical excitation as the perimeter frames do. Thus, the horizontal mass at each level is equal to half of the total mass of the building calculated for that level, but the vertical mass at each floor is equal to half of the mass of the floor portion extending to the first interior frame plus the mass of the tributary exterior wall. The horizontal mass at each floor level is about 4 times the vertical mass.

The mean and the maximum values of the element damage index, the element ductility demand, the element dissipated hysteretic energy, the interstory drift, the global drift, the global damage index, and the total dissipated hysteretic energy for the combined horizontal and vertical excitations (HV) and the horizontal excitation (H) are compared in Tables 5.1 through 5.3. As these tables show, there is no significant change in the maximum and the mean values of the response parameters for any frame model.

Interestingly, in many cases the bi-directional excitation has produced a smaller demand. For example, the mean interstory drift of mmwed has reduced by 13% as a result of the application of the combined horizontal and vertical components of the earthquakes.

To investigate the effect of the vertical ground acceleration in more depth, a detailed study of the response of the middle column in the first story of mmsb is presented. This column has undergone the maximum damage for most ground motions. Figure 5.1a shows the time history of the axial force in this column developed under Northridge earthquake, the ground motion that causes the largest response among all the ground motions. The time history of the bending moment at the base of the column is shown in Figure 5.1b. The axial force P (positive for compression) and the bending moment M (positive counterclockwise) are normalized with respect to P_0 and M_0, respectively. P_0 is the plastic axial force of the column cross section in the absence of bending moment (squash load) and M_0 is the plastic bending moment of the column cross section in the absence of axial force. The solid curves represent the response under the bi-directional and the dashed curves represent the response under the horizontal excitation. Due to the negligible difference in the response, the curves are almost coincident and cannot be easily distinguished.

A simple failure envelope for the column may be expressed as the following equation:

$$\left|\frac{P}{P_0}\right| + \left|\frac{M}{M_0}\right| = 1 \qquad (5.1)$$

The time history of the sum on the left-hand side of Equation (5.1) is shown in Figure 5.1c. As Figure 5.1a shows, the axial force in the column remains close to the axial force resulting from the gravity loads ($P/P_0 = 0.077$). The maximum axial force ratio under the

horizontal component is 0.093 and under the combined horizontal and vertical components is 0.106. The time history of the axial force in the latter case also has a high frequency content. The time history of the bending moment at the base of the column is practically the same in both cases. The maximum bending moment ratio under the horizontal component is 0.985 and under the combined horizontal and axial components is 0.863. Figure 5.1c shows that the time history of the sum on the left-hand side of Equation (5.1) (interaction parameter) is almost the same in both cases. It is clear that for this column, the failure is controlled by the bending moment. The maximum interaction parameter under the horizontal component is 0.947 and under the combined horizontal and vertical components is 1.057. The maximum in the latter case occurs at the time when the bending moment reaches its maximum value, and at this time the axial force in the column is even less than the axial force in the case of the horizontal excitation.

Figure 5.2 shows the response of the middle column in the sixth story of the braced frame on soil profile type S_B under Northridge earthquake. Contrary to the moment–resisting frame, in this case the failure mainly results from the axial force. However, the effect of the vertical ground acceleration on the axial force is negligible.

Based on the foregoing discussion, the effect of the vertical component of ground motion on seismic demands is negligible because the vertical mass is small compared to the horizontal mass and the axial force and the bending moment in the interior columns which are the critical elements under earthquake excitation, are not significantly affected by the vertical component of ground motion.

5.3 Geometric Nonlinearity

Geometric nonlinearity (sometimes called P-Δ effect) is the nonlinearity that results from the changing geometry of the structure as it deflects. In a geometrically nonlinear structure or element the stiffness matrix is a function of the displacements. There are different approaches to account for geometric nonlinearity in structural analysis. *Large strain* formulation assumes that the strains are not infinitesimal and that the rotations may be large. It should be applied when the strains in a material exceed a few percent and the changing geometry due to this deformation can no longer be neglected. *Large deflection* formulation allows for large rotations, but the strains should remain small. *Stress stiffening* is based on the assumption of small strains and rotations; it uses a first order approximation of the rotations to capture some nonlinear rotation effects.

The strains in the components of a steel frame arising during an earthquake are generally small, hence a large deflection analysis procedure is used to study the effect of geometric nonlinearity on the results of the dynamic analysis of steel frames. Large rotation-small strain problems are solved by using a corotational (or convected coordinate) approach. The strain-displacement relationship in this approach has the following form:

$$\mathbf{B}_t = \mathbf{B}_0 \mathbf{T}_t \tag{5.2}$$

where $\mathbf{B}_0$ is the usual small strain-displacement matrix in the original element coordinate system and $\mathbf{T}_t$ is the orthogonal transformation matrix relating the original element coordinates to the convected element coordinates. $\mathbf{T}_t$ is computed by separating the rigid body rotation from the total deformation, $\mathbf{U}_t$. The element tangent stiffness matrix is then

$$\mathbf{K}_e = \iiint_{vol} \mathbf{T}_t^T \mathbf{B}_0^T \mathbf{C} \mathbf{B}_0 \mathbf{T}_t \, dV \tag{5.3}$$

where **C** is the material property matrix. The vector of nodal point forces equivalent to the element stresses is

$$\mathbf{F}_t = \iiint_{vol} \mathbf{T}_t^T \mathbf{B}_0^T \mathbf{C} \mathbf{B}_0 \mathbf{U}_t^d \, dV \tag{5.4}$$

$\mathbf{U}_t^d$ is the element deformation which causes straining and is obtained by decomposing the displacement field.

The solution process can be summarized as a three-step procedure for each element:

1. Determining the updated transformation matrix, $\mathbf{T}_t$, for the element.
2. Extracting the deformational displacement, $\mathbf{U}_t^d$, from the total element displacement, $\mathbf{U}_t$, for computing the stresses as well as the equivalent nodal forces.
3. Updating the node rotations after the rotational increments in $\mathbf{U}_t$ are computed.

All three steps are implemented by using the concept of a rotational pseudovector.

Large deflection formulation includes initial stress effects (stress stiffening) as a subsequence. The effect of stress stiffening is accounted for by generating an additional stiffness matrix, called stress stiffness matrix, which augments the regular nonlinear stiffness matrix.

To observe the effect of the geometric nonlinearity on the dynamic response, the twelve story moment-resisting frame with strong columns and weak beams on soil profile type S_B (mmsb) has been analyzed with and without considering the geometric nonlinearity. The statistics of the response parameters in each case is given in Table 5.4 for both ground motion levels BSE-1 and BSE-2. As the table shows, the consideration of geometric nonlinearity in the analysis procedure has no effect on the response under BSE-1 ground motion level. However, a small increase in the maximum and the mean

values of the response parameters under BSE-2 ground motion is noticed when the geometric nonlinearity is accounted for. For example, the maximum ductility demand of the columns and the maximum interstory drift are respectively underestimated by 10% and 9% as a result of ignoring geometric nonlinearity. Considering the dispersion of the results of the dynamic analyses, this effect is not significant and does not change the expected structural performance level. The P-Δ effect for the braced frames is even less important, because they generally have a smaller interstory drift than the moment-resisting frames. The insignificance of geometric nonlinearity in the response of perimeter lateral-force-resisting systems has been mainly caused by the relatively small gravity loads of their tributary area. It must be assured that the columns in the interior frames are designed with sufficient strength to resist the additional moments resulting from the P-Δ effect. If the interior frames are designed so that they provide no lateral resistance or stability (hinged-base columns), then the exterior frames act to stabilize the deflected interior frames through floor diaphragms. In this case the gravity force used in the calculation of the secondary actions at each story is half of the total weight of that story (assuming that there are two lateral-force-resisting frames in the direction under consideration). This means that if the columns in the interior frames of this study were hinged at the base, the gravity force used in the calculation of the P-Δ actions would be larger by a factor of almost 4. In that case geometric nonlinearity could cause a more pronounced effect.

5.4 Participation of Nonstructural Elements

The nonstructural elements in a building are not usually isolated from the lateral-force-resisting system. The stiffness and strength of the nonstructural elements is not explicitly addressed in the design procedures, but their contribution to the response, especially during the initial excitation, may be important. In this study, the effect of in-plane masonry infills on the seismic response of steel frames is investigated.

Masonry infill panels are found in most frame systems. Although they are basically intended to perform as architectural components, infill panels do resist lateral forces. The additional stiffness and strength provided by the infills may change the magnitude and the distribution of the seismic demands calculated in a bare lateral-force-resisting system. Steel infilled frame buildings showed a good performance during the 1906 San Francisco earthquake and other subsequent earthquakes. This good performance can be explained by the fact that the infill provides a significant bracing mechanism for the frame and the steel frame members have adequate ductility to accommodate the demands imposed on them by the infill. In addition, a significant amount of energy is dissipated by the cracking of the infill and the friction between the infill and the frame. Behavior of infilled frame systems subjected to in-plane lateral forces depends on many factors, such as mechanical properties of both the frame and infill materials, geometry of the infill panel, connection of the infill to the surrounding frame members, and stress or lateral deformation levels. To model the infill panels the equivalent strut concept of the *NEHRP Guidelines* is used. The equivalent strut concept was first introduced by Polyacov (Polyacov 1960). Since then, many others have proposed procedures to determine the properties of the equivalent strut. It has been found

that a strut width equal to one-eighth of the diagonal dimension of the infill panel provides good correlation with experimental results (Angel et al. 1994). The *Guidelines* use the equation proposed by Mainstone (Mainstone 1971) to determine the elastic in-plane stiffness of solid unreinforced masonry infill panels. The elastic in-plane stiffness is represented with an equivalent diagonal compression strut which has the same thickness and modulus of elasticity as the infill panel it represents. Its width, a, is given by:

$$a = 0.175(\lambda_1 h_c)^{-0.4} r_i \tag{5.5}$$

where

$$\lambda_1 = \left(\frac{E_i t_i \sin 2\theta}{4 E_f I_c h_i} \right)^{\frac{1}{4}} \tag{5.6}$$

and

h_c = height of column between centerlines of beams, in.

h_i = height of infill panel, in.

E_f = modulus of elasticity of frame material, psi.

E_i = modulus of elasticity of infill material, psi.

I_c = moment of inertia of column cross section, $in.^4$

r_i = diagonal length of infill panel, in.

t_i = thickness of infill panel, in.

θ = angle the tangent of which is the infill height-to-length aspect ration, radians.

Equation (5.5) has been used to calculate the width of the equivalent strut representing the infill panels in this study where they are treated as being solid. It is assumed that the masonry infill panels are 6 in. thick and made of clay masonry units with a compressive strength of 10 ksi, using type M mortar. The specified compressive

strength of masonry, f'_m, is then 4 ksi (UBC, Table 21-D). The modulus of elasticity for masonry infills, E_i, is estimated in accordance with Section 2106.2.12.1 of the UBC:

$$E_i = 750 f'_m \tag{5.7}$$

which gives a value of 3000 ksi for the modulus of elasticity. Based on the above properties for the masonry infills and the dimensions of the panels in each story, a strut width of 45" is calculated for panels in all stories.

For the purpose of global response analysis, the compression strut may be placed concentrically across the diagonals of the frame, effectively forming a concentrically braced frame system. However, this configuration does not yield the forces imposed on the columns and beams by the infill. To determine these forces, in the analytical model each compression strut is replaced by two eccentric spars as shown in Figure 5.3. The cross sectional area of each spar is half of the cross sectional area of the equivalent strut. They are modelled as compression-only spars using LINK10 element in ANSYS computer program. These elements have a linear force-deformation relationship up to a stress f'_m; their failure after reaching a stress of f'_m, is accounted for by deactivating the overstressed elements using the "element birth and death" option.

Incorporating the nonstructural elements into the frame models increases the fundamental frequency by a factor of more than 2; the fundamental frequency of mmsb changes from 0.45 Hz to 1.24 Hz and that of mmse changes from 0.59 Hz to 1.31 Hz. A new set of ground motion scale factors and Rayleigh's damping constants are calculated based on these frequencies and used in the analysis of the models with nonstructural elements.

The statistics of the response parameters for the twelve story moment-resisting frames with and without nonstructural elements are compared in Table 5.5. The C.O.V. of the response parameters of the models with nonstructural elements is large, and therefore, a considerable difference is observed between the maximum and the mean response parameters. The participation of the nonstructural elements produces a higher demand in the beams and a much higher demand in the columns of the moment-resisting frames. For example, the maximum column ductility demand has increased from 5.0 to 22.6, from 14.3 to 27.3, and from 9.2 to 19.4 for mmsbd, mmsbm, and mmsed, respectively. The maximum beam ductility demand has not significantly changed for mmsbd, but has almost doubled for the other two models. Interestingly, the maximum interstory drift has remained unchanged and the mean interstory drift for mmsbd and mmsed has been reduced. The mean global drift has also significantly decreased for all models. The total beam dissipated hysteretic energy has decreased by an order of magnitude and comparing its value with the elemental dissipated hysteretic energy suggests that the nonlinearities must have been concentrated in a few beam elements.

The unusually high ductility demands in the columns can be explained by the failure pattern of the masonry infill panels. Locating the overstressed panels in the frame models indicates that in almost all the 27 analyzed cases, the failure of the infill panels has been initiated in the first story and progressed upward. In the majority of cases, the failure of the panels does not extend beyond the fourth story. Therefore, while the infill panels in the lower stories fail, the infill panels in the rest of the frame remain intact and add a significant stiffness and strength to the upper stories. As a result of developing a "soft story" band in the lower part of the frame, the nonlinearities are localized into this

region, giving rise to high ductility demands for the elements in these stories. For example, the maximum ductility demand of 22.6 for mmsbd (Table 5.5), belongs to the right interior column in the first story. Investigation of the infill panels in this case shows that all the panels in the first two stories have failed, but the rest of them are intact. When Northridge earthquake is applied to this frame, no panel fails and the maximum column ductility demand will reduce form 5.0 to 0.6 due to participation of nonstructural elements. The failure pattern of the infill panels also explains the reduction in the global drift; the increased stiffness of the upper stories obviously tends to decrease the roof displacement. The maximum interstory drift does not seem to change significantly, but a closer look at the results indicates that the maximum interstory drift increases significantly in the "soft stories" and decreases in the rest of stories. For instance, the maximum interstory drift for the first story of mmsbd without nonstructural elements is 0.017 and for the same frame with nonstructural elements is 0.030 (which is also the global maximum). The global maximum interstory drift for mmsb without nonstructural elements is 0.029 which occurs in the tenth story, but will be reduced to 0.004 as a result of incorporating nonstructural elements. Although the maximum interstory drift of each story has significantly changed, the global maximum has almost remained the same. The failure of the infill panels in the lower stories also localizes the demands in the beams of the "soft" stories with a significant reduction in the demands for the beams in the rest of the structure. The low total beam dissipated hysteretic energy indeed implies that most of the beams behave elastically.

5.5 Damping Representation

This section describes how the representation of damping in a dynamic nonlinear time history analysis can affect the results. Damping of structural vibrations results from miscellaneous sources of energy dissipation in the structure, but is commonly represented by an equivalent viscous-damping matrix, **C**. Most finite element or frame analysis computer programs use Rayleigh's damping defined as

$$\mathbf{C} = a_0\mathbf{M} + a_1\mathbf{K} \tag{5.8}$$

where **M** is the mass matrix, **K** is the initial stiffness matrix and a_0 and a_1 are arbitrary proportionality factors. These factors are determined in terms of two specified modal frequencies ω_m and ω_n to give the desired damping ratios in the corresponding modes m and n. Once defined, **C** will remain constant throughout the analysis that may be unrealistic during the nonlinear response since the frequencies associated with modes m and n will generally be different from ω_m and ω_n as a result of stiffness changes. In other words, **C** will correspond to a new (unknown) modal damping ratio for modes m and n each time the stiffness matrix changes.

5.5.1 Proposed Approach to Model Damping

Consider a simple oscillator of mass m, elastic spring constant k, post-yield spring constant k_p, and viscous-damping coefficient c. The damping ratio,

$$\xi = \frac{c}{2\sqrt{mk}} \tag{5.9}$$

is determined so that the equivalent viscous damping produces the same decay rates as the actual damping mechanism under free-vibration conditions. If c remains constant, an incursion into the post-yield loading of the spring will increase the damping ratio by a

factor of $\sqrt{\frac{k}{k_p}}$. This is obviously a physically invalid picture of the behavior of structural systems. Although the damping characteristics of a structural system may actually change as a result of nonlinear behavior, these changes do not alter ξ by the above factor. While damping ratio of structural systems is usually in the range of 0.02 to 0.08, the factor $\sqrt{\frac{k}{k_p}}$, depending upon the post-yield stiffness, can be very large during the post-yield loading and result in ξ values much higher than the actual ratio. The spurious damping ratio can be avoided by modifying the value of c during yield incursions to control ξ. This, of course, is legitimate because c is only an equivalent viscous-damping parameter. It should be noted that energy dissipation during nonlinear response is caused by both damping and hysteresis and the fact that more energy is dissipated during nonlinear response than during elastic response does not imply that viscous damping has substantially increased. In other words, in a nonlinear analysis hysteretic energy dissipation (also called hysteretic damping) is taken into account by modelling of material nonlinear behavior and viscous damping is only required to represent other sources of energy dissipation during the nonlinear response which are often the same as those during the linear response.

By analogy, in multi-degree-of-freedom systems one may consider modifying the damping matrix **C**, given by Equation (5.8), during nonlinear response to obtain constant modal damping ratios for two specified (dominant) modes m and n each time the stiffness matrix changes. This approach will require calculation of frequencies ω_m and ω_n during

nonlinear response which are needed to determine the proportionality factors a_0 and a_1 in Equation (5.8). ω_m and ω_n must be obtained by solving the general eigenvalue problem

$$\mathbf{K} - \omega^2 \mathbf{M} = \mathbf{0} \tag{5.10}$$

In this study, however, a more practical approach which does not require the calculation of frequencies and ensures a constant viscous damping throughout the entire analysis will be pursued. This approach uses a damping matrix of the form

$$\mathbf{C} = \mathbf{M} \sum_b a_b \left[\mathbf{M}^{-1}\mathbf{K}\right]^b \qquad (-\infty < b < \infty) \tag{5.11}$$

in which as many terms may be included as desired. If ξ denotes the vector of modal damping ratios and **a** denotes the vector of coefficients a_b, it can be shown (Chopra 1995; Clough and Penzien 1975) that

$$\xi = \frac{1}{2}\mathbf{Q}\mathbf{a} \tag{5.12}$$

or,

$$\mathbf{a} = 2\mathbf{Q}^{-1}\xi \tag{5.13}$$

where **Q** is a square matrix involving different powers of the modal frequencies:

$$Q_{ij} = \omega_i^{2b_j - 1} \tag{5.14}$$

This form is indeed an extended Rayleigh's damping matrix which by satisfying the orthogonality condition allows the relationship between the damping matrix, **C**, and the modal damping ratio vector, ξ, to be easily established using Equations (5.11) through (5.14).

To ensure that the modal damping ratios will conform with the prescribed values over a wide range of frequencies, the damping matrix is calculated using nine terms. First, a set of nine frequencies and a set of nine b values are selected. Then, **Q** is

calculated from Equation (5.14). Substituting for **Q** and ξ into Equation (5.13), vector **a** is obtained which is used to calculate the damping matrix, **C**, from Equation (5.11). The damping matrix so obtained must be updated during the nonlinear response based on the tangent stiffness matrix **K**. It should be noted that using the additional terms in Equation (5.11) guarantees that the prescribed modal damping ratios exist in all those modes which are determined from the same stiffness matrix. It does not eliminate the necessity for updating the damping matrix. Unless **C** changes accordingly, any change in **K** will alter the modal damping ratio which corresponds to any given frequency.

In this study the constants a_b were evaluated to give a modal damping ratio of 0.05 corresponding to the 9 arbitrarily chosen frequencies in the range of 0.001 to 100 rad/s. As Figure 5.4 shows, the modal damping ratio for any frequency in the range of 10^{-5} to 10^{6} will also be very close to 0.05.

A computer code has been developed for dynamic nonlinear time history analysis of mass-spring (stick) models of structural systems. The code, written in MATLAB programming language, uses Equation (5.11) to update the damping matrix in the step-by-step solution procedure.

5.5.2 Simple Oscillator

The effect of damping ratio variation during nonlinear response is investigated by subjecting a simple oscillator to a number of earthquake ground motions. Two different models are considered for damping. In the *constant-c* model, the viscous-damping coefficient, c, remains constant during the entire response. This implies that ξ, being 0.05

during the elastic response, increases by a factor of $\sqrt{\frac{k}{k_p}}$ during the post-yield loading of the spring. The ratio $\sqrt{\frac{k}{k_p}}$ is assumed to be 100. In the *varying-c* model, on the other hand, the viscous-damping coefficient, c, is modified during the analysis to give a constant ξ of 0.05 throughout the entire response. Using the two-step scaling procedure described in Section 3.4.1, the first three earthquakes listed in Table 3.1 are anchored to the UBC design response spectrum for seismic zone 4. Maximum relative displacement (d), maximum imparted energy per unit mass (I.E.), and maximum dissipated hysteretic energy per unit mass (D.H.E.), are computed for three ductility demand levels of 3, 6, and 12 at several oscillator frequencies. Ductility is defined as the ratio of the maximum displacement to the yield displacement. Imparted energy is the sum of the kinetic, elastic, and dissipated energies. Oscillator frequency, f, is the elastic frequency, defined as

$$f = \frac{1}{2\pi}\sqrt{\frac{k}{m}} \tag{5.15}$$

Figure 5.5 shows the average nonlinear response spectra of displacement, imparted energy, and dissipated hysteretic energy for the ground motions considered. In this figure, the solid lines show the response of the *constant-c* model and the dashed lines show the response of the *varying-c* model. The results of the two approaches are different; the *constant-c* model (the one commonly used) generally results in a lower response.

Let us define

$$r = \frac{R_v}{R_c} \tag{5.16}$$

where R_c is the average maximum response of the *constant-c* model and R_v is the corresponding average maximum response of the *varying-c* model. The largest difference in the average maximum displacements occurs at $f = 0.1$ Hz for a ductility of 12 with $r = 2.18$. The largest difference in the average maximum imparted and hysteretic energies for frequencies higher than 0.2 Hz, is represented by r values of 1.25 and 1.43, respectively. Energies are negligible when frequency is less than 0.2 Hz. It should be noted that in few instances where the response of the *constant-c* model is larger than that of the *varying-c* model, the ratio is between 0.9 and 1.0. Noting that the accuracy of the results is always limited by the uncertainty in the estimation of the damping ratio, this difference is not significant.

It is then concluded that using the *constant-c* model which produces spuriously large damping ratios during nonlinear response, generally leads to an underestimation of the seismic demands calculated for a simple oscillator.

5.5.3 Multi-Degree-Of-Freedom Systems

To investigate the significance of damping representation in dynamic nonlinear analysis of multi-story buildings, the stick model of a twelve story building is analyzed once with a *constant damping matrix* (Rayleigh's damping) corresponding to 5% modal damping in the first and second modes of vibration and once with a *varying damping matrix* (extended Rayleigh's damping) assuming a constant 5% modal damping over a wide frequency range.

This stick model corresponds to the previously designed moment-resisting frame on soil profile type S_B, mmsbd . The dynamic properties of the stick model are

determined to represent both elastic and nonlinear behavior of the actual frame as accurately as possible. The fundamental period of vibration of the twelve-DOF stick model is 2.2 seconds.

The stick model is subjected to the first three earthquake ground motions used in the analysis of the actual frames. Table 5.6 summarizes the results of the analyses by showing the average maximum interstory drifts obtained using both constant and varying damping matrix assumptions. The table also shows the response ratio defined as d_v / d_c, where d_c is the average maximum interstory drift of the *constant-C* model and d_v is the corresponding average maximum interstory drift of the *varying-C* model. Although the top story itself does not yield under any of the three ground motions, it experiences the largest response ratio. The time histories of top-story drift are shown in Figure 5.6.

The stick model is also analyzed after reducing the yield force of each story to 20% of the yield force in the original design. The average maximum results obtained from analyzing this case are also shown in Table 5.6. The first story shows the largest response ratio. Figure 5.7 shows the time histories of first-story drift under the three earthquakes. Note that as a result of the large reduction in the yield force, the interstory drifts are unrealistic and must be regarded only as an illustration. As inferred from the analysis results, for high levels of nonlinear behavior (displacement ductility demand) implementation of a constant damping matrix may produce some error in the estimation of seismic demands.

Similar to a simple Oscillator, using a constant Rayleigh's damping matrix in dynamic analysis of a multi-degree-of-freedom system generates spurious modal damping ratios during the nonlinear response of the system, but unless the response is

highly nonlinear, the effect of these spurious damping ratios is negligible. An extended Rayleigh's damping matrix which is continuously updated during the nonlinear response can be used to control the modal damping ratios over a wide frequency range so that spurious modal damping ratios will no longer arise. The issue of specifying an accurate damping ratio which represents the true damping characteristics of a structural system at all times, still remains. However, since the modal damping ratios of a structural system vary within a rather narrow range, specifying a constant average modal damping ratio throughout the entire analysis is encouraged.

CHAPTER 6

SUMMARY AND CONCLUSIONS

6.1 Summary

It was the objective of this study to evaluate the expected performance of low and medium-rise steel frames designed in accordance with the requirements of the 1997 Uniform Building Code and also to indicate the effect of vertical ground motion, geometric nonlinearity, participation of nonstructural elements, and damping model on the structural performance. This objective was successfully achieved by dynamic nonlinear time history analysis of several steel frames which were designed to represent different combinations of height, lateral-force-resisting system, soil profile type, and frame-member proportioning.

The frame models were made up of nonlinear beam elements with large-deflection and spread-plasticity capabilities. The element formulation allowed an accurate representation of axial force and bending moment. Actual accelerograms scaled to a design spectrum-related intensity and design spectrum-compatible simulated accelerograms were used to define the ground motion. The expected performance was evaluated based on interstory drift, ductility demand, dissipated hysteretic energy, and Park-Ang damage index. The guidelines provided in FEMA-273 was used to assign a performance level to each structure. Also, a simple procedure for estimating the maximum interstory drift from a proposed damage index was developed.

6.2 Conclusions

Based on the results of the performed dynamic nonlinear time history analyses, the following general conclusions were obtained:

1. Structures built on ground rock (soil profile type S_B) and designed to satisfy all the requirements of the Code, are expected to sustain a light damage after a 10%/50 earthquake (design-level earthquake) with their probable performance close to the Immediate Occupancy level. Even in the worst case, which is unlikely, still some margin against partial or total collapse exists and the performance is close to Life Safety level. In the event of a 2%/50 earthquake (Maximum Considered Earthquake), special moment-resisting frames most likely undergo a moderate to significant damage and their performance is close to Life Safety level, with a slight chance of reaching close to Collapse Prevention level in the worst case. Special concentrically braced frames, however, are most probably on the verge of experiencing partial or total collapse (Collapse Prevention level) and in the worst case fail.
2. Given the same earthquake level, the structures built on soft soil (soil profile type S_E) and satisfying all the requirements of the Code are generally subjected to more damage than those built on ground rock. Under a 10%/50 earthquake a moderate damage is expected to occur to special moment-resisting frames and a substantial damage is expected to occur to special concentrically braced frames. The probable performances are close to Life Safety and Collapse Prevention levels, respectively. In the worst case, the moment-resisting frames are significantly damaged and the braced frames fail. A 2%/50 earthquake most likely brings moment-resisting and braced frames to the state of imminent collapse with a possibility of failure.

3. The use of weak columns and strong beams in the moment-resisting frames will lead to an increased damage. Very likely, the frames on ground rock will resist the 10%/50 earthquakes with moderate damage and the 2%/50 earthquakes with significant damage. There is a chance of partial or total collapse under the 2%/50 earthquakes. Weak column-strong beam design on soft soil will most likely result in a significant damage represented by Collapse Prevention level under the 10%/50 ground motions. The risk of failure during a 2%/50 earthquake is high.
4. In general, special moment-resisting frames exhibit a more desirable performance than special concentrically braced frames and the performance is better on ground rock than on soft soil. This suggests that the earthquake design forces for braced frames and structures on soft soil profile have to be raised to provide an improved performance at least identical to the expected performance of moment-resisting frames on ground rock.
5. The limiting values of different response parameters presently used to determine the performance level (acceptance criteria) are not consistent. The designer has to make a decision as to which criterion is most appropriate for the case under consideration. The lack of reliable acceptance criteria is a major drawback in the current performance-based design practice.
6. The simulated accelerograms generated by the spectral-representation-based algorithm adopted in this study prove to yield unbiased estimates of the mean value of the response parameters for a wide range of structures with different periods of vibration. For medium-rise frames, these accelerograms produce less dispersion in the results of dynamic analysis than the actual "seed" accelerograms scaled to the spectral

acceleration at the fundamental frequency of the structure. For low-rise frames the dispersion is slightly higher when simulated accelerograms are used. In addition, the scaling of ground motions to the spectral acceleration at the fundamental frequency of the structure should be carried out each time a new frequency is encountered, but the generation of spectrum-compatible accelerogram for an actual earthquake is done only once. Therefore, the use of simulated accelerograms seems to be an efficient alternative to the other scaling procedures.

7. The effect of vertical component of ground motion on seismic demands of perimeter lateral-force-resisting systems is negligible. In perimeter frames the vertical inertia forces are small compared to the horizontal inertia forces, because the interior frames, while offering negligible lateral-force resistance, are capable of carrying the forces that result from vertical excitation of the building. Axial force and bending moment in the interior columns of the designed frames, which were the most critical elements under earthquake excitation, were not significantly affected by the vertical component of ground motion.
8. Geometric nonlinearity or P-Δ effect may be neglected in the analysis of perimeter lateral-force-resisting frames in a building with fixed-base interior columns, but it must be assured that the interior columns have sufficient capacity to resist the secondary moments resulting from P-Δ effect. The insensitivity of the results of dynamic analysis to geometric nonlinearity in this case is due to the smallness of the gravity load applied to the frame.
9. Participation of nonstructural elements like masonry infill panels in both elastic and nonlinear response is important. Analysis shows that during a ground motion, in a

frame with infill panels the failure of the panels initiates from the first story and progresses upward. The failure of the infill panels is unlikely to extend beyond the first few stories of the frame. While the infill panels in the lower stories fail, the infill panels in the rest of the frame remain intact and add a significant stiffness and strength to the upper stories. Localization of nonlinearities in the soft story band in the lower part of the frame produces high ductility demands for the elements and also increases the interstory drift in these stories. Elemental demands and interstory drift in the upper stories, on the other hand, will be reduced. Due to this new distribution of stiffness through the height of the frame, it is probable that roof displacement decreases. The magnitude of the maximum interstory drift in a frame with nonstructural elements is not much different from that in a frame without nonstructural elements; only the location of the maximum interstory drift is shifted to a lower story. In general, participation of nonstructural elements can change the performance level by inducing unusually high demands in a few elements of the lateral-force-resisting system.

10. Using a constant Rayleigh's damping matrix in dynamic analysis of a structural system generates spurious modal damping ratios during the nonlinear response of the system, but unless the response is highly nonlinear, the effect of these spurious damping ratios is negligible. An extended Rayleigh's damping matrix which is continuously updated during the nonlinear response can be used to control the modal damping ratios over a wide frequency range so that spurious modal damping ratios will no longer arise. The issue of specifying an accurate damping ratio which represents the true damping characteristics of a structural system at all times, still

remains. However, since the modal damping ratios of a structural system vary within a rather narrow range, specifying a constant average modal damping ratio throughout the entire analysis is encouraged.

11. A simple but efficient method was proposed to estimate the mean interstory drift of low and medium-rise steel frames. The method is based on the observation that if the roof displacement in pushover analysis of a frame is set equal to the mean roof displacement obtained from a series of dynamic analyses performed on the same frame, then the interstory drifts computed from the pushover analysis are in close agreement with the average maximum interstory drifts obtained from the dynamic analyses. First, the roof displacement is estimated using a SDOF analogy which was shown to yield acceptable results. Then the point corresponding to this displacement is located on the base shear-global drift curve. If the story shear-interstory drift curves of all stories are available, the load factor associated with this point can be used to obtain the interstory drift of each story from those curves and to select the maximum value of the interstory drift. Otherwise, the stiffness reduction damage index $D_k = 1-K/K_0$ is calculated at the target point where K is the initial stiffness and K_0 is the secant stiffness at the target point. This damage index has a fair linear relationship with the maximum average interstory drift and can be used to estimate it. Alternatively, D_k may be directly used in the assessment of the performance. The recommended limiting values of this parameter for IO, LS, and CP performance levels for moment-resisting frames are 0.1, 0.4, and 0.8, and for braced frames are 0.1, 0.2, and 0.3.

6.3 Recommendation for Further Study

It is recommended that the present study be continued by developing a probabilistic framework for damage assessment which will allow obtaining the confidence interval for the performance levels. This framework can then be used to determine a design coefficient that modifies the current earthquake-design-force expressions for performance control.

APPENDIX I

TABLES

Table 1.1 Earthquake design levels (SEAOC 1995).

Earthquake design level	Recurrence interval	Probability of being exceeded
Frequent	43 years	50% in 30 years
Occasional	72 years	50% in 50 years
Rare	475 years	10% in 50 years
Very rare	970 years	10% in 100 years

Table 1.2 Maximum interstory drifts associated with structural performance levels (FEMA-273).

Performance level	IO	LS	CP
Steel moment frames	0.7%	2.5%	5%
Braced steel frames	0.5%	1.5%	2%
Concrete frames	1%	2%	4%

Table 2.1 Uniform dead loads.

	Detail	DL (psf)
Roof	2″ reinforced concrete deck	25
	uncoated, corrugated iron	2
	3″ cinder fill	15
	suspended ceiling	10
	5-ply felt and gravel roofing	6
	mechanical and electrical equipment	15
	structural system	15
	total	**88**
Floor	2″ reinforced concrete deck	25
	uncoated, corrugated iron	2
	suspended ceiling	10
	3″ cinder fill	15
	1″ cement finish	12
	mechanical and electrical equipment	15
	structural system	15
	partition	20
	total	**114**
Exterior walls	4″ light concrete plastered on one side	25
	porcelain-enameled steel curtain wall	17.5
	total	**42.5**

Table 2.2 Lateral-force vertical distribution factors for the twelve story building.

Story level	h_x (ft)	w_xh_x	$w_xh_x/\Sigma w_ih_i$
1	18	51336	0.019
2	30	83850	0.031
3	42	117390	0.043
4	54	150930	0.055
5	66	184470	0.068
6	78	218010	0.080
7	90	251550	0.092
8	102	285090	0.105
9	114	318630	0.117
10	126	352170	0.129
11	138	385710	0.142
12	150	325650	0.120
Σ	-	2724786	1.00

Table 2.3 Lateral-force vertical distribution factors for the two story building.

Story level	h_x (ft)	w_xh_x	$w_xh_x/\Sigma w_ih_i$
1	18	51336	0.441
2	30	65130	0.559
Σ	-	116466	1.00

Table 2.4 Lateral force applied at each story level to a twelve story perimeter frame (kips).

Story level	SMRF		SCBF	
	Soil profile type S_B	Soil profile type S_E	Soil profile type S_B	Soil profile type S_E
1	13.6	23.1	22.3	45.4
2	22.2	37.7	36.4	74.2
3	30.7	52.3	50.4	102.9
4	39.3	66.8	64.5	131.6
5	48.6	82.6	79.8	162.7
6	57.1	97.1	93.8	191.4
7	65.7	111.7	107.9	220.0
8	75.0	127.5	123.1	251.2
9	83.6	142.1	137.2	279.8
10	92.2	156.7	151.3	308.6
11	101.5	172.5	166.5	339.6
12	169.3	287.9	219.3	447.5

Table 2.5 Lateral force applied at each story level to a two story perimeter frame (kips).

Story level	Soil profile type S_B	Soil profile type S_E
1	143.8	129.4
2	182.2	164.0

Table 2.6 Sections selected for SCWB-B design.

	Story	Section	A (in.^{2})	I (in.^{4})	d (in.)	Z (in.^{3})
Columns	1-2	W14x500 +2PL24x2	243.0	19407	23.60	2087
	3-5	W14x730	215.0	14300	22.42	1660
	6-8	W14x665	196.0	12400	21.64	1480
	9-12	W14x455	134.0	7190	19.02	936
Beams	1-2	W24x408	119.0	15100	28.54	1250
	3-5	W24x370	108.0	13400	27.99	1120
	6-8	W24x306	89.8	10700	27.13	922
	9-12	W24x207	60.7	6820	25.71	606

Table 2.7 Sections selected for WCSB-B design.

	Story	Section	A (in.^{2})	I (in.^{4})	d (in.)	Z (in.^{3})
Columns	1-2	W14x730	215.0	14300	22.42	1660
	3-5	W14x398	117.0	6000	18.29	801
	6-8	W14x342	101.0	4900	17.54	672
	9-12	W14x233	68.5	3010	16.04	436
Beams	1-2	W24x370 +2PL16x2	172.0	27790	32.00	2080
	3-5	W24x370 +2PL16x2	172.0	27790	32.00	2080
	6-8	W24x335 +2PL16x2	162.4	25843	31.52	1965
	9-12	W24x492	144.0	19100	29.65	1550

Table 2.8 Sections selected for SCWB-E design.

	Story	Section	A (in.^{2})	I (in.^{4})	d (in.)	Z (in.^{3})
Columns	1-2	W14x730 +2PL24x2	311.0	28612	26.42	2832
	3-5	W14x730 +2PL24x2	311.0	28612	26.42	2832
	6-8	W14x665 +2PL24x2	292.0	25812	25.64	2615
	9-12	W14x730	215.0	14300	22.42	1660
Beams	1-2	W24x335 +2PL16x2	162.4	25843	31.52	1965
	3-5	W24x335 +2PL16x2	162.4	25843	31.52	1965
	6-8	W24x450	132.0	17100	29.09	1410
	9-12	W24x335	98.4	11900	27.52	1020

Table 2.9 Sections selected for WCSB-E design.

	Story	Section	A (in.^{2})	I (in.^{4})	d (in.)	Z (in.^{3})
Columns	1-2	W14x665 +2PL24x2	292.0	25812	25.64	2615
	3-5	W14x605	178.0	10800	20.92	1320
	6-8	W14x500	147.0	8210	19.60	1050
	9-12	W14x342	101.0	4900	17.54	672
Beams	1-2	W36x588	172.0	43500	39.84	2550
	3-5	W36x588	172.0	43500	39.84	2550
	6-8	W36x588	172.0	43500	39.84	2550
	9-12	W36x588	172.0	43500	39.84	2550

Table 2.10 Sections selected for SCBF-B design.

	Story	Section	A (in.^{2})
Columns	1-2	W14x605	178.0
	3-5	W14x398	117.0
	6-8	W14x233	68.5
	9-12	W14x109	32.0
Braces	1-2	2L8x8x3/4	22.9
	3-5	2L8x8x5/8	19.2
	6-8	2L8x8x5/8	19.2
	9-12	2L8x8x1/2	15.5
Beams	1-12	W24x76	22.4

Table 2.11 Sections selected for SCBF-E design.

	Story	Section	A (in.^{2})
Columns	1-2	W14x730 +2PL24x2	311.0
	3-5	W14x730	215.0
	6-8	W14x426	125.0
	9-12	W14x176	51.8
Braces	1-2	4L8x8x3/4	45.8
	3-5	2L8x8x9/8	33.5
	6-8	2L8x8x1	30.0
	9-12	2L8x8x3/4	22.9
Beams	1-12	W24x76	22.4

Table 2.12 Sections selected for the two story SMRF design.

	Section	A (in.^{2})	I (in.^{4})	d (in.)	Z (in.^{3})
Columns	W14x370	109.0	5440	17.92	736
Beams	W24x162	47.7	5170	25.00	468

Table 3.1 Selected ground motion records.

Ground	Earthquake name	Station component	Station name
Rock	Imperial Valley	S00E	El Centro
	Kern County	S69E	Taft
	San Fernando	S16E	Pacoima Dam
	Michoacan, Mexico City	N00E	Caleta De Campo
	Nahanni Aftershock	360	Battlement Creek
	Loma Prieta	360	Calaveras Array
	Loma Prieta	137	Apeel Array 9
	Northridge	270	LA, Griffith Observatory
	San Fernando	S69E	Lake Hughes, Array 4
Soil	Loma Prieta	255	Hollister Airport
	Loma Prieta	243	Anderson Dam
	Kern County	S00W	Hollywood Storage
	San Fernando	N90E	Hollywood Storage
	San Fernando	S00W	Hollywood Storage
	Northridge	210	Littlerock
	Northridge	90	Norwalk
	Imperial Valley	140	El Centro Array 4
	Imperial Valley	140	El Centro Array 5

Table 4.1 Acceptance criteria for moment-resisting frames.

Performance level	IO	LS	CP
Component ductility (FEMA-273)	3	12	16
Interstory drift (FEMA-273)	0.007	0.025	0.050
Modified Park-Ang damage index	0.4	0.8	1.0

Table 4.2 Statistics of the response of the twelve story moment-resisting frames.

Frame model		mmsbd	mmsbm	mmwbd	mmwbm	mmsed	mmwed
Beam D.I.	Maximum	2.0	3.6	0.6	1.2	2.4	1.8
	Mean	0.8	1.4	0.4	0.5	1.5	0.9
	C.O.V.	0.58	0.60	0.20	0.41	0.29	0.46
Column D.I.	Maximum	1.6	4.9	3.1	6.1	3.2	8.0
	Mean	0.7	1.5	1.5	3.6	1.8	5.3
	C.O.V.	0.53	0.83	0.59	0.34	0.33	0.29
Beam ductility	Maximum	5.8	10.7	1.7	3.5	7.2	6.5
	Mean	2.5	4.7	1.0	1.6	4.8	2.9
	C.O.V.	0.58	0.52	0.28	0.49	0.25	0.55
Column ductility	Maximum	5.0	14.3	10.8	17.8	9.2	23.9
	Mean	2.2	4.9	4.9	12.6	5.9	17.9
	C.O.V.	0.59	0.73	0.56	0.28	0.30	0.23
Normalized unit beam D.H.E.	Maximum	24.0	47.4	0.73	8.7	28.7	6.8
	Mean	3.3	9.9	0.1	1.1	11.3	2.2
	C.O.V.	2.25	1.41	2.76	2.43	0.82	1.05
Normalized unit column D.H.E.	Maximum	14.2	64.0	52.0	90.1	35.8	137.8
	Mean	2.0	10.6	9.9	32.9	13.2	53.1
	C.O.V.	2.22	1.80	1.56	0.71	0.73	0.78

Table 4.2 Statistics of the response of the twelve story moment-resisting frames (continued).

Frame model		mmsbd	mmsbm	mmwbd	mmwbm	mmsed	mmwed
Interstory drift	Maximum	0.029	0.047	0.032	0.055	0.027	0.063
	Mean	0.013	0.021	0.016	0.037	0.020	0.046
	C.O.V.	0.54	0.48	0.49	0.28	0.21	0.22
Global drift	Maximum	0.008	0.015	0.008	0.012	0.014	0.018
	Mean	0.007	0.011	0.006	0.010	0.011	0.012
	C.O.V.	0.11	0.13	0.12	0.13	0.16	0.24
Global D.I.	Maximum	1.2	2.7	2.0	4.1	1.9	4.0
	Mean	0.5	1.0	0.8	2.0	1.1	2.6
	C.O.V.	0.50	0.62	0.63	0.42	0.29	0.33
Normalized unit total beam D.H.E.	Maximum	3.1	10.1	0.0	0.2	4.3	0.2
	Mean	0.4	2.1	0.0	0.0	1.8	0.1
	C.O.V.	2.32	1.41	2.79	2.46	0.76	1.12
Normalized unit total column D.H.E.	Maximum	0.9	4.8	6.3	20.6	1.7	10.9
	Mean	0.1	0.7	1.0	4.7	0.6	4.9
	C.O.V.	2.45	1.95	1.88	1.24	0.75	0.71

Table 4.3 Acceptance criteria for braced frames (FEMA-273).

Performance level		IO	LS	CP
Interstory drift		0.005	0.015	0.020
Brace ductility	Tension	1	6	8
	Compression	0.8	5	7
Column ductility	Tension	1	3	5
	Compression	force-controlled		

Table 4.4 Statistics of the response of the twelve story braced frames.

Frame model		bbd	bbm	bed	bem
Brace ductility (tension)	Maximum	3.0	6.2	9.7	16.7
	Mean	1.6	3.9	4.9	10.3
	C.O.V.	0.47	0.36	0.41	0.28
Brace ductility (compression)	Maximum	4.8	6.3	11.3	16.9
	Mean	1.8	4.1	5.7	11.6
	C.O.V.	0.65	0.33	0.38	0.23
Column ductility (tension)	Maximum	1.6	2.6	3.3	4.3
	Mean	0.9	1.3	1.7	2.8
	C.O.V.	0.38	0.46	0.40	0.28
Column A.C.F. ratio	Maximum	1.2	1.2	1.1	1.2
	Mean	1.1	1.1	1.1	1.2
	C.O.V.	0.05	0.04	0.03	0.04
Normalized unit brace D.H.E.	Maximum	14.5	69.9	50.4	136.9
	Mean	2.6	24.3	26.7	88.6
	C.O.V.	1.73	0.69	0.48	0.43
Normalized unit column D.H.E.	Maximum	50.8	107.5	34.5	105.9
	Mean	9.3	29.6	20.3	63.0
	C.O.V.	1.69	0.99	0.51	0.51
Interstory drift	Maximum	0.020	0.023	0.045	0.065
	Mean	0.011	0.018	0.024	0.045
	C.O.V.	0.32	0.26	0.34	0.21
Global drift	Maximum	0.007	0.014	0.011	0.037
	Mean	0.006	0.010	0.009	0.021
	C.O.V.	0.07	0.18	0.12	0.37
Normalized unit total brace D.H.E.	Maximum	5.0	25.6	8.1	63.3
	Mean	0.8	7.9	5.7	34.5
	C.O.V.	2.03	0.83	0.36	0.44
Normalized unit total column D.H.E.	Maximum	1.3	3.5	0.8	3.6
	Mean	0.2	1.5	0.4	2.4
	C.O.V.	1.66	0.52	0.48	0.43

Table 4.5 Statistics of the response of the two story frame models.

Frame model		lbd	lbm	led	lem
Beam D.I.	Maximum	0.6	1.3	1.0	2.3
	Mean	0.6	1.1	0.8	1.5
	C.O.V.	0.05	0.14	0.14	0.24
Column D.I.	Maximum	0.8	3.5	2.0	7.2
	Mean	0.7	1.8	1.3	3.3
	C.O.V.	0.08	0.37	0.25	0.46
Beam ductility	Maximum	1.9	4.5	3.5	7.2
	Mean	1.8	3.5	2.9	4.8
	C.O.V.	0.07	0.17	0.16	0.24
Column ductility	Maximum	2.4	11.9	6.8	23.8
	Mean	2.1	5.7	4.2	10.6
	C.O.V.	0.1	0.41	0.27	0.49
Normalized unit beam D.H.E.	Maximum	0.5	10.1	5.1	27.8
	Mean	0.3	5.7	2.3	12.3
	C.O.V.	0.22	0.38	0.51	0.53
Normalized unit column D.H.E.	Maximum	1.8	31.1	14.9	76.6
	Mean	1.1	15.3	6.6	32.6
	C.O.V.	0.32	0.47	0.51	0.54
Interstory drift	Maximum	0.012	0.047	0.028	0.094
	Mean	0.010	0.024	0.018	0.043
	C.O.V.	0.07	0.37	0.24	0.47
Global drift	Maximum	0.010	0.033	0.020	0.066
	Mean	0.009	0.018	0.014	0.031
	C.O.V.	0.06	0.31	0.20	0.44
Global D.I.	Maximum	0.6	2.7	1.6	5.5
	Mean	0.5	1.4	1.0	2.5
	C.O.V.	0.07	0.36	0.24	0.44
Normalized unit total beam D.H.E.	Maximum	0.1	2.1	0.9	6.6
	Mean	0.0	1.0	0.4	2.6
	C.O.V.	0.24	0.45	0.60	0.61
Normalized unit total column D.H.E.	Maximum	0.3	8.3	3.2	21.5
	Mean	0.2	3.3	1.3	8.1
	C.O.V.	0.34	0.61	0.58	0.65

Table 4.6 Estimation of the mean roof displacement and the mean interstory drift.

Frame model	ω (rad/s)	S_a (in./s^2)	Δ_r (in.)	Δ_{rd} (in.)	D_k	δ	δ_d
mmsbd	2.82	69.4	12.2	12.5	0.03	0.005	0.013
mmsbm	2.82	138.8	24.4	20.3	0.25	0.020	0.021
mmsed	3.73	220.2	22.2	19.8	0.29	0.022	0.020
mmwbd	2.91	71.6	11.8	11.4	0.10	0.010	0.016
mmwbm	2.91	143.2	23.7	18.7	0.37	0.028	0.037
mmwed	3.79	223.5	21.8	22.2	0.51	0.037	0.046
bbd	3.41	83.9	10.1	11.1	0.01	0.003	0.011
bbm	3.41	167.8	20.2	18.3	0.33	0.025	0.018
bed	4.52	266.8	18.3	16.5	0.28	0.022	0.024
bem	4.52	533.6	36.6	38.5	0.67	0.048	0.045
lbd	8.86	217.9	3.3	3.2	0.14	0.012	0.010
lbm	8.86	435.8	6.7	6.6	0.49	0.036	0.024
led	8.86	347.6	5.3	5.1	0.37	0.028	0.018
lem	8.86	695.2	10.6	11.3	0.70	0.050	0.043

Table 5.1 Comparison of the responses of the twelve story moment-resisting frames to horizontal (H) and combined horizontal and vertical (HV) ground accelerations.

Frame model		mmsbd		mmsed		mmwbd		mmwed	
Excitation		H	HV	H	HV	H	HV	H	HV
Beam D.I.	Maximum	2.0	2.0	2.4	2.2	0.6	0.6	1.8	1.8
	Mean	0.8	0.9	1.5	1.4	0.4	0.4	0.9	0.9
Column D.I.	Maximum	1.6	1.5	3.2	2.9	3.1	2.9	8.0	6.4
	Mean	0.7	0.7	1.8	1.7	1.5	1.5	5.3	4.6
Beam ductility	Maximum	5.8	5.8	7.2	6.4	1.7	1.9	6.5	6.6
	Mean	2.5	2.8	4.8	4.6	1.0	1.1	2.9	2.9
Column ductility	Maximum	5.0	4.7	9.2	8.2	10.8	9.9	23.9	21.5
	Mean	2.2	2.3	5.9	5.6	4.9	4.9	17.9	15.5
Normalized unit beam D.H.E.	Maximum	24.0	24.1	28.7	28.6	0.7	1.1	6.8	6.8
	Mean	3.3	4.7	11.3	10.9	0.1	0.2	2.2	2.2
Normalized unit column D.H.E.	Maximum	14.2	12.8	35.8	33.6	52.0	48.6	137.8	113.1
	Mean	2.0	2.5	13.2	12.7	9.9	11.6	53.1	45.6
Interstory drift	Maximum	0.029	0.028	0.027	0.025	0.032	0.030	0.063	0.056
	Mean	0.013	0.014	0.020	0.019	0.016	0.016	0.046	0.040
Global drift	Maximum	0.008	0.008	0.014	0.014	0.008	0.008	0.018	0.017
	Mean	0.007	0.007	0.011	0.011	0.006	0.006	0.012	0.012
Global D.I.	Maximum	1.2	1.2	1.9	1.7	2.0	1.9	4.0	3.4
	Mean	0.5	0.6	1.1	1.1	0.8	0.8	2.6	2.3
Normalized unit total beam D.H.E.	Maximum	3.1	3.0	4.3	4.3	0.0	0.0	0.2	0.2
	Mean	0.4	0.6	1.8	1.7	0.0	0.0	0.1	0.1
Normalized unit total column D.H.E.	Maximum	0.9	0.8	1.7	1.6	6.3	6.0	10.9	10.1
	Mean	0.1	0.2	0.6	0.6	1.0	1.3	4.9	4.6

Table 5.2 Comparison of the responses of the twelve story braced frames to horizontal (H) and combined horizontal and vertical (HV) ground accelerations.

Frame model		bbd		bed	
Excitation		H	HV	H	HV
Brace ductility (tension)	Maximum	3.0	2.9	9.7	9.2
	Mean	1.6	1.8	4.9	4.6
Brace ductility (compression)	Maximum	4.8	5.0	11.3	10.7
	Mean	1.8	2.1	5.7	5.5
Column ductility (tension)	Maximum	1.6	0.9	3.3	3.3
	Mean	0.9	0.7	1.7	1.7
Column A.C.F. ratio	Maximum	1.2	1.2	1.1	1.1
	Mean	1.1	1.1	1.1	1.1
Normalized unit brace D.H.E.	Maximum	14.5	15.0	50.4	51.0
	Mean	2.6	3.5	26.7	27.5
Normalized unit column D.H.E.	Maximum	50.8	55.9	34.5	37.0
	Mean	9.3	15.7	20.3	20.1
Interstory drift	Maximum	0.020	0.019	0.045	0.043
	Mean	0.011	0.012	0.024	0.023
Global drift	Maximum	0.007	0.007	0.011	0.011
	Mean	0.006	0.006	0.009	0.009
Normalized unit total brace D.H.E.	Maximum	5.0	5.0	8.1	8.4
	Mean	0.8	1.1	5.7	5.9
Normalized unit total column D.H.E.	Maximum	1.3	1.5	0.8	0.7
	Mean	0.2	0.4	0.4	0.4

Table 5.3 Comparison of the responses of the two story frames to horizontal (H) and combined horizontal and vertical (HV) ground accelerations.

Frame model		lbd		led	
Excitation		H	HV	H	HV
Beam D.I.	Maximum	0.6	0.6	1.0	1.1
	Mean	0.6	0.6	0.8	0.8
Column D.I.	Maximum	0.8	0.7	2.0	1.9
	Mean	0.7	0.7	1.3	1.2
Beam ductility	Maximum	1.9	1.9	3.5	3.5
	Mean	1.8	1.8	2.9	2.8
Column ductility	Maximum	2.4	2.3	6.8	6.4
	Mean	2.1	2.1	4.2	4.1
Normalized unit beam D.H.E.	Maximum	0.5	0.5	5.1	5.2
	Mean	0.3	0.3	2.3	2.2
Normalized unit column D.H.E.	Maximum	1.8	1.5	14.9	14.0
	Mean	1.1	1.0	6.6	6.4
Interstory drift	Maximum	0.012	0.011	0.028	0.026
	Mean	0.010	0.010	0.018	0.018
Global drift	Maximum	0.010	0.009	0.020	0.020
	Mean	0.009	0.009	0.014	0.014
Global D.I.	Maximum	0.6	0.6	1.6	1.5
	Mean	0.5	0.5	1.0	1.0
Normalized unit total beam D.H.E.	Maximum	0.1	0.1	0.9	0.9
	Mean	0.0	0.0	0.4	0.4
Normalized unit total column D.H.E.	Maximum	0.3	0.3	3.2	3.0
	Mean	0.2	0.2	1.3	1.3

Table 5.4 Effect of geometric nonlinearity on the calculated response parameters.

Frame model		mmsbd		mmsbm	
Geometric Nonlinearity		Yes	No	Yes	No
Beam D.I.	Maximum	2.0	2.0	3.6	3.4
	Mean	0.8	0.8	1.4	1.4
Column D.I.	Maximum	1.6	1.6	4.9	4.5
	Mean	0.7	0.7	1.5	1.4
Beam ductility	Maximum	5.8	5.8	10.7	9.9
	Mean	2.5	2.5	4.7	4.5
Column ductility	Maximum	5.0	5.0	14.3	12.9
	Mean	2.2	2.2	4.9	4.7
Normalized unit beam D.H.E.	Maximum	24.0	24.5	47.4	44.4
	Mean	3.3	3.3	9.9	9.5
Normalized unit column D.H.E.	Maximum	14.2	13.9	64.0	59.2
	Mean	2.0	1.9	10.6	9.9
Interstory drift	Maximum	0.029	0.029	0.047	0.043
	Mean	0.013	0.013	0.021	0.021
Global drift	Maximum	0.008	0.008	0.015	0.014
	Mean	0.007	0.007	0.011	0.011
Global D.I.	Maximum	1.2	1.2	2.7	2.5
	Mean	0.5	0.5	1.0	1.0
Normalized unit total beam D.H.E.	Maximum	3.1	3.1	10.1	10.5
	Mean	0.4	0.4	2.1	2.1
Normalized unit total column D.H.E.	Maximum	0.9	0.9	4.8	4.3
	Mean	0.1	0.1	0.7	0.7

Table 5.5 Effect of nonstructural elements on the response of the twelve story moment-resisting frames.

Frame model		mmsbd		mmsbm		mmsed	
Nonstructural elements		Yes	No	Yes	No	Yes	No
Beam D.I.	Maximum	1.8	2.0	7.4	3.6	3.8	2.4
	Mean	0.8	0.8	2.8	1.4	1.6	1.5
Column D.I.	Maximum	6.3	1.6	9.8	4.9	6.4	3.2
	Mean	1.8	0.7	4.0	1.5	2.5	1.8
Beam ductility	Maximum	6.1	5.8	22.4	10.7	12.4	7.2
	Mean	2.7	2.5	9.1	4.7	5.4	4.8
Column ductility	Maximum	22.6	5.0	27.3	14.3	19.4	9.2
	Mean	6.0	2.2	12.6	4.9	8.7	5.9
Normalized unit beam D.H.E.	Maximum	5.7	24.0	38.3	47.4	16.0	28.7
	Mean	1.4	3.3	9.7	9.9	3.3	11.3
Normalized unit column D.H.E.	Maximum	19.2	14.2	54.5	64.0	27.3	35.8
	Mean	5.4	2.0	15.6	10.6	6.9	13.2
Interstory drift	Maximum	0.030	0.029	0.046	0.047	0.025	0.027
	Mean	0.011	0.013	0.022	0.021	0.014	0.020
Global drift	Maximum	0.006	0.008	0.015	0.015	0.007	0.014
	Mean	0.003	0.007	0.007	0.011	0.005	0.011
Global D.I.	Maximum	3.7	1.2	6.1	2.7	3.7	1.9
	Mean	1.0	0.5	2.3	1.0	1.3	1.1
Normalized unit total beam D.H.E.	Maximum	0.2	3.1	5.5	10.1	1.1	4.3
	Mean	0.1	0.4	1.1	2.1	0.2	1.8
Normalized unit total column D.H.E.	Maximum	1.2	0.9	3.4	4.8	1.4	1.7
	Mean	0.3	0.1	1.0	0.7	0.3	0.6

Table 5.6 Average maximum interstory drifts of the 12-DOF stick models.

Story	Original model			Model with reduced yield force		
	d_c (in.)	d_v (in.)	r	d_c (in.)	d_v (in.)	r
1	1.054	1.048	0.99	3.011	3.815	1.27
2	1.275	1.277	1.00	0.490	0.437	0.89
3	1.275	1.289	1.01	0.736	0.489	0.66
4	1.265	1.271	1.01	0.537	0.519	0.97
5	1.175	1.199	1.02	0.517	0.515	1.00
6	1.246	1.273	1.02	0.986	1.041	1.06
7	1.368	1.391	1.02	0.589	0.572	0.97
8	1.365	1.353	0.99	0.518	0.527	1.02
9	1.505	1.485	0.99	3.784	3.774	1.00
10	1.561	1.599	1.02	1.461	1.194	0.82
11	1.286	1.327	1.03	0.691	0.791	1.15
12	0.686	0.752	1.10	0.362	0.431	1.19

APPENDIX II

FIGURES

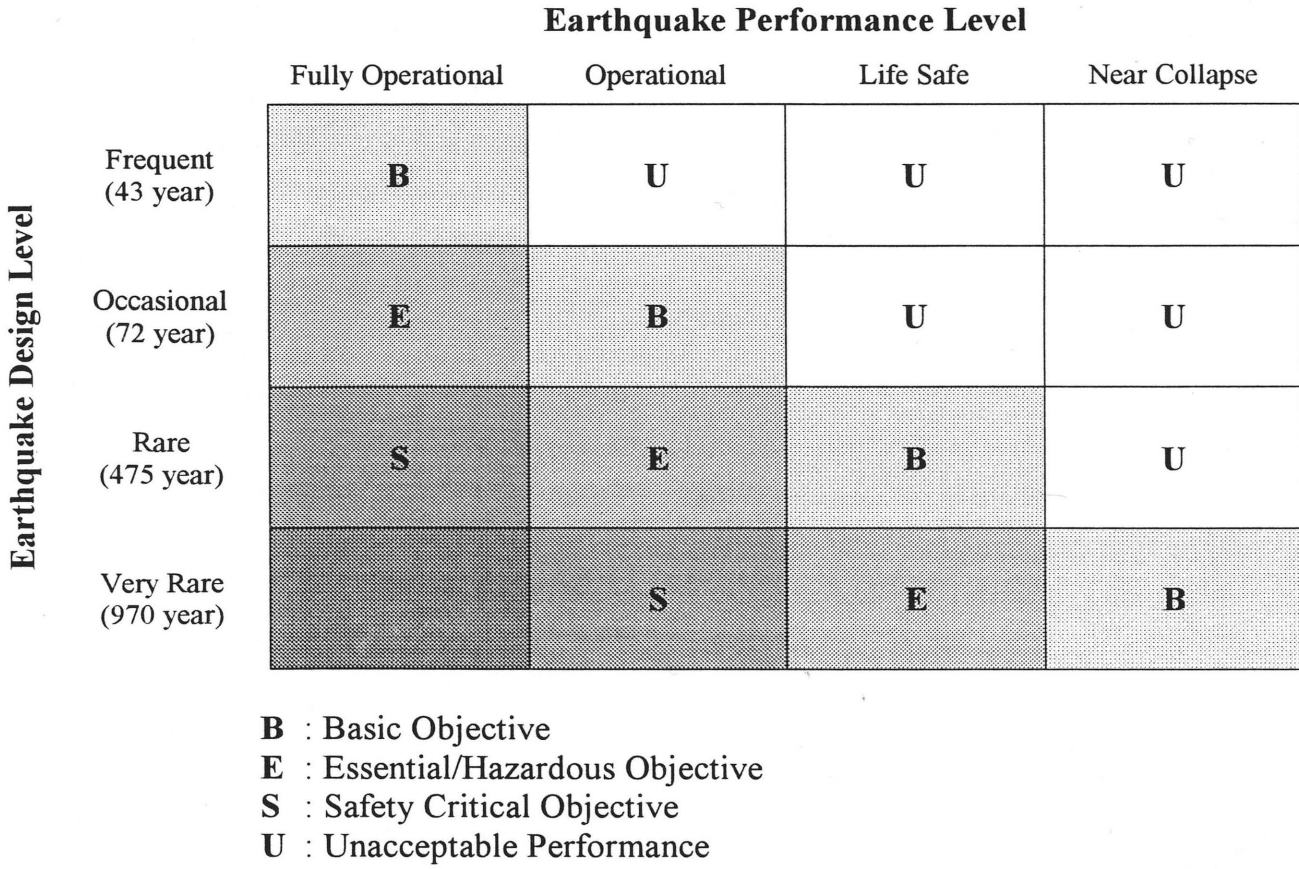

Figure 1.1 Recommended performance objectives for buildings (SEAOC 1995).

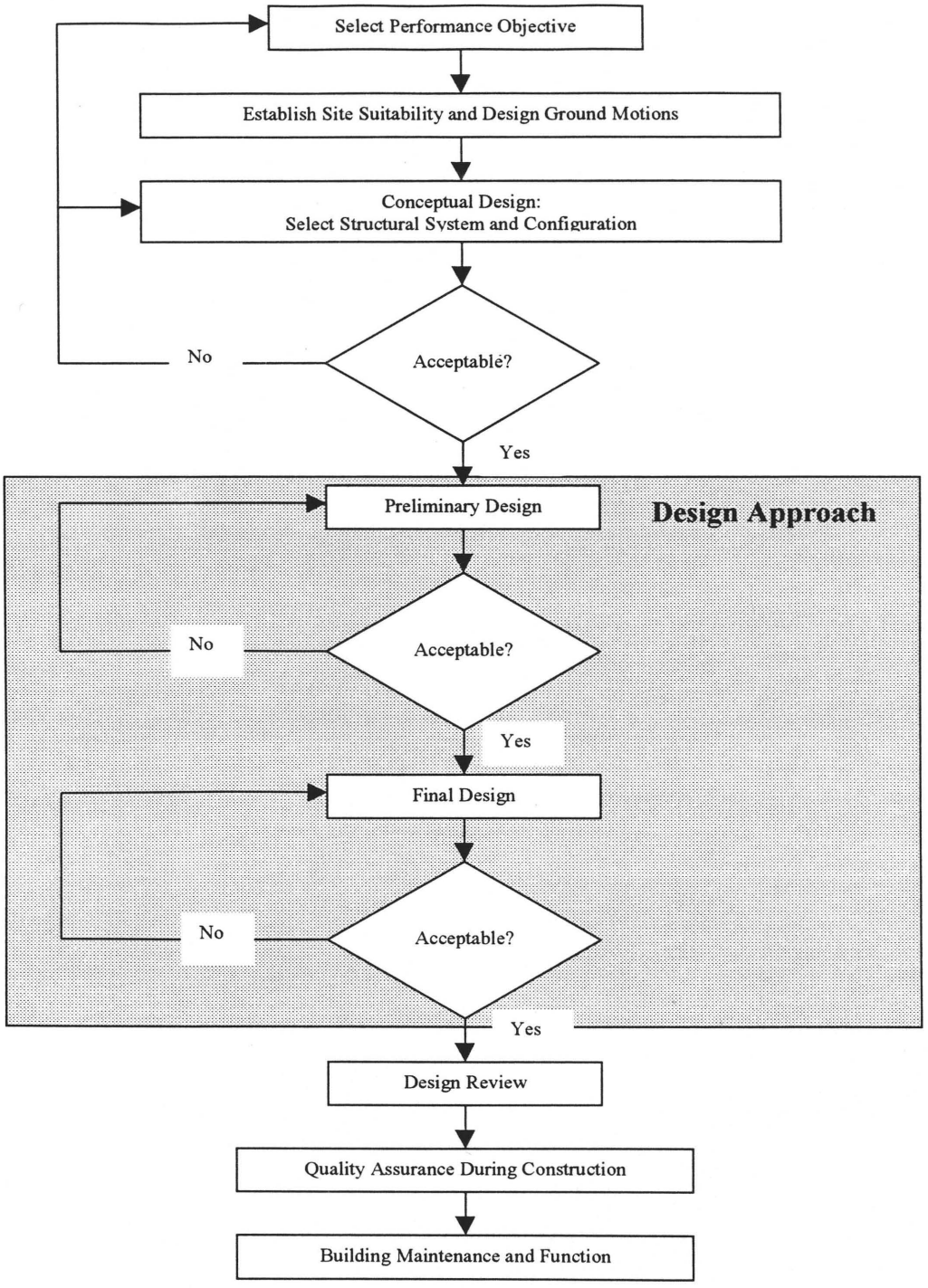

Figure 1.2 Methodology of performance-based engineering (SEAOC 1995).

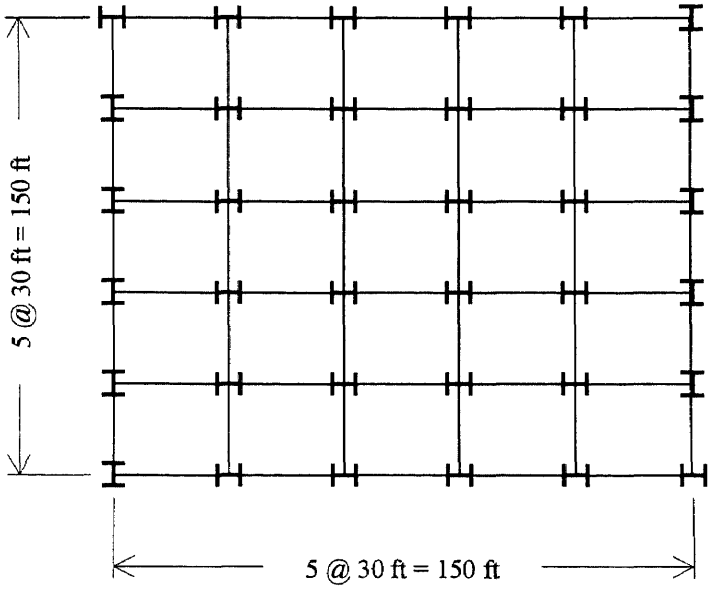

Figure 2.1 Plan view of the structural layout of the designed buildings.

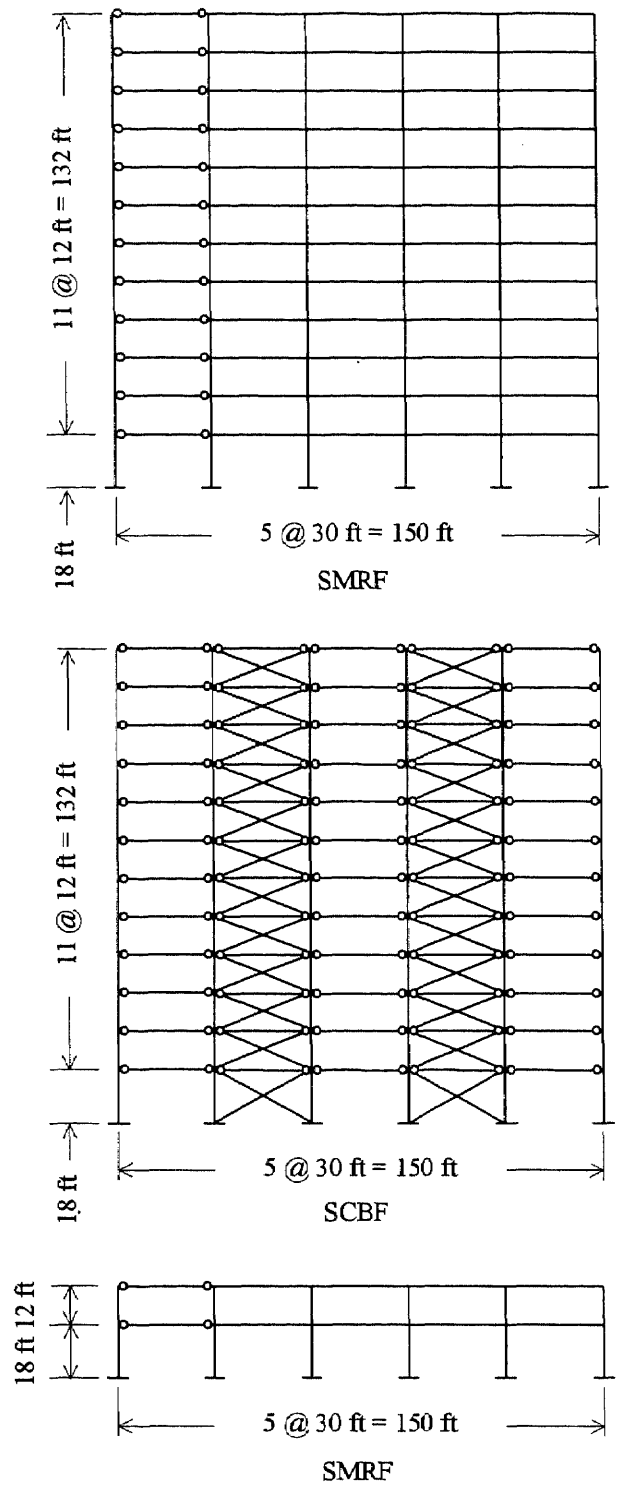

Figure 2.2 Configuration layout of the perimeter lateral-force-resisting frames.

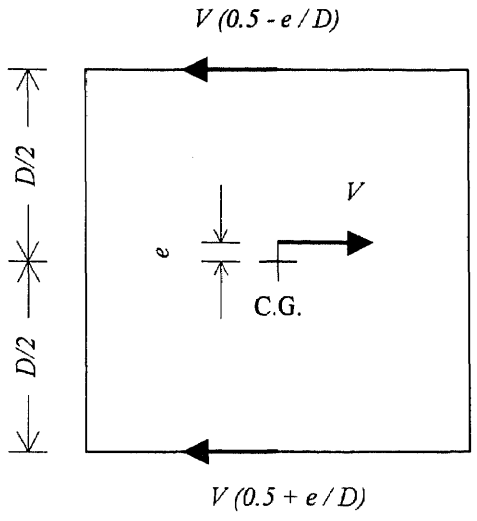

Figure 2.3 Distribution of the base shear between the perimeter frames.

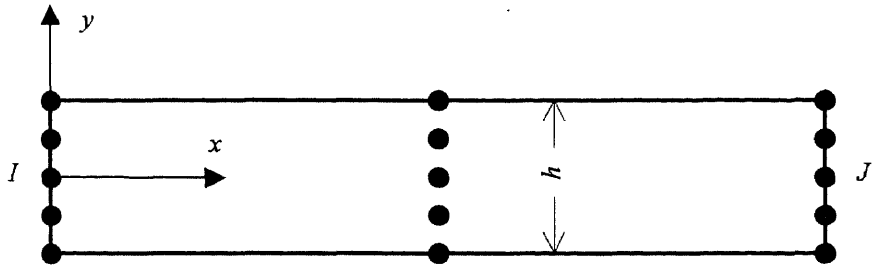

Figure 3.1 Two-dimensional nonlinear beam element.

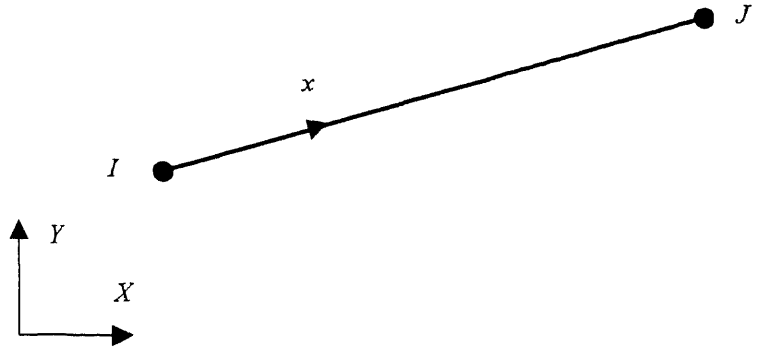

Figure 3.2 Two-dimensional spar element.

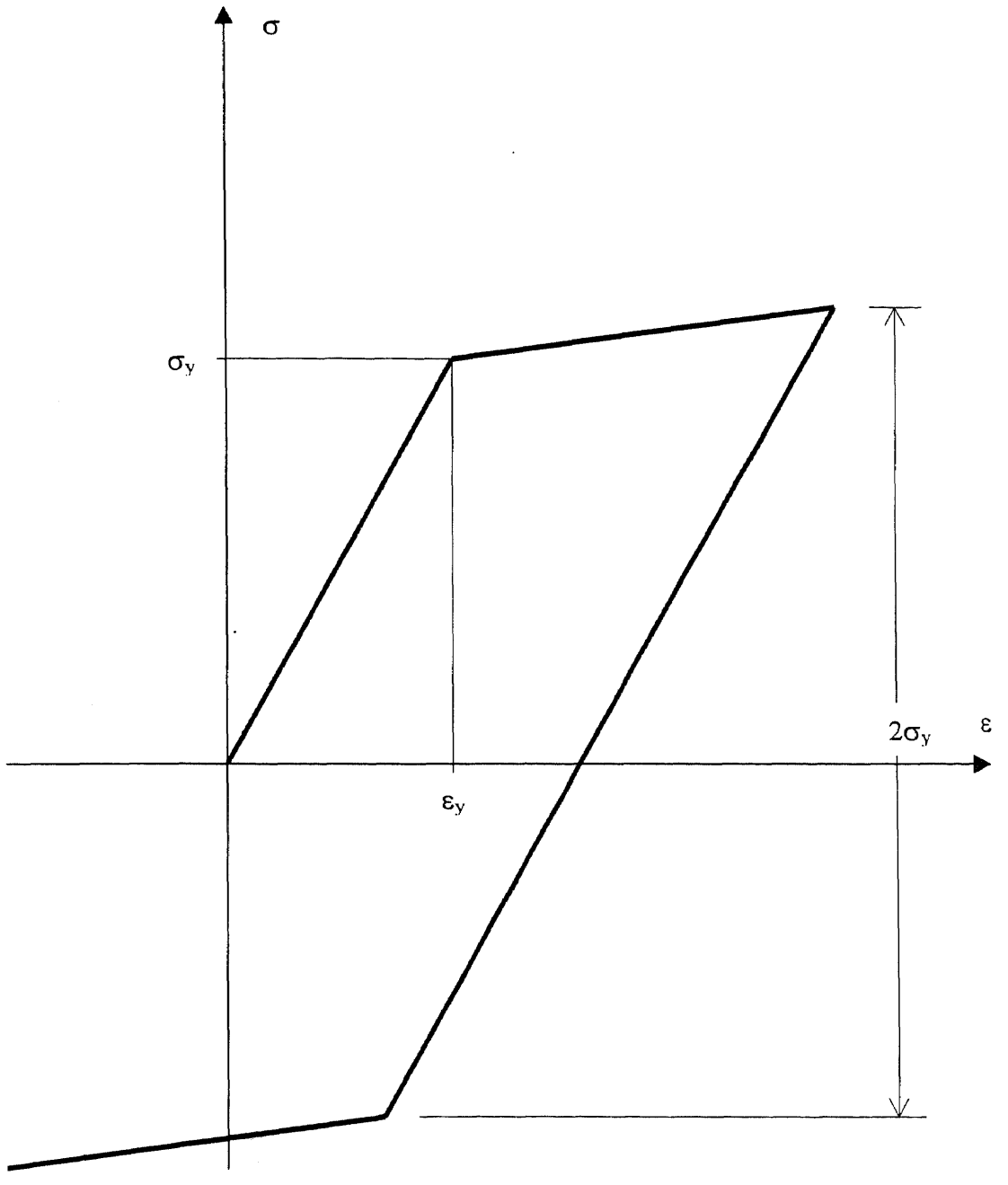

Figure 3.3 Bilinear material behavior with kinematic hardening.

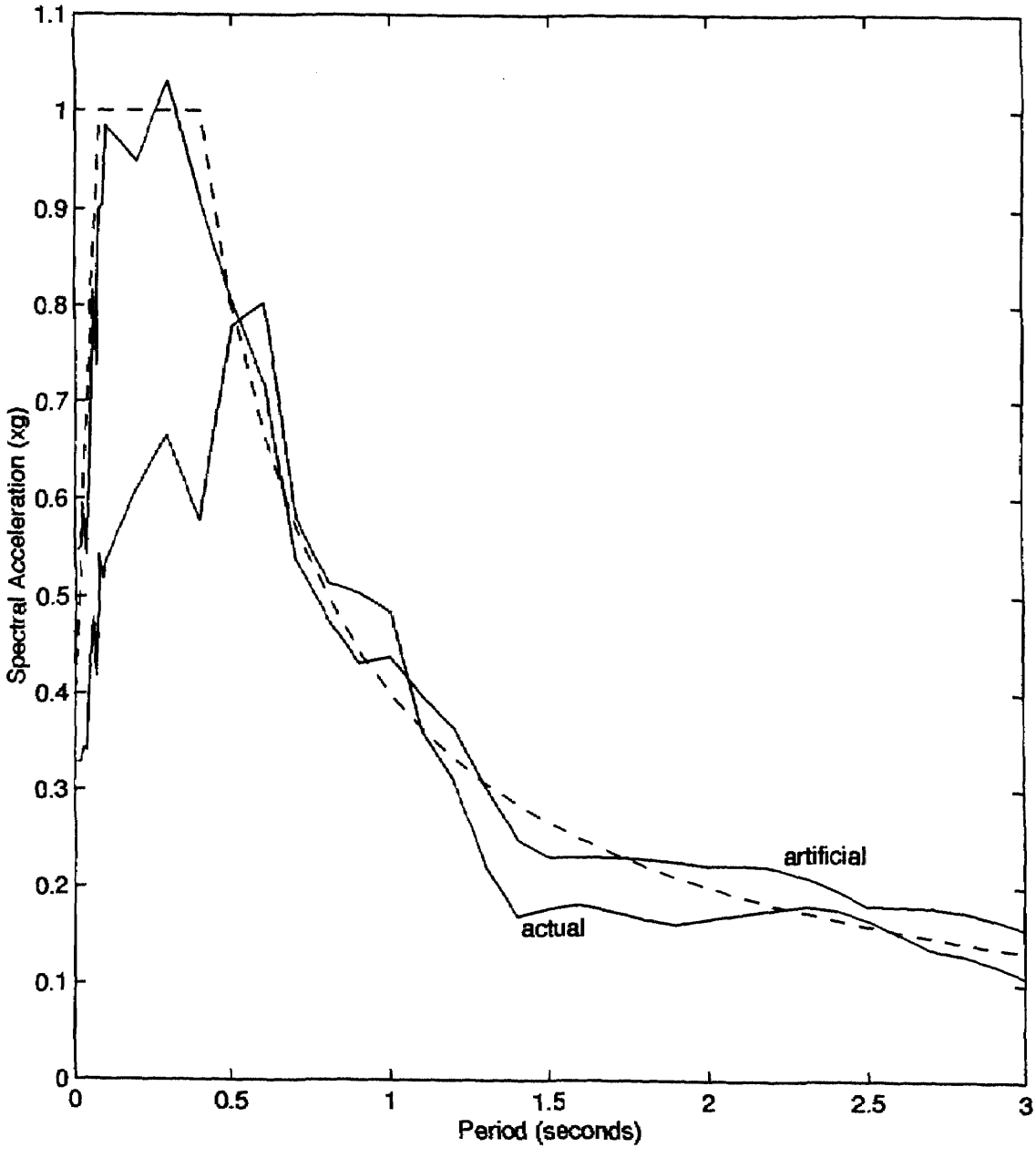

Figure 3.4 Acceleration response spectra of El Centro and the associated artificial accelerogram.

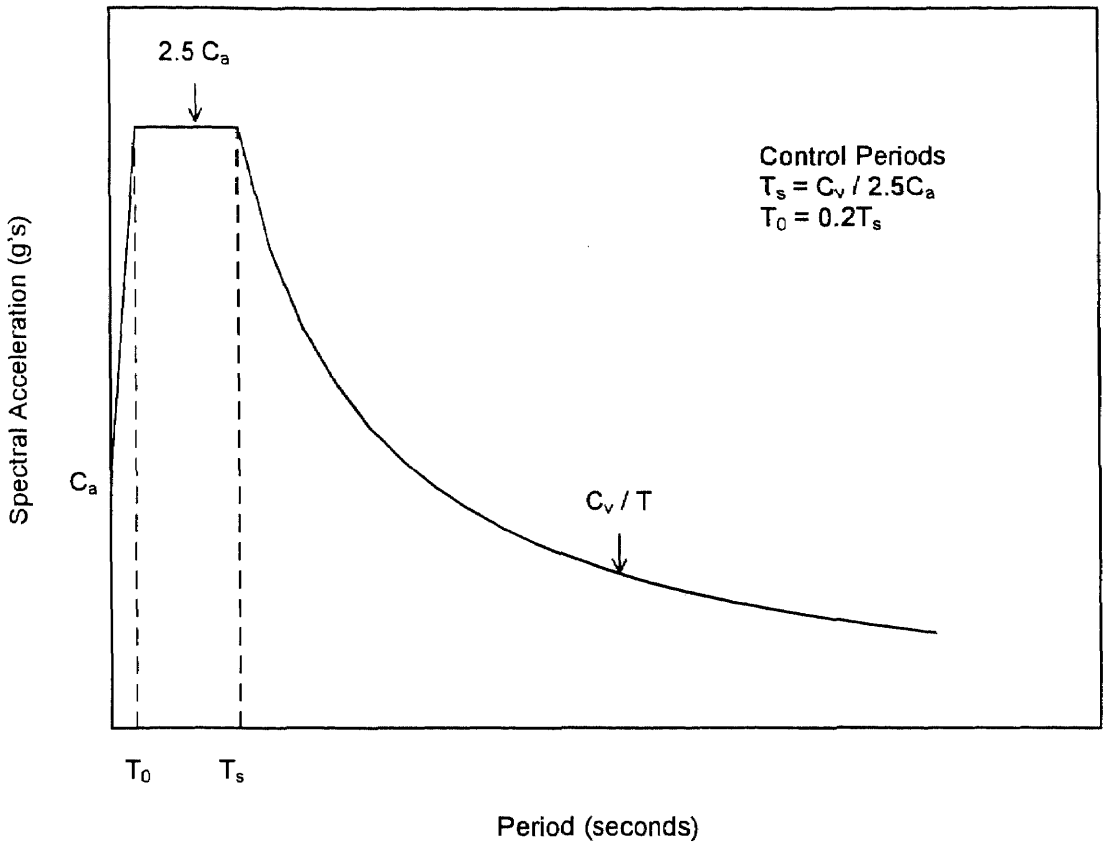

Figure 3.5 The UBC design response spectra.

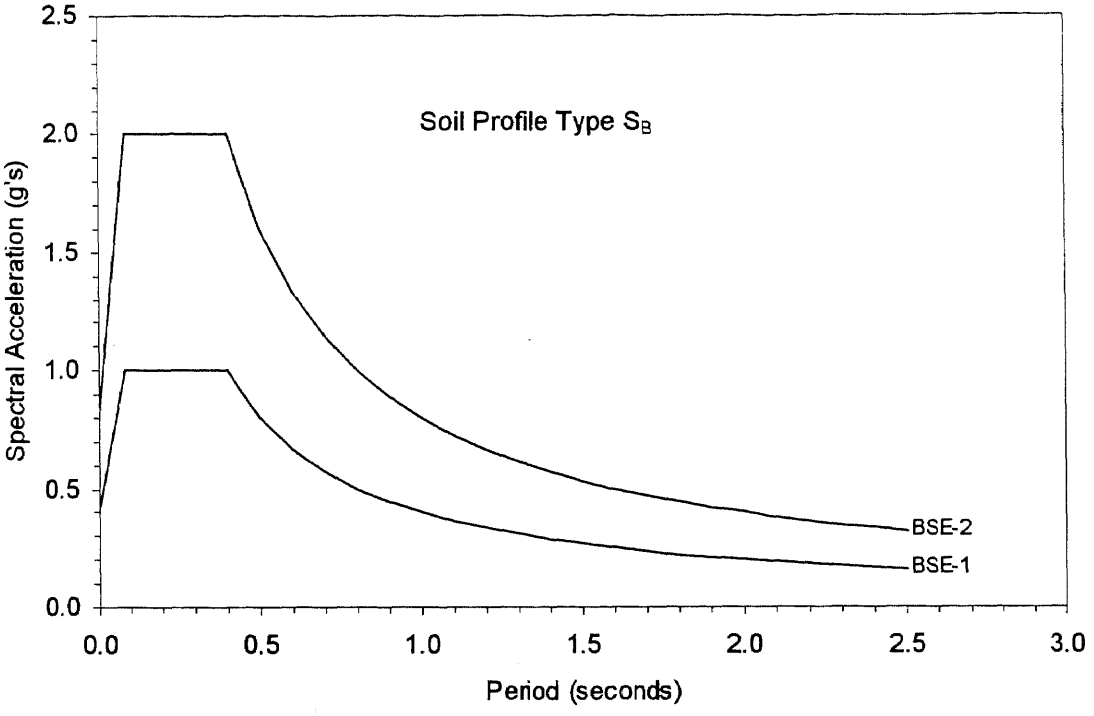

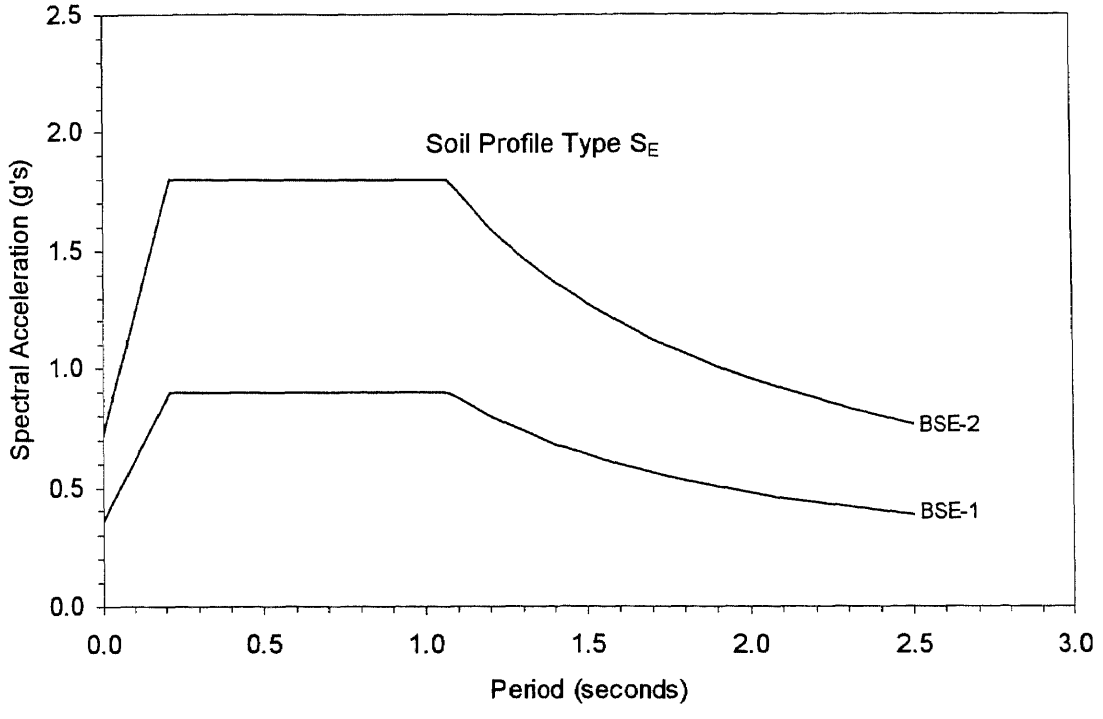

Figure 3.6 Acceleration response spectra for BSE-1 and BSE-2.

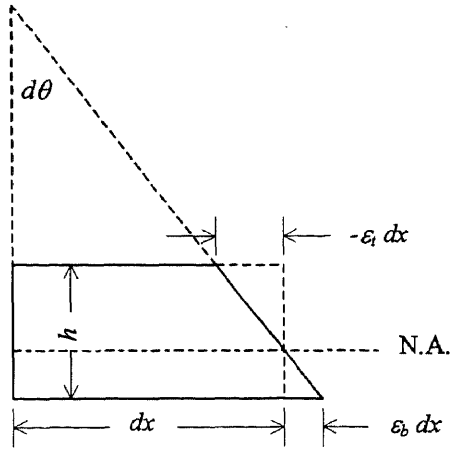

Figure 3.7 Definition of curvature.

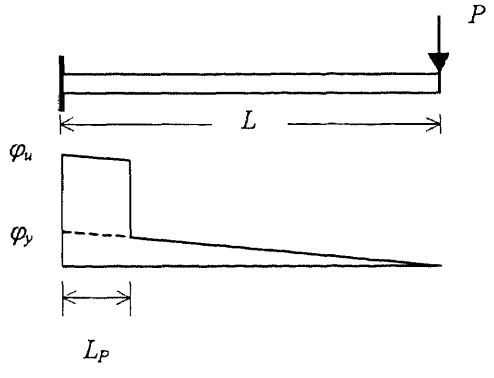

Figure 3.8 Curvature distribution for a cantilever beam.

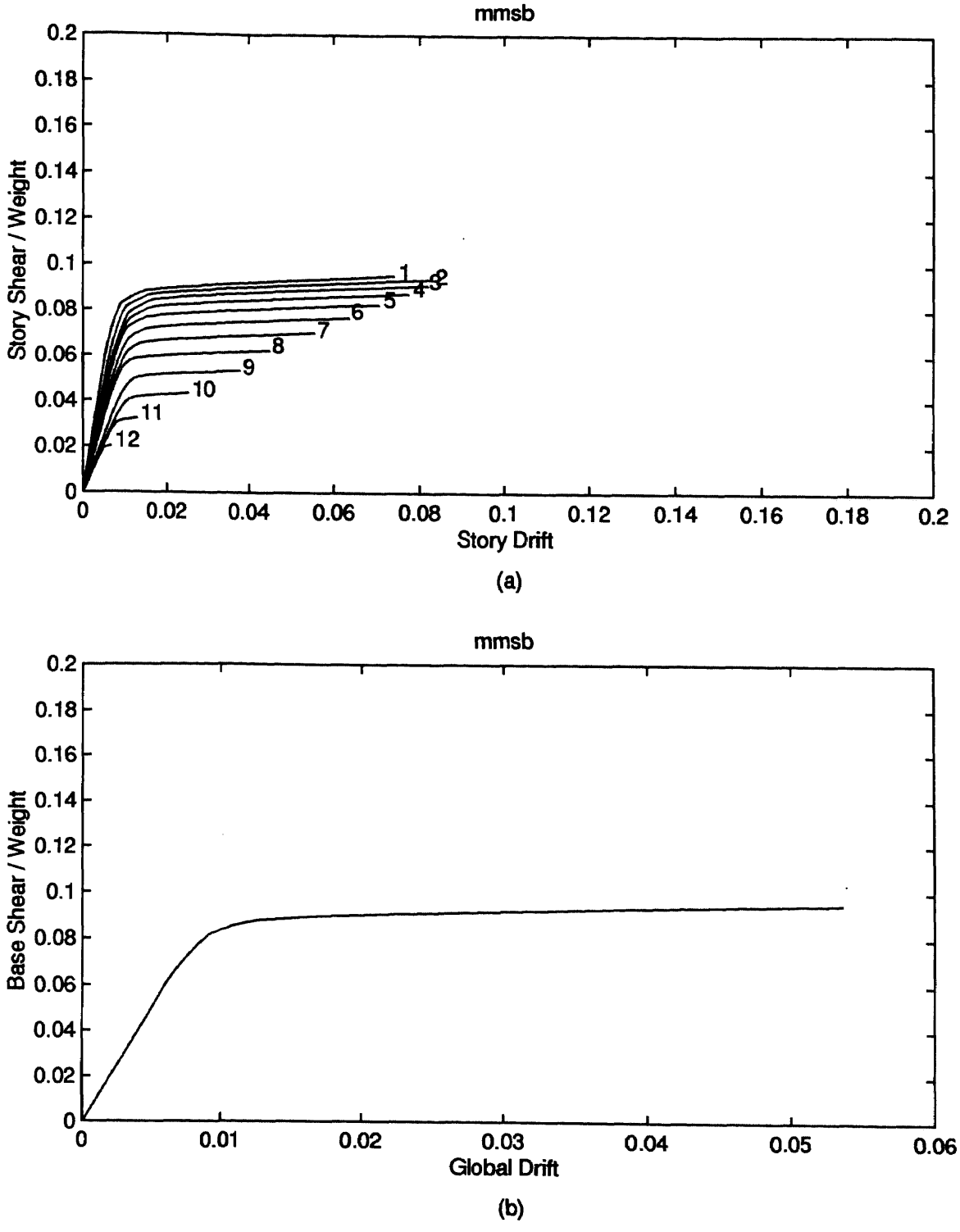

Figure 4.1 Pushover curves for mmsb: (a) story shear vs. interstory drift, (b) base shear vs. global drift.

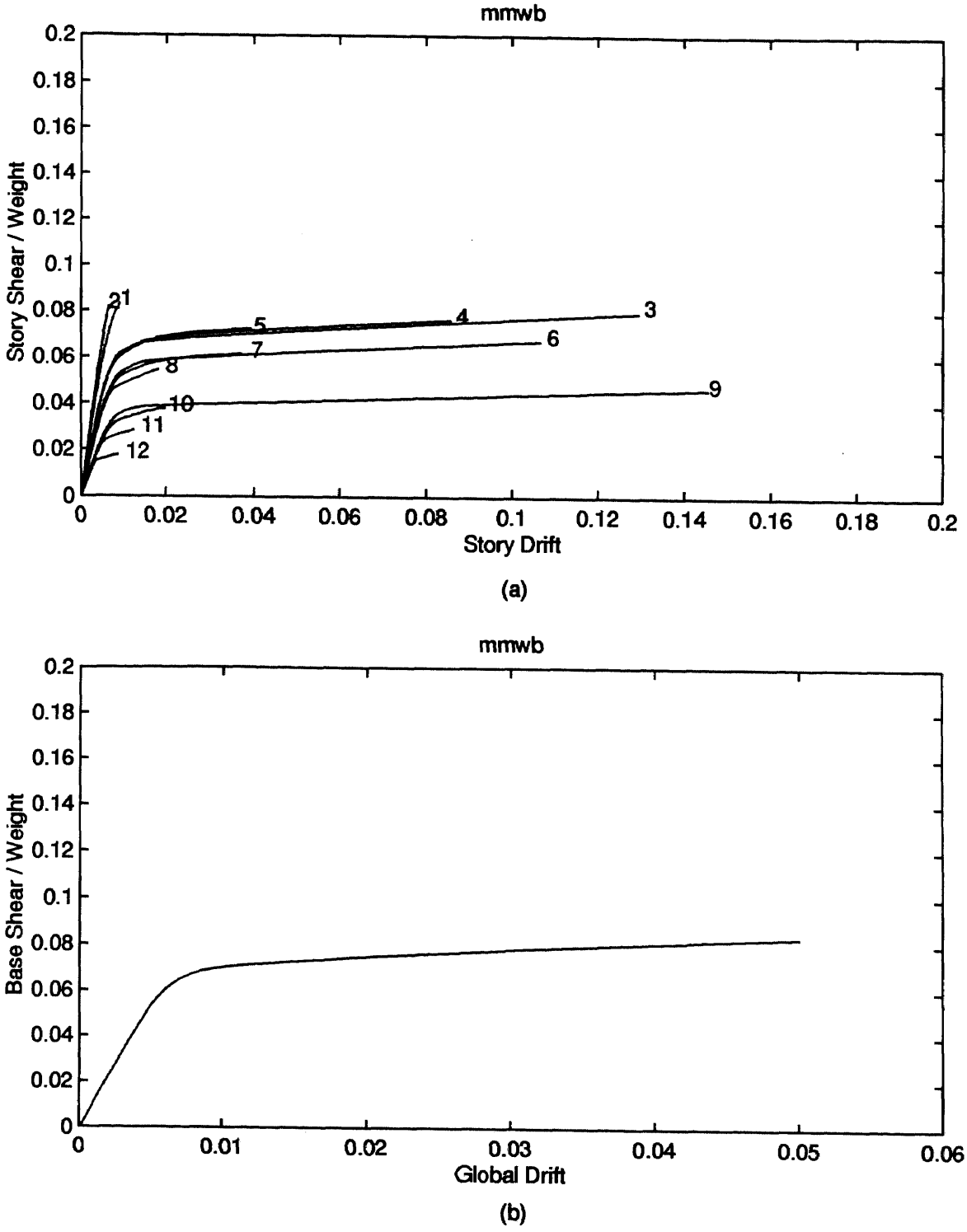

Figure 4.2 Pushover curves for mmwb: (a) story shear vs. interstory drift, (b) base shear vs. global drift.

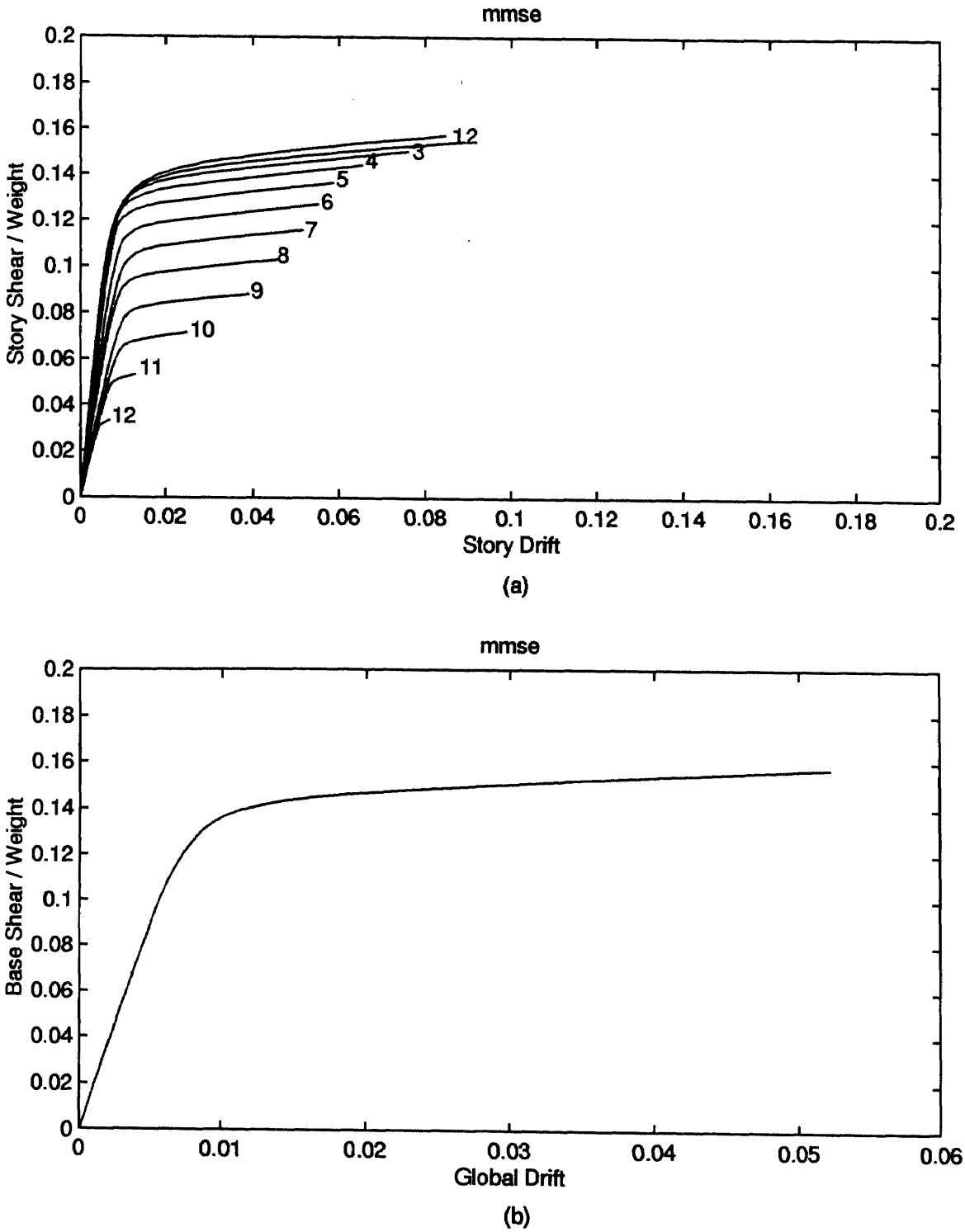

Figure 4.3 Pushover curves for mmse: (a) story shear vs. interstory drift, (b) base shear vs. global drift.

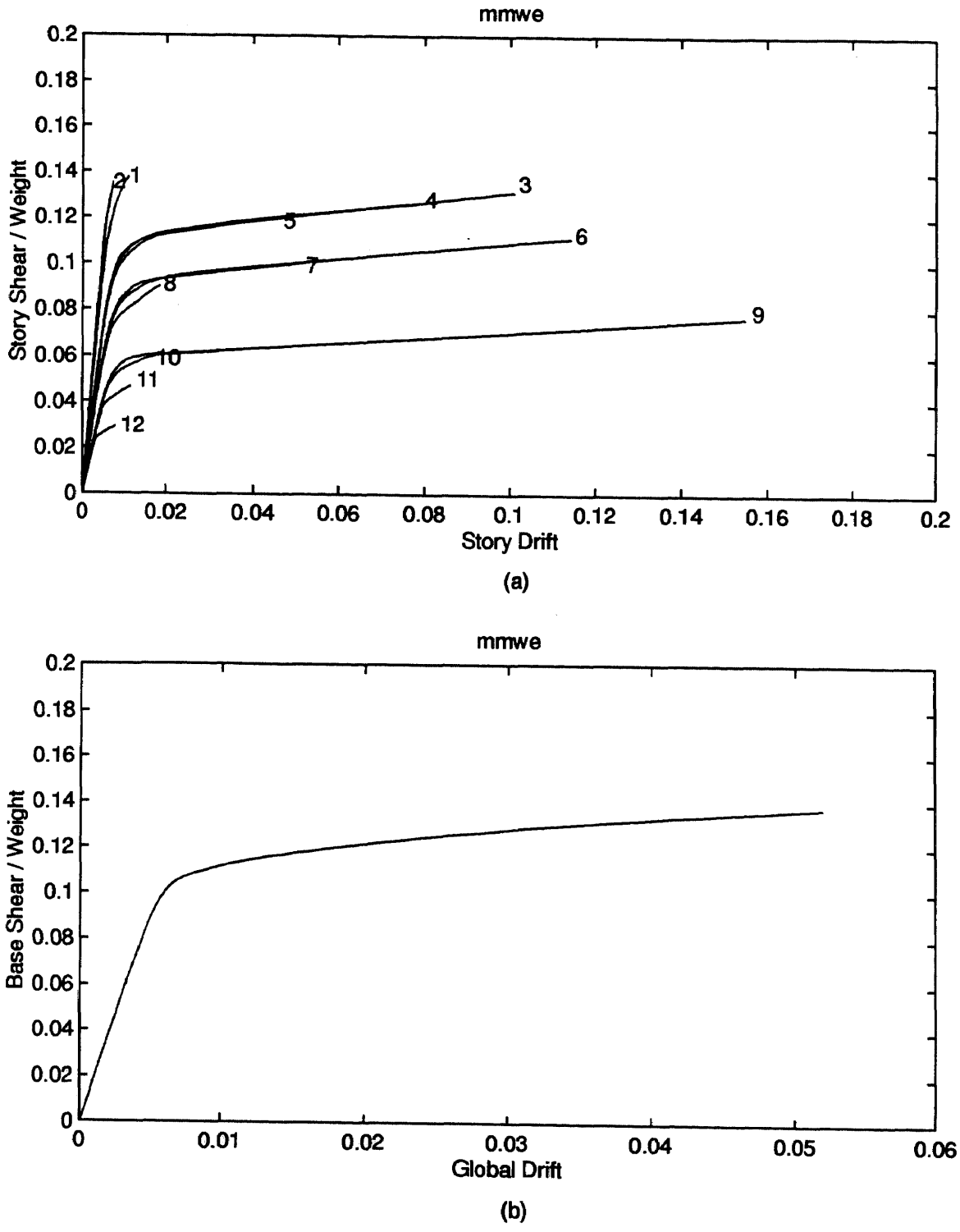

Figure 4.4 Pushover curves for mmwe: (a) story shear vs. interstory drift, (b) base shear vs. global drift.

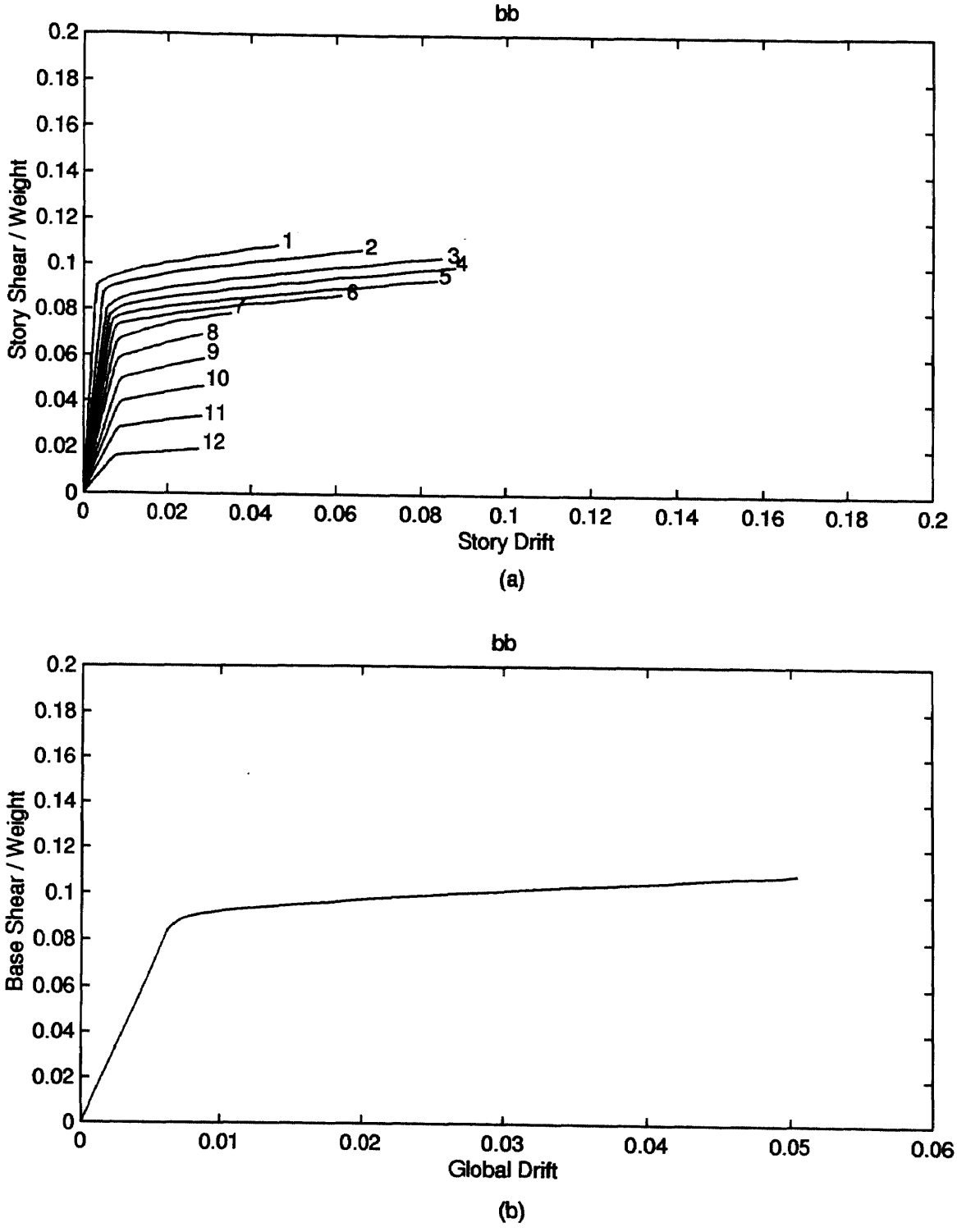

Figure 4.5 Pushover curves for bb: (a) story shear vs. interstory drift, (b) base shear vs. global drift.

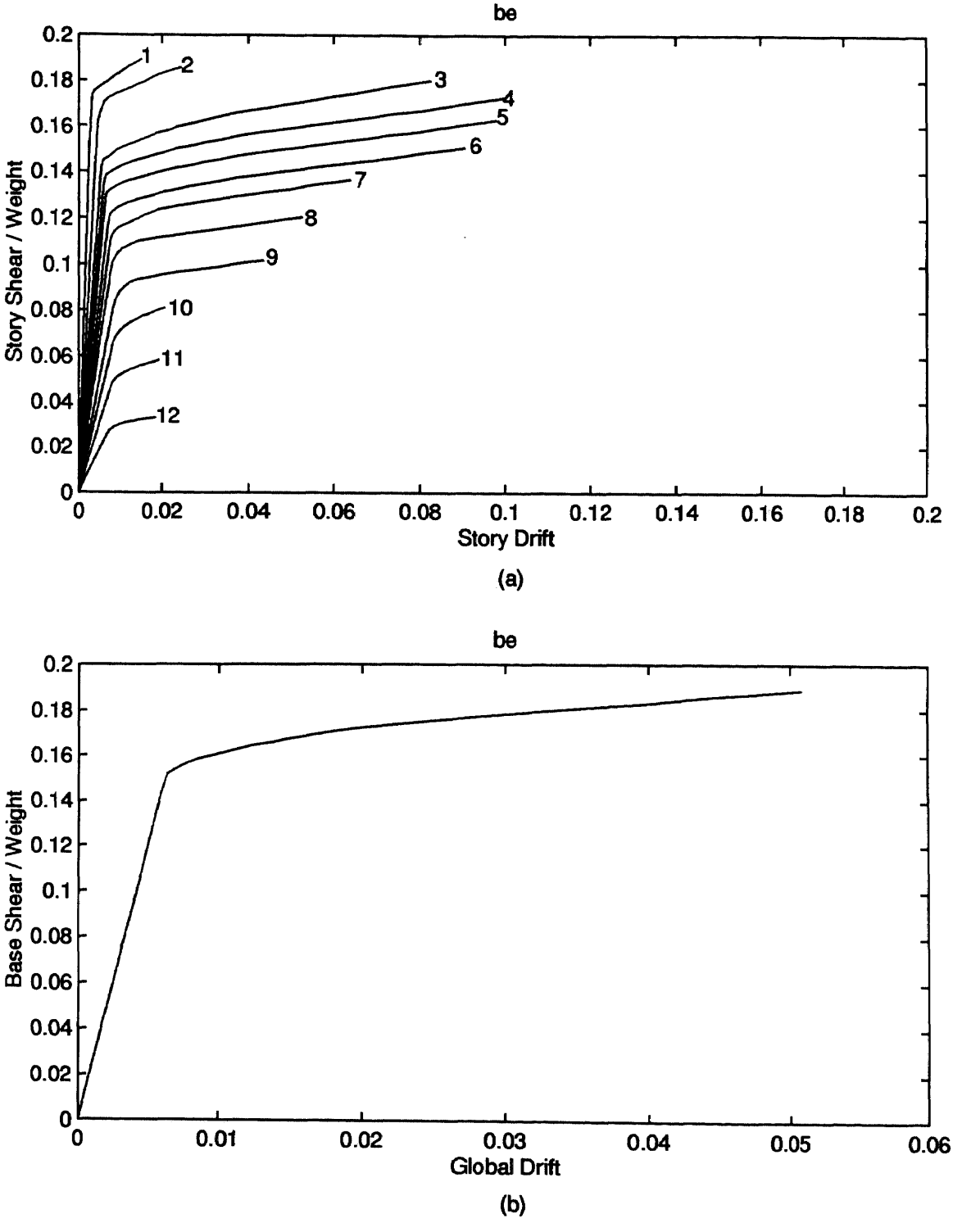

Figure 4.6 Pushover curves for be: (a) story shear vs. interstory drift, (b) base shear vs. global drift.

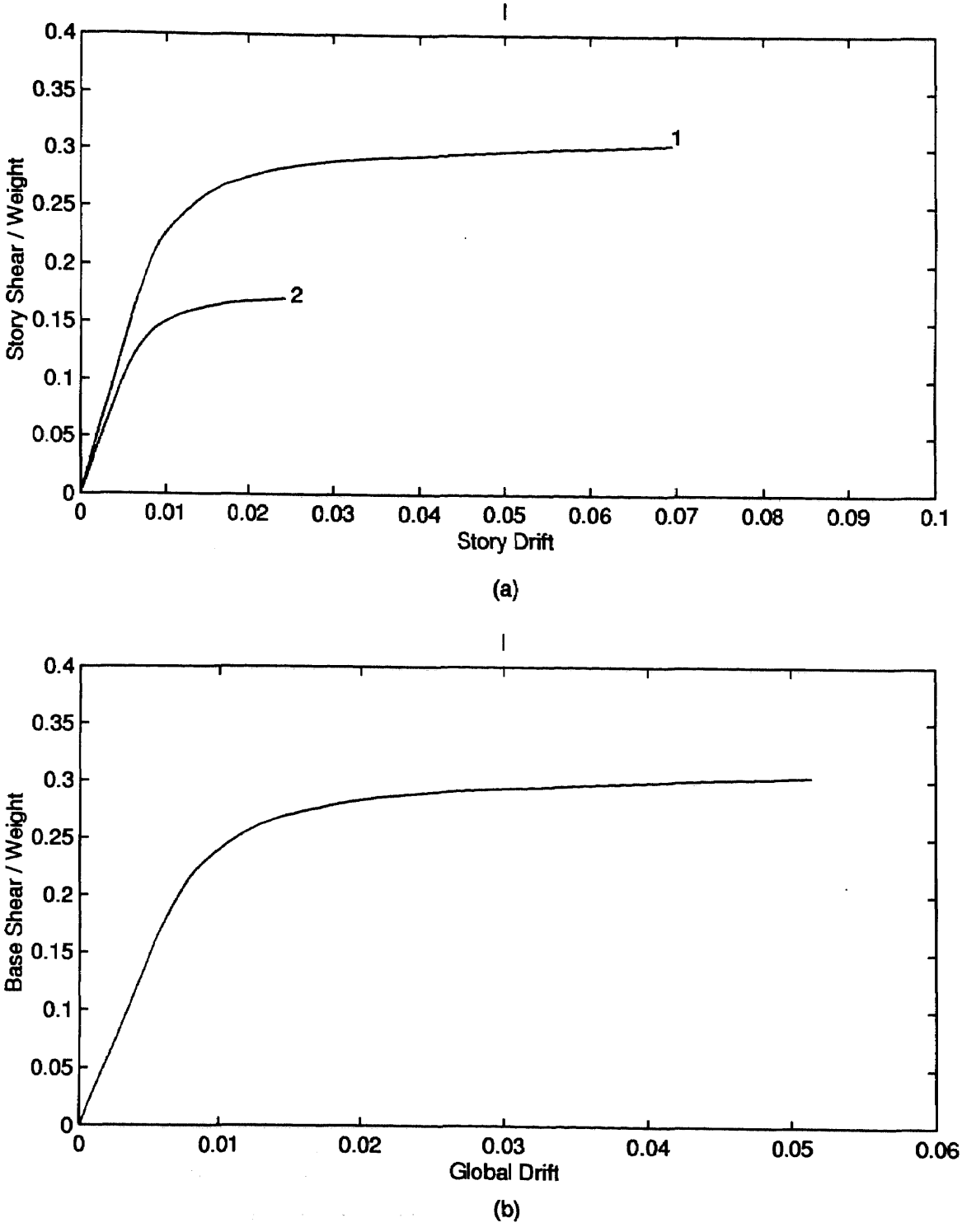

Figure 4.7 Pushover curves for l: (a) story shear vs. interstory drift, (b) base shear vs. global drift.

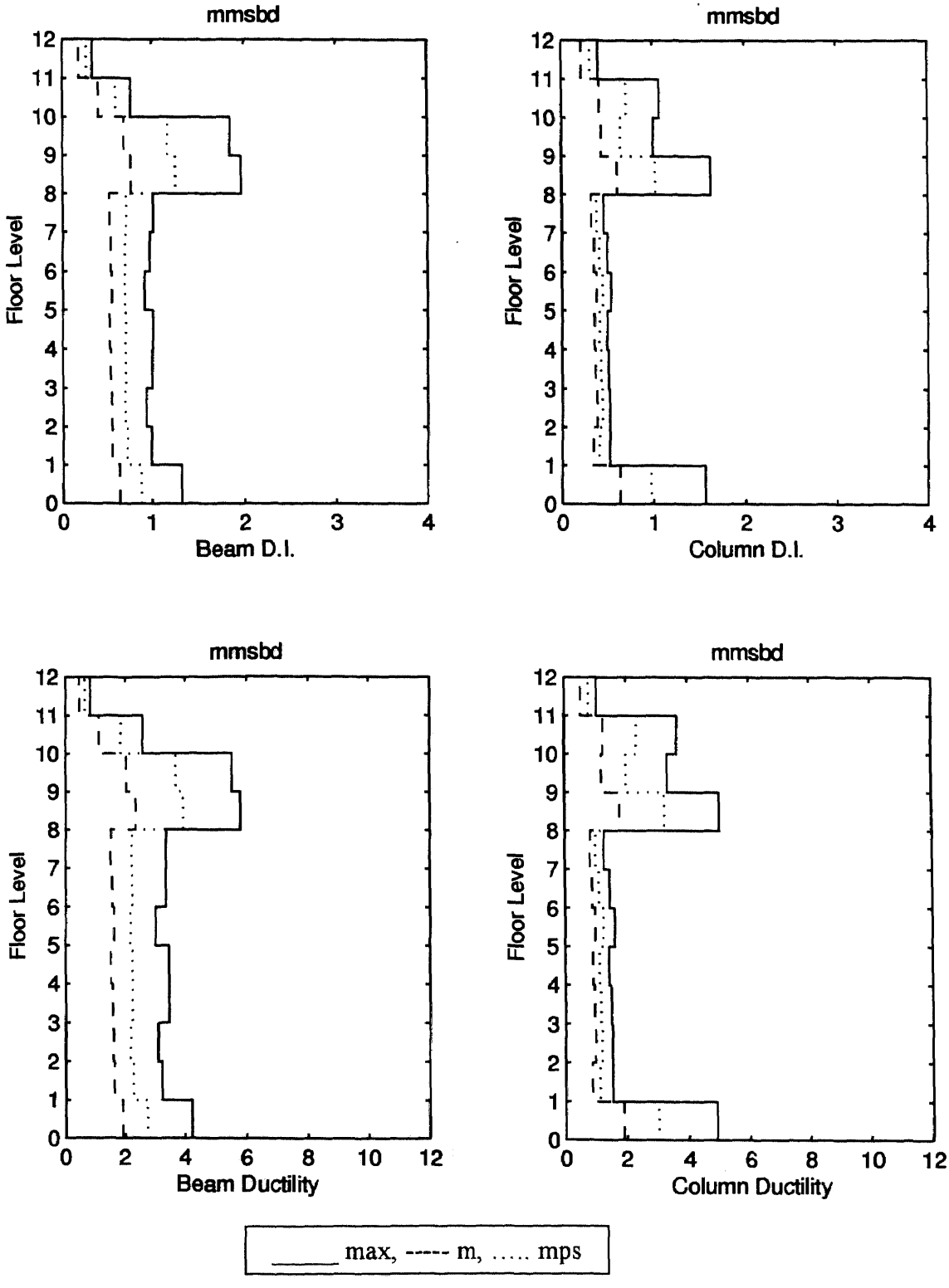

Figure 4.8 Story response of mmsbd: damage index and ductility.

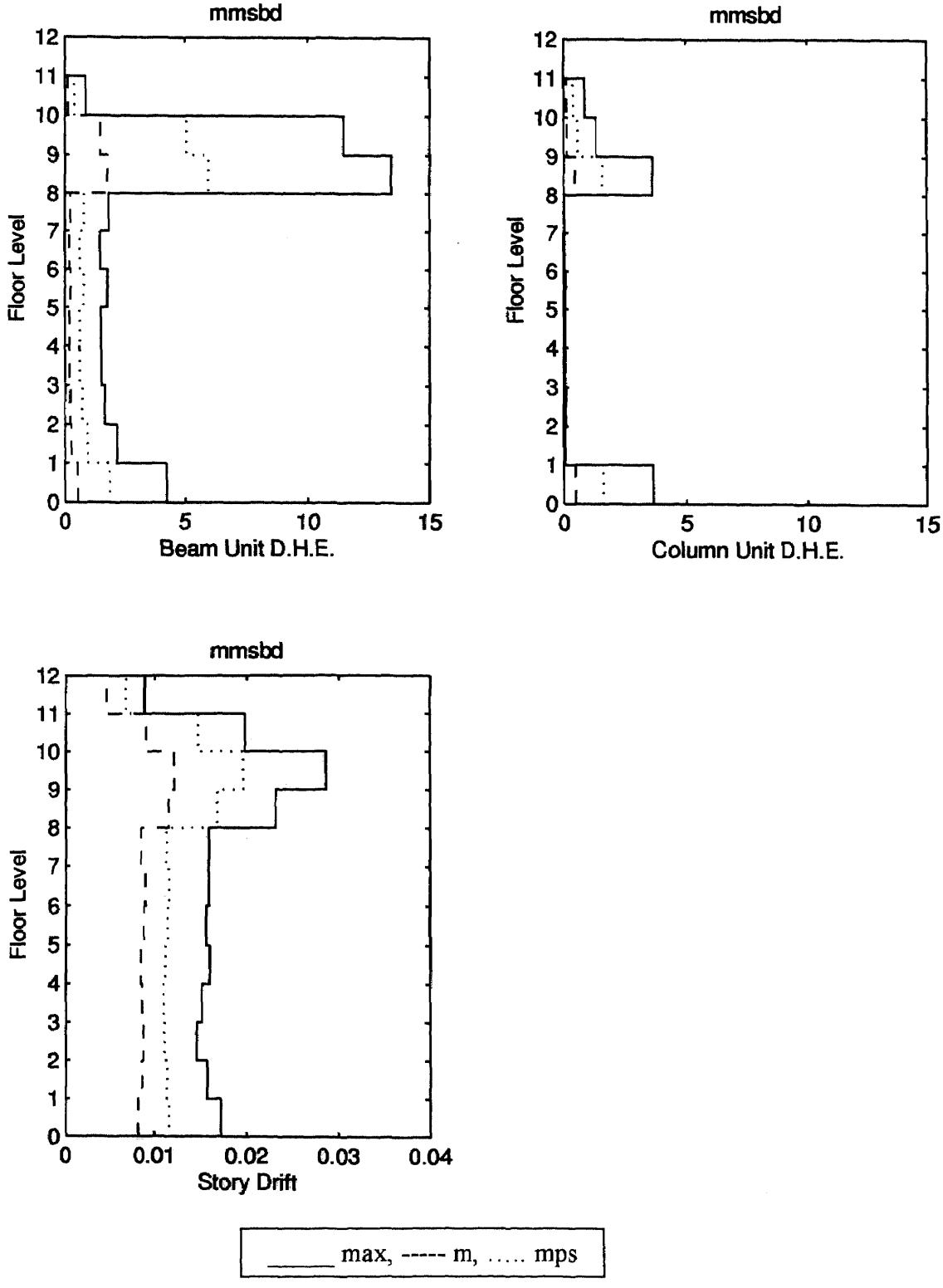

Figure 4.9 Story response of mmsbd: dissipated hysteretic energy and interstory drift.

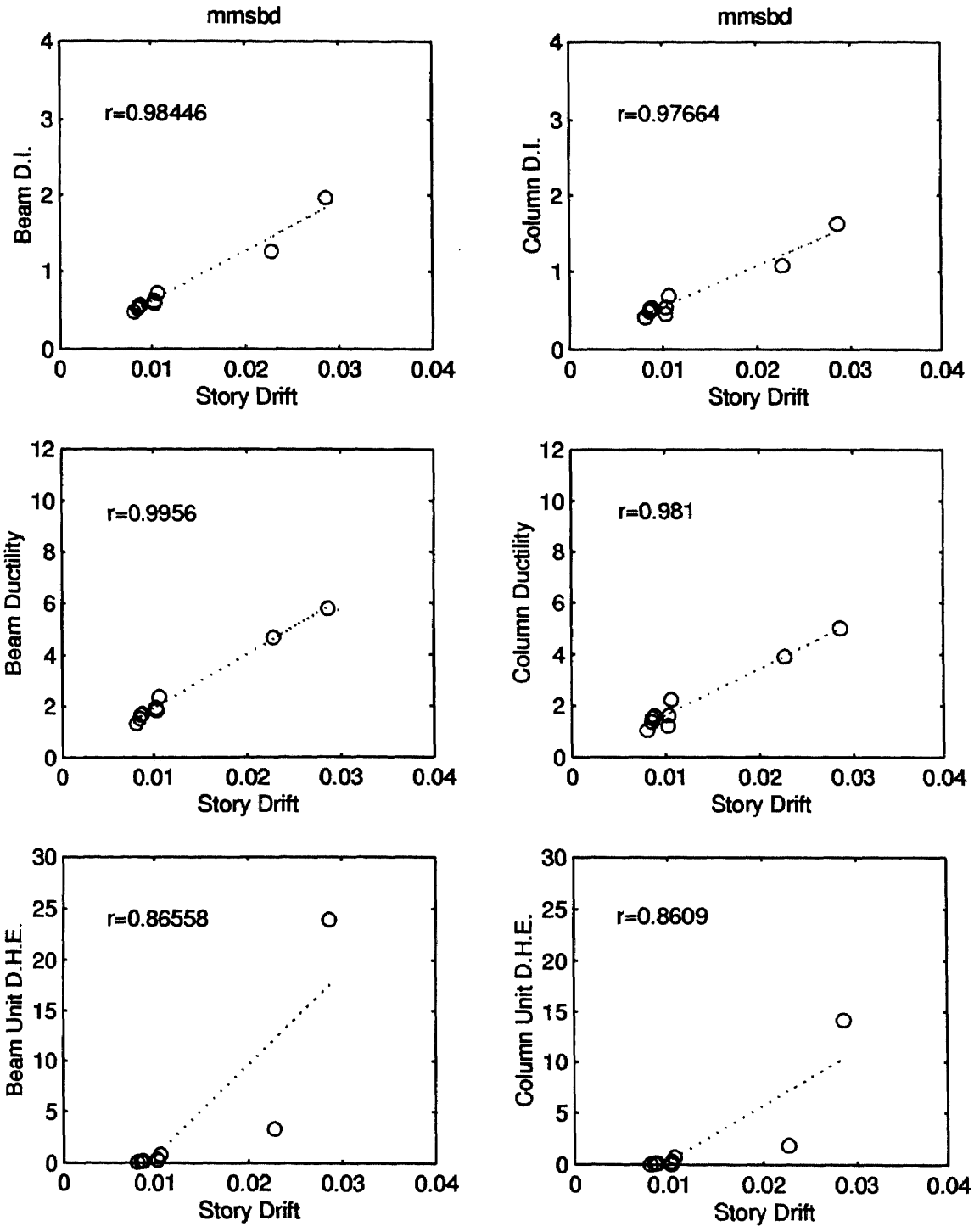

Figure 4.10 Element response of mmsbd.

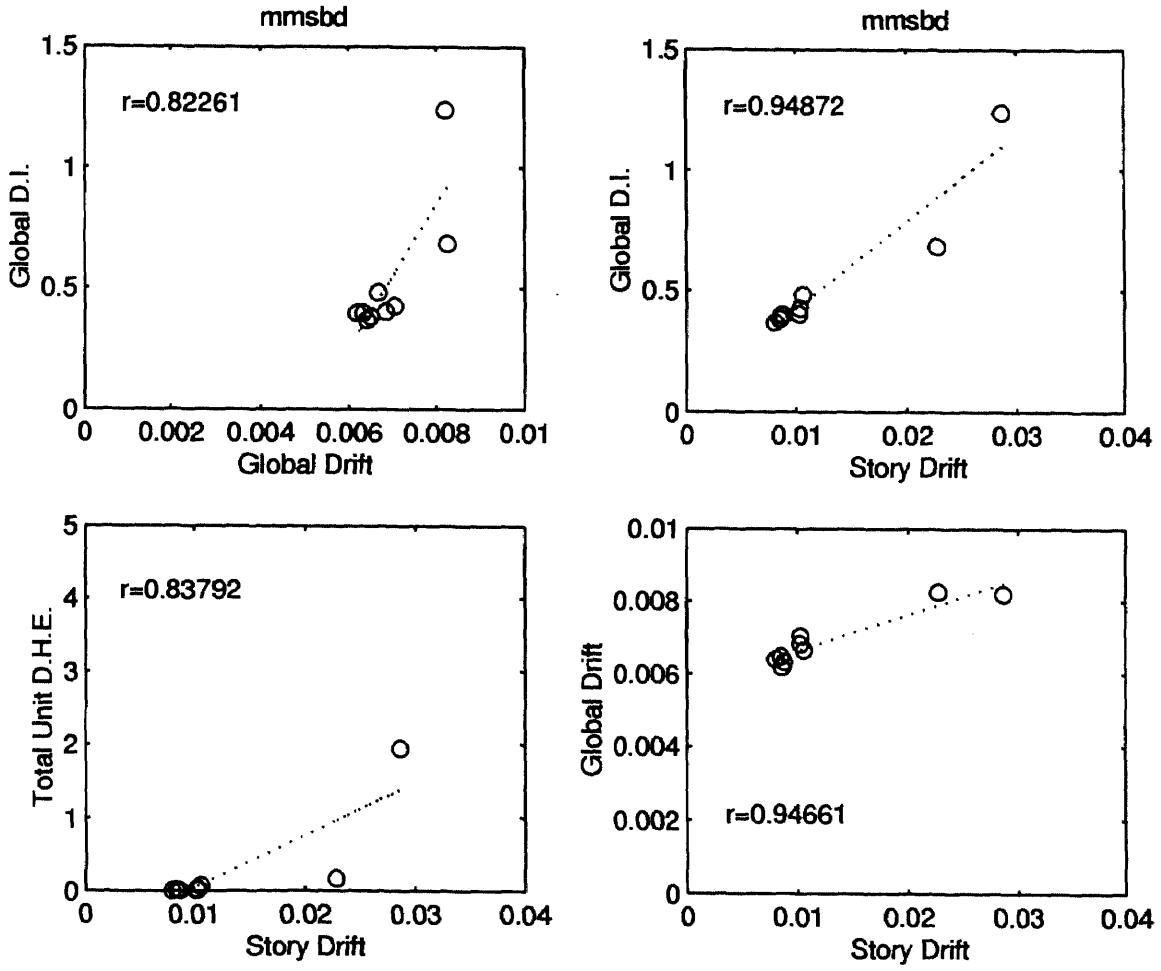

Figure 4.11 Global response of mmsbd.

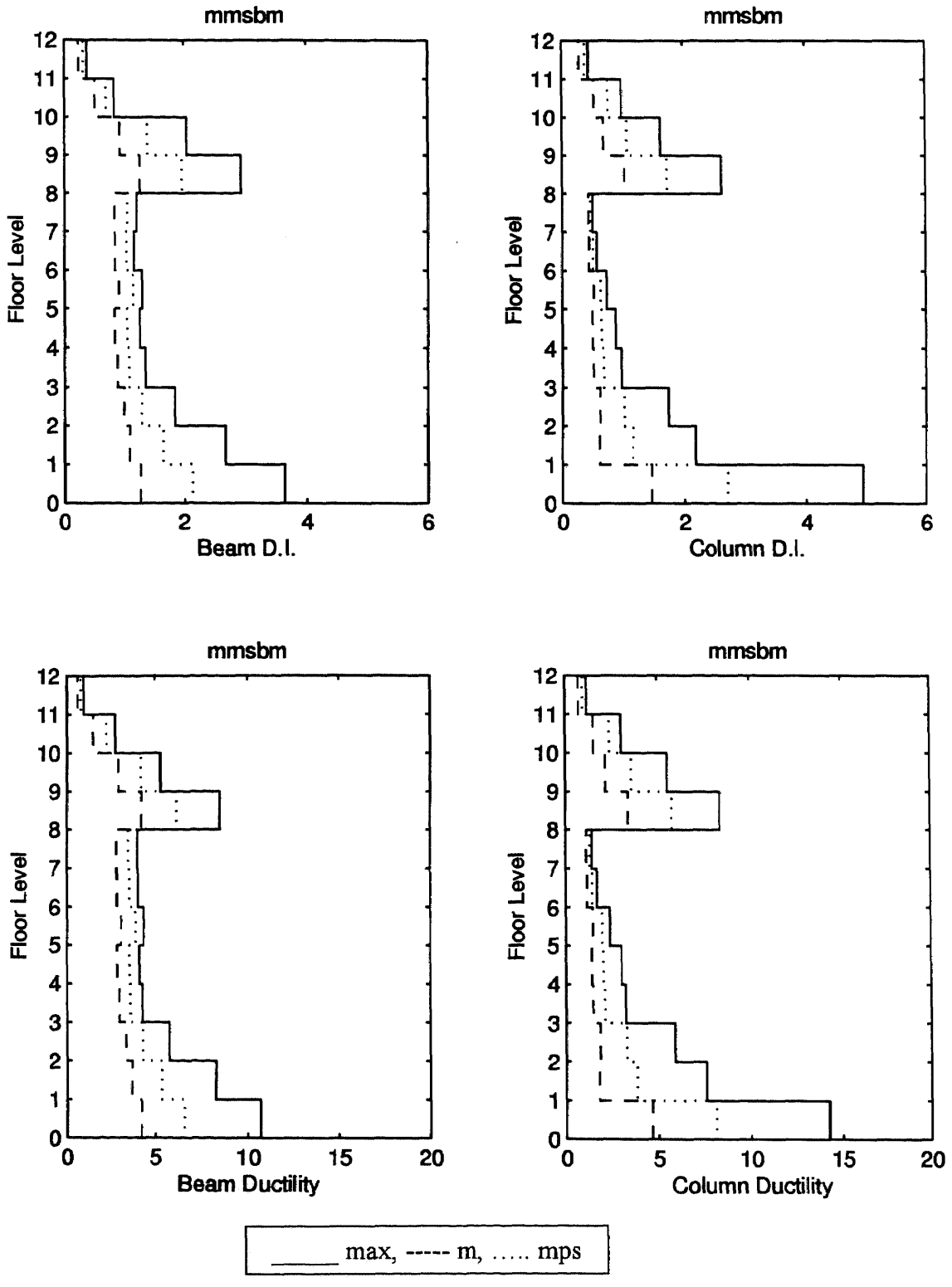

Figure 4.12 Story response of mmsbm: damage index and ductility.

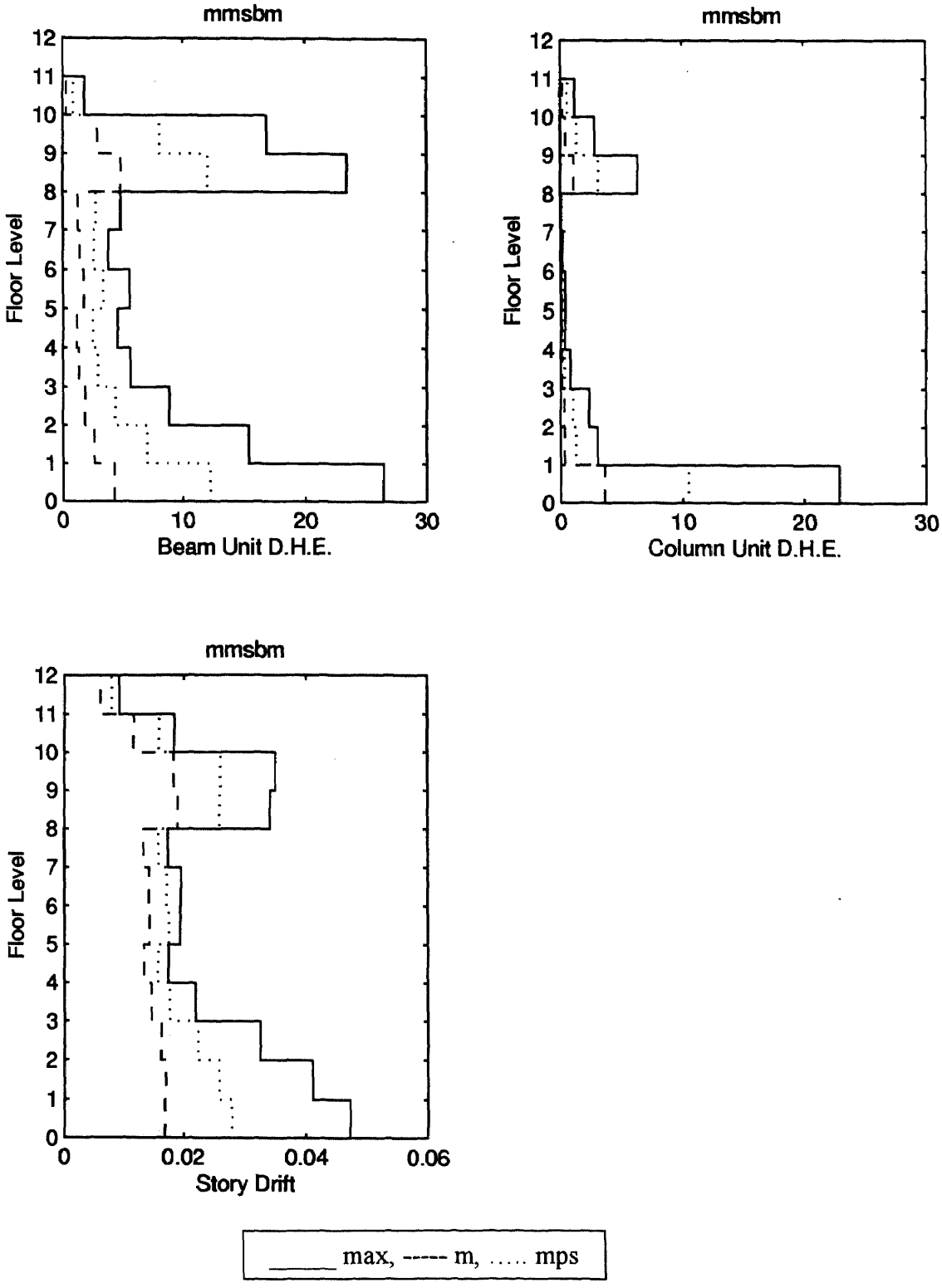

Figure 4.13 Story response of mmsbm: dissipated hysteretic energy and interstory drift

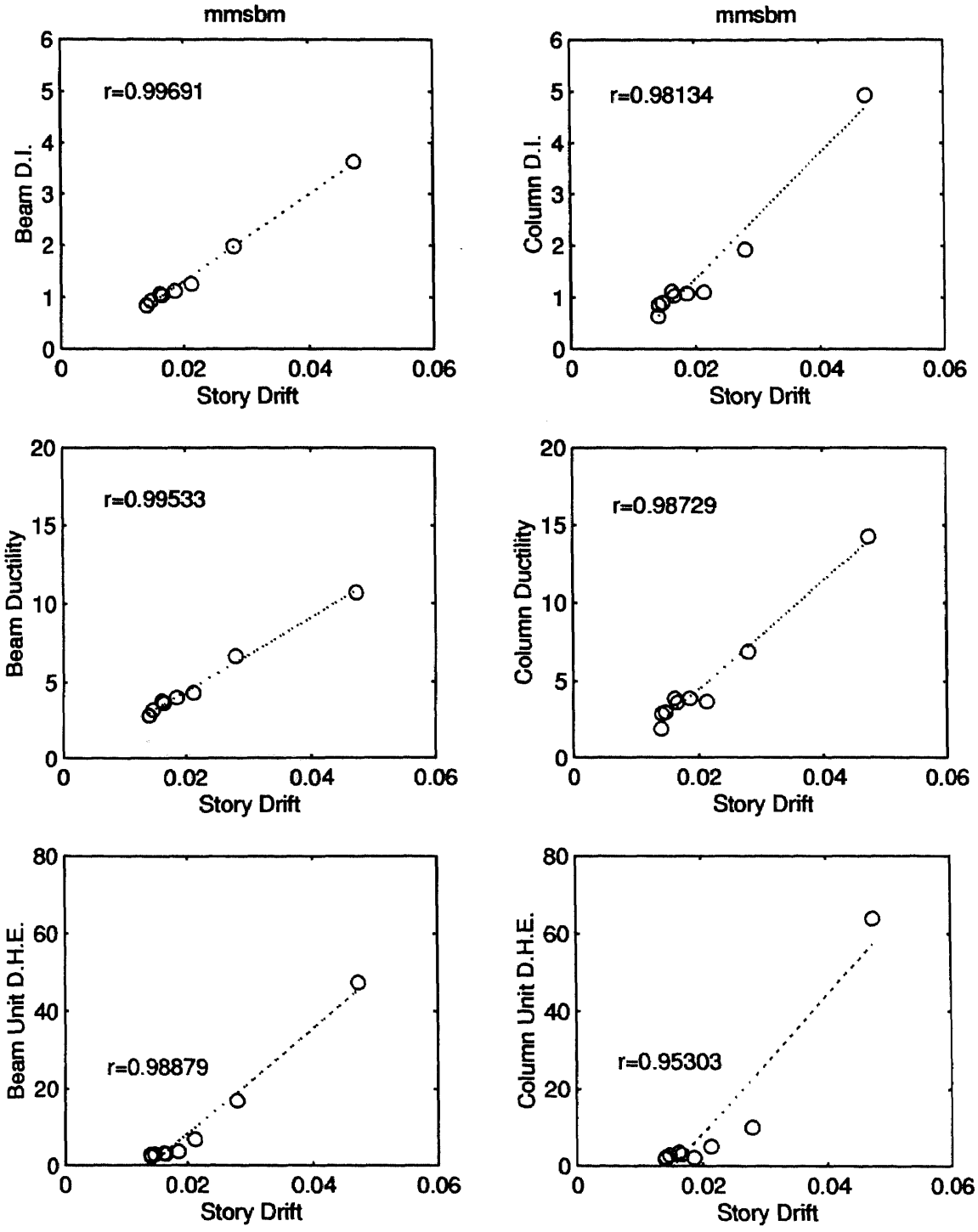

Figure 4.14 Element response of mmsbm.

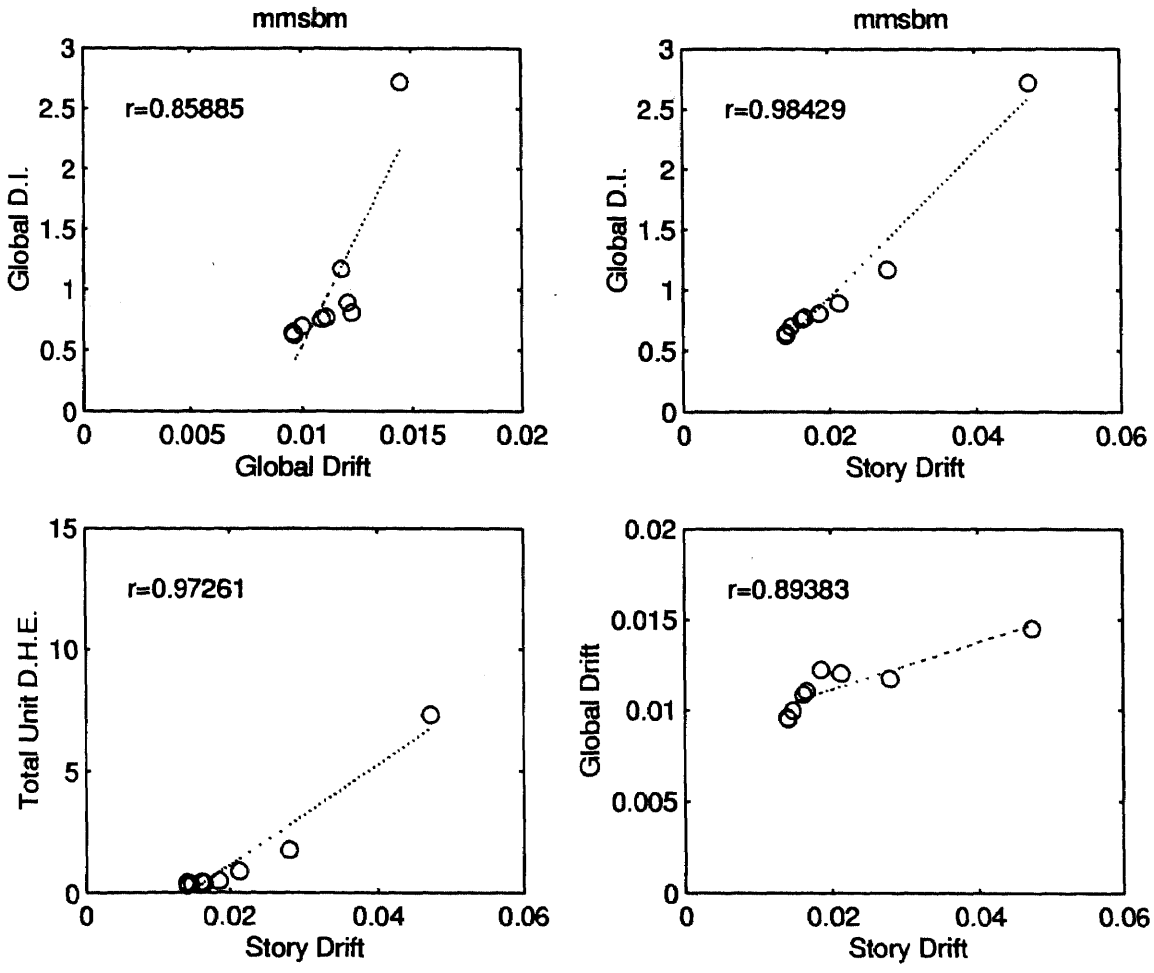

Figure 4.15 Global response of mmsbm.

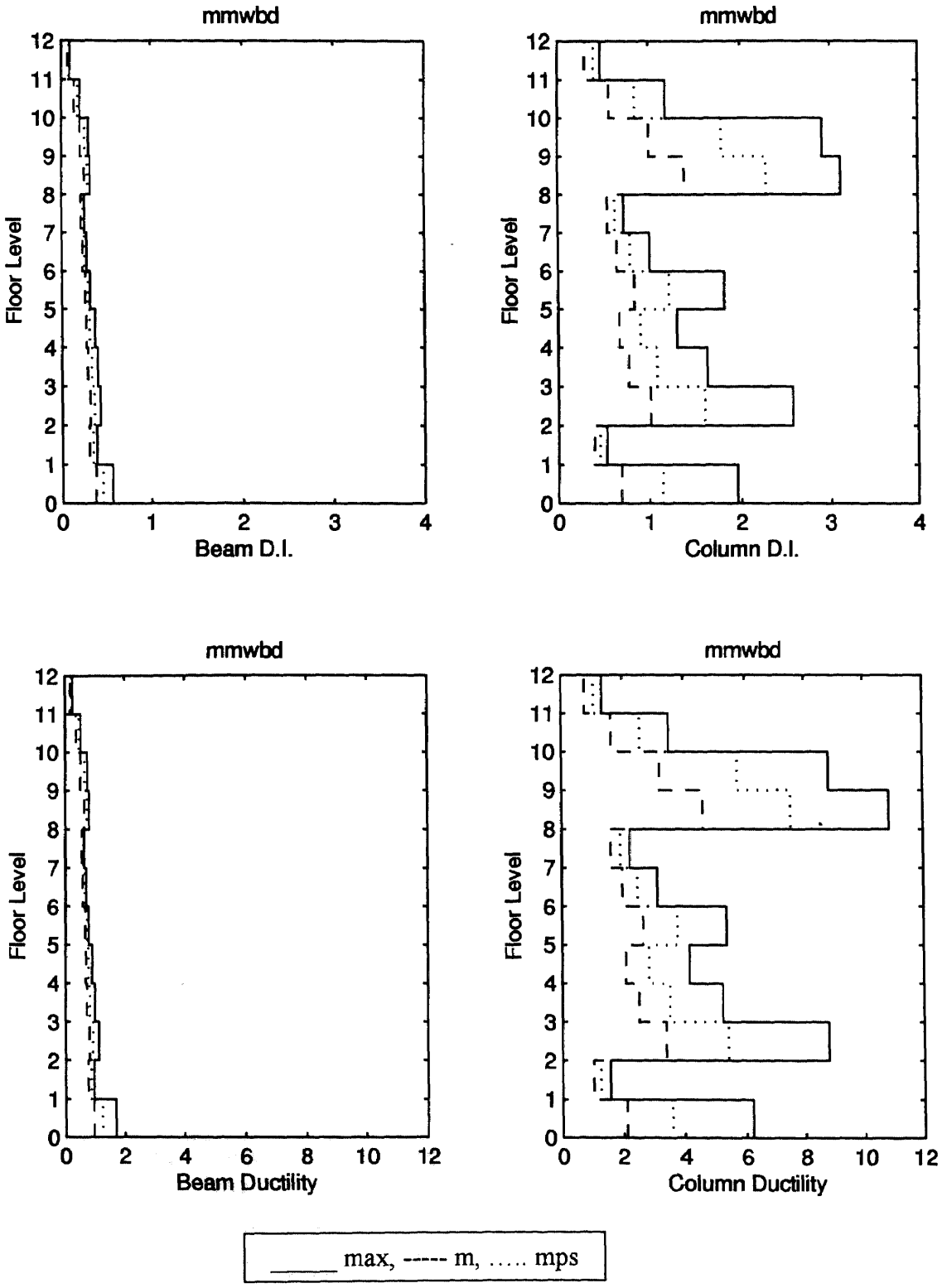

Figure 4.16 Story response of mmwbd: damage index and ductility.

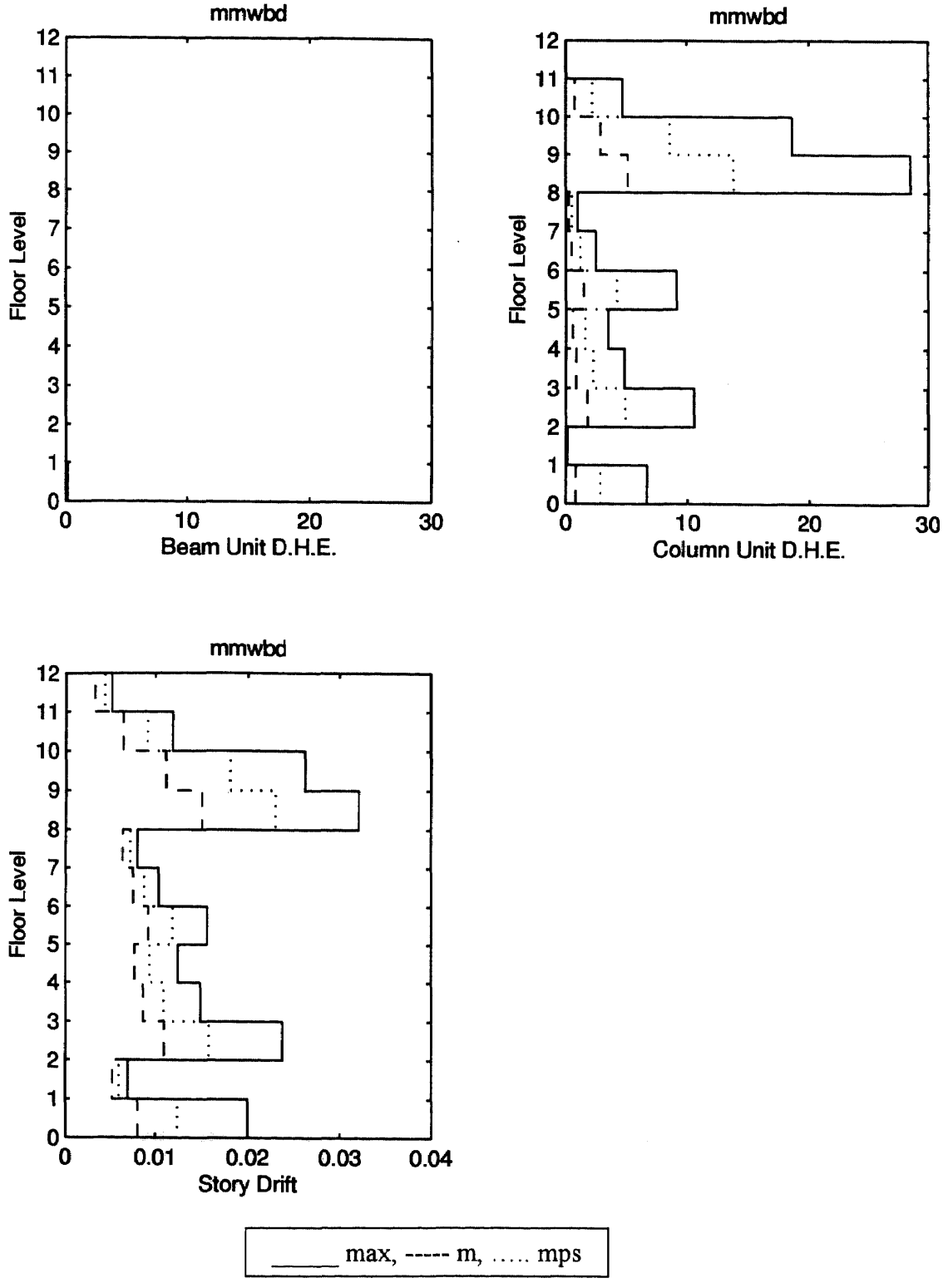

Figure 4.17 Story response of mmwbd: dissipated hysteretic energy and interstory drift.

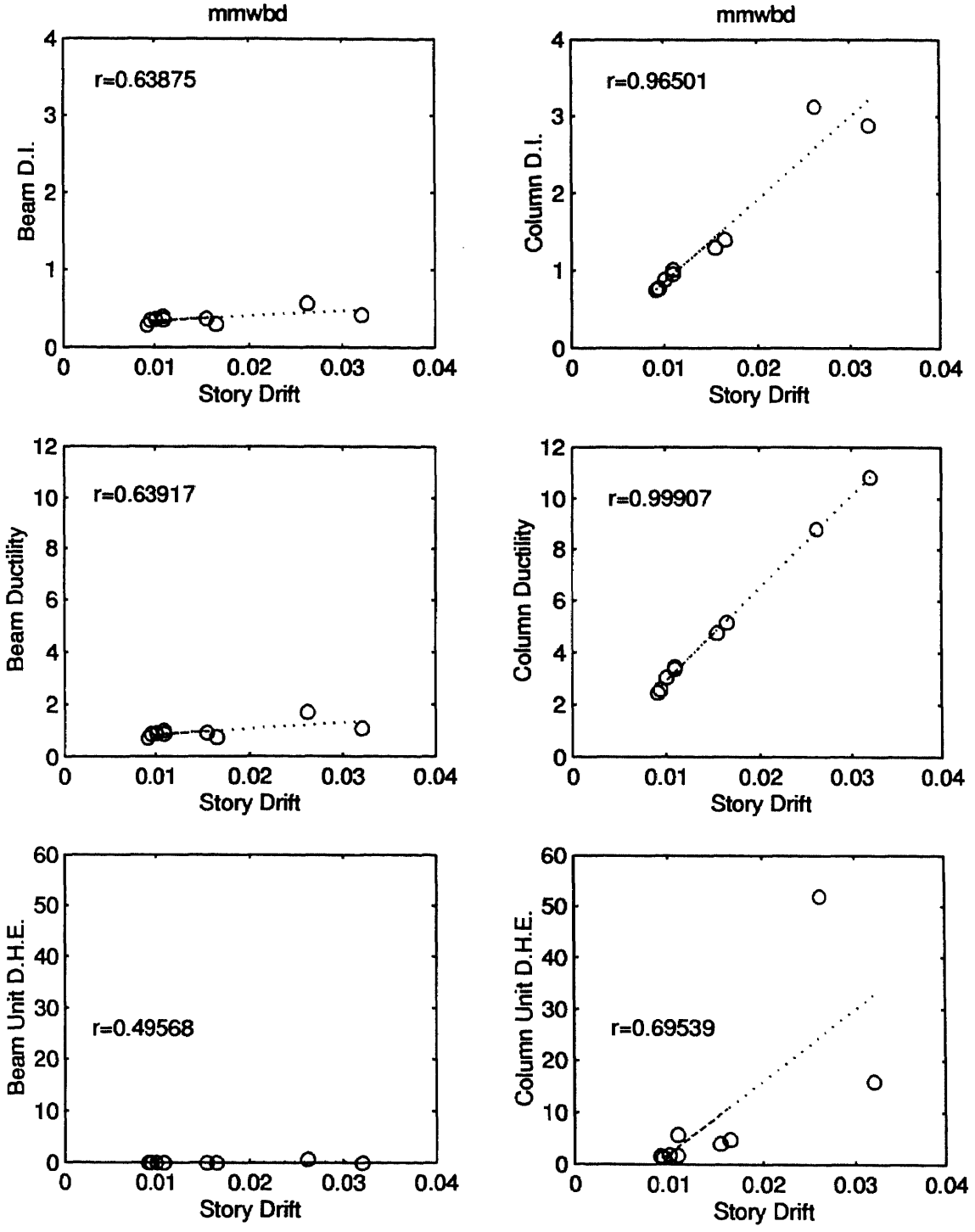

Figure 4.18 Element response of mmwbd.

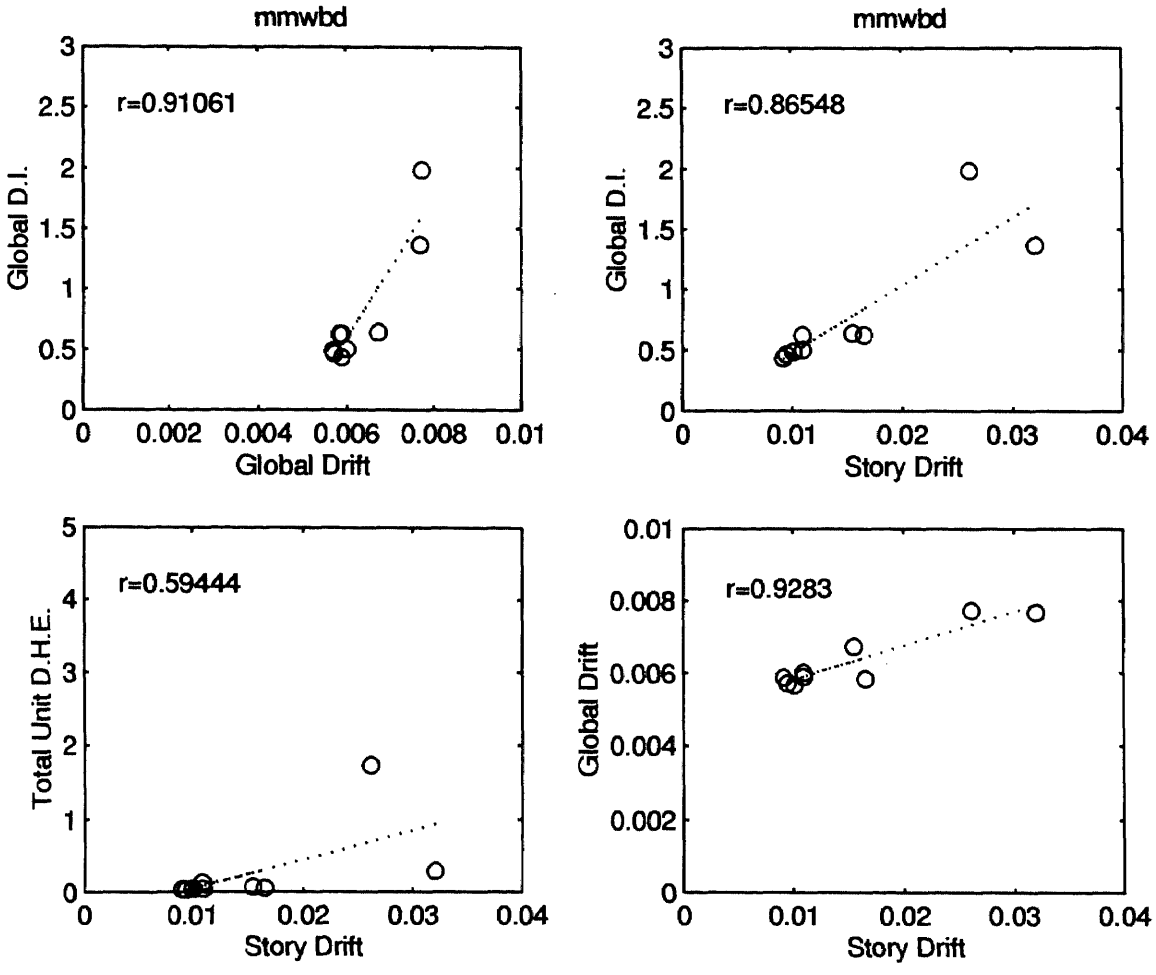

Figure 4.19 Global response of mmwbd.

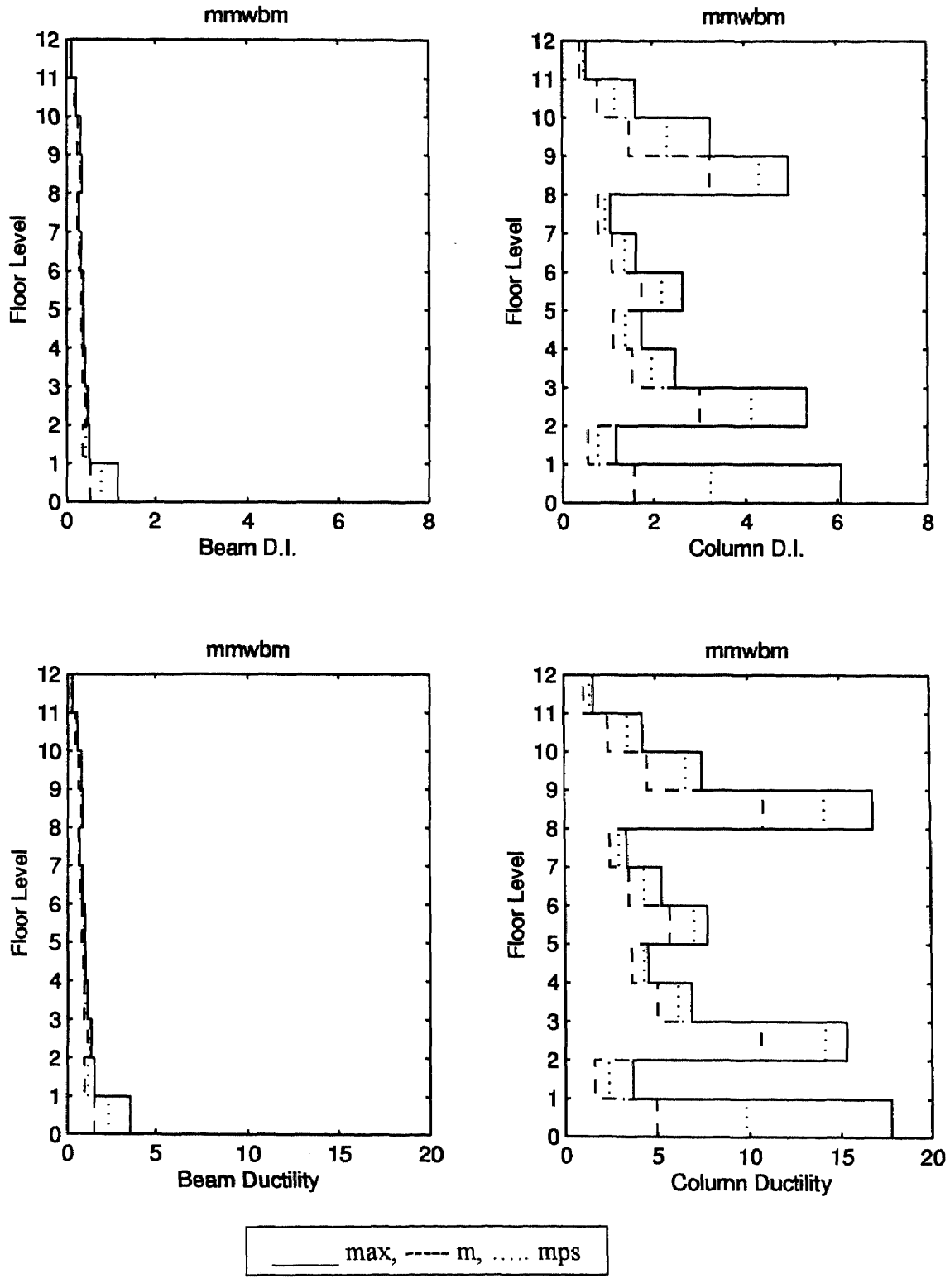

Figure 4.20 Story response of mmwbm: damage index and ductility.

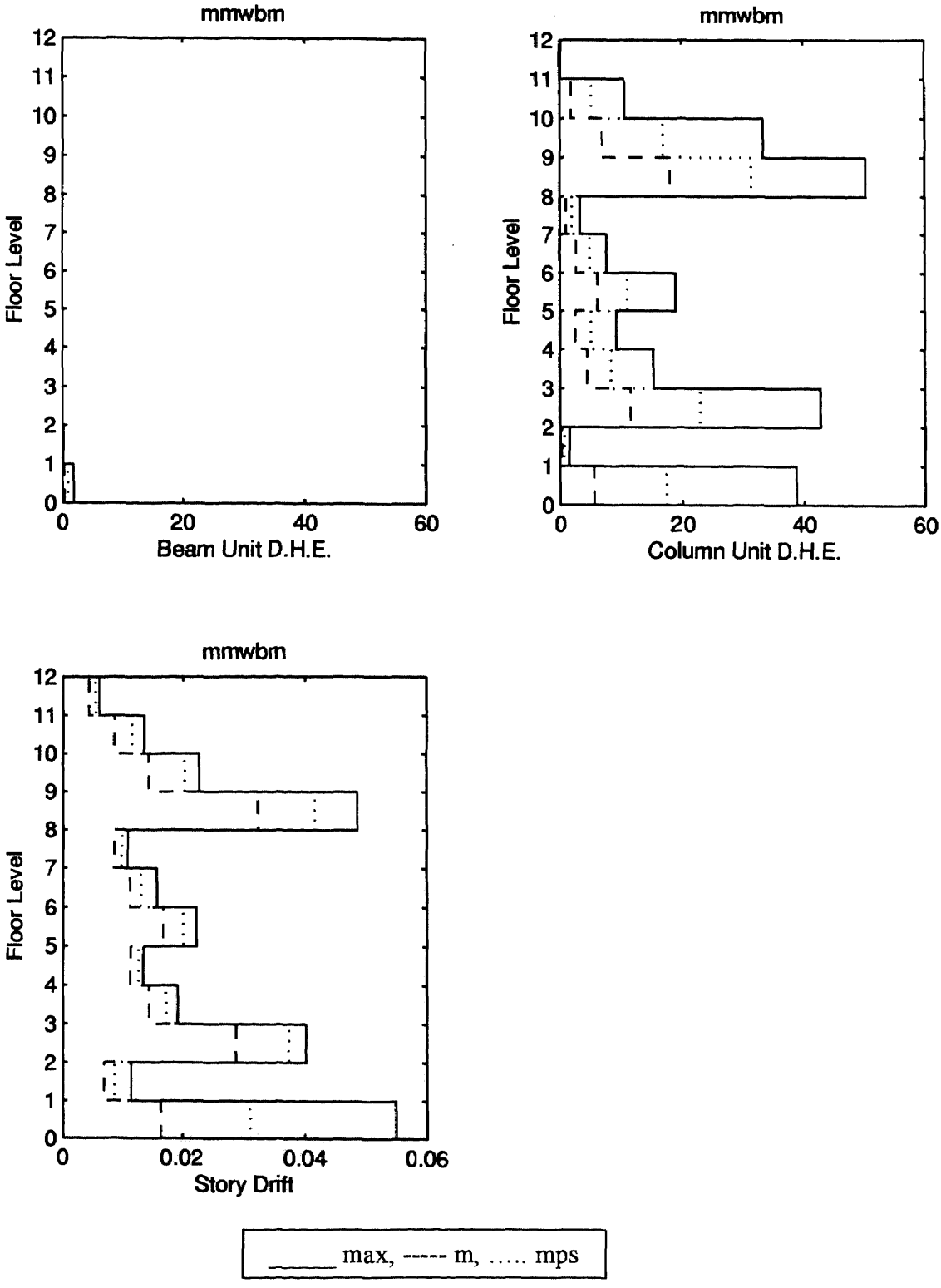

Figure 4.21 Story response of mmwbm: dissipated hysteretic energy and interstory drift.

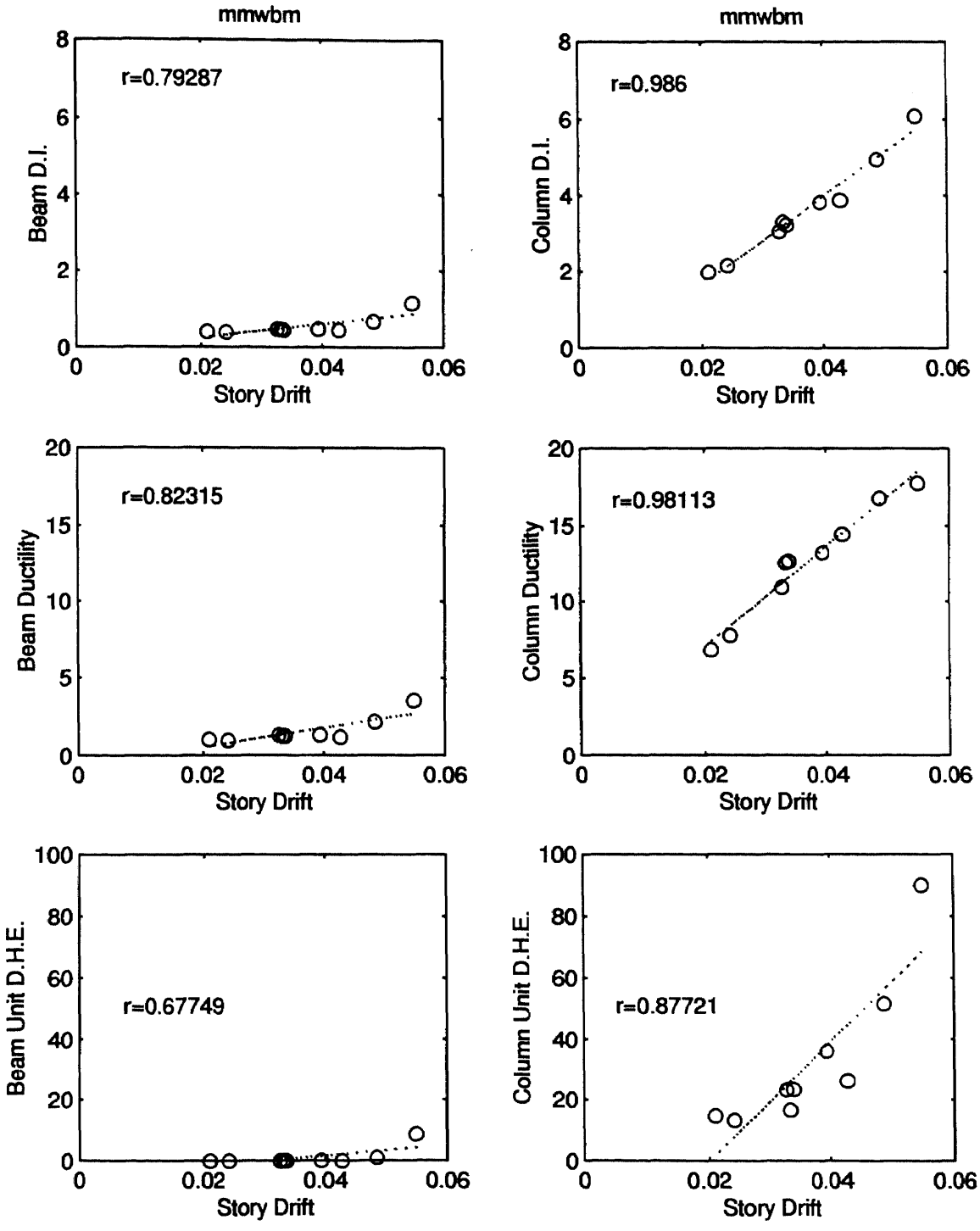

Figure 4.22 Element response of mmwbm.

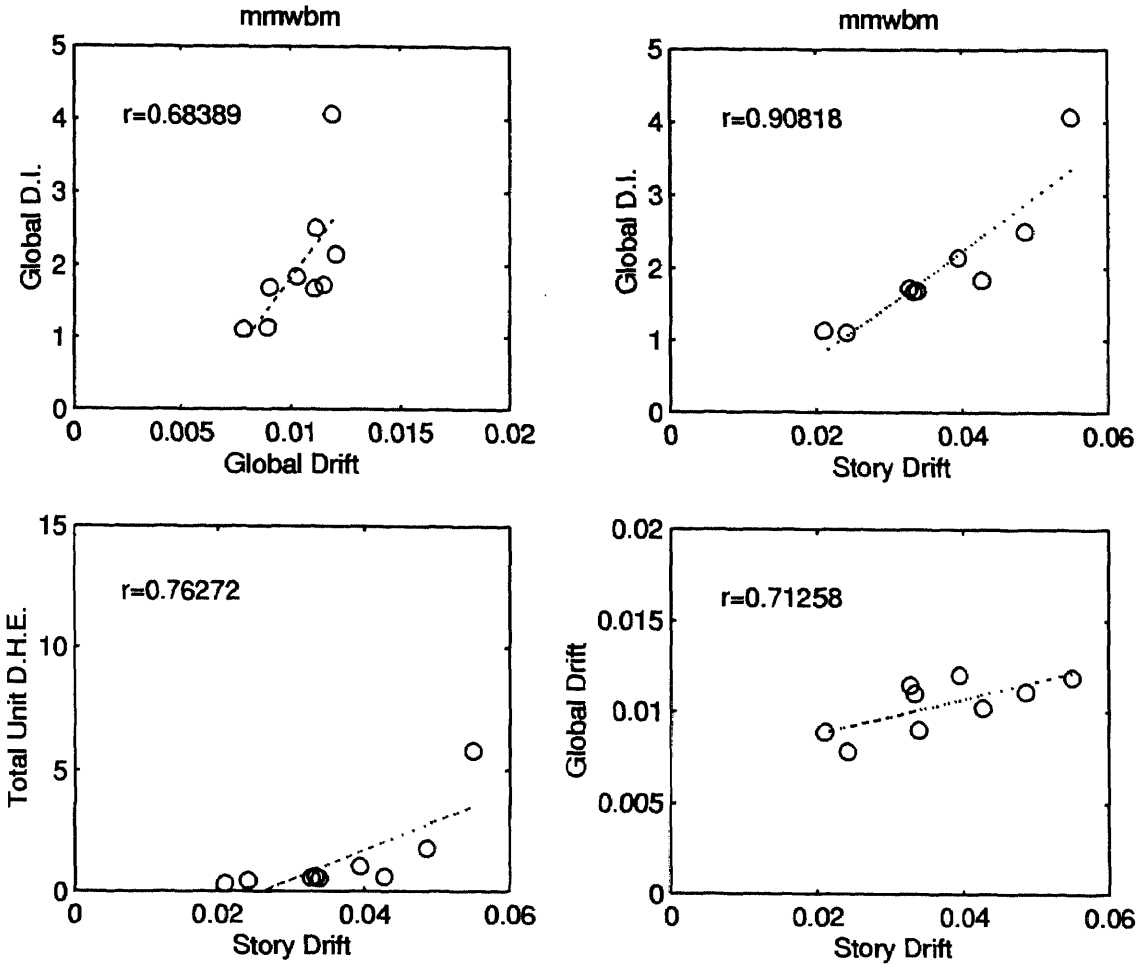

Figure 4.23 Global response of mmwbm.

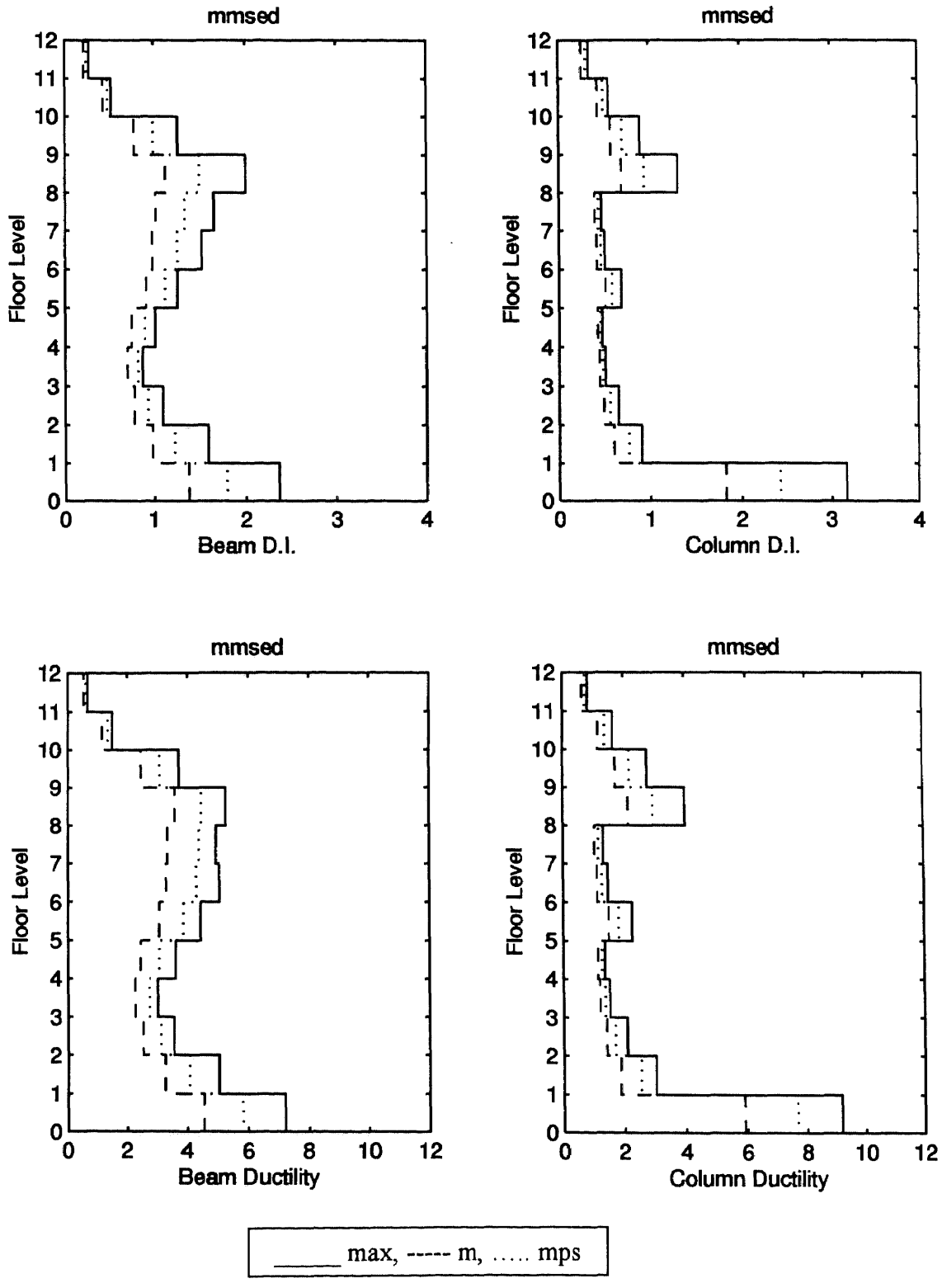

Figure 4.24 Story response of mmsed: damage index and ductility.

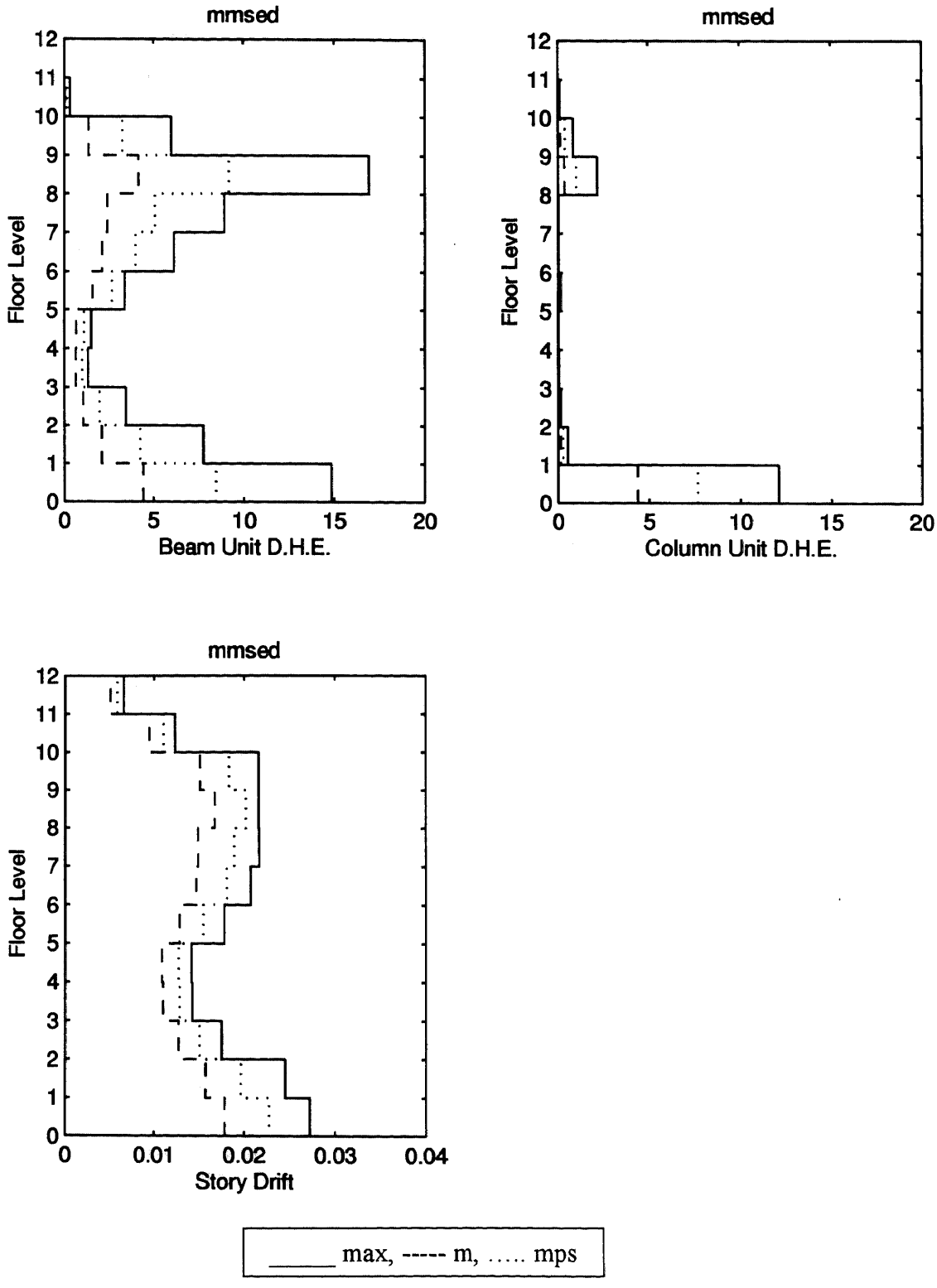

Figure 4.25 Story response of mmsed: dissipated hysteretic energy and interstory drift.

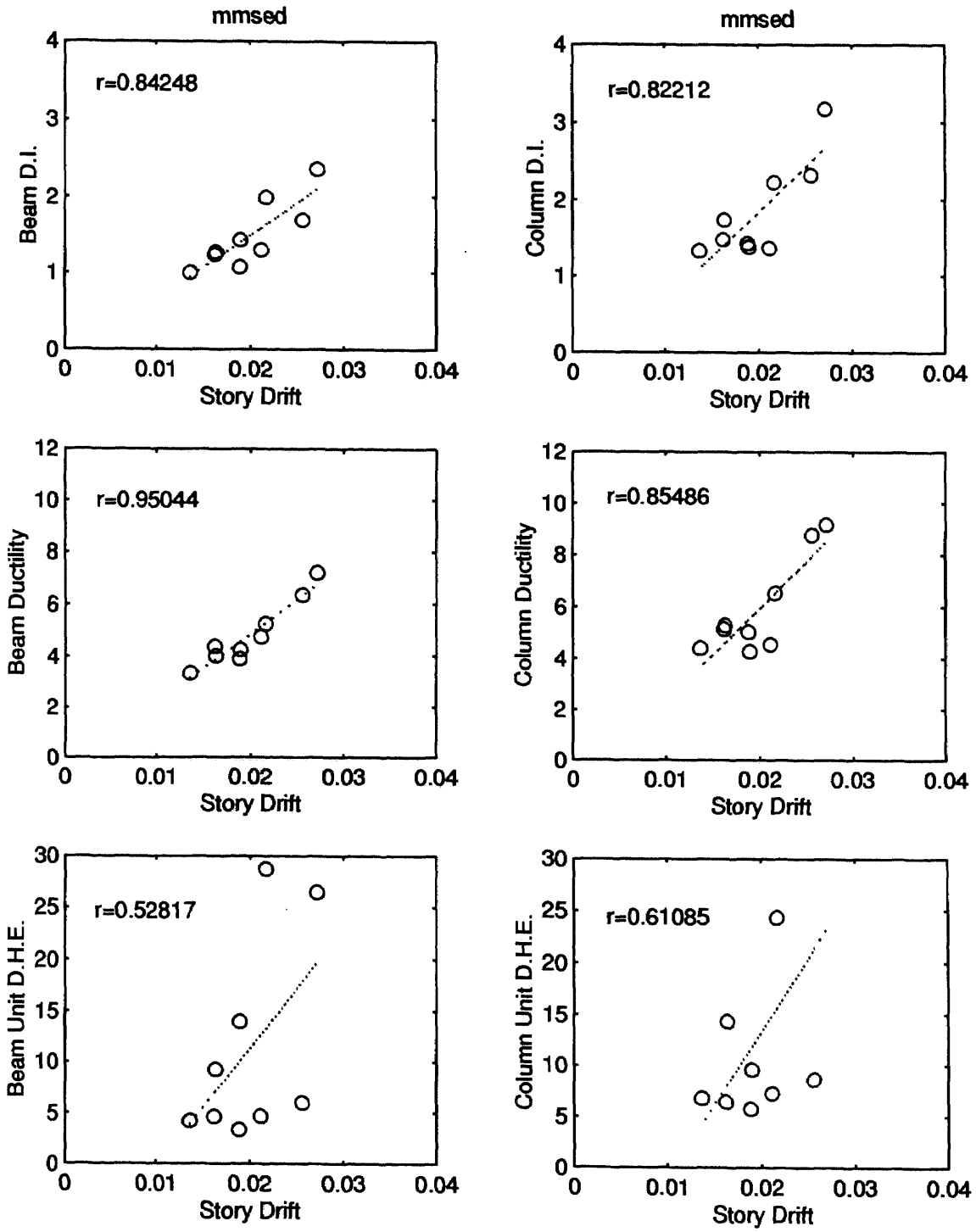

Figure 4.26 Element response of mmsed.

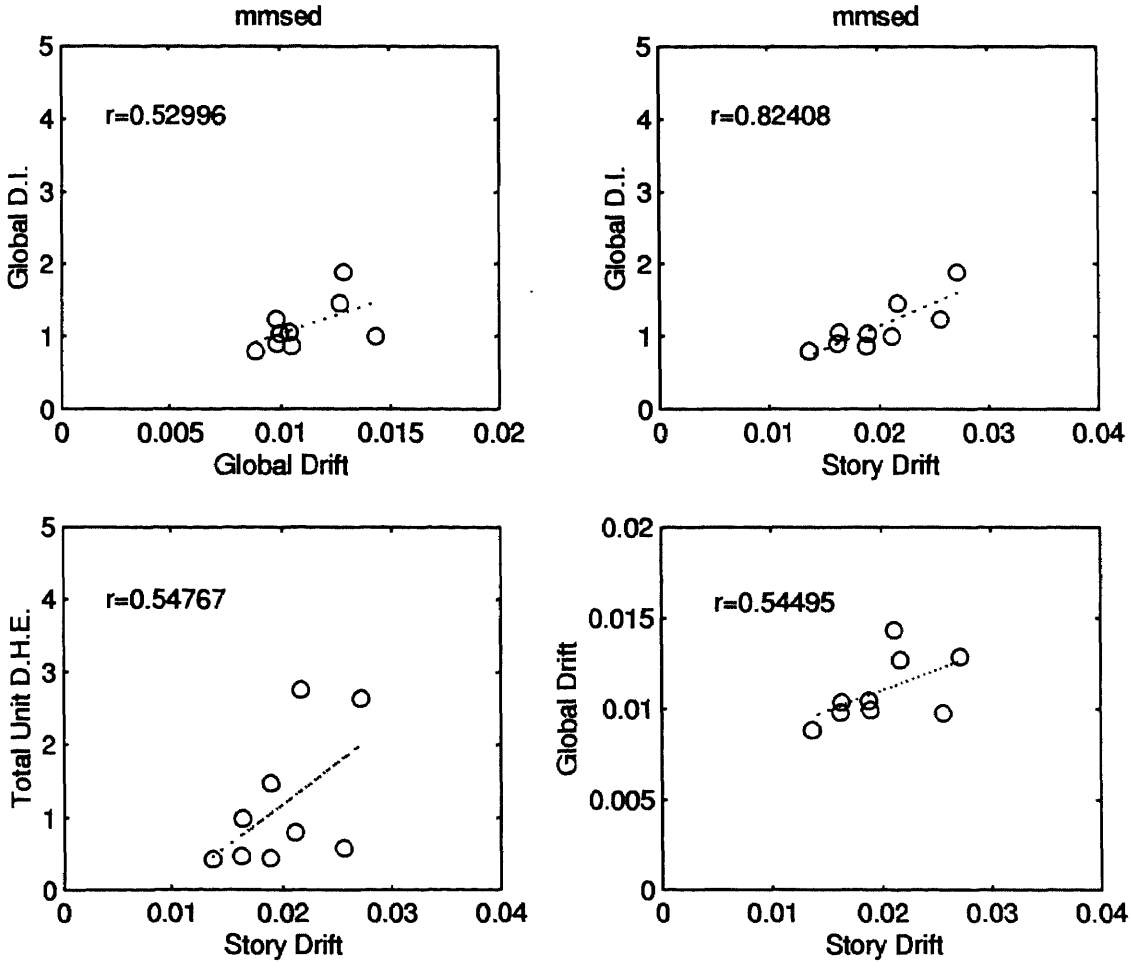

Figure 4.27 Global response of mmsed.

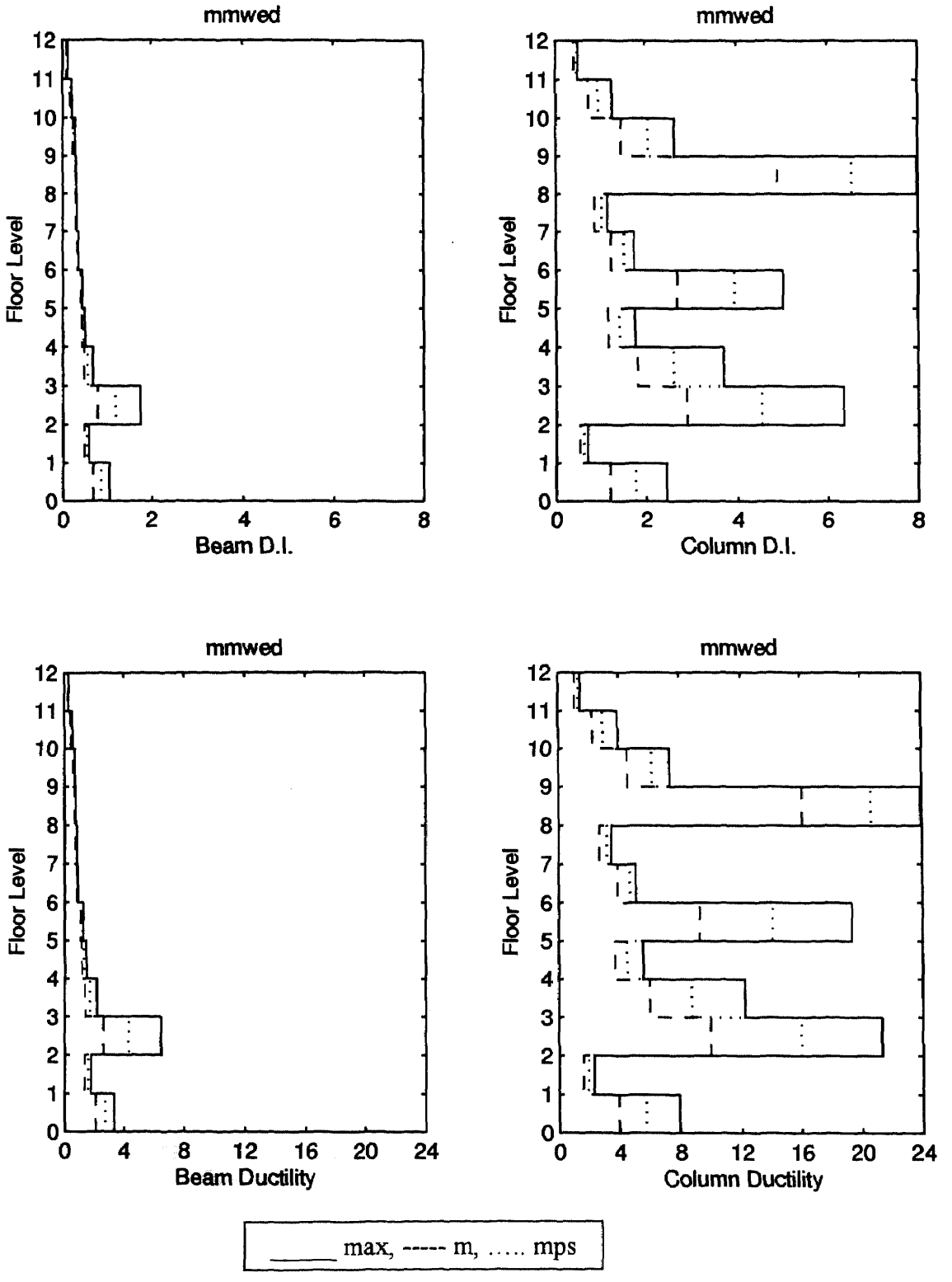

Figure 4.28 Story response of mmwed: damage index and ductility.

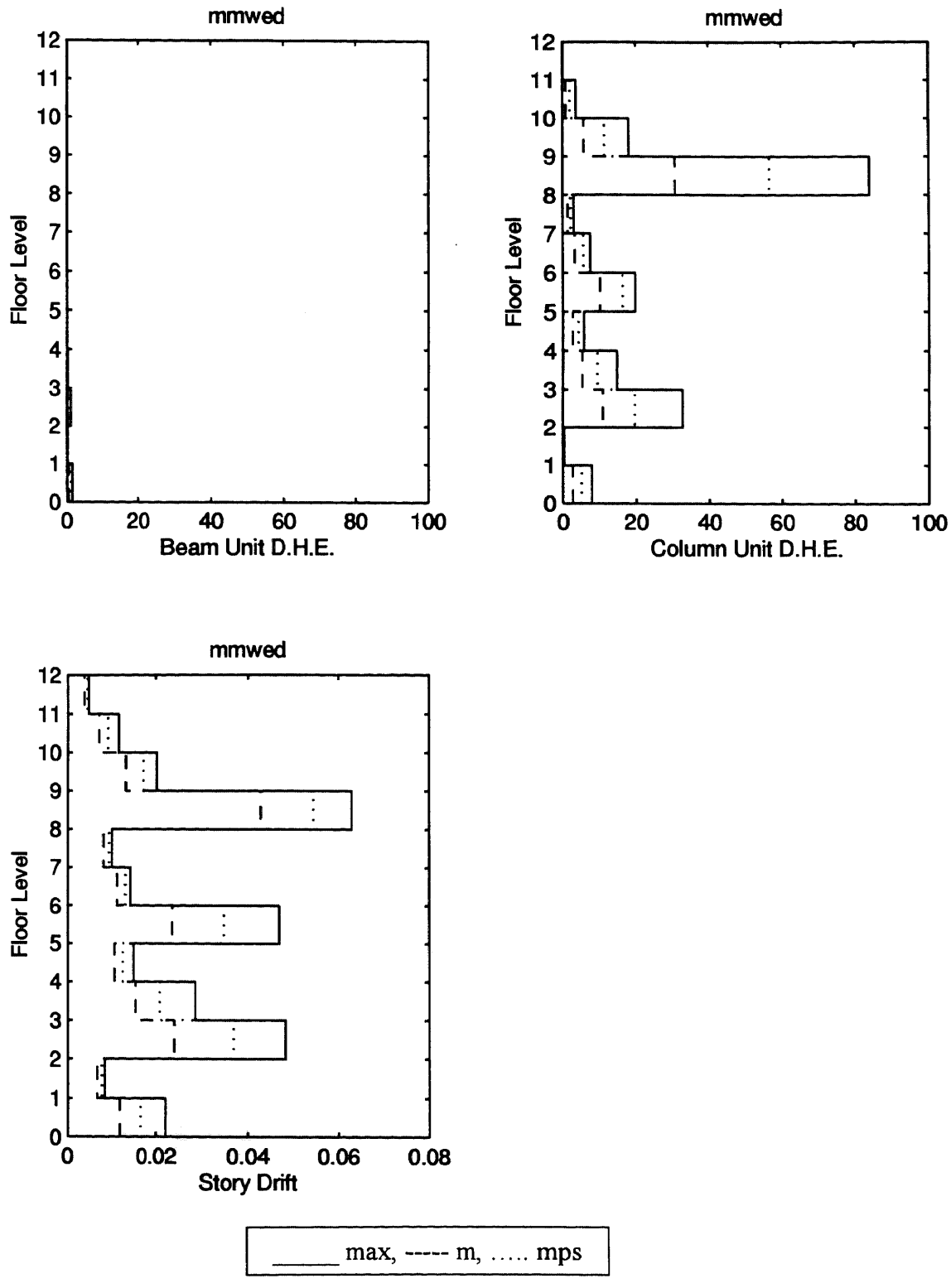

Figure 4.29 Story response of mmwed: dissipated hysteretic energy and interstory drift.

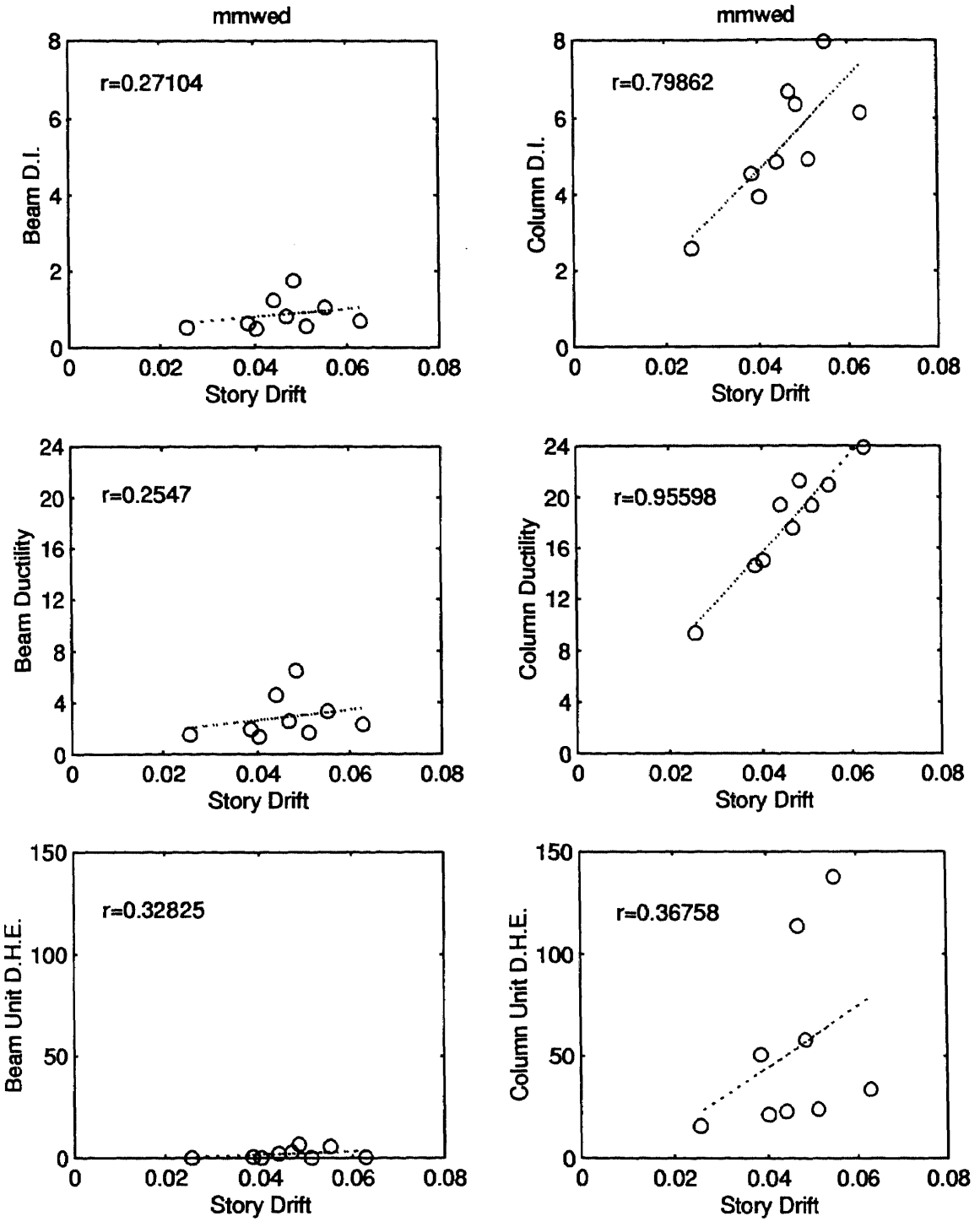

Figure 4.30 Element response of mmwed.

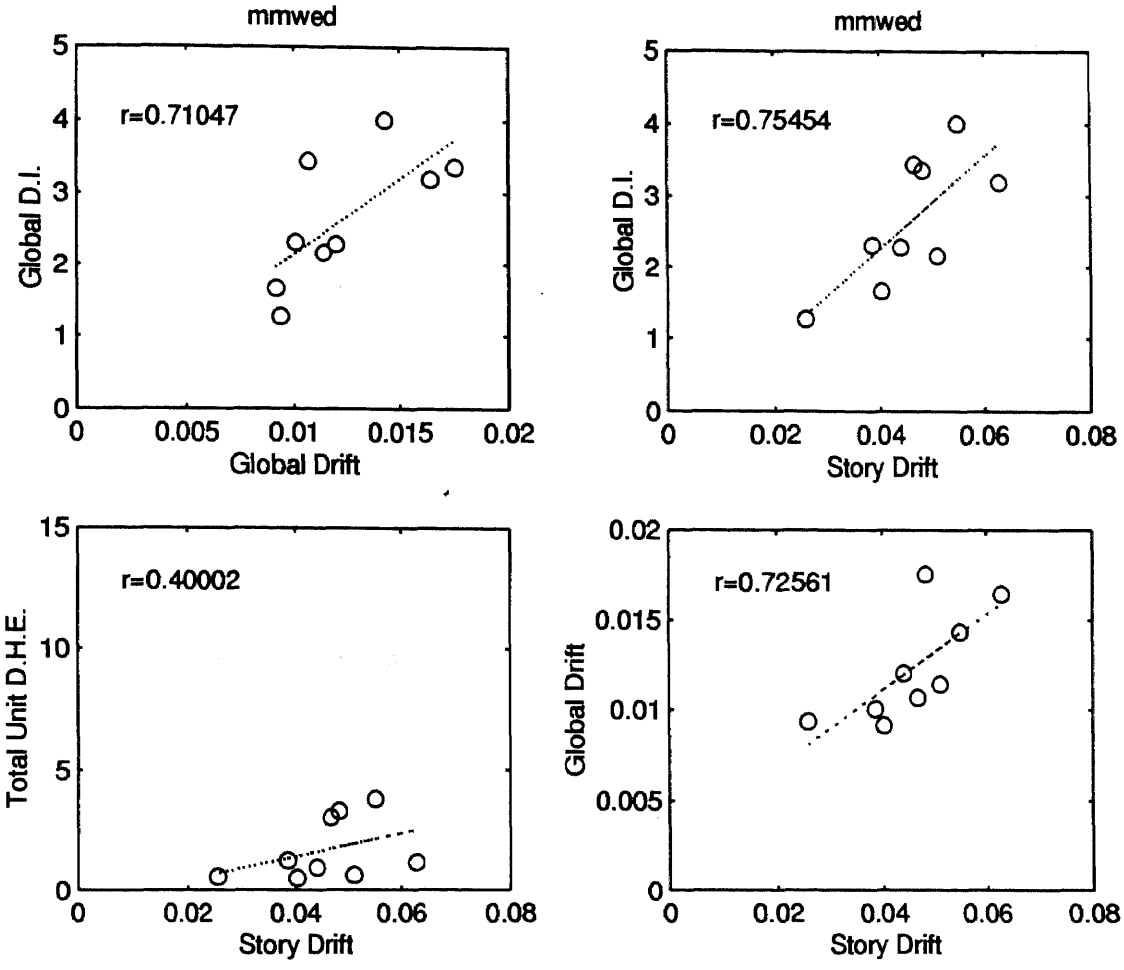

Figure 4.31 Global response of mmwed.

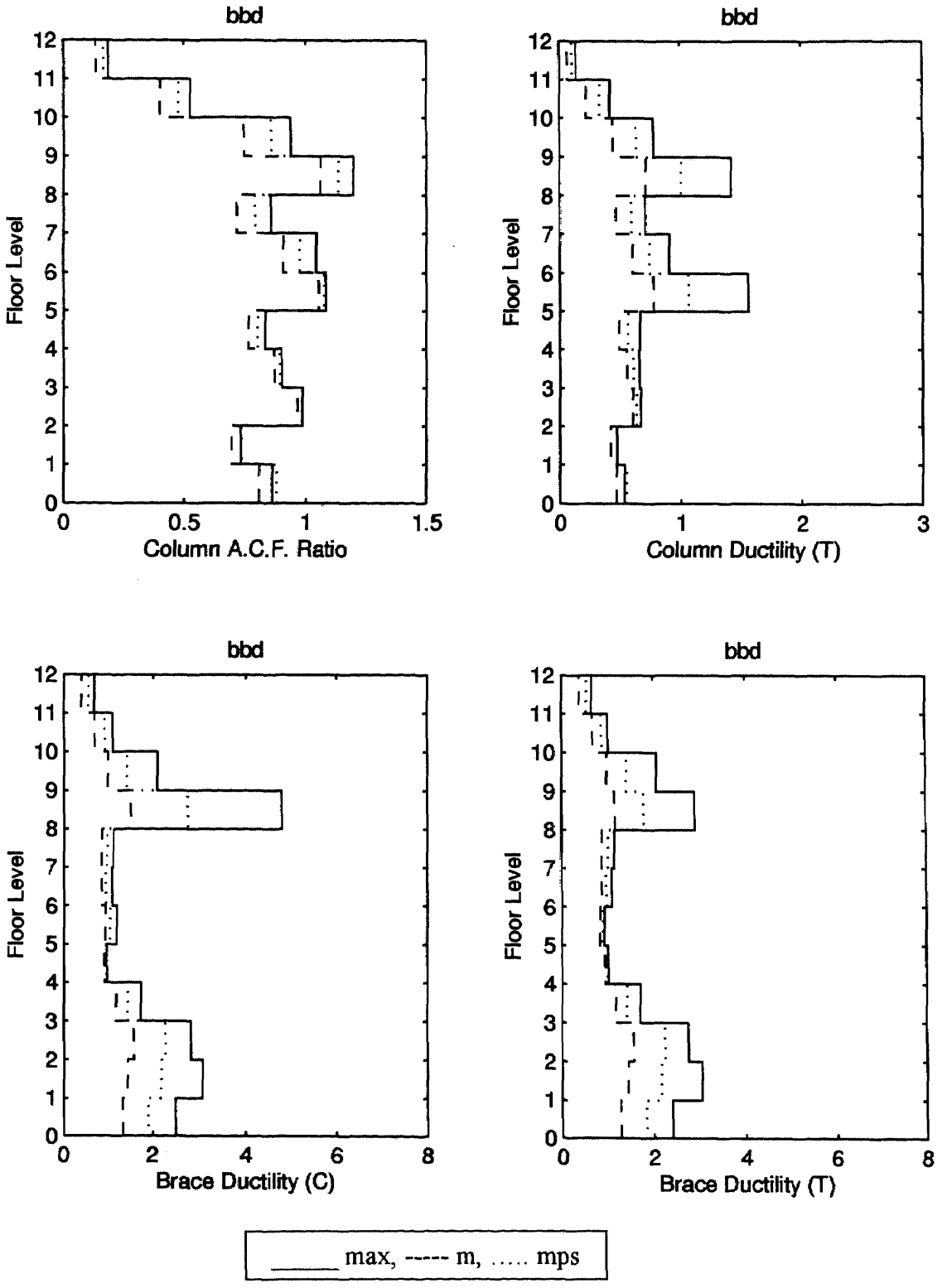

Figure 4.32 Story response of bbd: axial compressive force ratio and ductility.

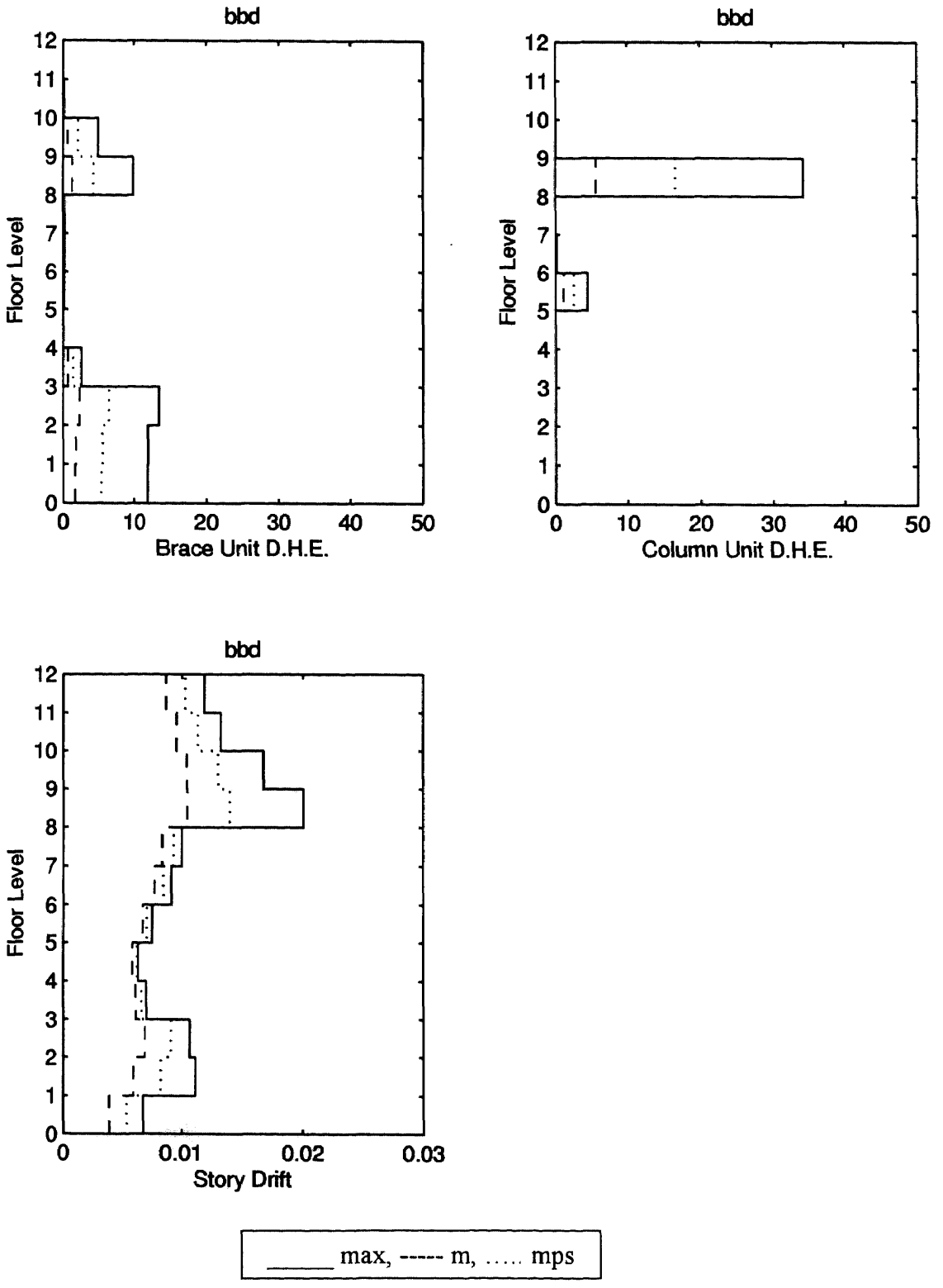

Figure 4.33 Story response of bbd: dissipated hysteretic energy and interstory drift.

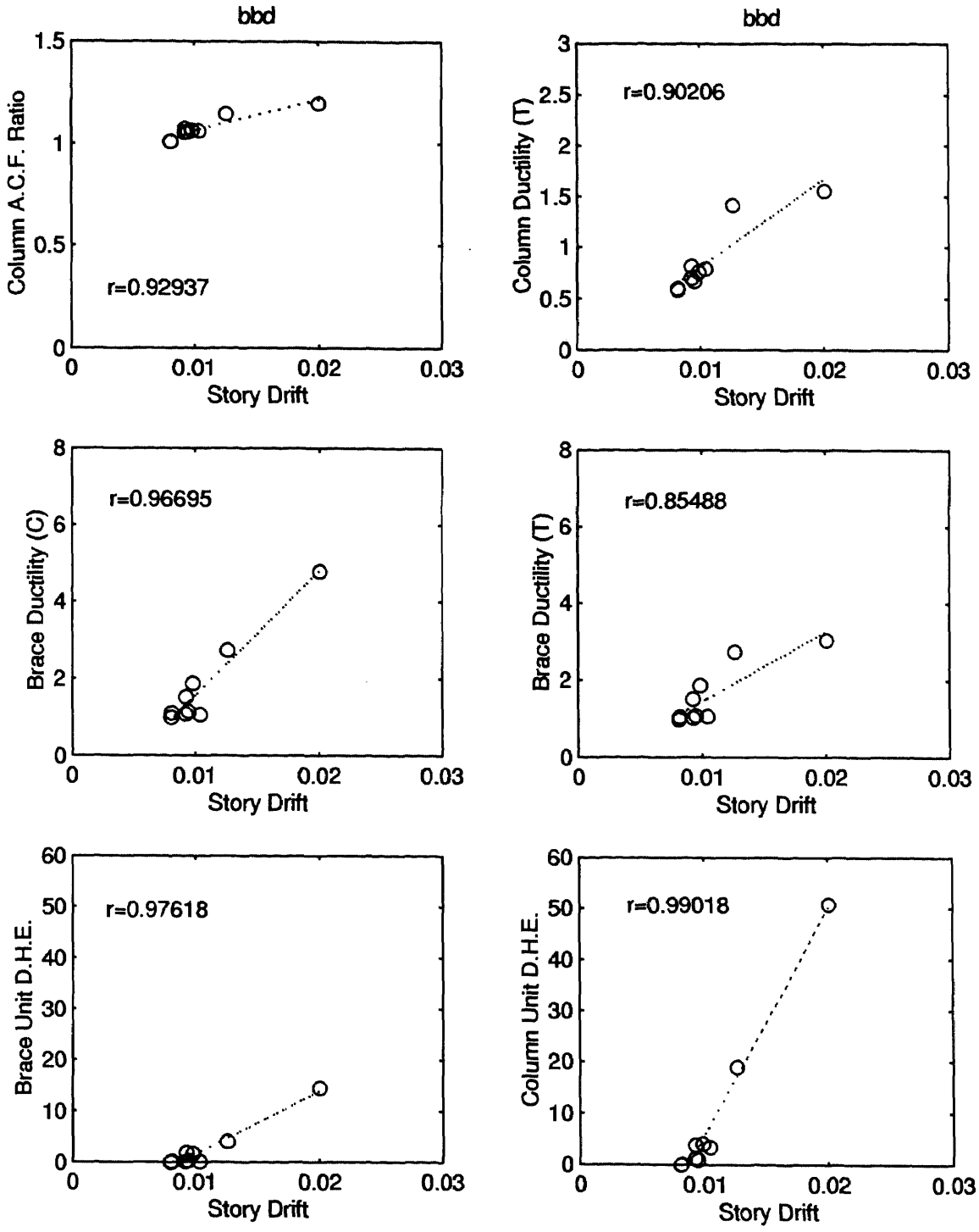

Figure 4.34 Element response of bbd.

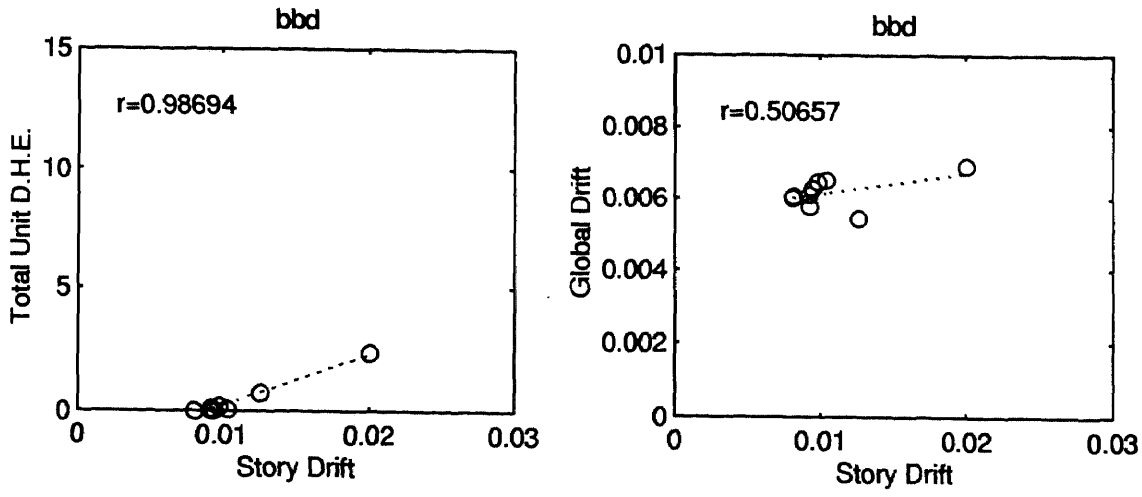

Figure 4.35 Global response of bbd.

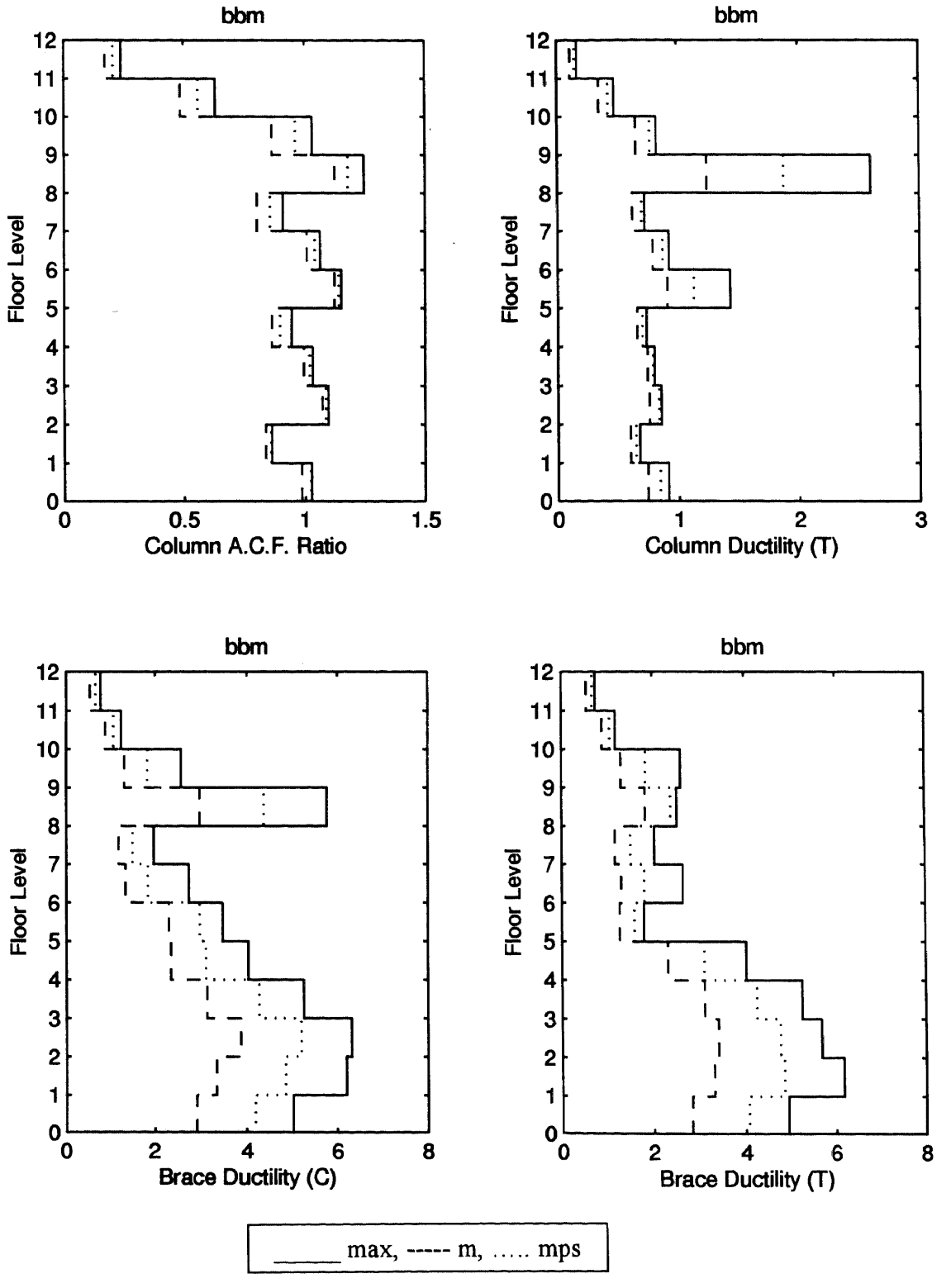

Figure 4.36 Story response of bbm: axial compressive force ratio and ductility.

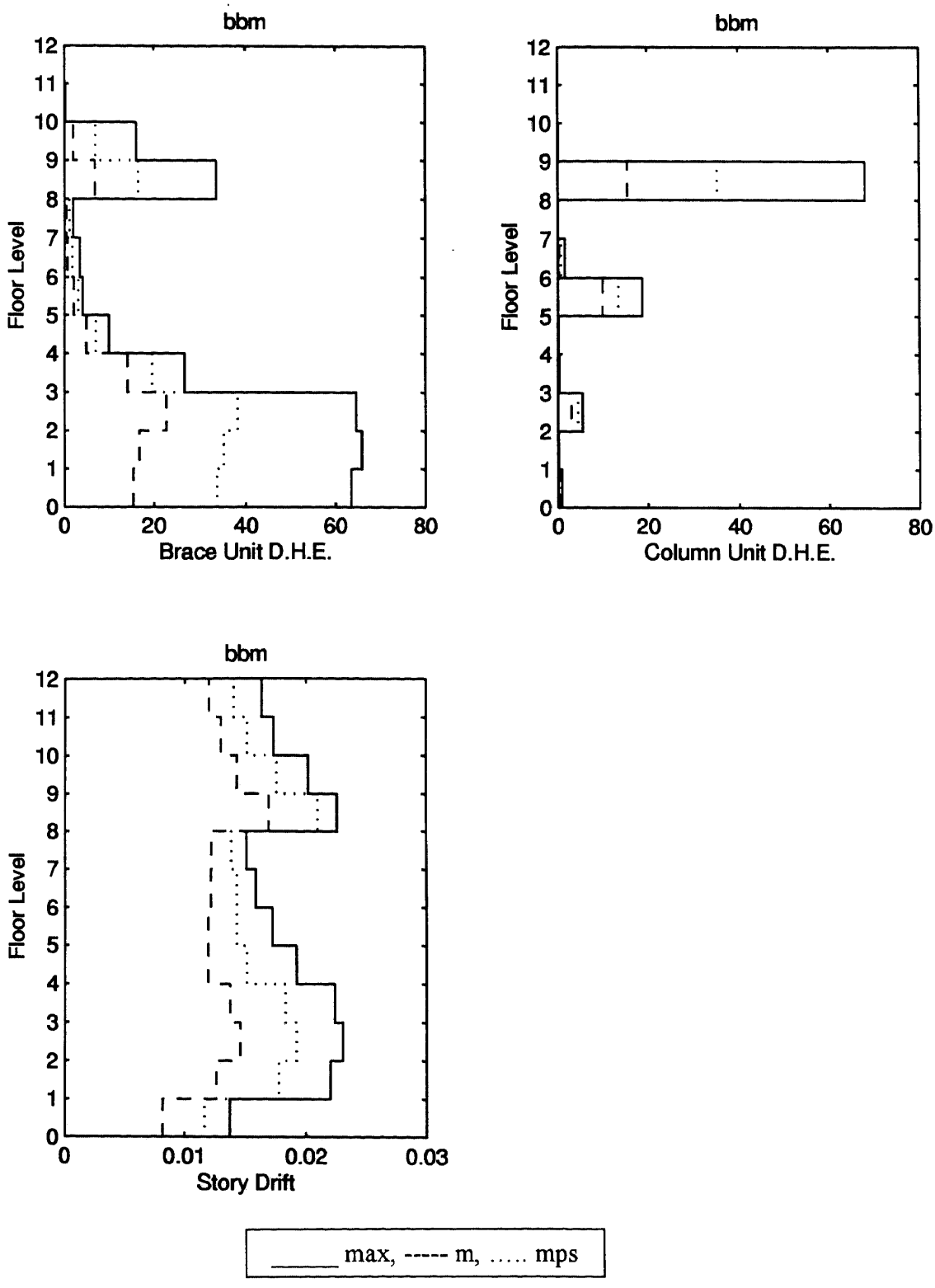

Figure 4.37 Story response of bbm: dissipated hysteretic energy and interstory drift.

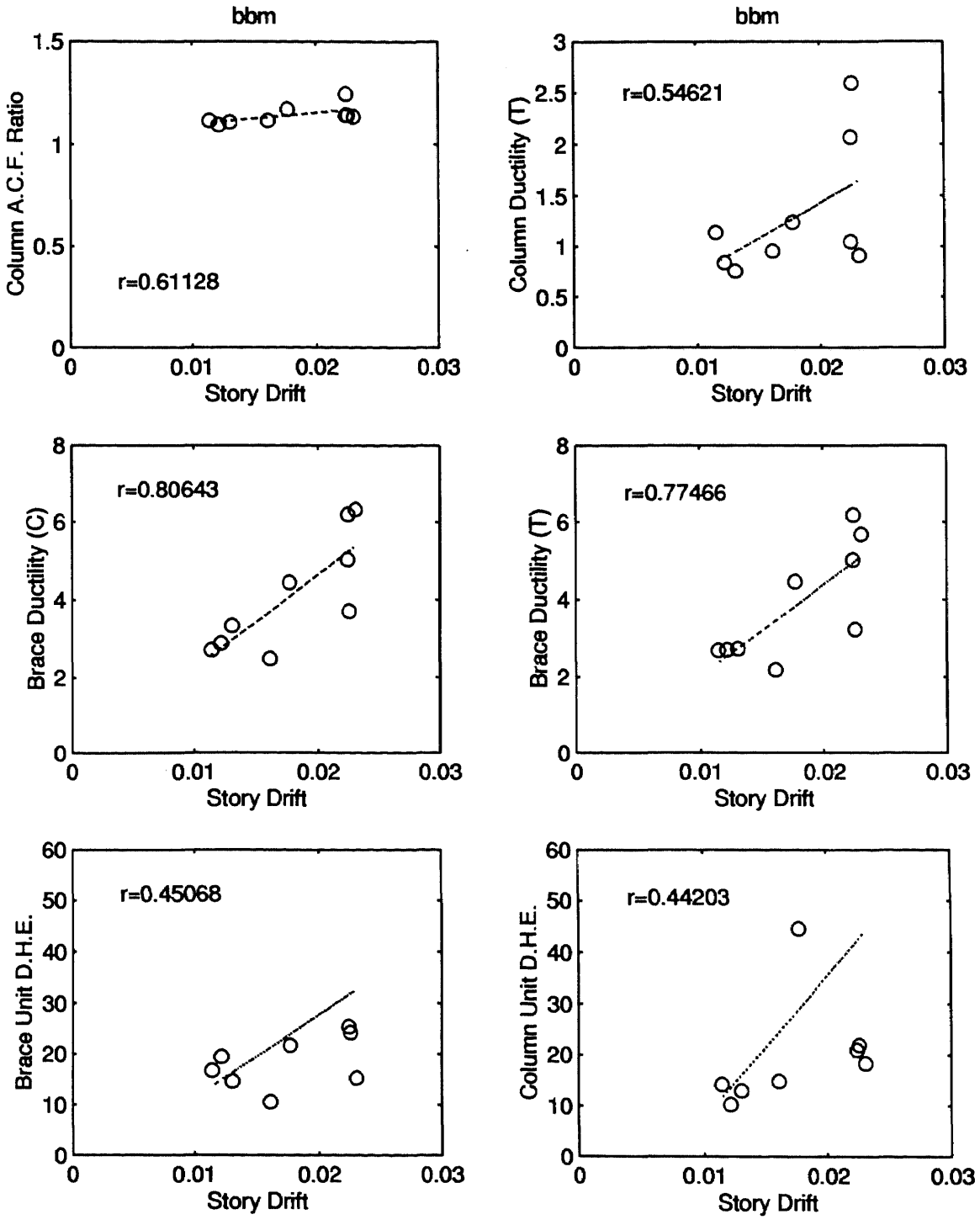

Figure 4.38 Element response of bbm.

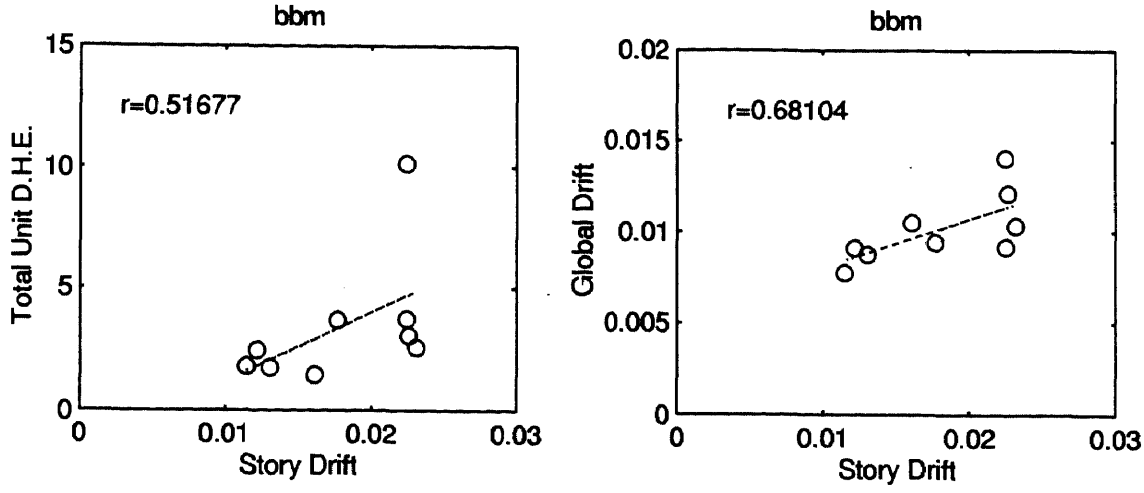

Figure 4.39 Global response of bbm.

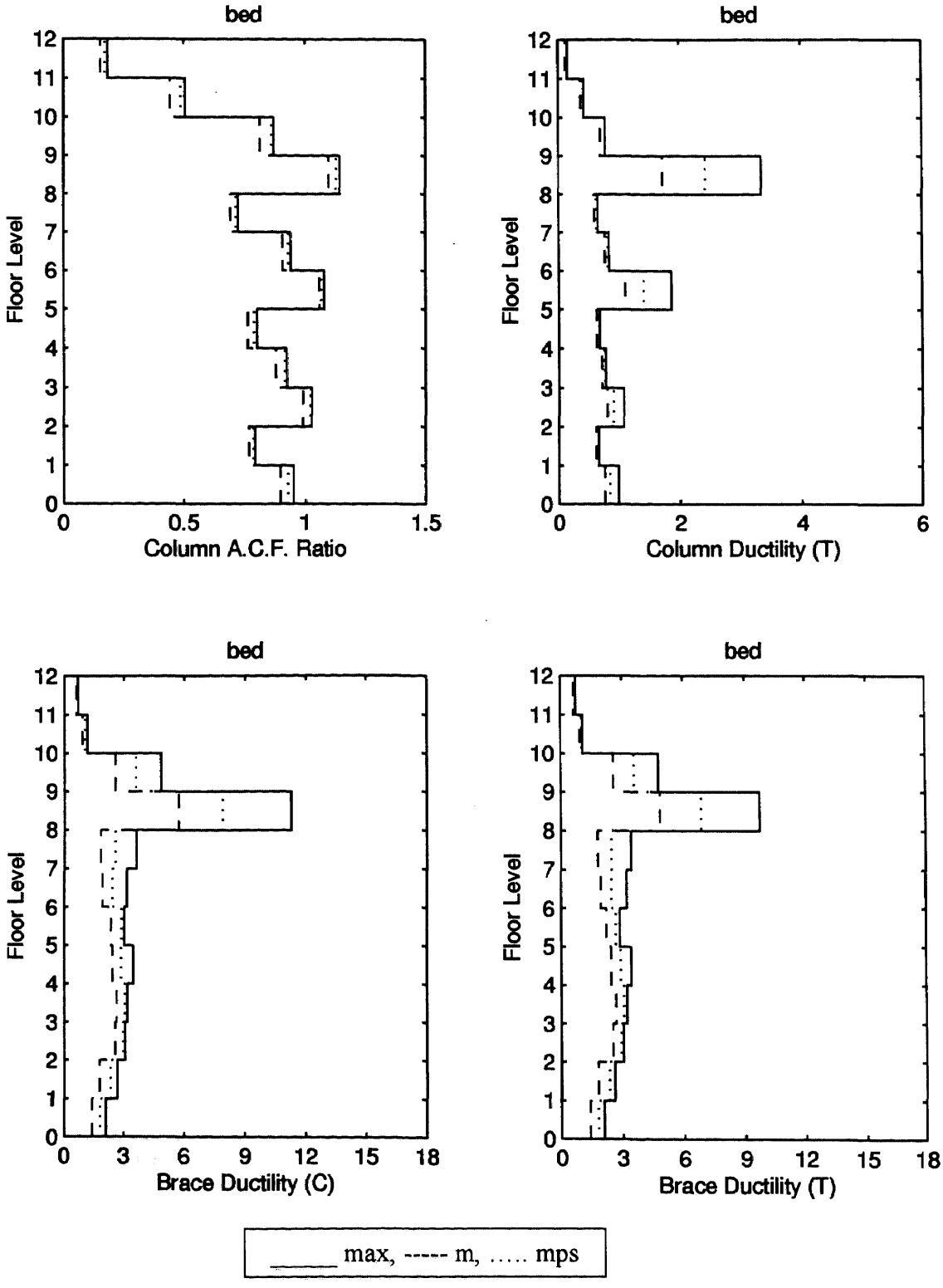

Figure 4.40 Story response of bed: axial compressive force ratio and ductility.

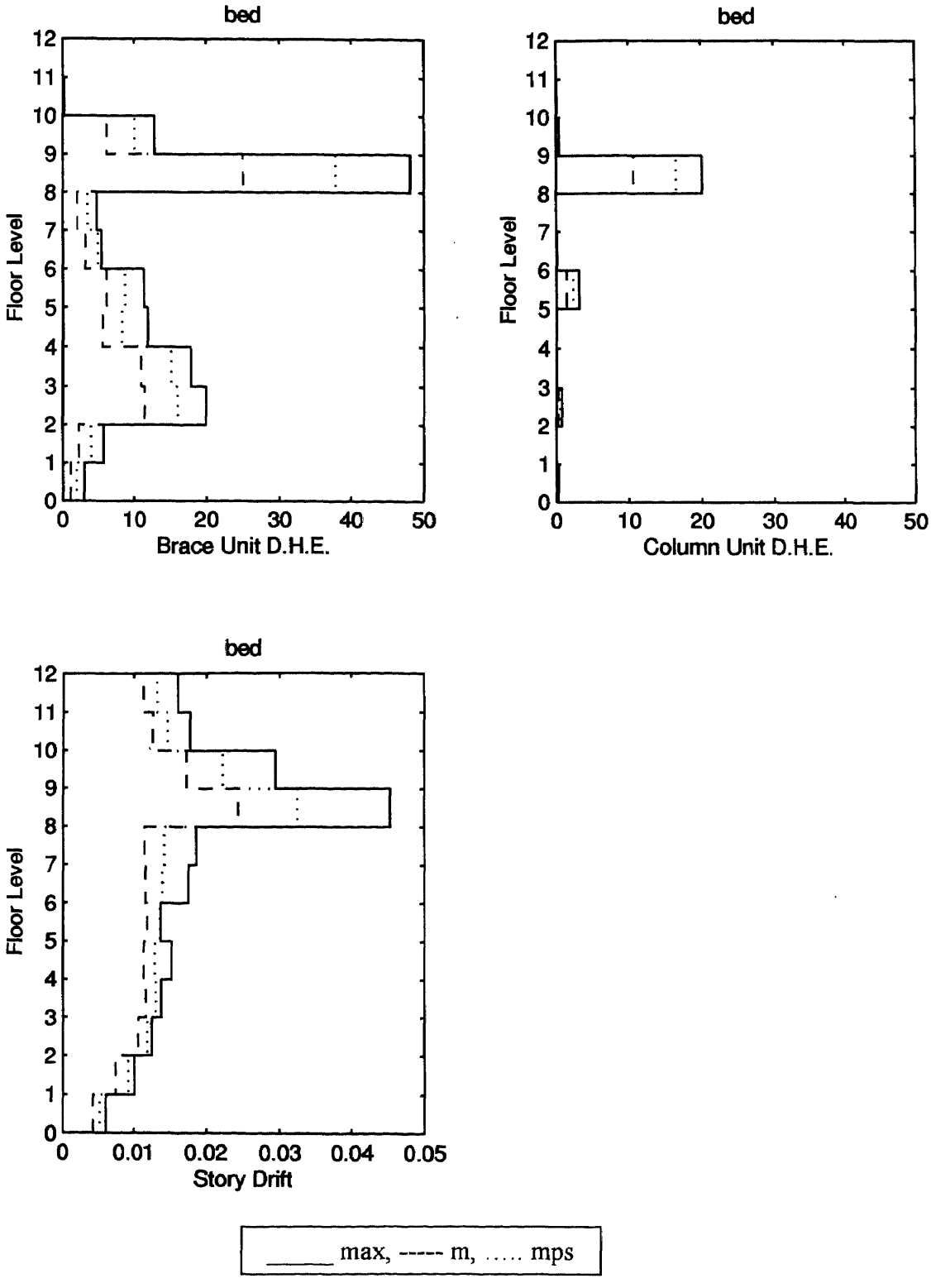

Figure 4.41 Story response of bed: dissipated hysteretic energy and interstory drift.

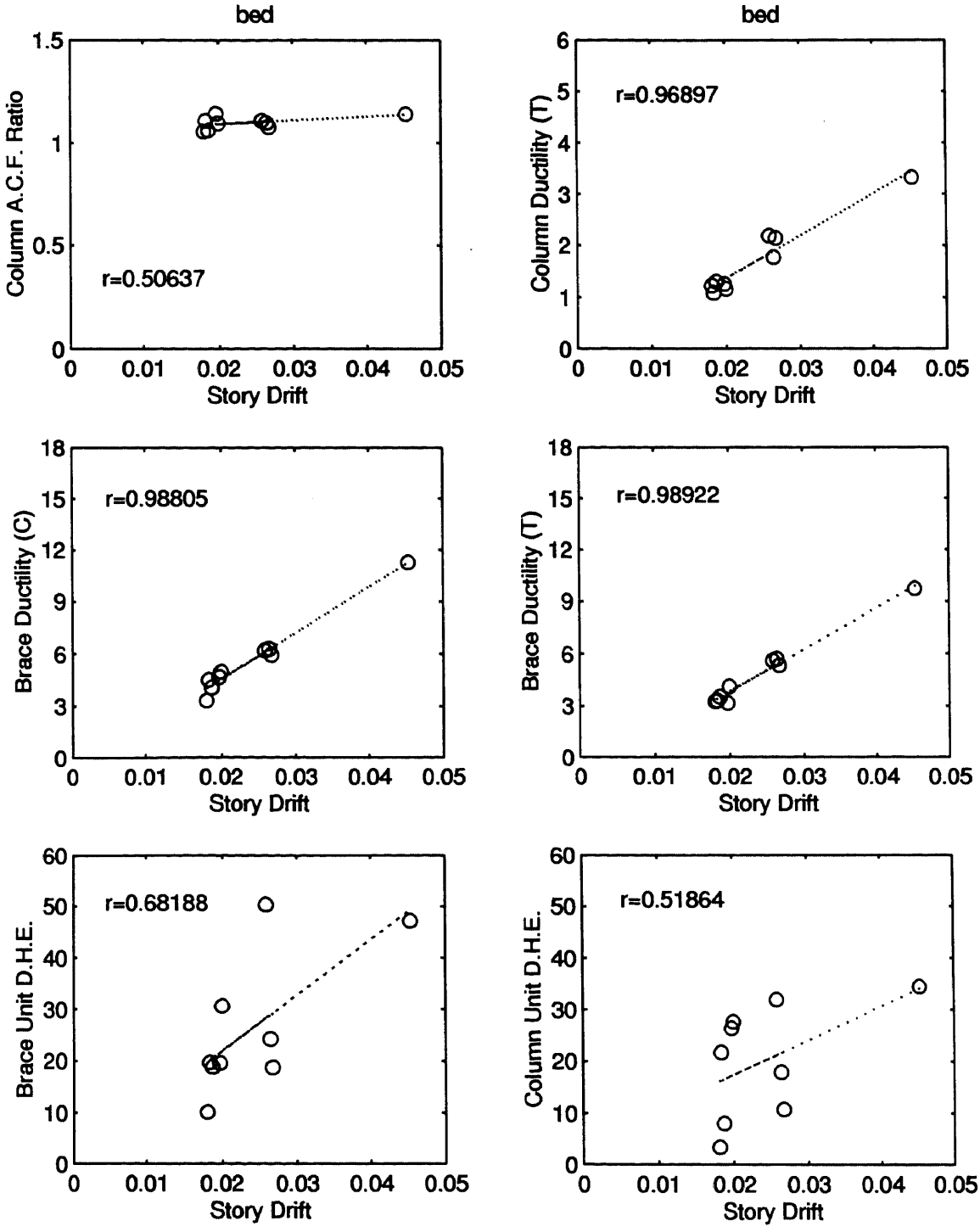

Figure 4.42 Element response of bed.

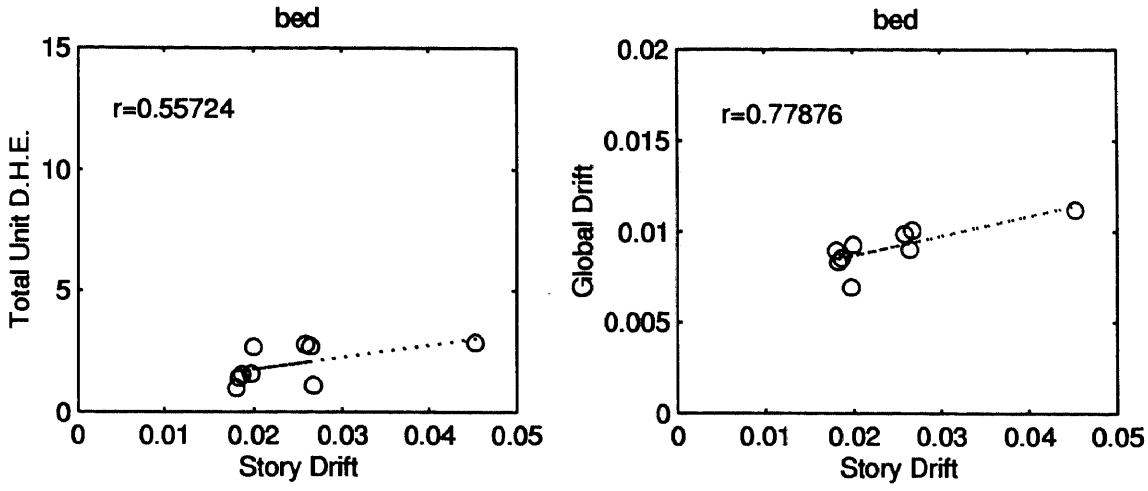

Figure 4.43 Global response of bed.

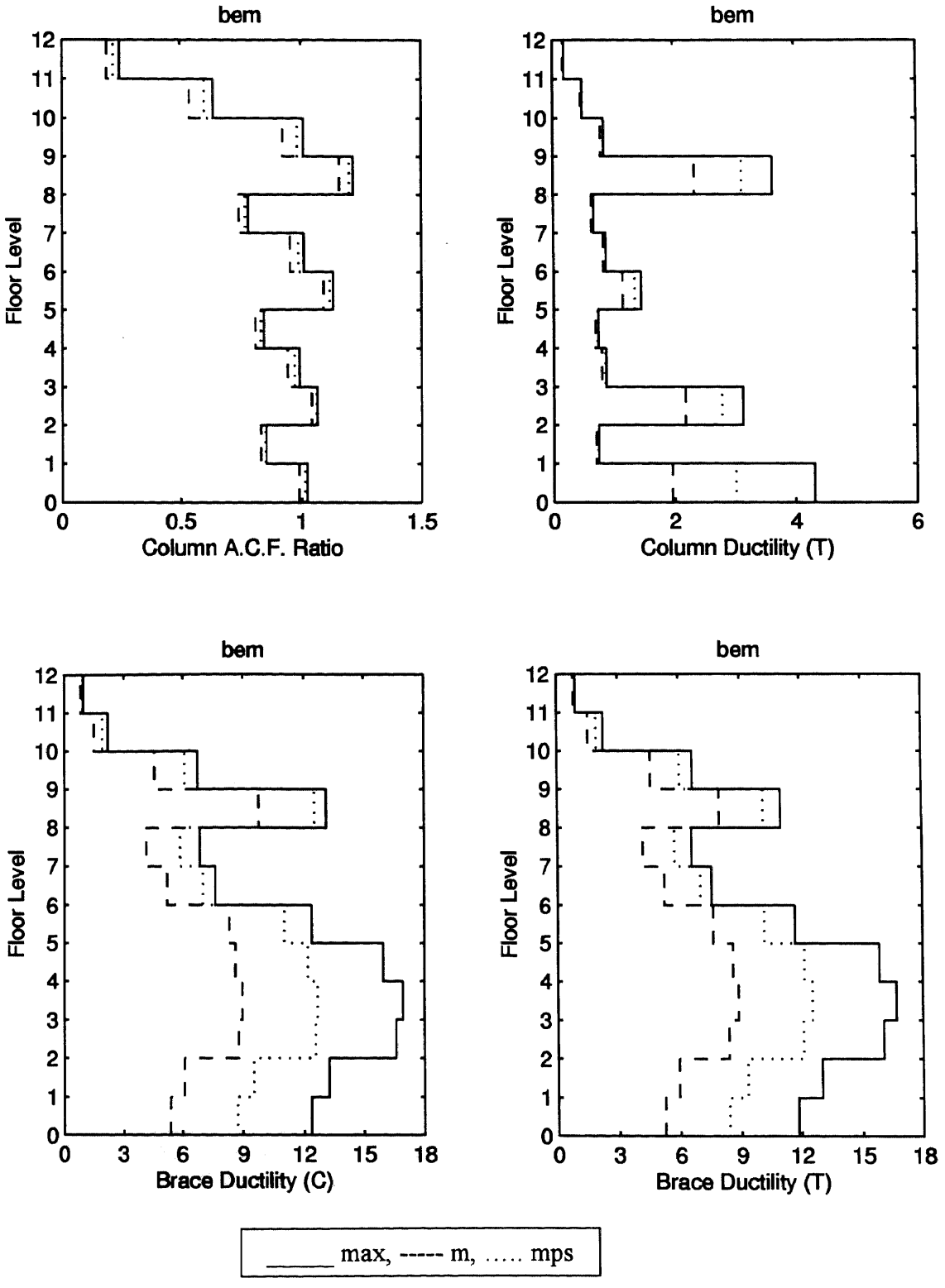

Figure 4.44 Story response of bem: axial compressive force ratio and ductility.

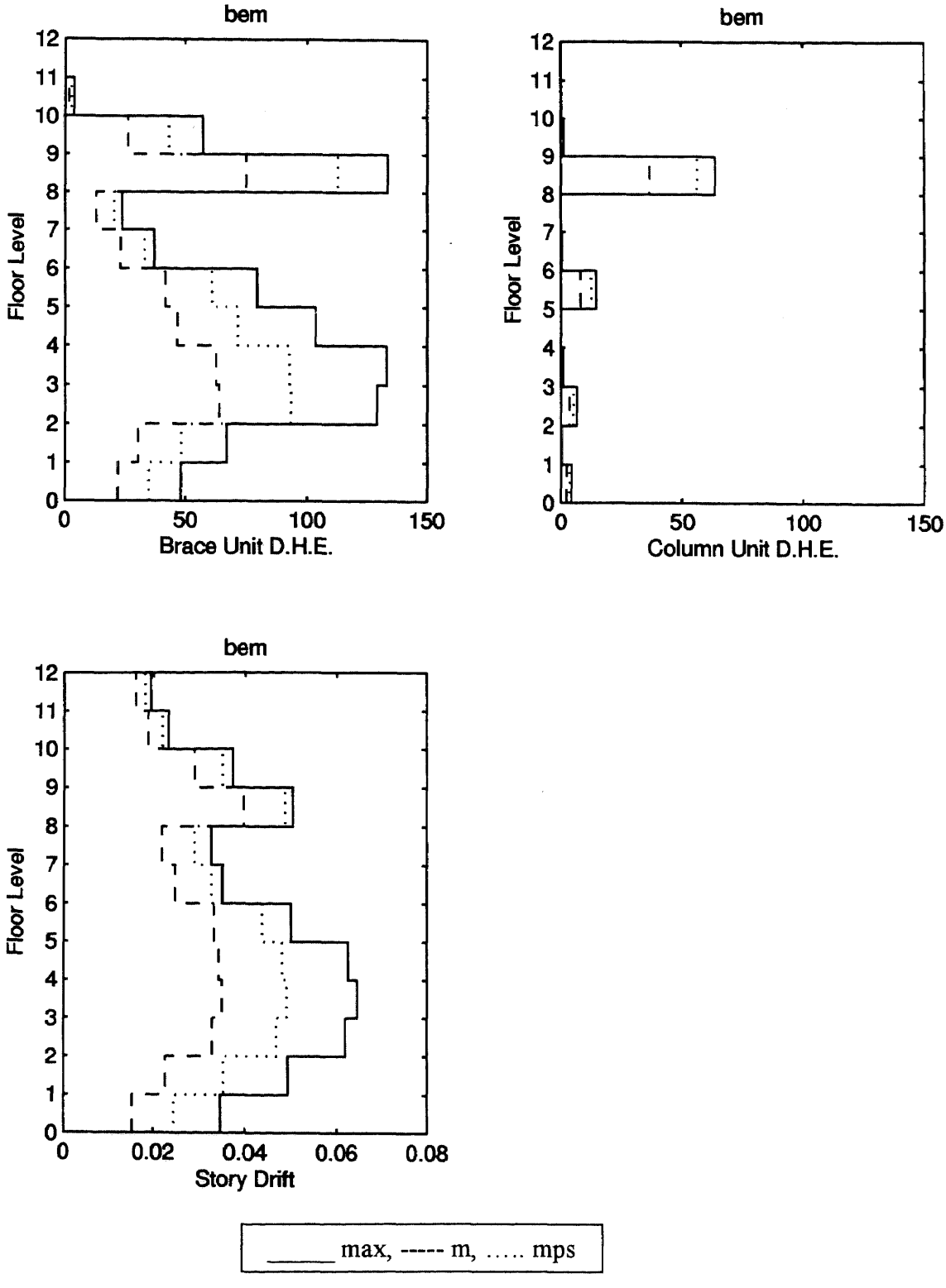

Figure 4.45 Story response of bem: dissipated hysteretic energy and interstory drift.

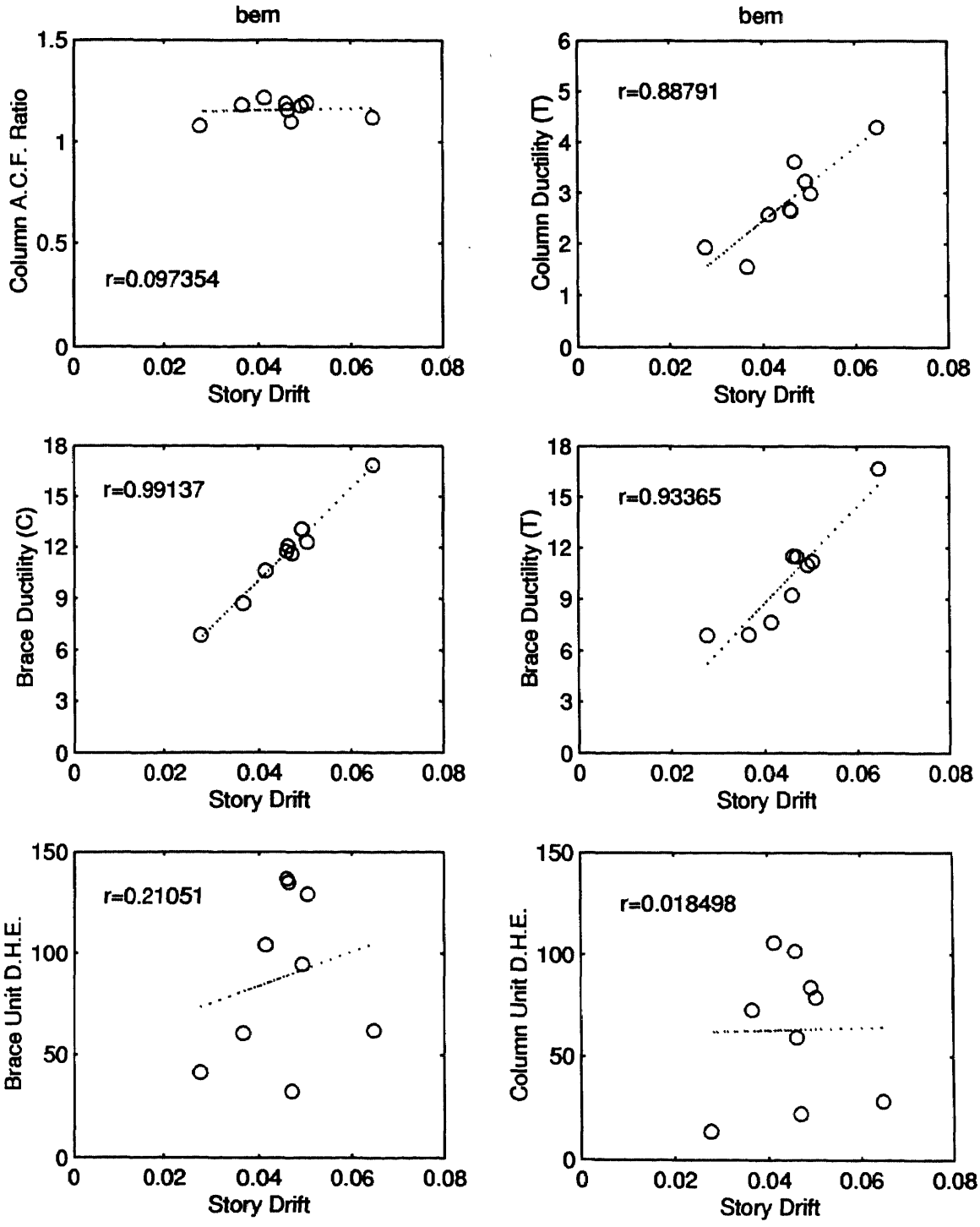

Figure 4.46 Element response of bem.

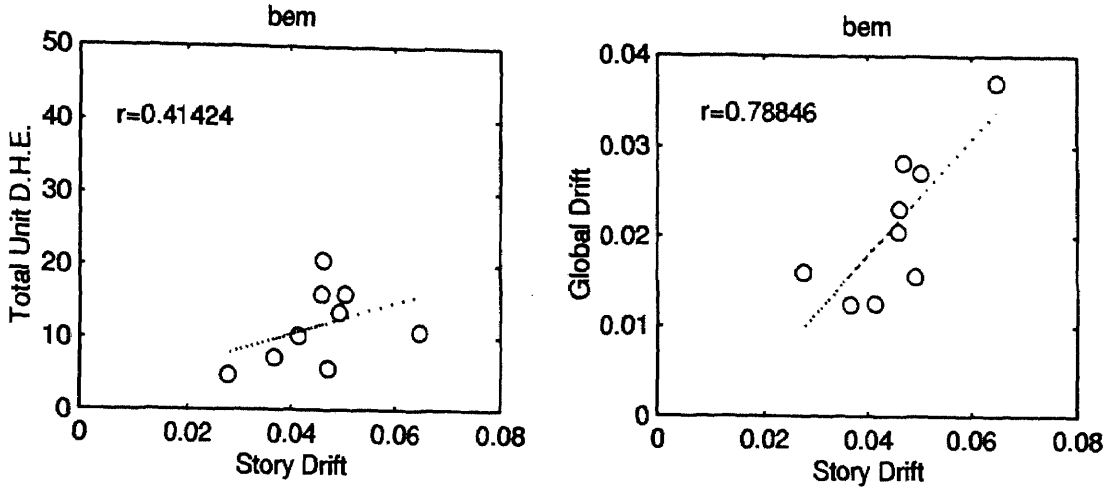

Figure 4.47 Global response of bem.

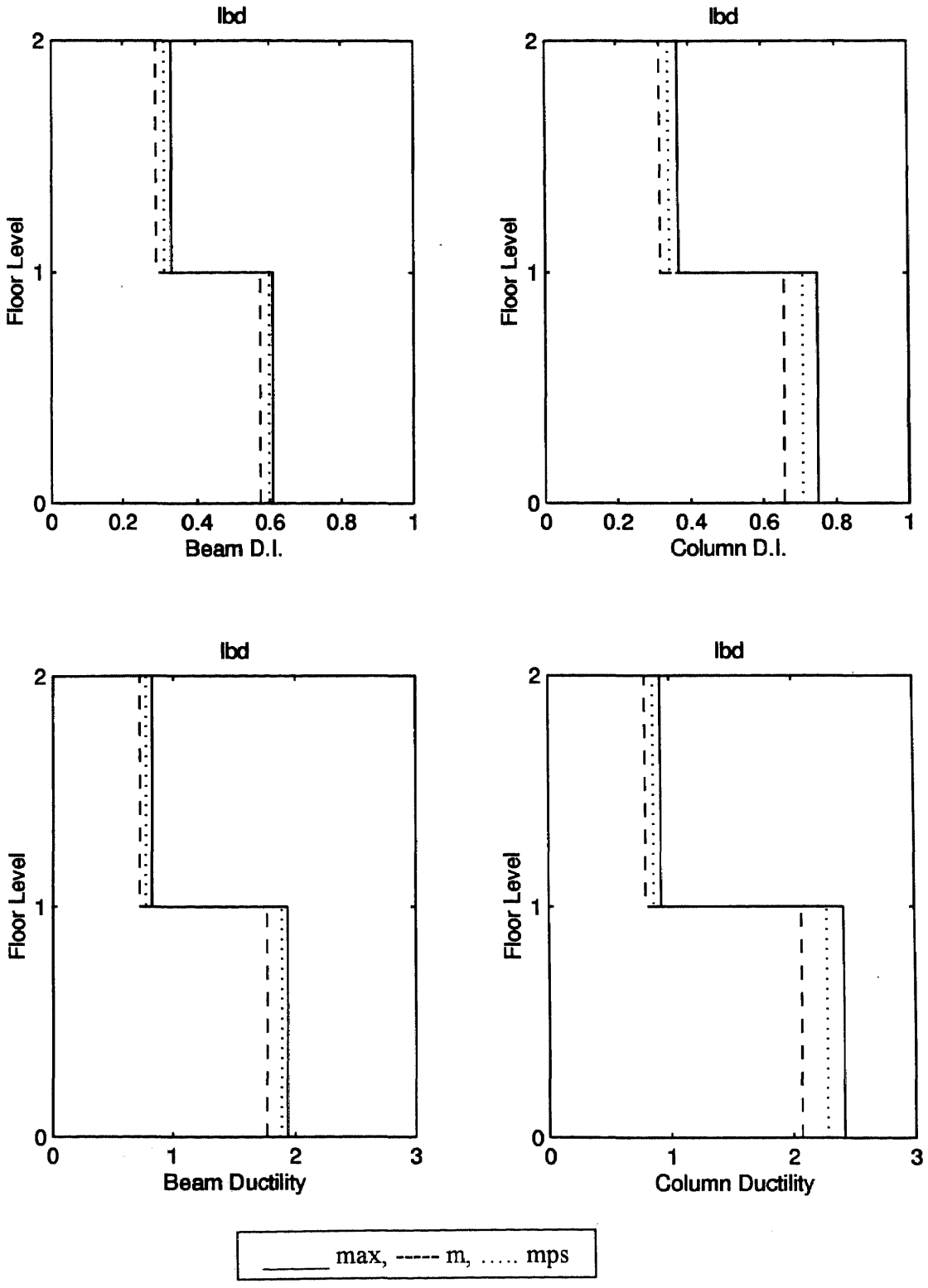

Figure 4.48 Story response of lbd: damage index and ductility.

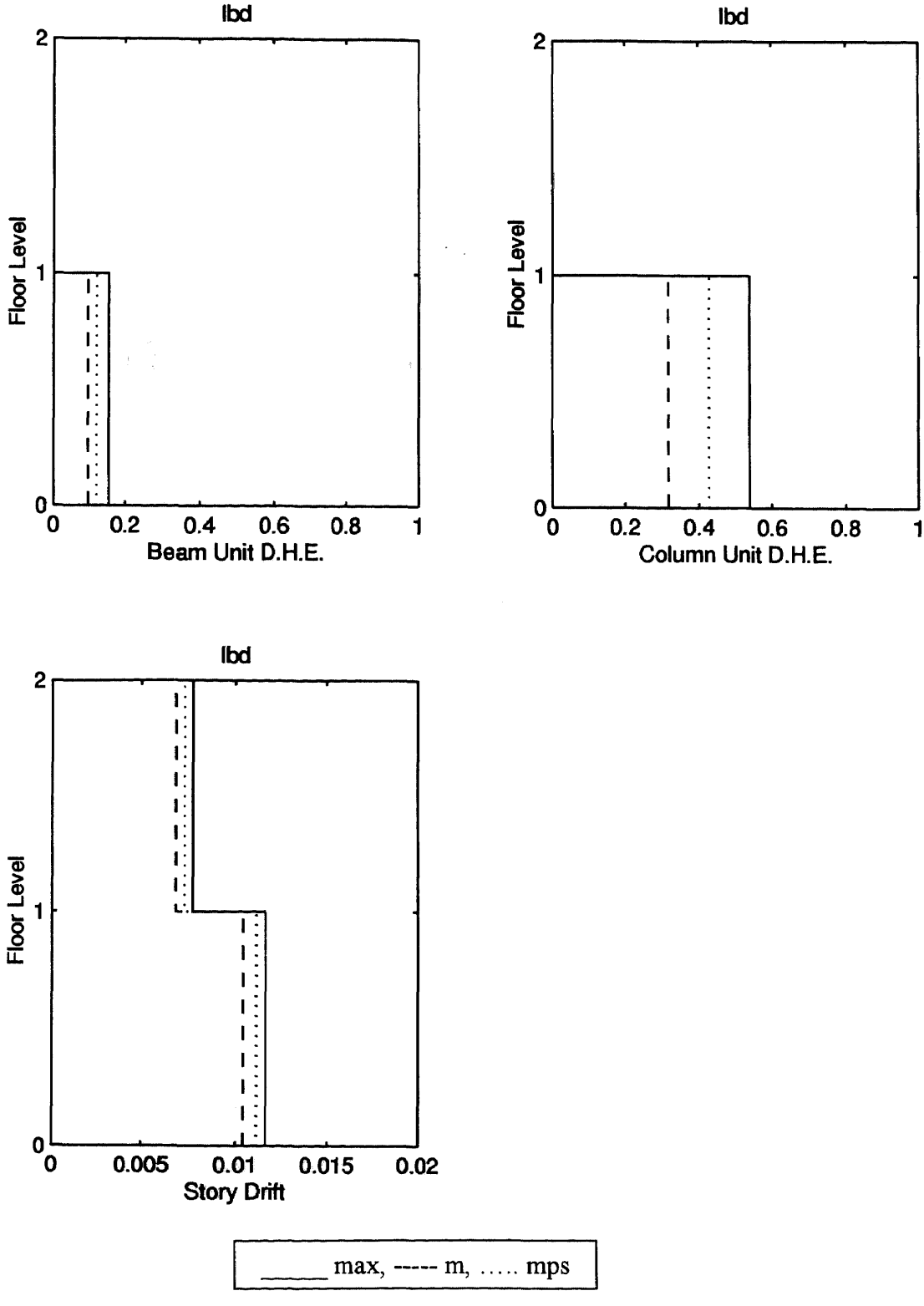

Figure 4.49 Story response of lbd: dissipated hysteretic energy and interstory drift.

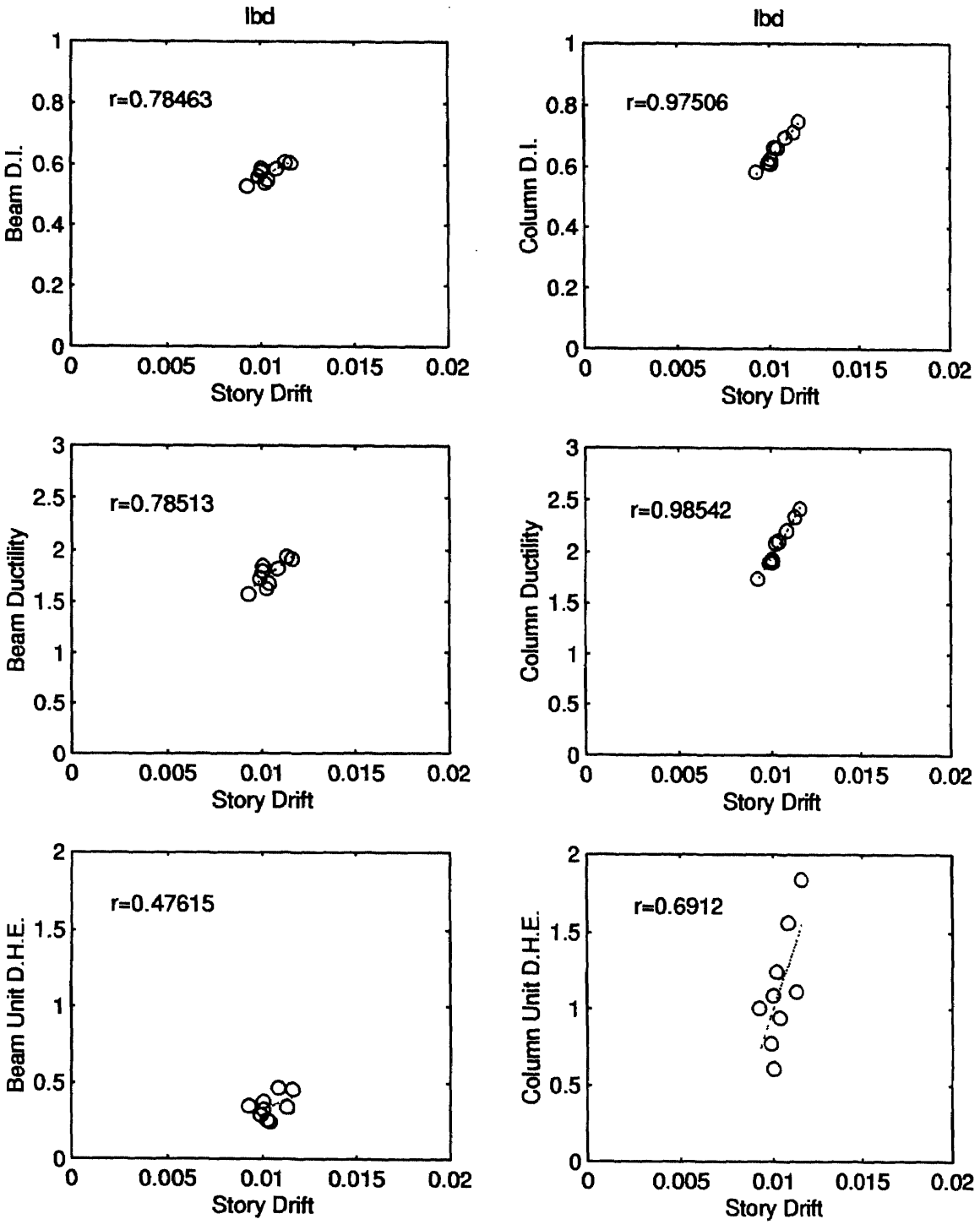

Figure 4.50 Element response of lbd.

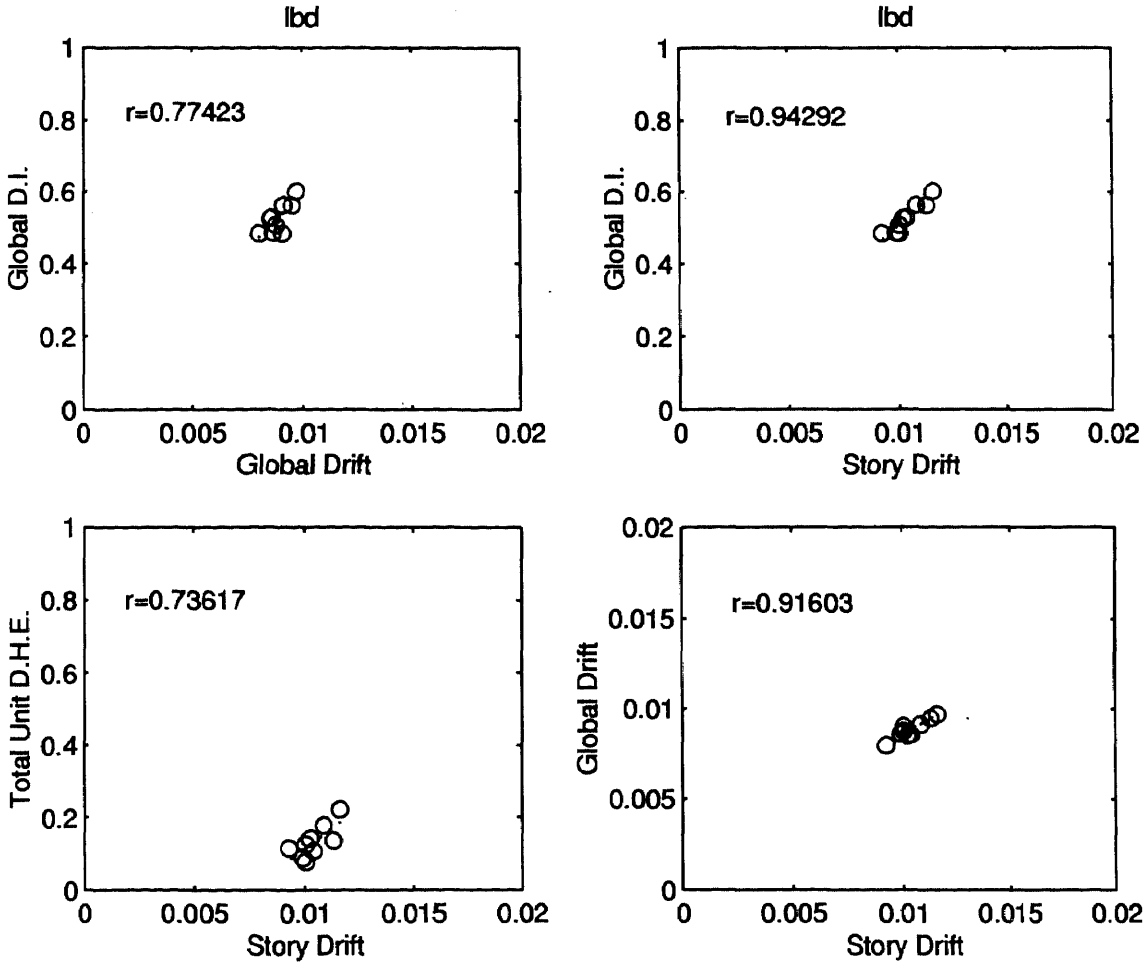

Figure 4.51 Global response of lbd.

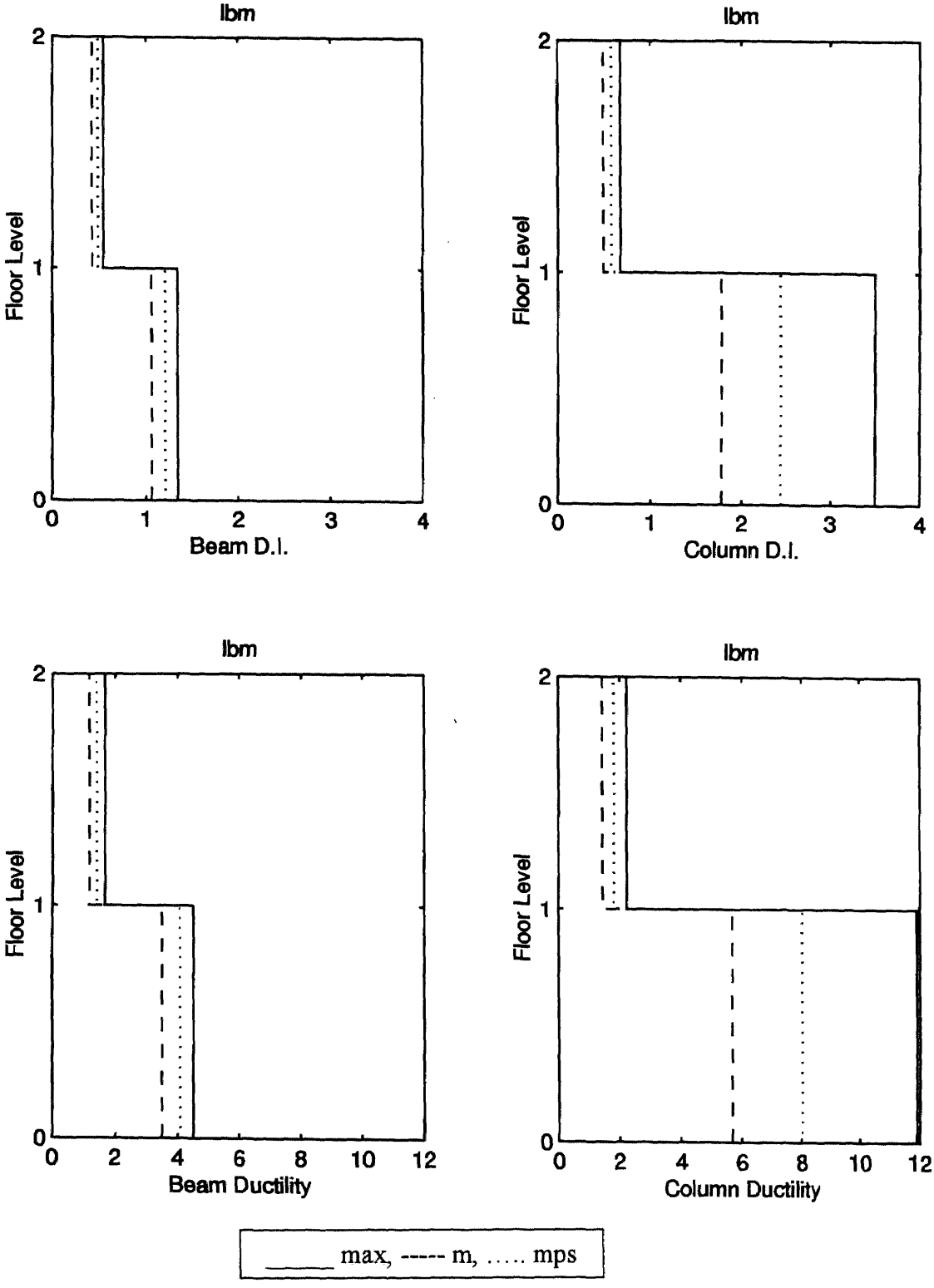

Figure 4.52 Story response of lbm: damage index and ductility.

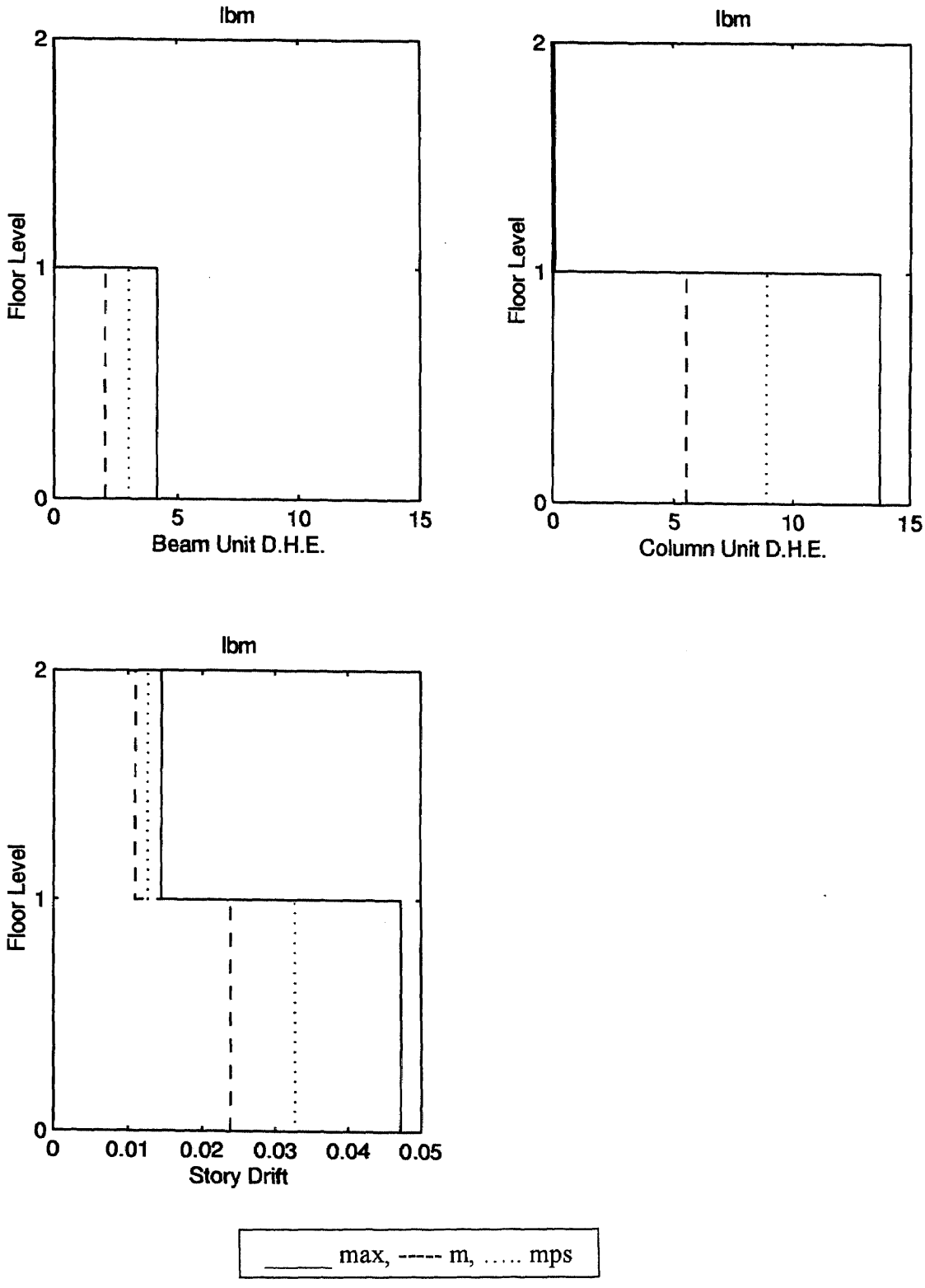

Figure 4.53 Story response of lbm: dissipated hysteretic energy and interstory drift.

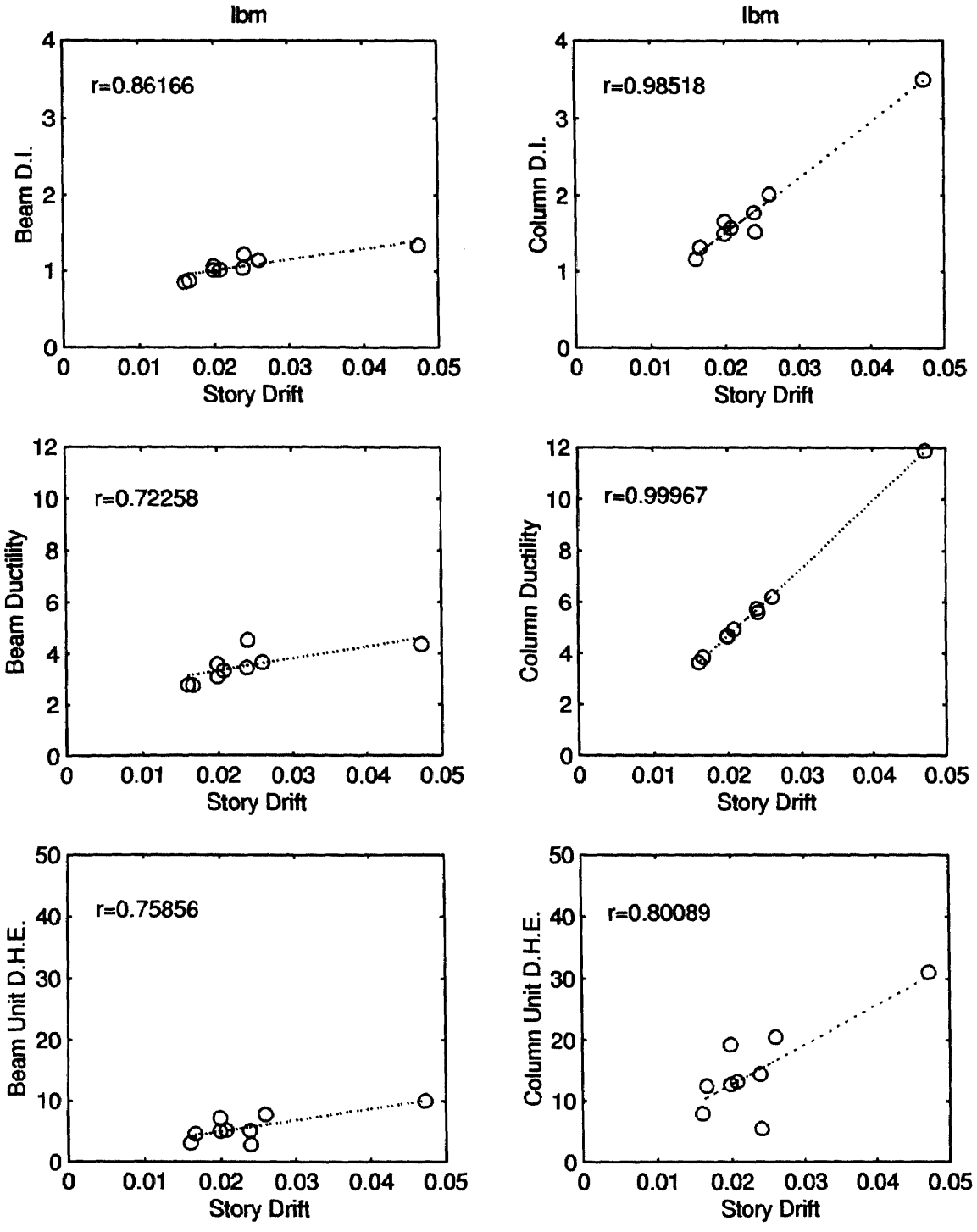

Figure 4.54 Element response of lbm.

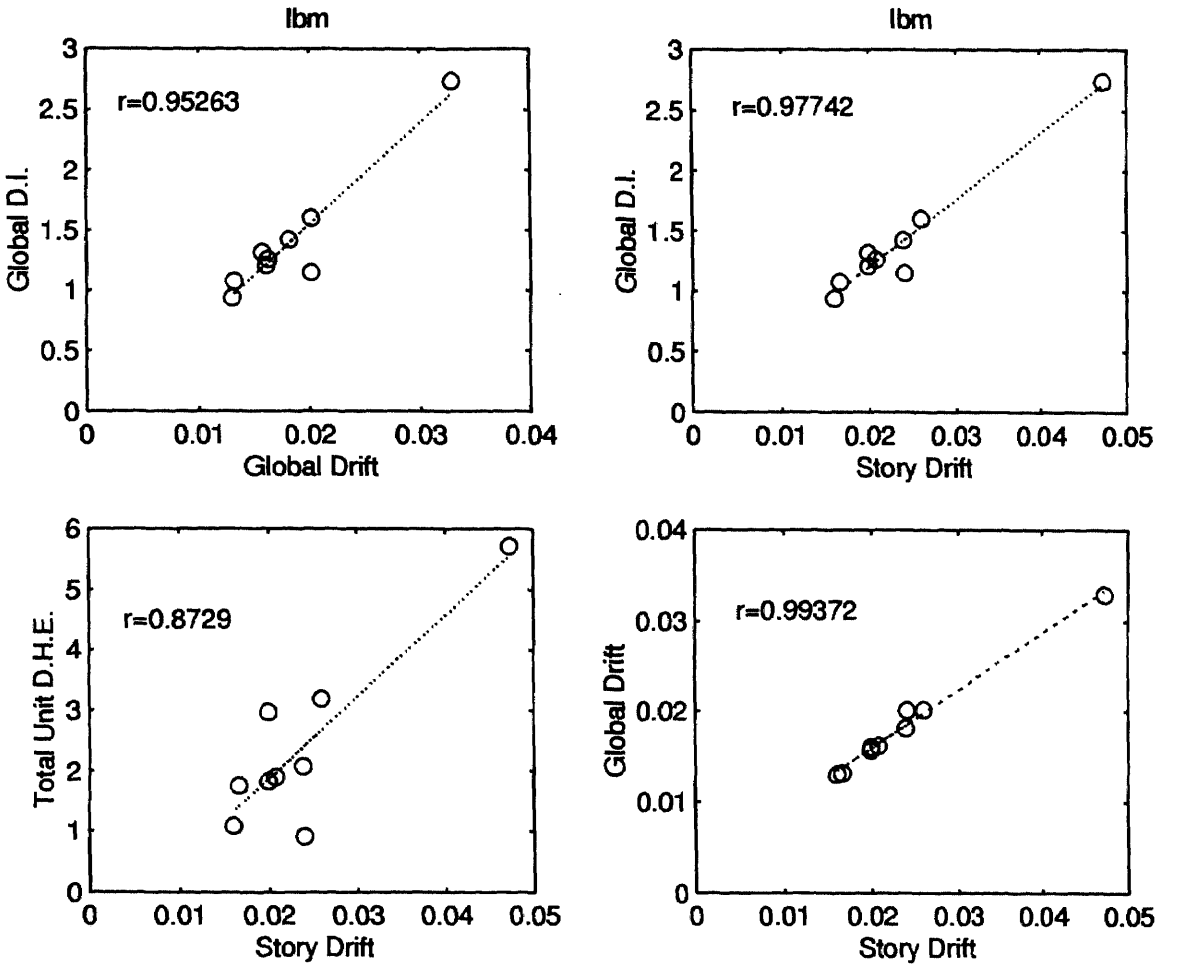

Figure 4.55 Global response of Ibm.

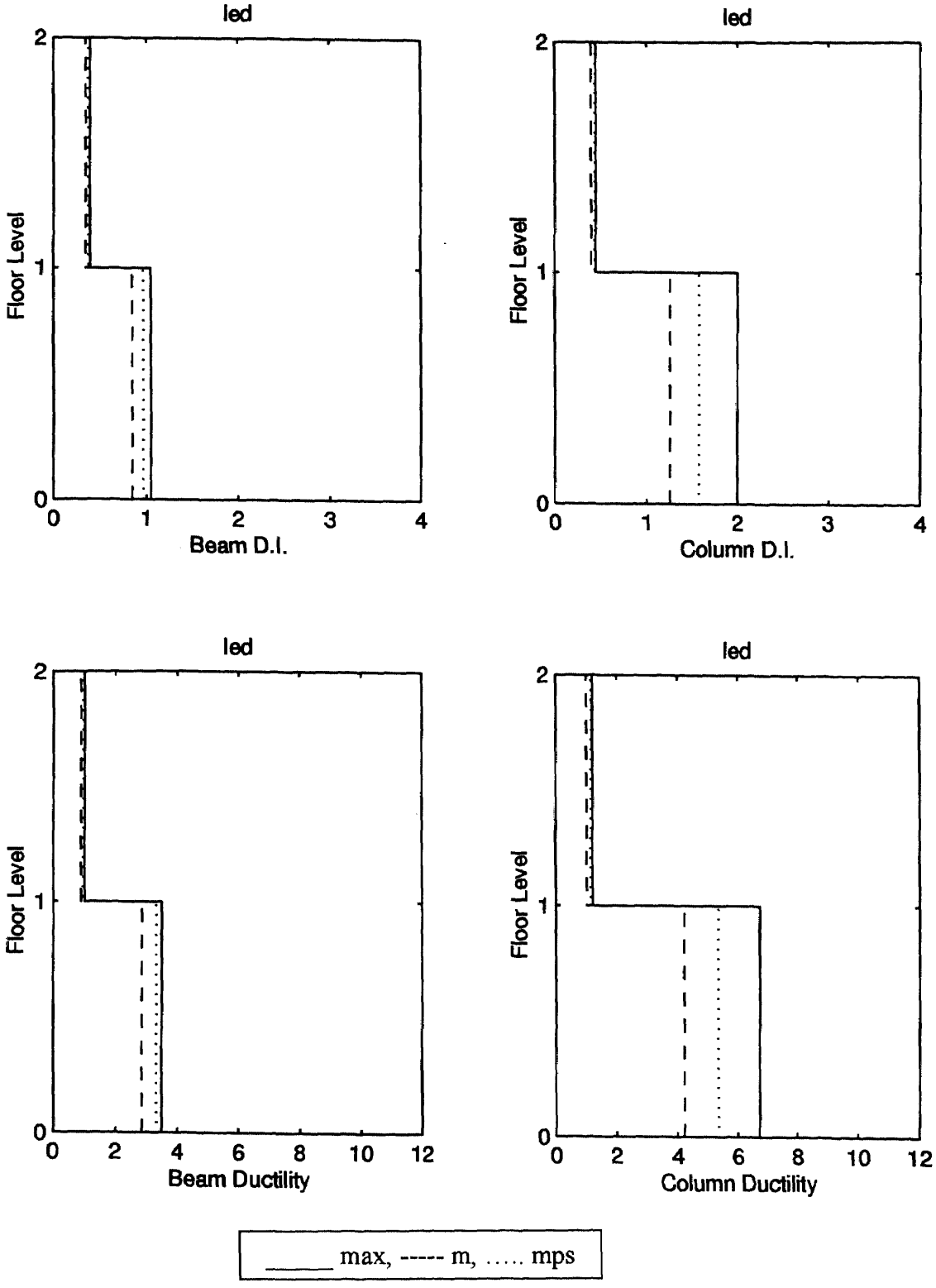

Figure 4.56 Story response of led: damage index and ductility.

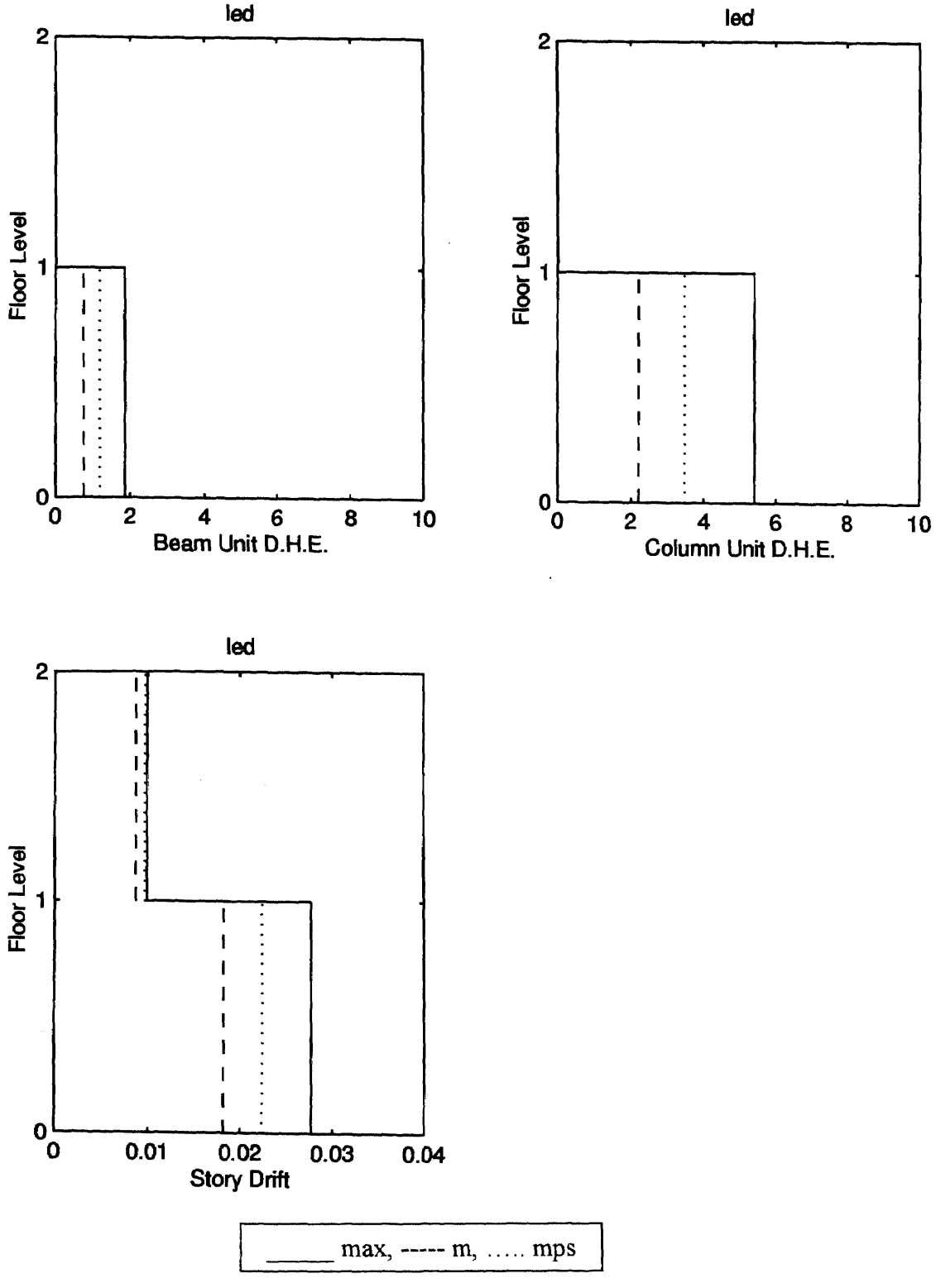

Figure 4.57 Story response of led: dissipated hysteretic energy and interstory drift.

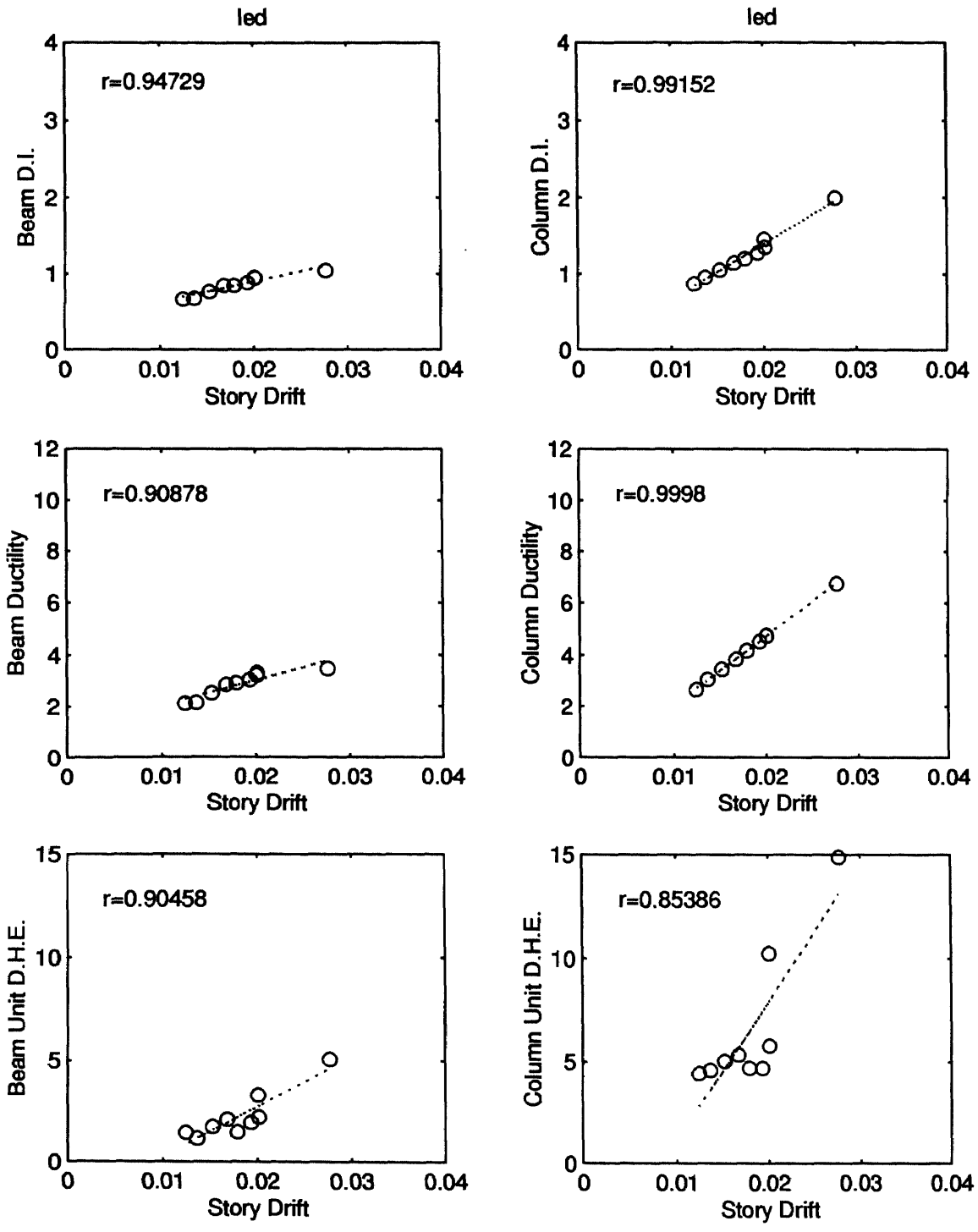

Figure 4.58 Element response of led.

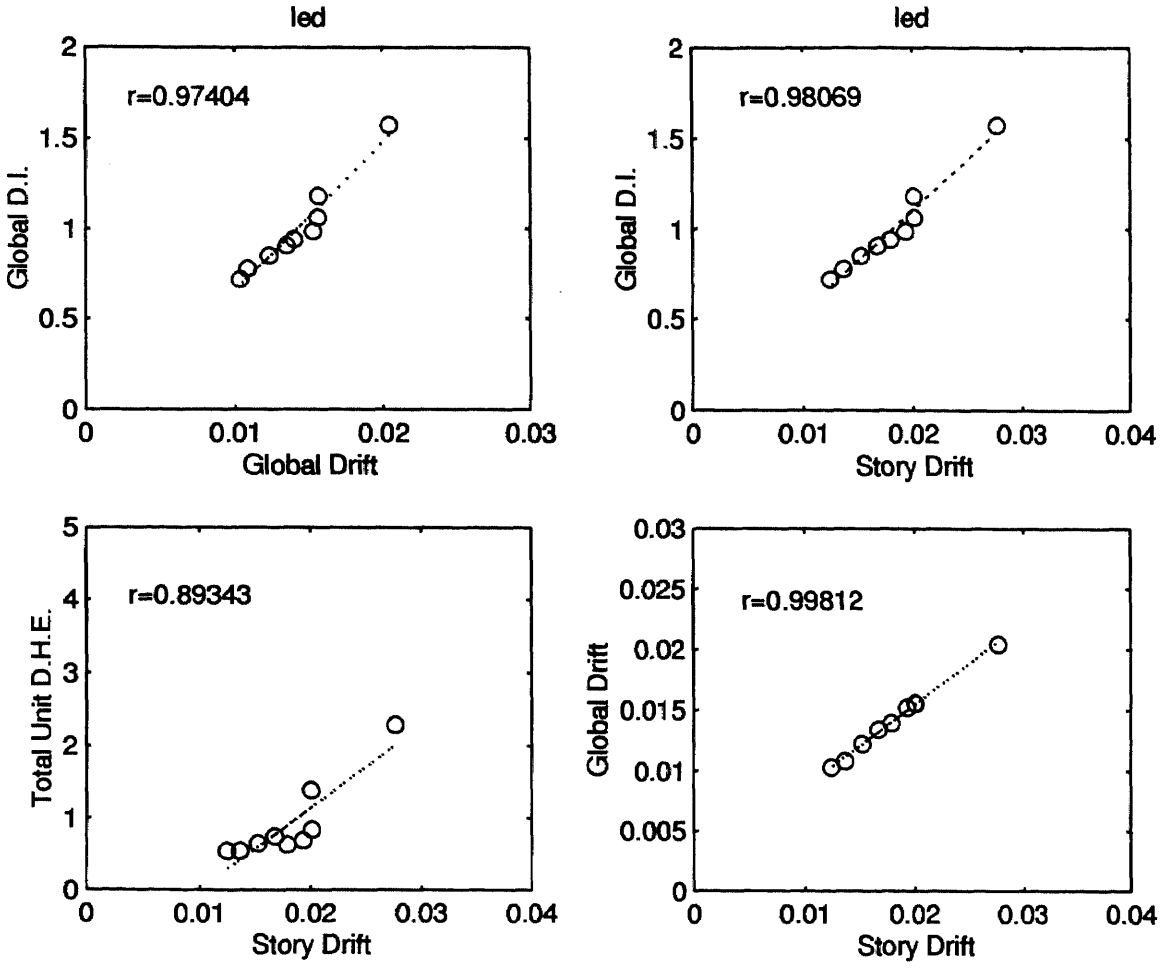

Figure 4.59 Global response of led.

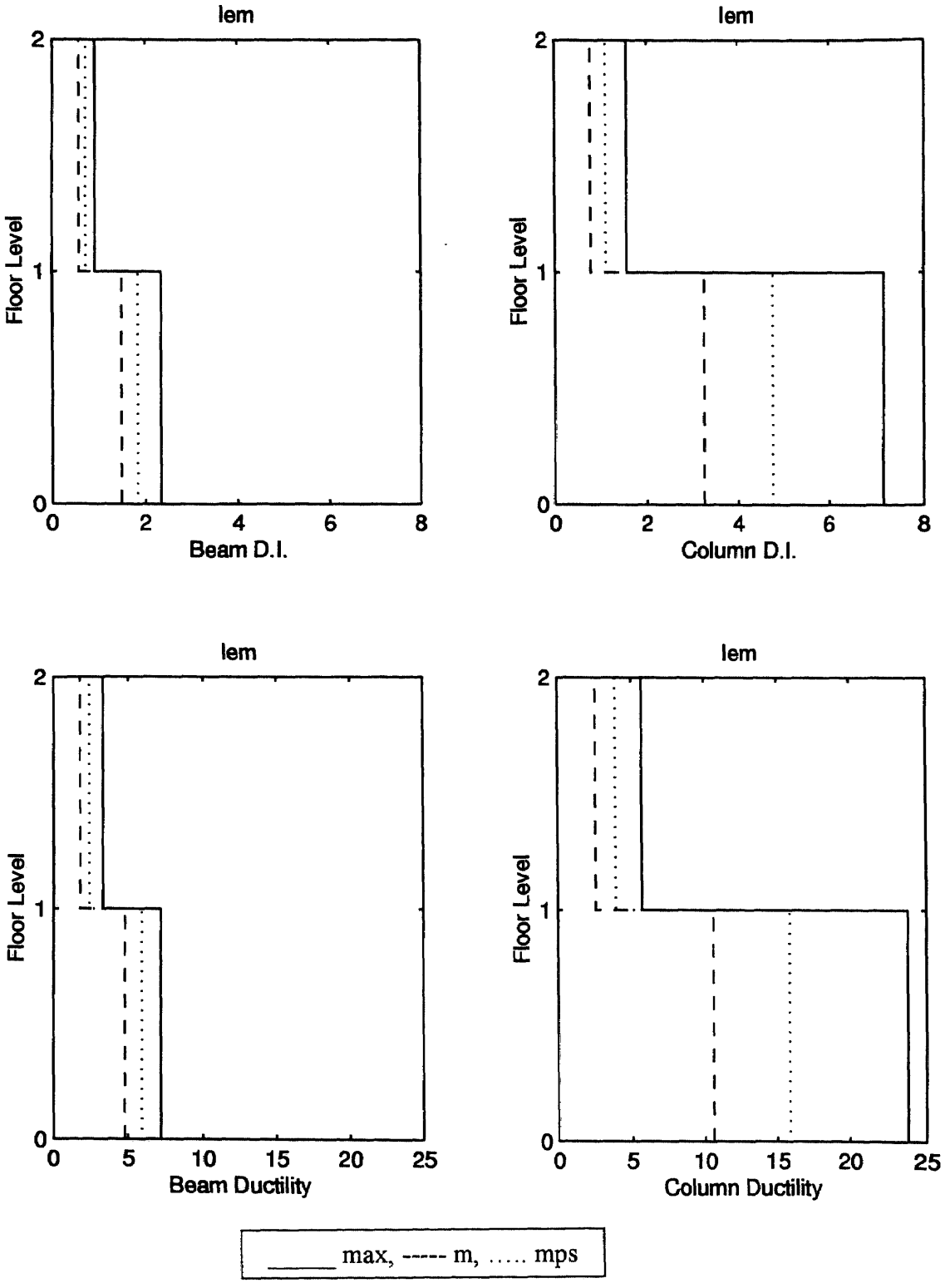

Figure 4.60 Story response of lem: damage index and ductility.

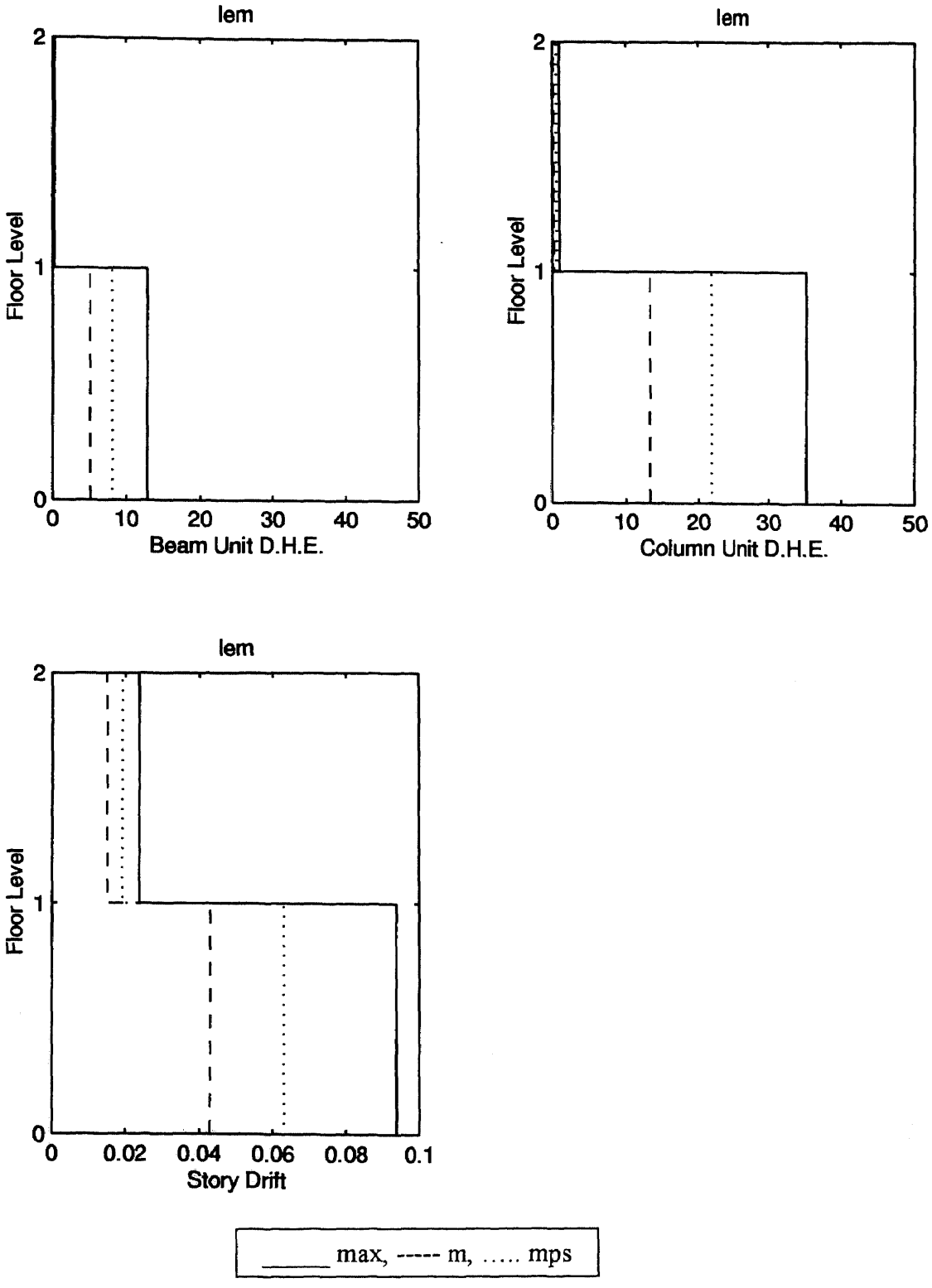

Figure 4.61 Story response of lem: dissipated hysteretic energy and interstory drift.

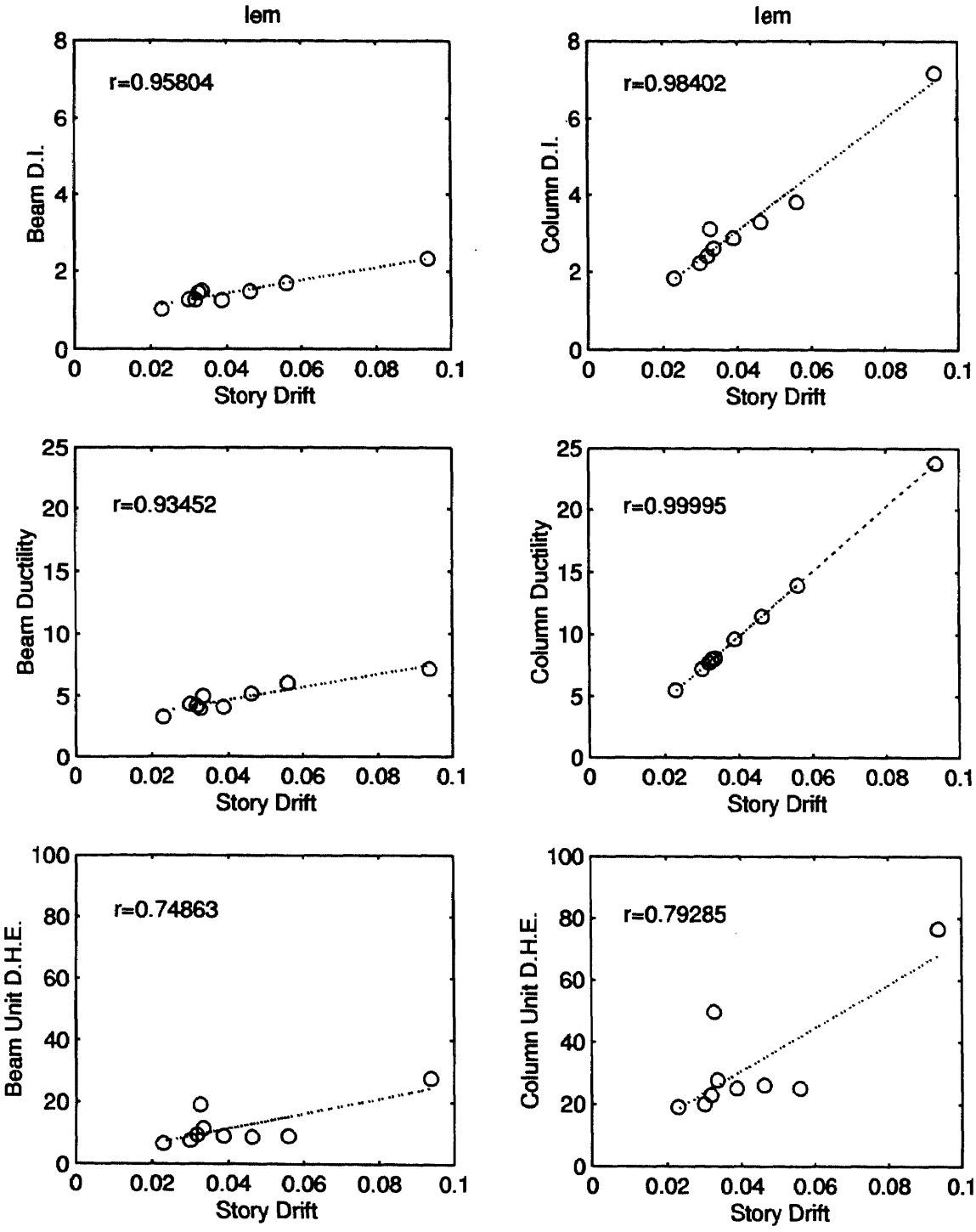

Figure 4.62 Element response of lem.

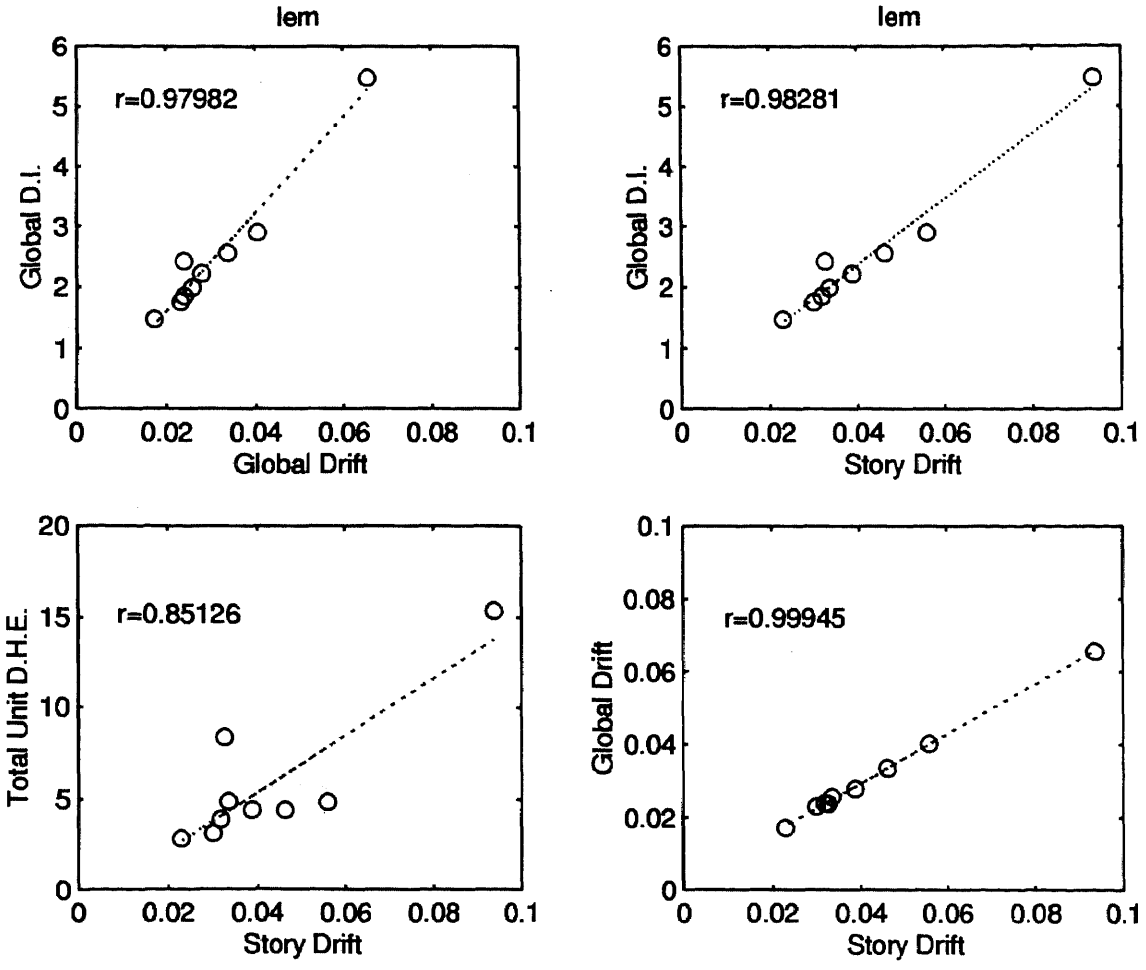

Figure 4.63 Global response of lem.

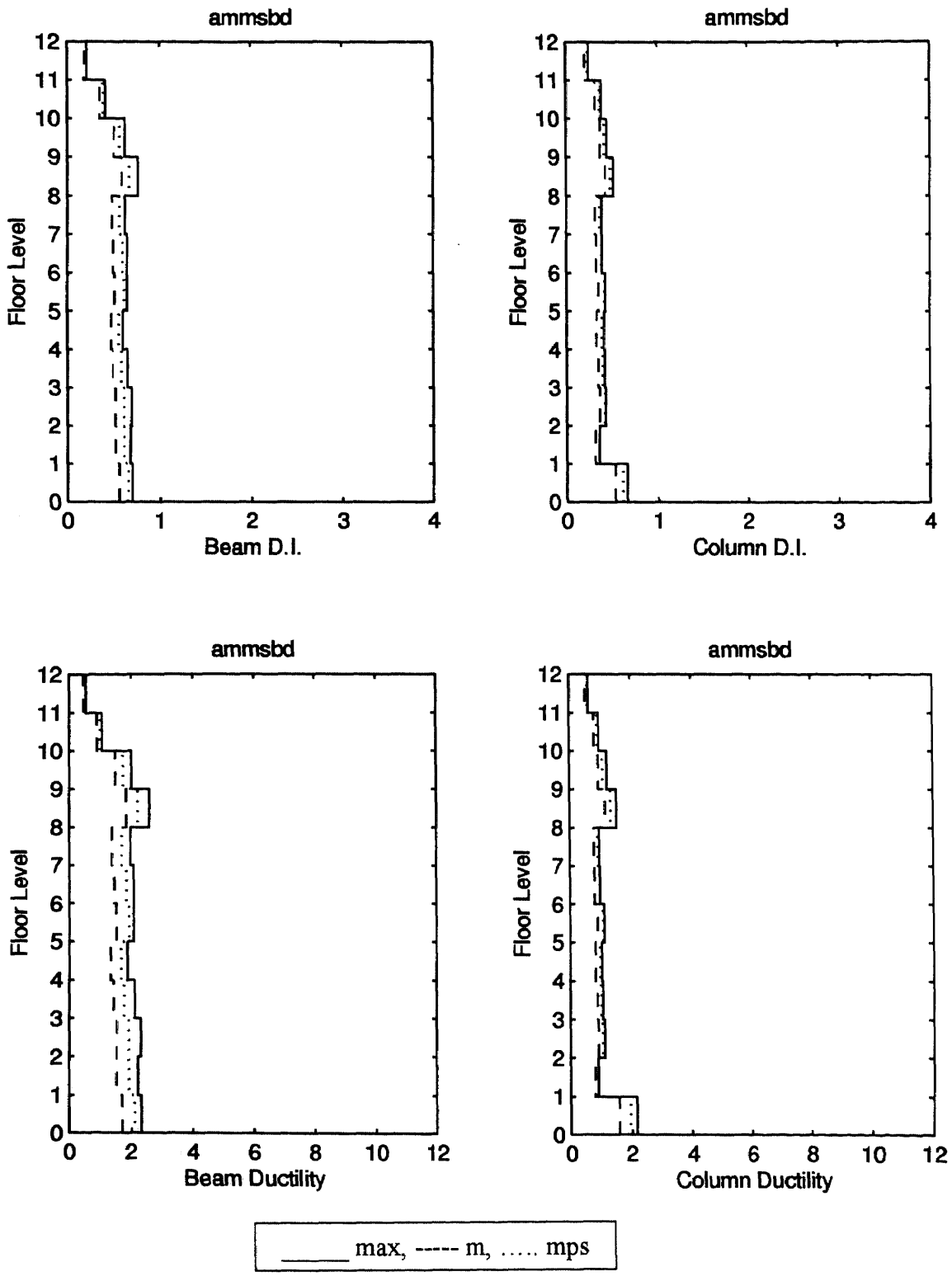

Figure 4.64 Story response of ammsbd: damage index and ductility.

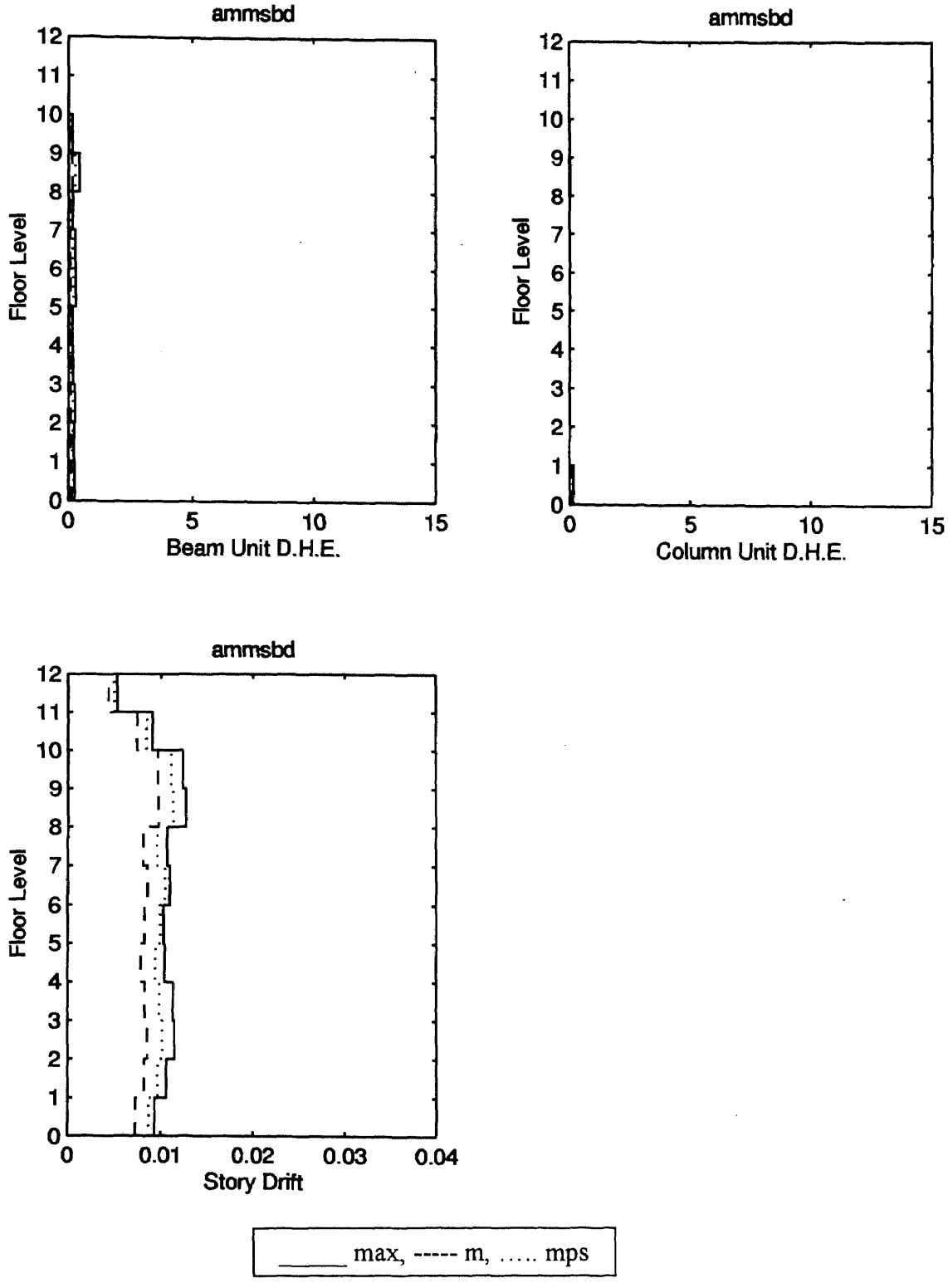

Figure 4.65 Story response of ammsbd: dissipated hysteretic energy and interstory drift.

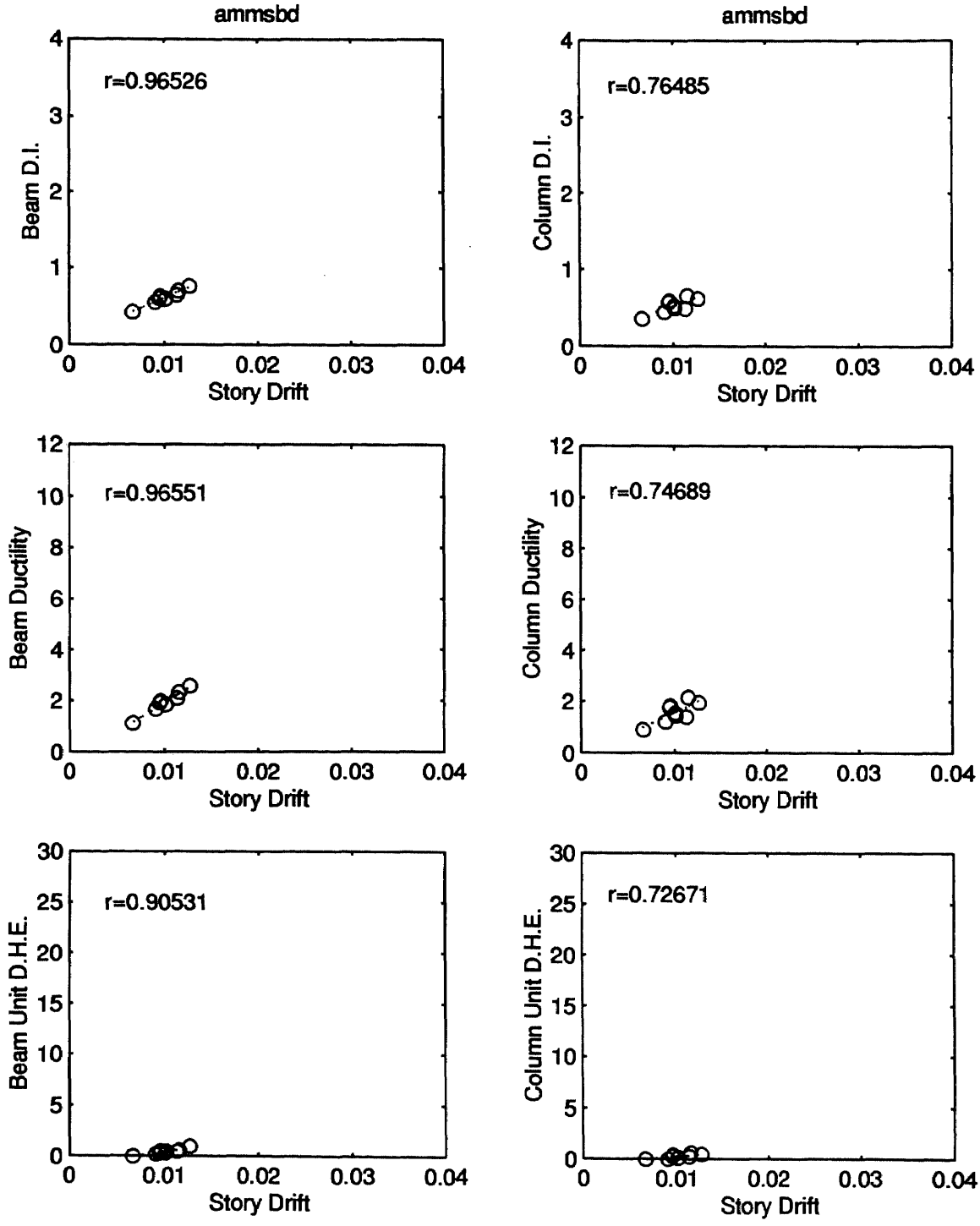

Figure 4.66 Element response of ammsbd.

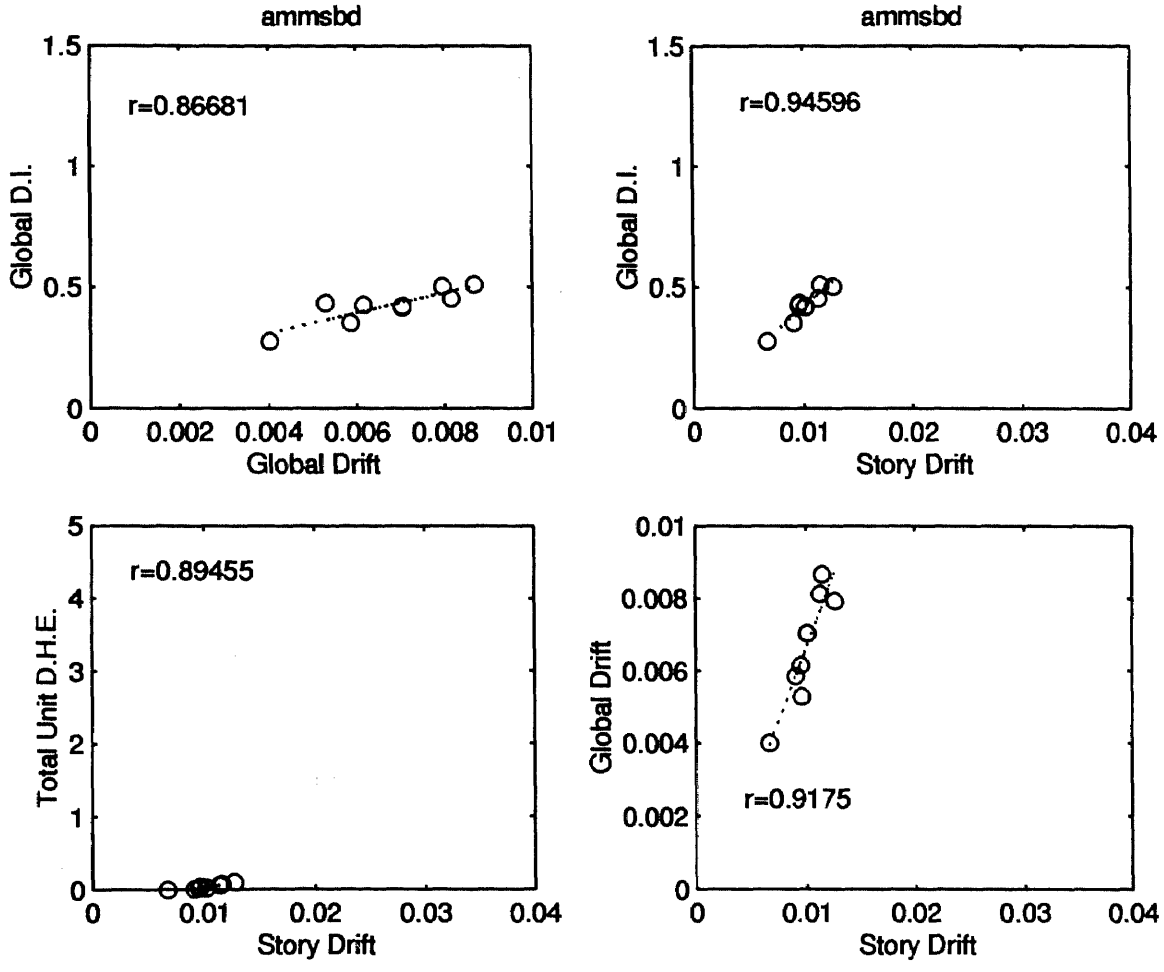

Figure 4.67 Global response of ammsbd.

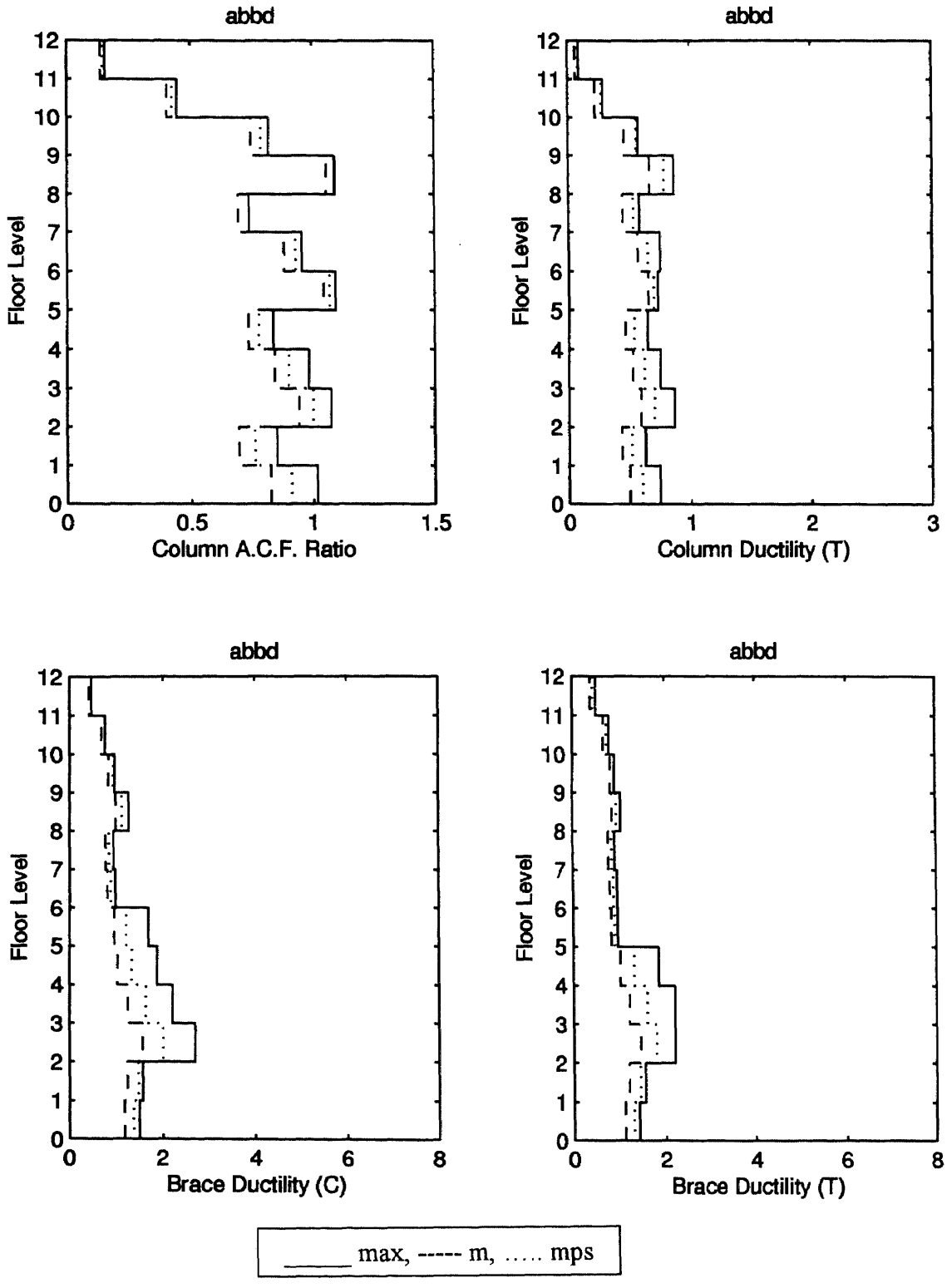

Figure 4.68 Story response of abbd: axial compressive force ratio and ductility.

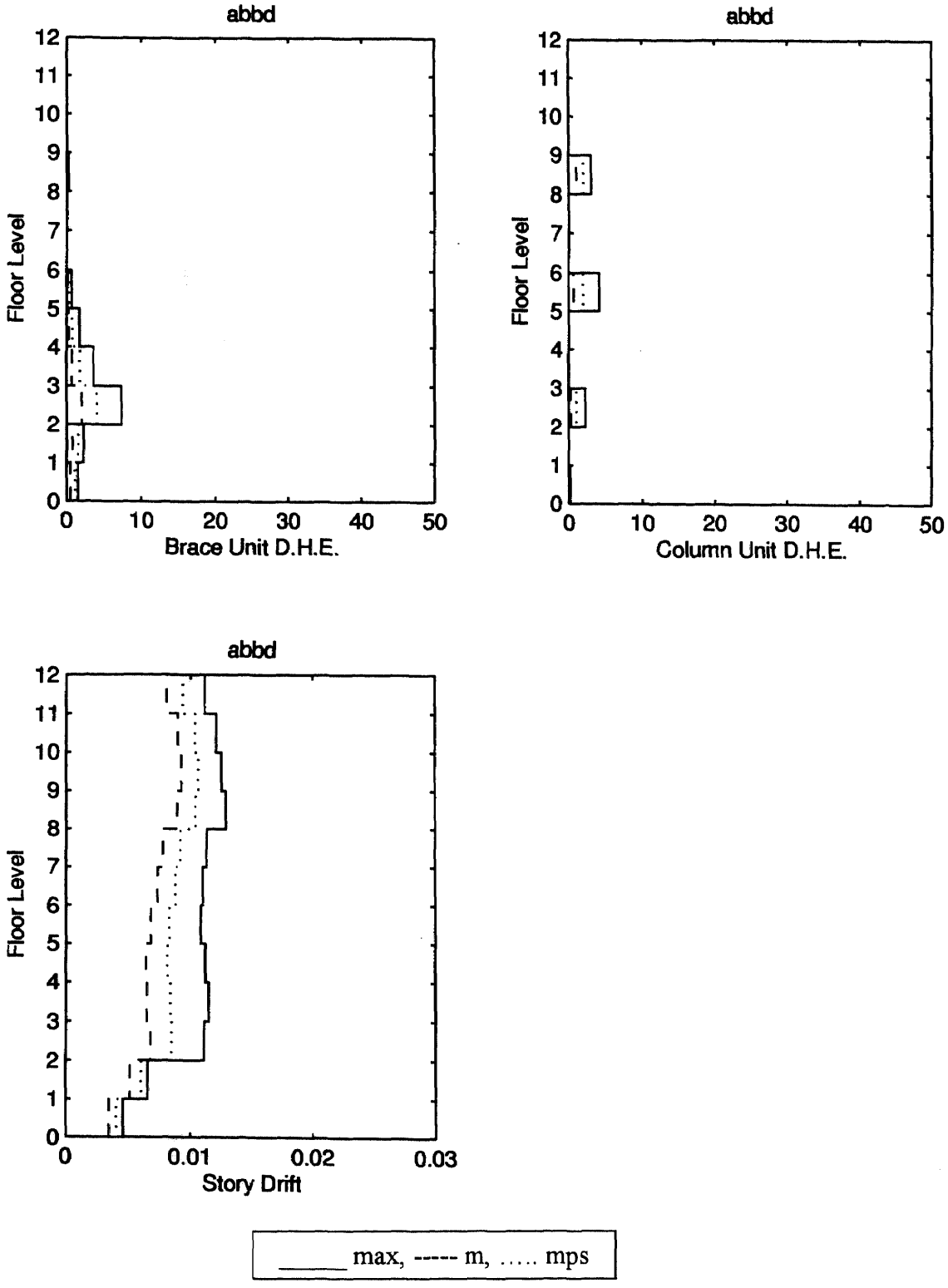

Figure 4.69 Story response of abbd: dissipated hysteretic energy and interstory drift.

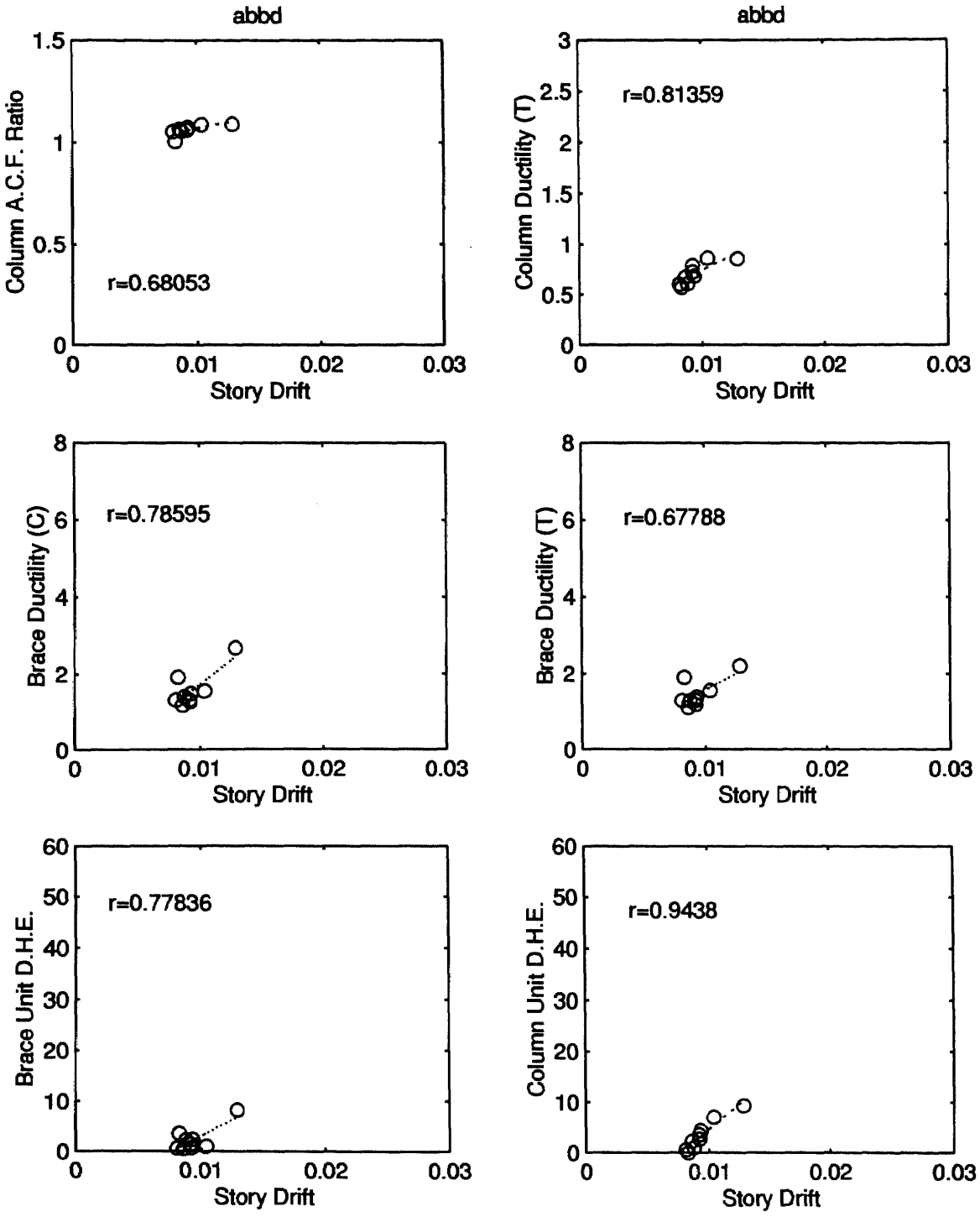

Figure 4.70 Element response of abbd.

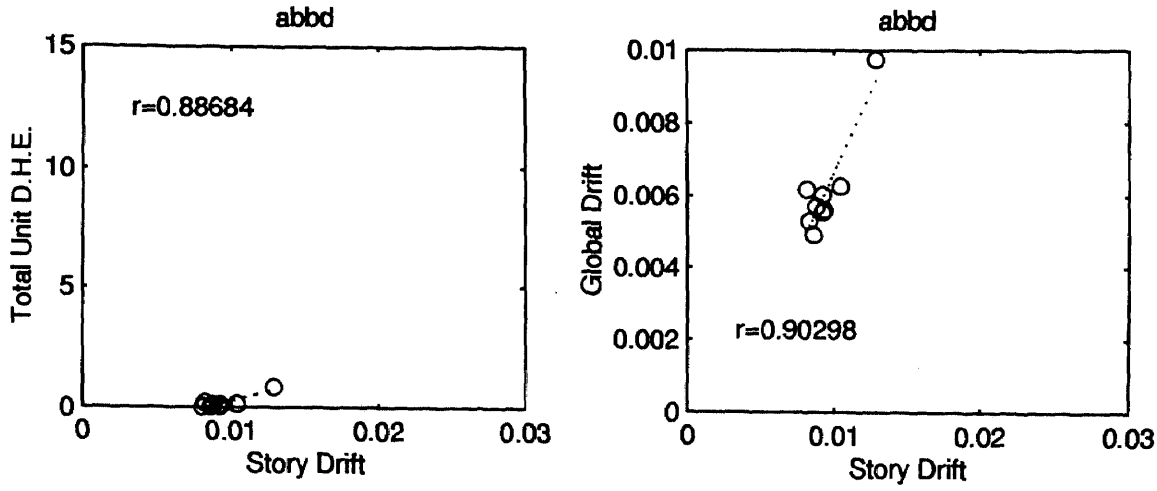

Figure 4.71 Global response of abbd.

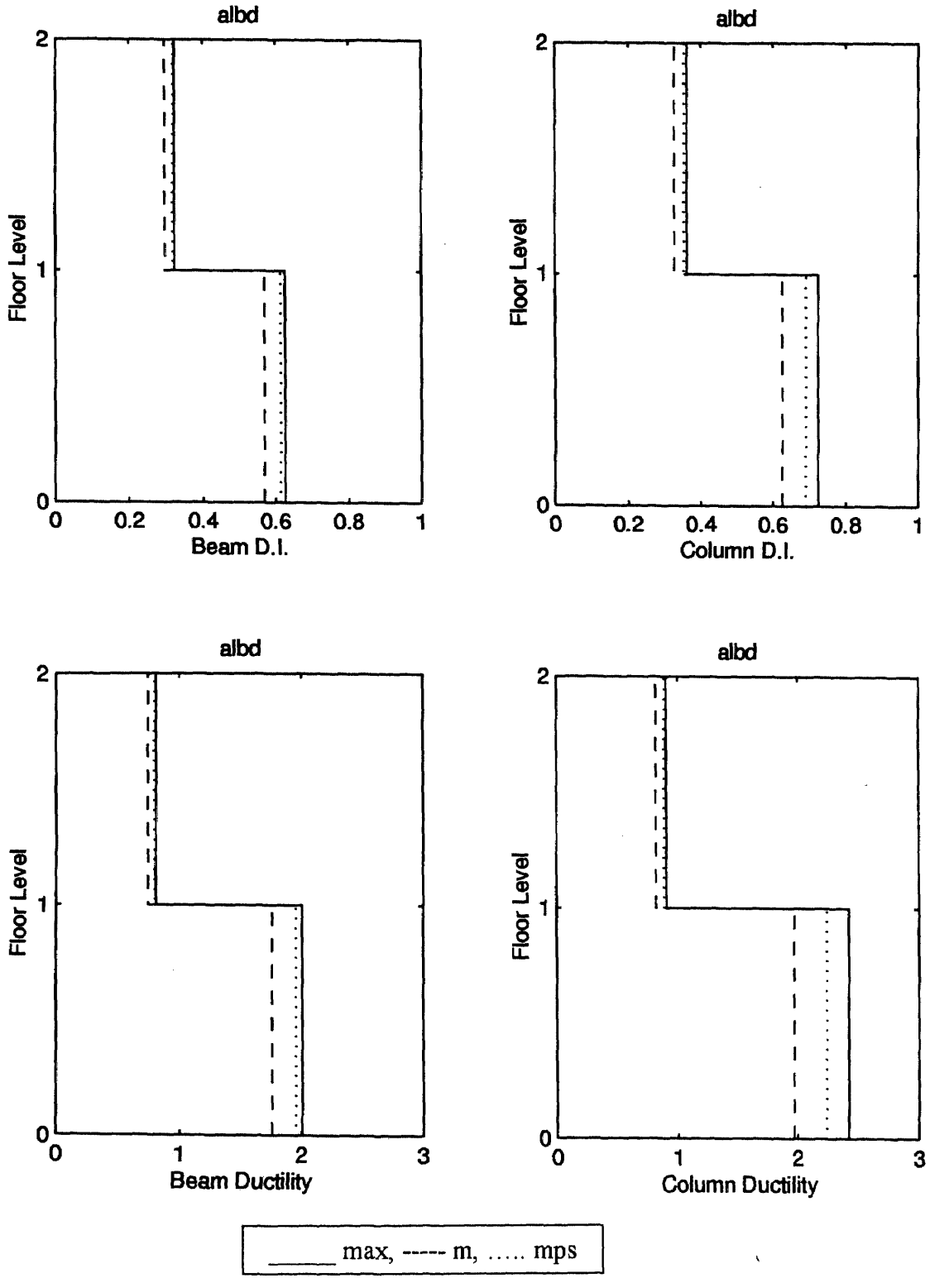

Figure 4.72 Story response of albd: damage index and ductility.

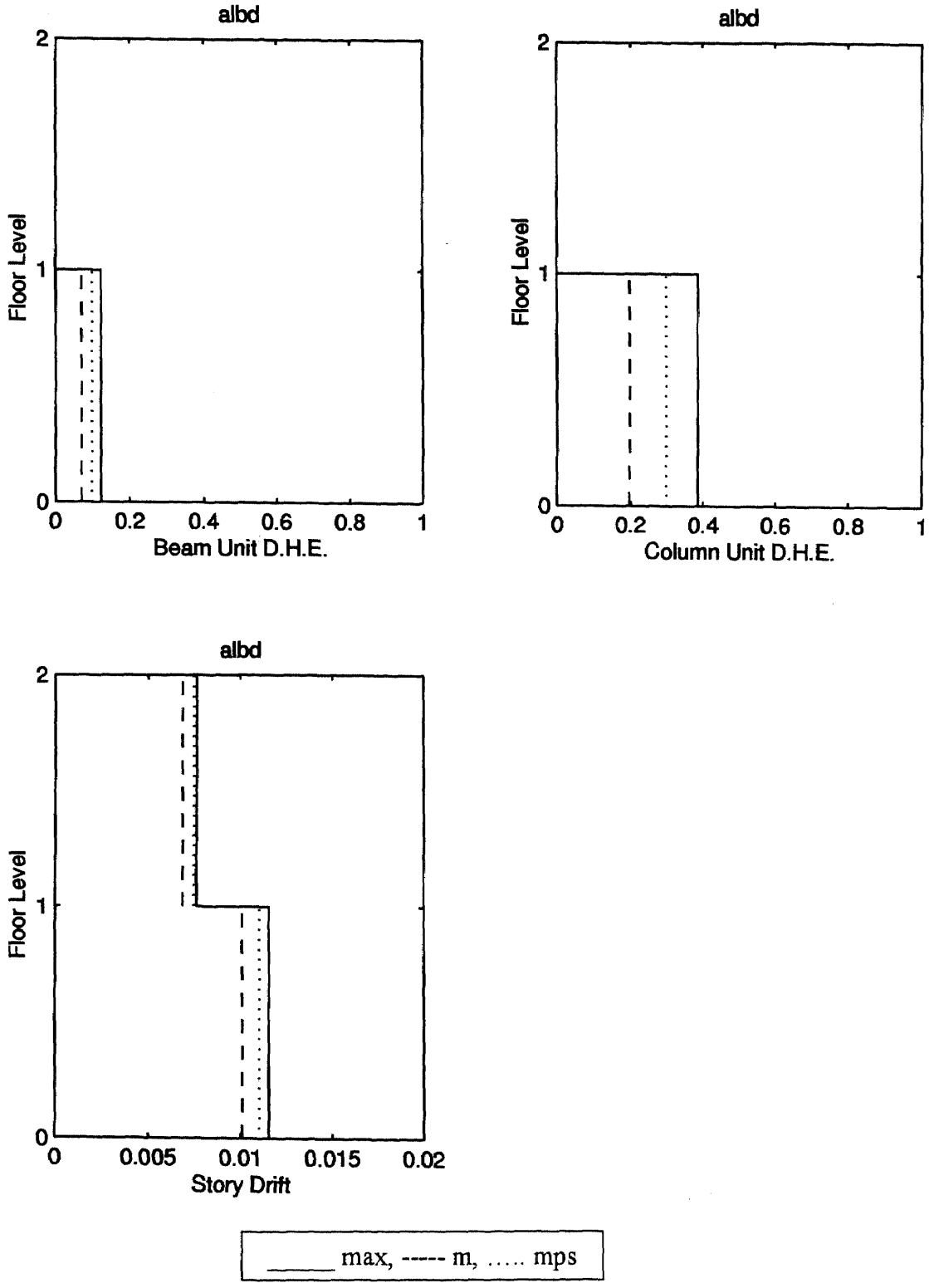

Figure 4.73 Story response of albd: dissipated hysteretic energy and interstory drift.

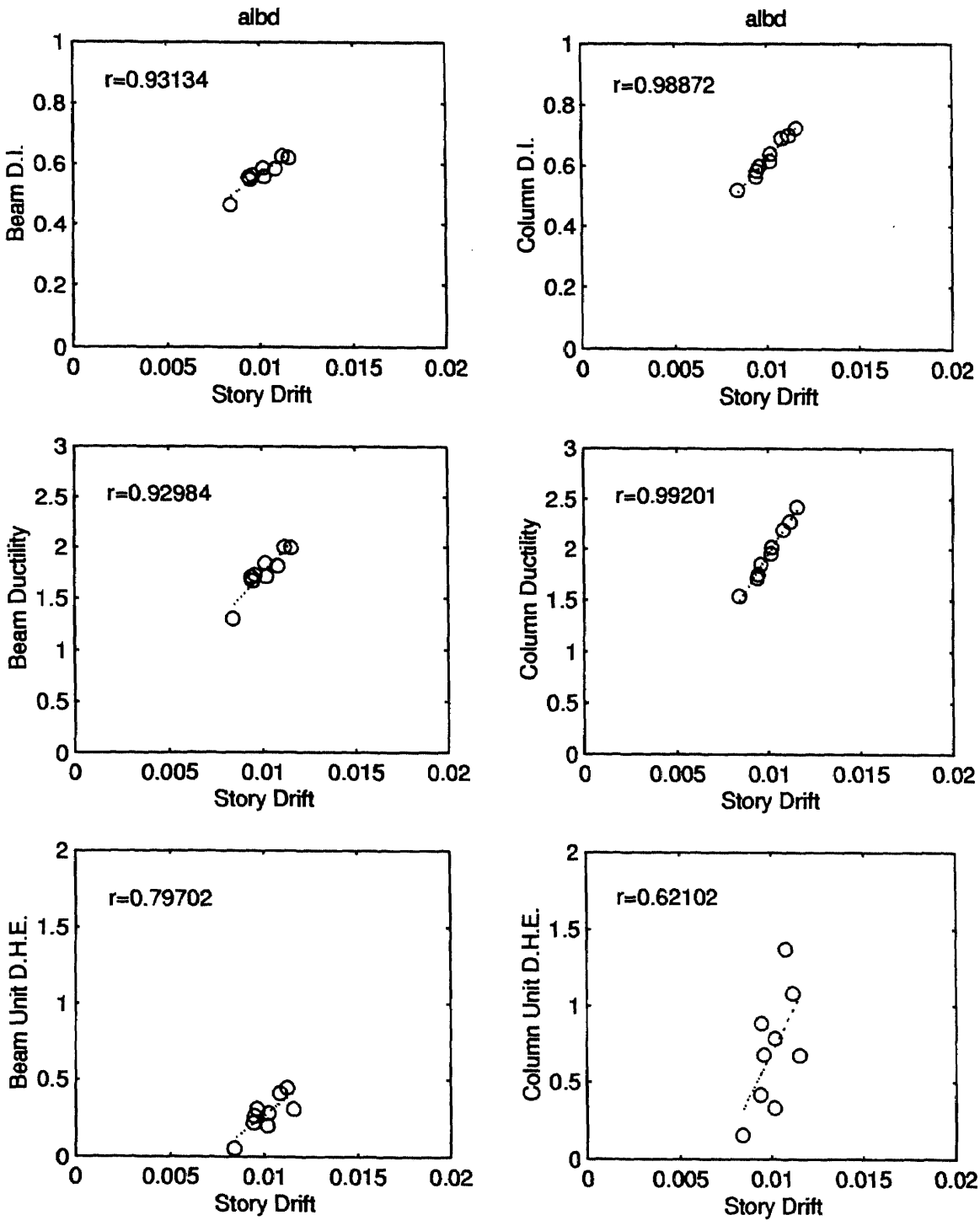

Figure 4.74 Element response of albd.

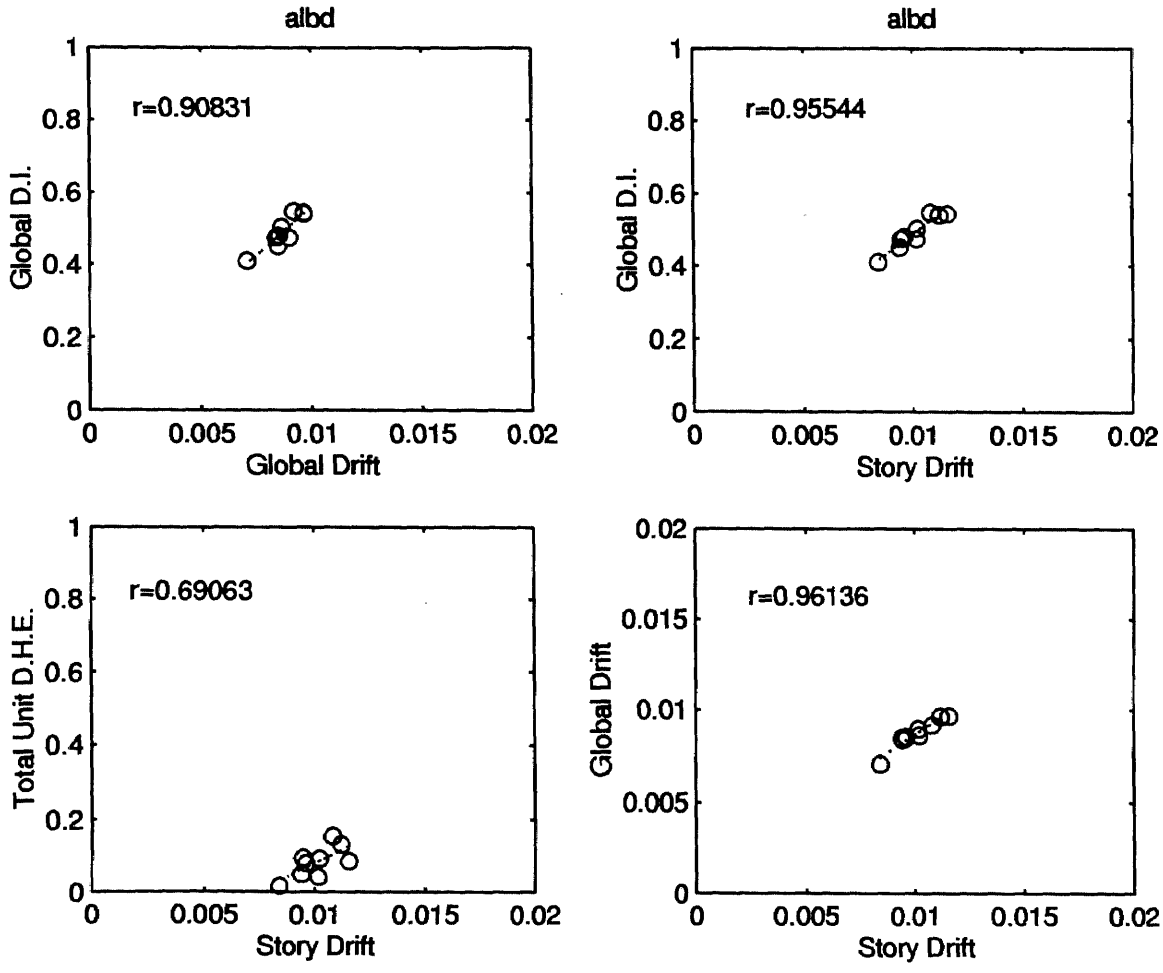

Figure 4.75 Global response of albd.

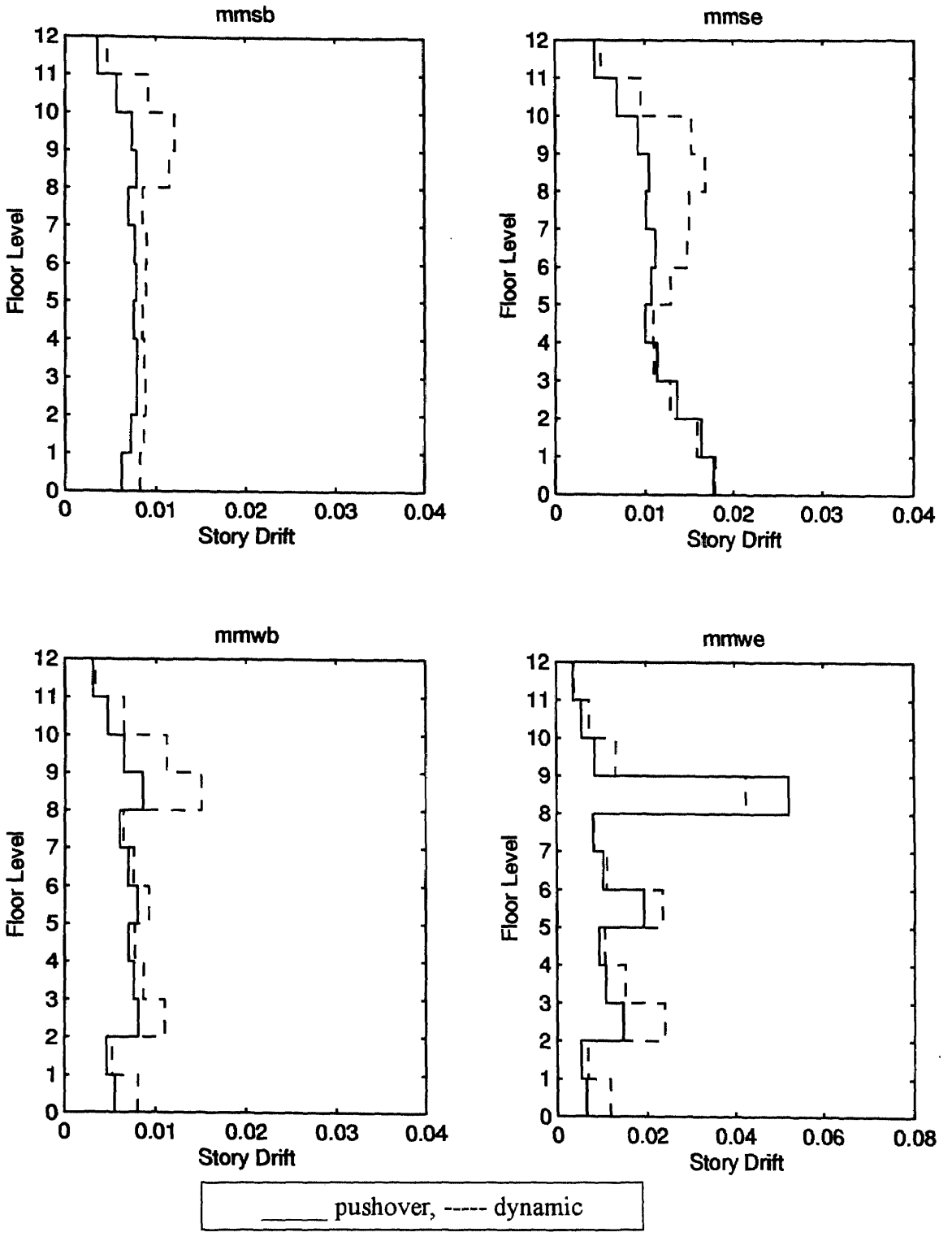

Figure 4.76 Comparison of interstory drifts obtained from pushover and dynamic analysis methods: twelve story moment-resisting frames.

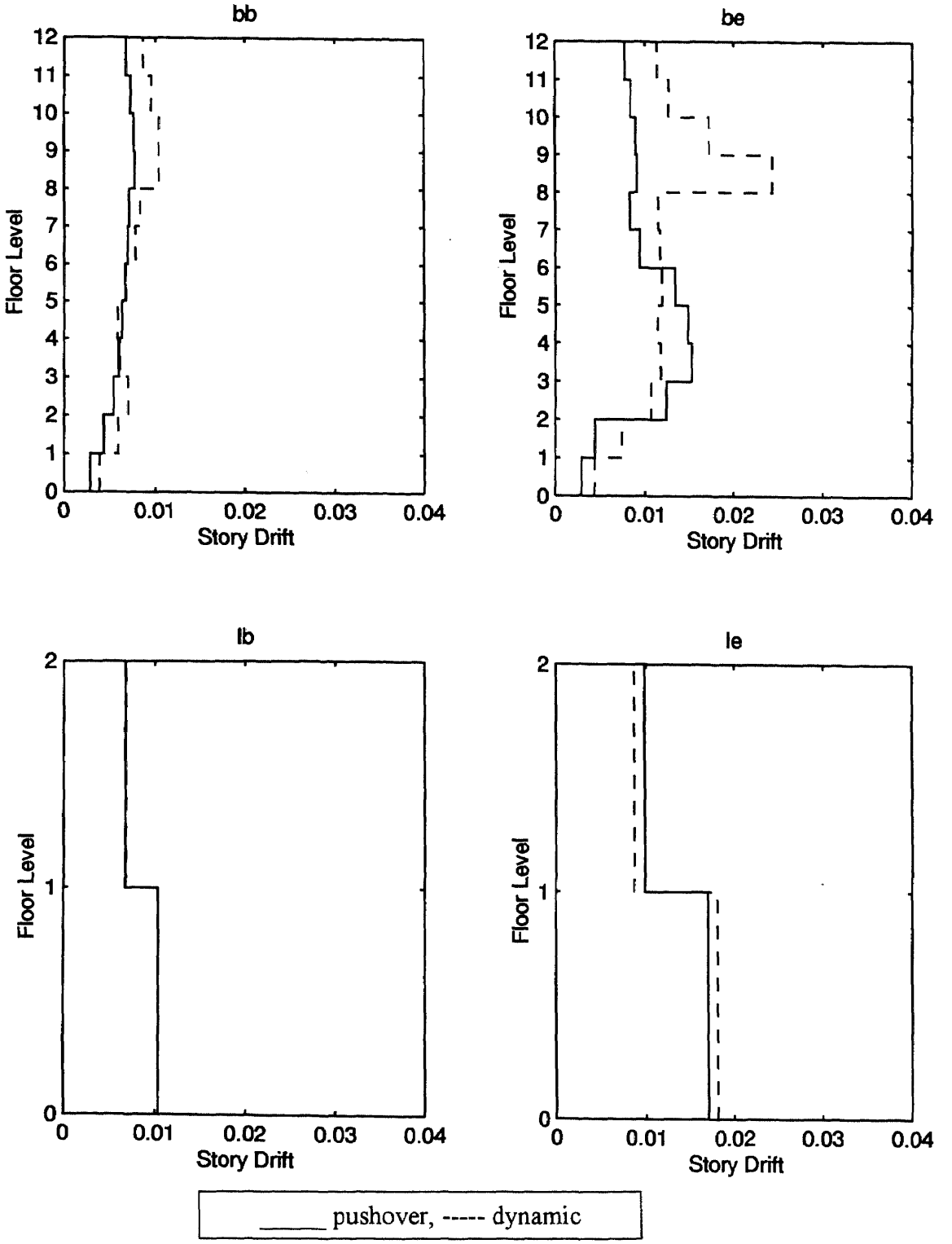

Figure 4.77 Comparison of interstory drifts obtained from pushover and dynamic analysis methods: braced and two story frames.

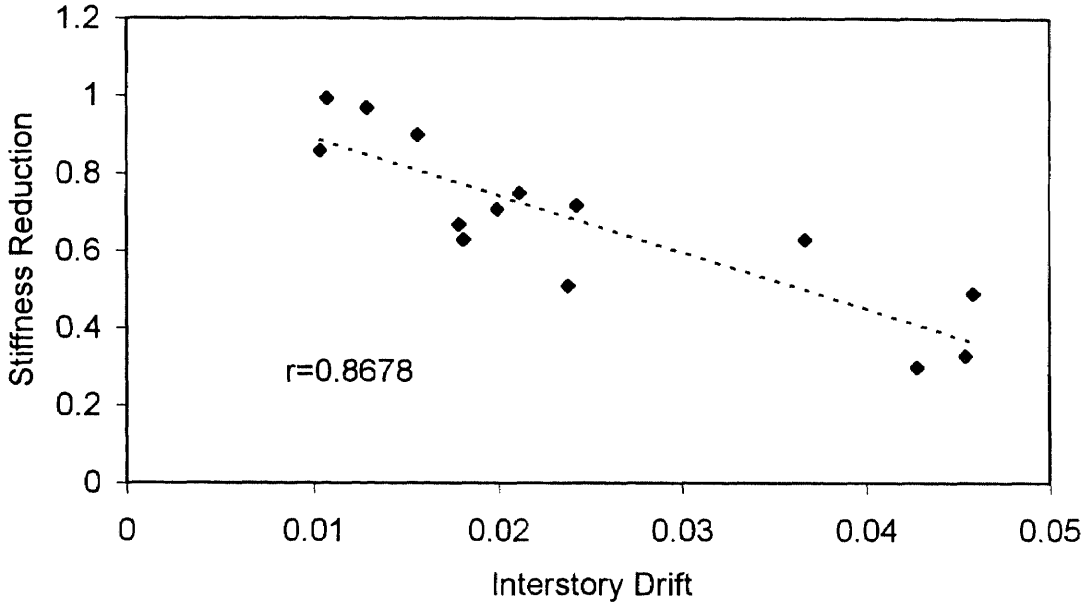

Figure 4.78 Correlation between stiffness reduction and interstory drift.

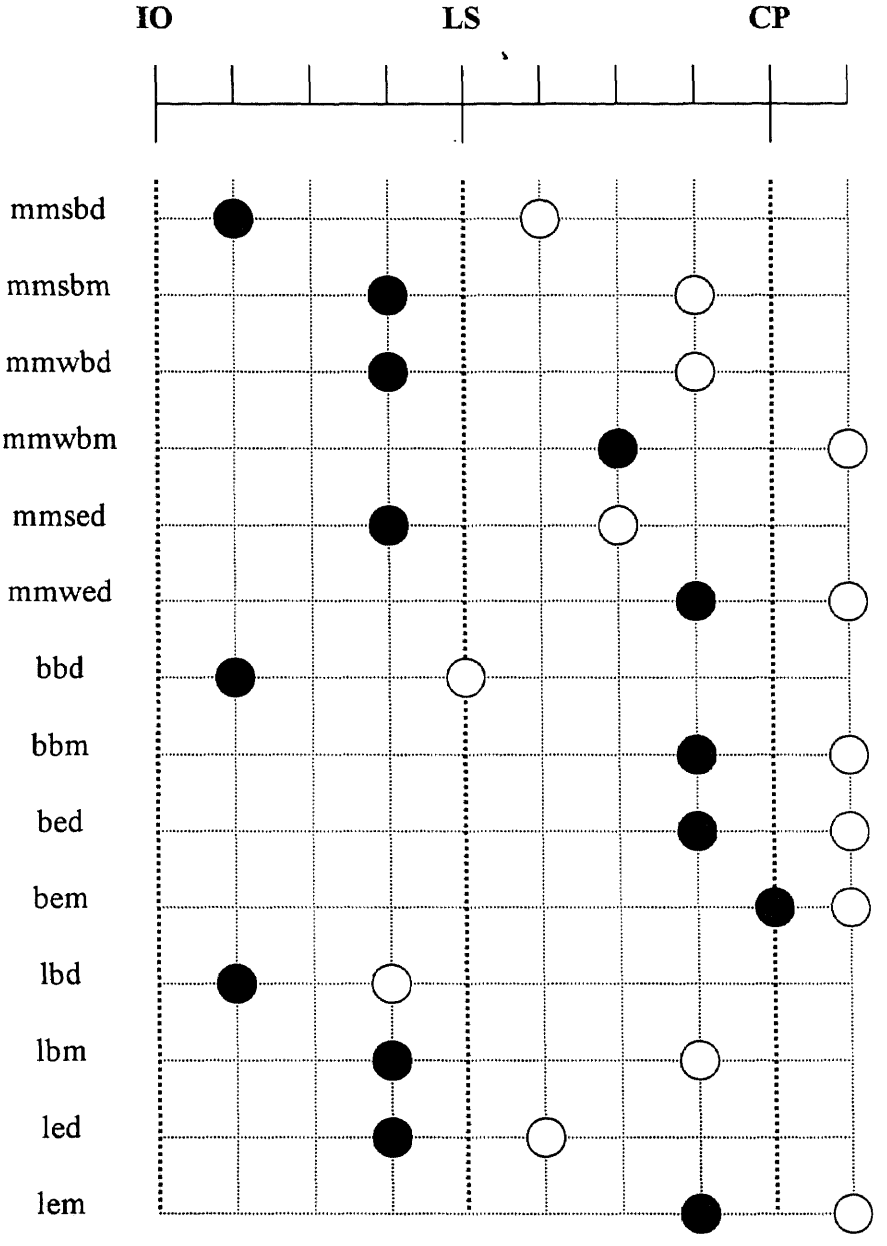

Figure 4.79 Probable and extreme performance levels of the designed frames.

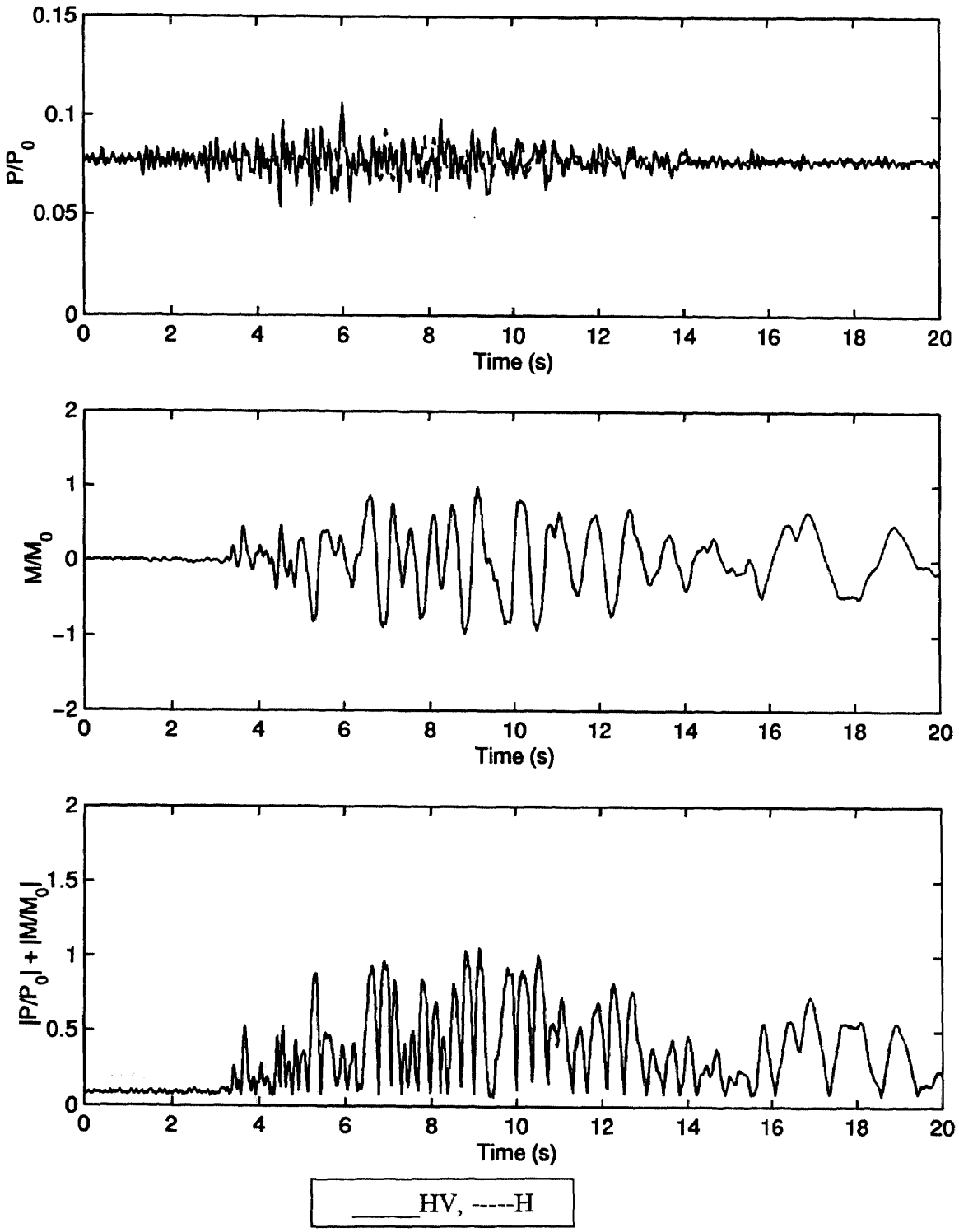

Figure 5.1 Effect of vertical ground acceleration on the column response in a moment-resisting frame: (a) axial force, (b) bending moment, (c) linear interaction.

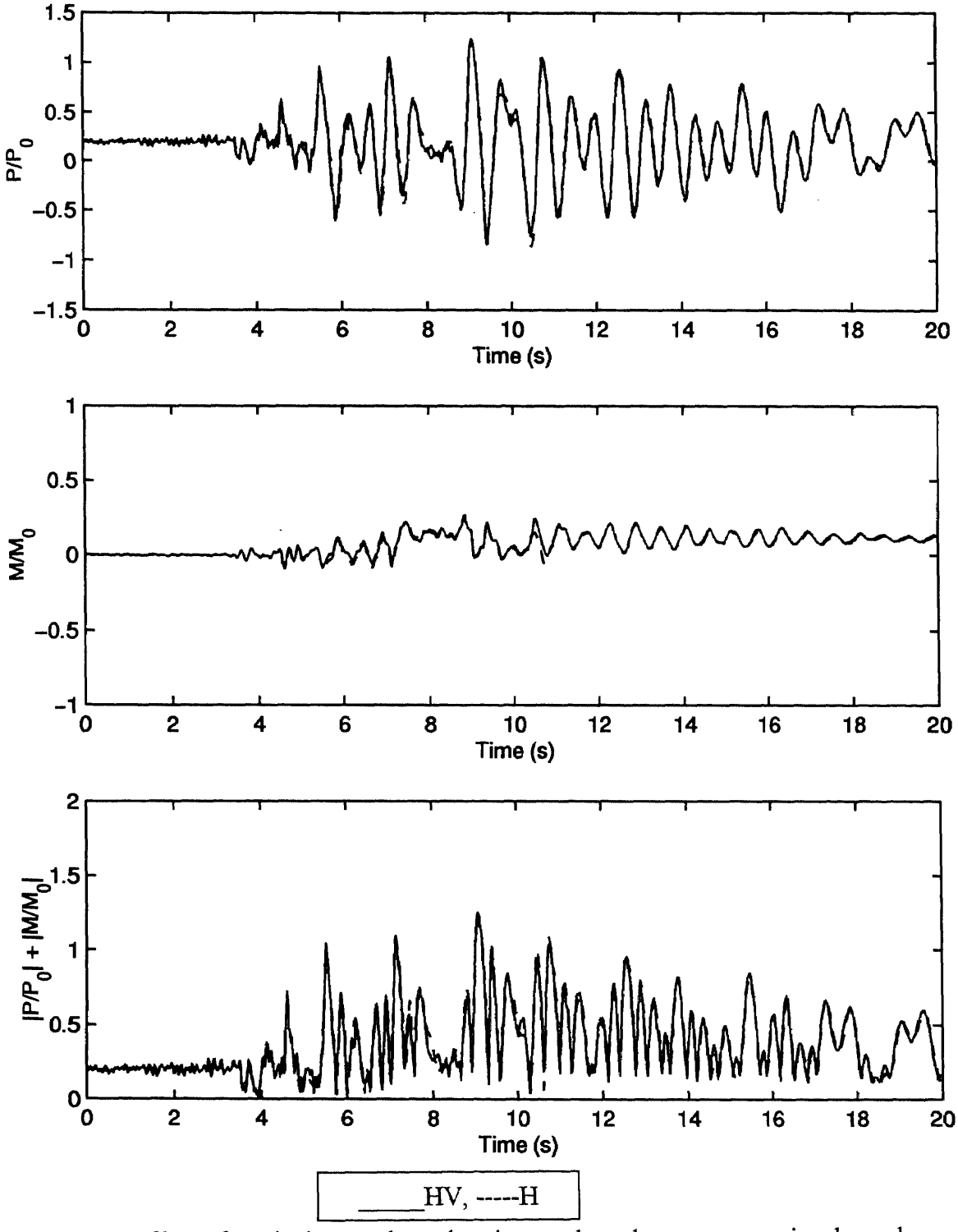

Figure 5.2 Effect of vertical ground acceleration on the column response in a braced frame: (a) axial force, (b) bending moment, (c) linear interaction.

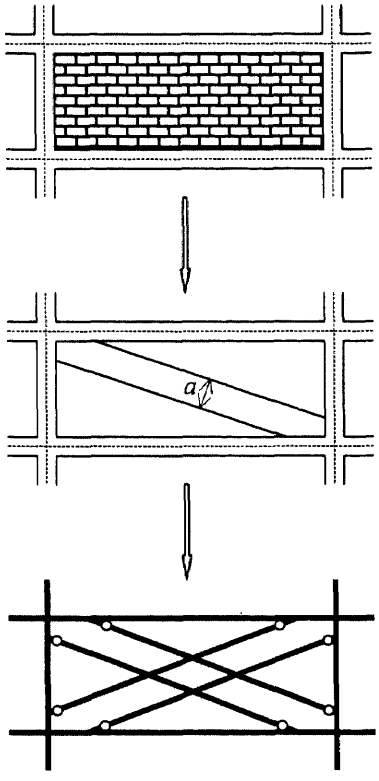

Figure 5.3 Modelling of masonry infill panels using the concept of equivalent strut.

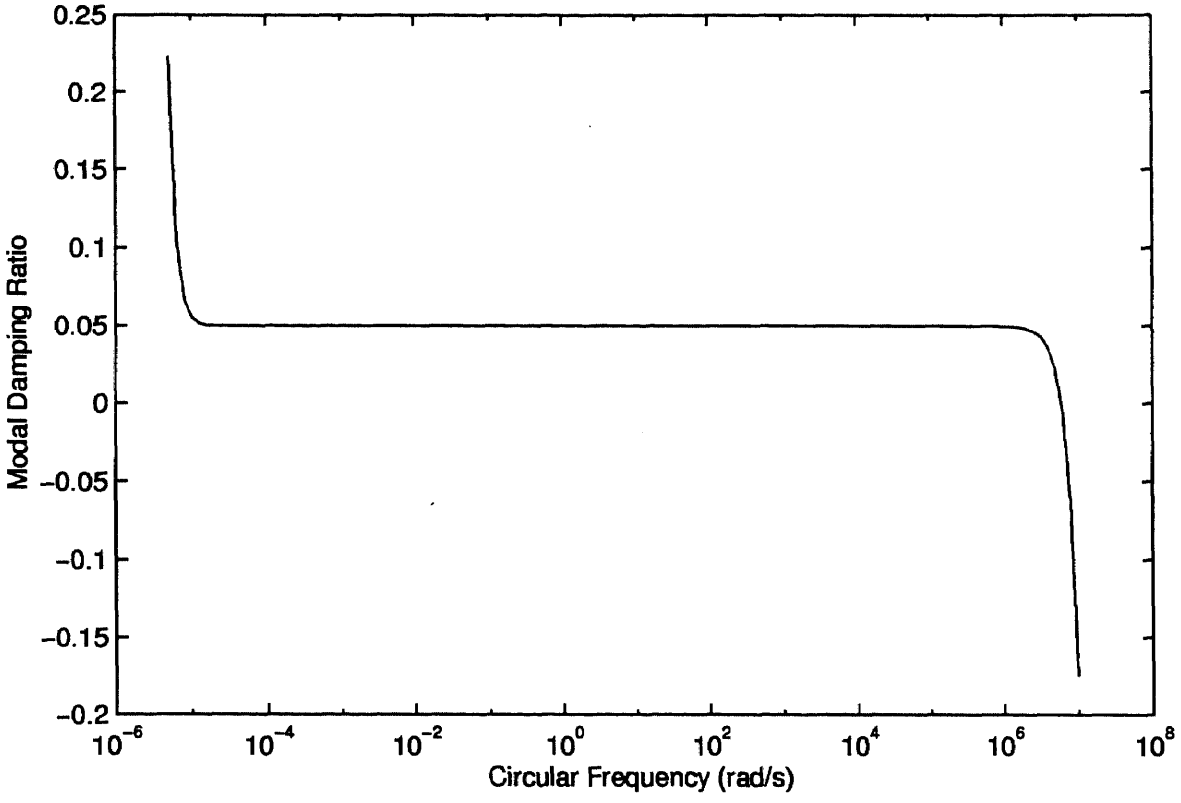

Figure 5.4 Variation of modal damping ratio with circular frequency.

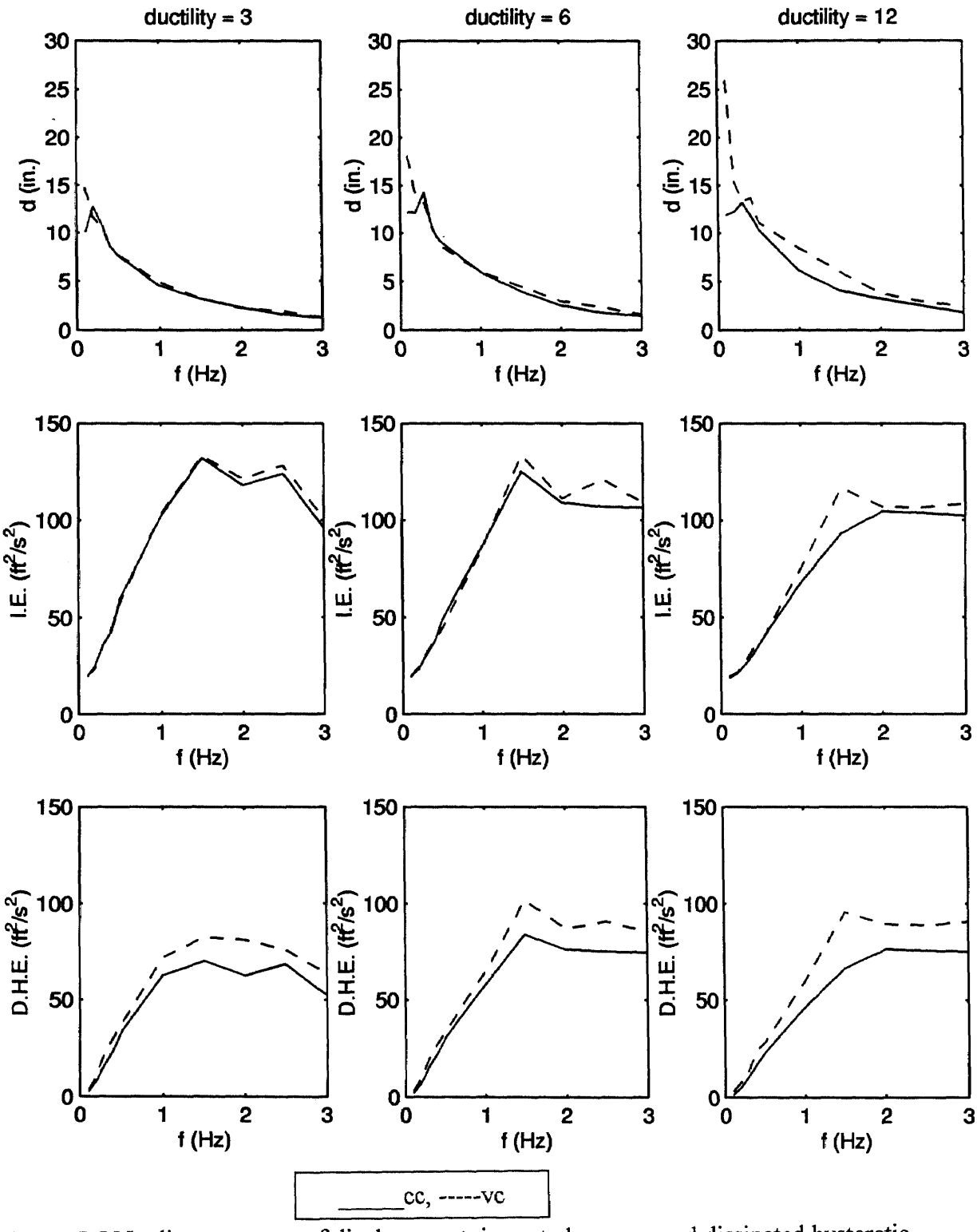

Figure 5.5 Nonlinear spectra of displacement, imparted energy, and dissipated hysteretic energy for the *constant-c* and *varying-c* models.

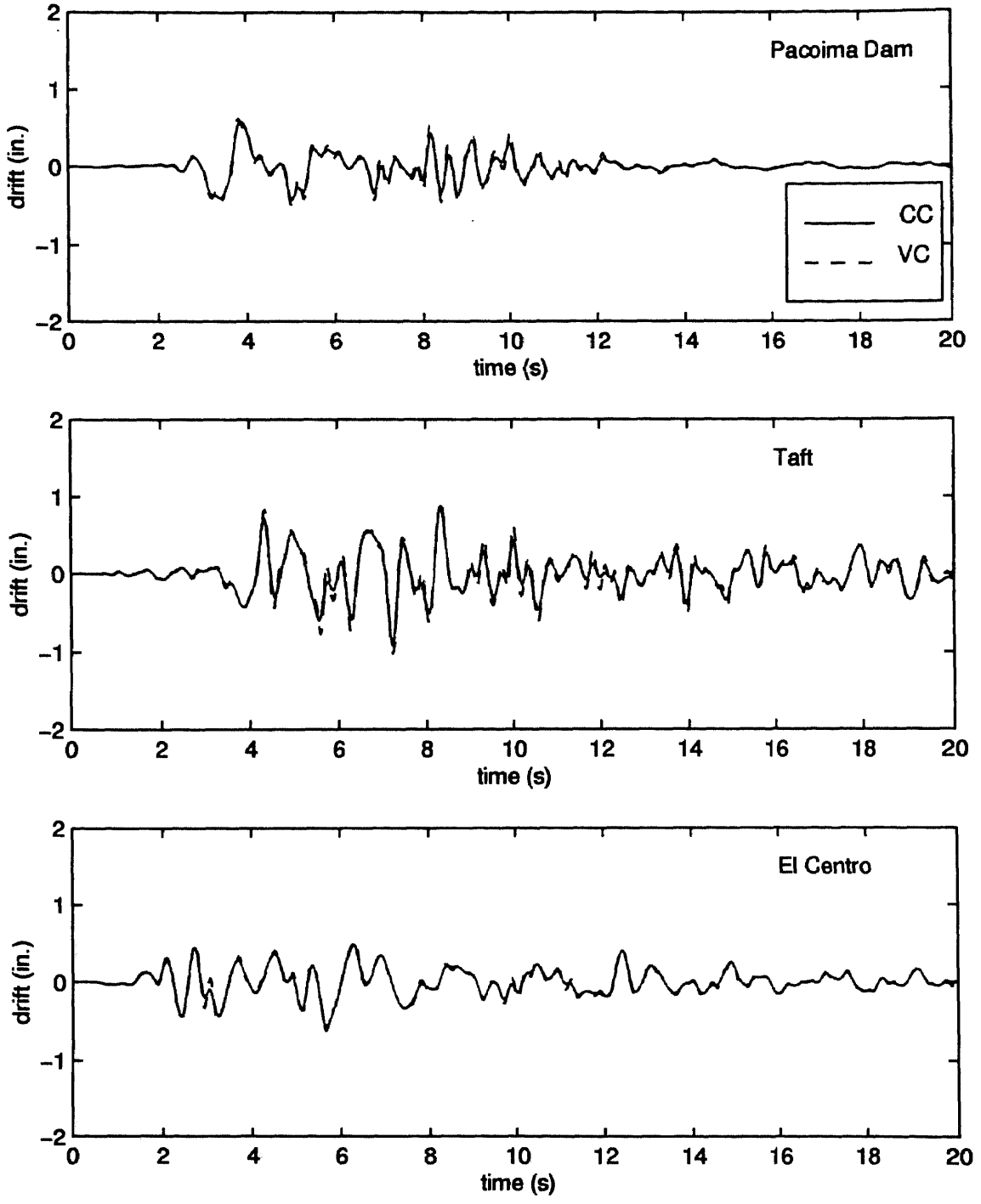

Figure 5.6 Time histories of top-story drift for the original 12-DOF stick model.

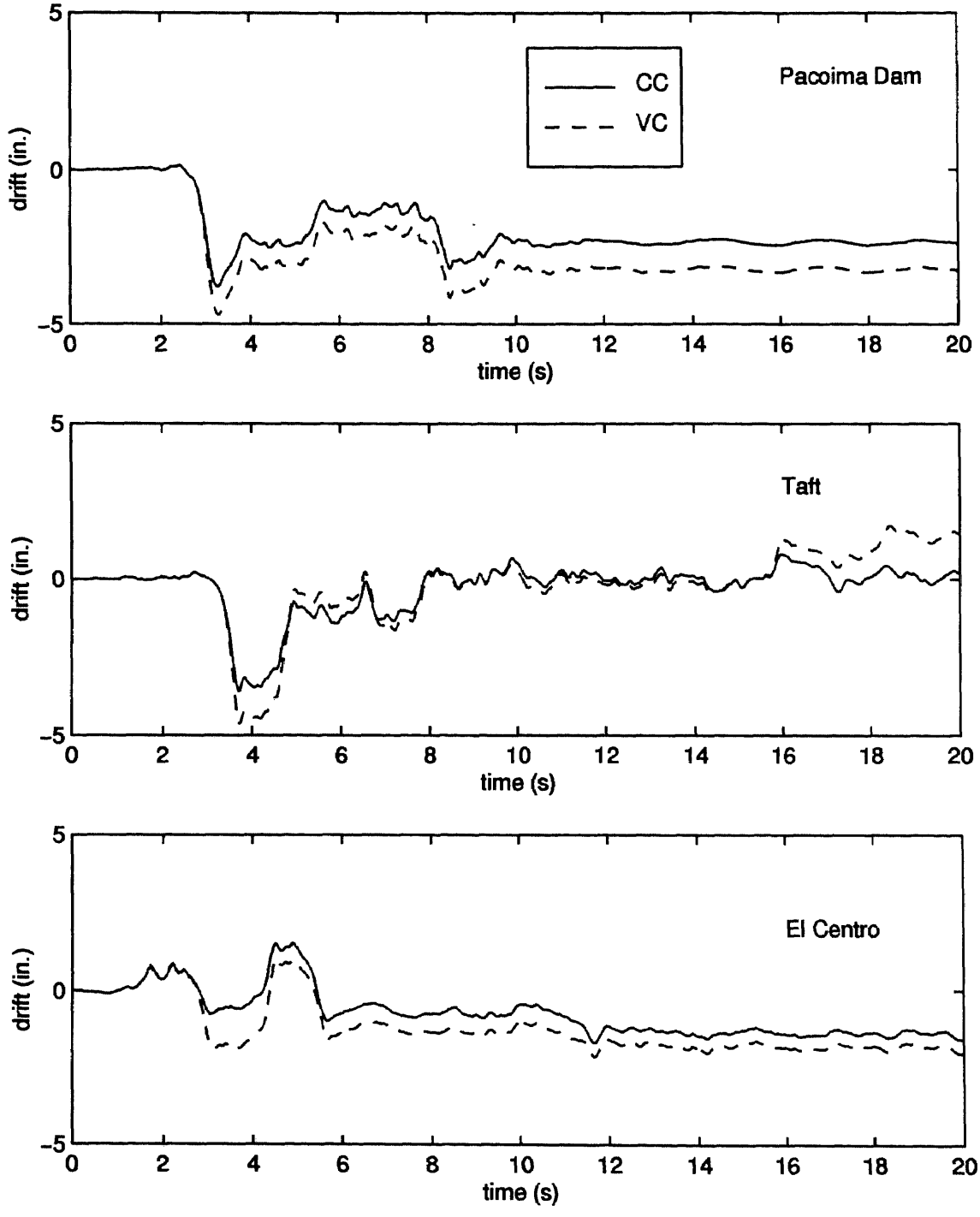

Figure 5.7 Time histories of first-story drift for the 12-DOF stick model with reduced yield force.

REFERENCES

AISC, *Manual of Steel Construction-Load and Resistance Factor Design*, American Institute of Steel Construction, 1994.

Anderson, J. C., and Bertero, V. V., "Effects of Gravity Loads and Vertical Ground Acceleration on the Seismic Response of Multistory Frames," *Proc. 5th WCEE*, Rome, Italy, 1971, pp. 2914-2923.

Angel, R., Abrams, D. P., Shapiro, D., Uzarski, J., Webster, M., "Behavior of Reinforced Concrete Frames with Masonry Infills," *Structural Research Series No. 589*, University of Illinois at Urbana-Champaign, Urbana, IL, 1994.

Ballio, G., Calado, L., and Castiglioni, C. A., "Low Cycle Fatigue Behavior of Structural Steel Members and Connections," *Fatigue Fract. Engng Mater. Struct.*, Vol. 20, No. 8, 1997, pp. 1129-1146.

Ballio, G., and Castiglioni, C. A., "An Approach to the Seismic Design of Steel Structures Based on Cumulative Damage Criteria," *Earthquake Engineering and Structural Dynamics*, Vol. 23, 1994, pp. 969-986.

Bathe, K. J., *Finite Element Procedures in Engineering Analysis*, Prentice-Hall, Englewood Cliffs, NJ, 1982.

Biddah, A., and Heidebrecht, A. C., "Seismic Performance of Moment-Resisting Steel Frame Structures Designed for Different Levels of Seismic Hazard," *Earthquake Spectra*, Vol. 14, No. 4, November 1998, pp. 597-627.

Chai, Y. H., Romstad, K. M., and Bird, S. M., "Energy-Based Damage Model for High-Intensity Seismic Loading," *Journal of Structural Engineering*, ASCE, Vol. 121, No. 5, May 1995, pp. 857-864.

Chopra, A. K., *Dynamics of Structures: Theory and Applications to Earthquake Engineering*, Prentice-Hall, Englewood Cliffs, NJ, 1995.

Clough, R. W., and Penzien, J., *Dynamics of Structures*, McGraw-Hill, New York, NY, 1993.

Court, A. B., and Kowalsky, M. J., "Performance-Based Engineering of Buildings-A Displacement Design Approach," *Proc. SEWC 98*, San Francisco, CA, 1998, Paper No. T109-1.

Daali, M. L., and Korol, R. M., "Low Cycle Fatigue Damage Assessment in Steel Beams," *Structural Engineering and Mechanics*, Vol. 3, No. 4, 1995, pp. 341-358.

Deodatis, G., "Non-stationary Stochastic Vector Processes: Seismic Ground Motion Application," *Probabilistic Engineering Mechanics*, Vol. 11, 1996, pp. 149-168.

DiPasquale, E., and Cakmak, A. S., "Identification of the Serviceability Limit State and Detection of Seismic Structural Damage," *Technical Report NCEER-88-0022*, National Center for Earthquake Engineering Research, State University of New York, Buffalo, NY, 1988.

Ghobarah, A., Abou-Elfath, H., and Biddah, A., "Response-Based Damage Assessment of Structures," *Earthquake Engineering and Structural Dynamics*, Vol. 28, 1999, pp. 79-104.

Hamburger, R. O., "Implementing Performance Based Seismic Design in Structural Engineering Practice," *Proc. 11th WCEE*, Mexico City, Mexico, 1996, Paper No. 2121.

FEMA, *NEHRP Recommended Provisions for Seismic Regulations for New Buildings (FEMA 222A, 223A)*, Building Seismic Safety Council, Washington, D.C., 1994.

FEMA, *NEHRP Guidelines for the Seismic Rehabilitation of Buildings (FEMA-273)*, Applied Technology Council, Redwood City, CA, 1997.

FEMA, *NEHRP Commentary on the Guidelines for the Seismic Rehabilitation of Buildings (FEMA-274)*, Applied Technology Council, Redwood City, CA, 1997.

Foutch, D. A., Yun, S. Y., and Lee, K., "Comparative Reliability of Linear and Nonlinear Approaches to Demand Characterization in Steel Structures," *Proc. SEWC 98*, San Francisco, CA, 1998 Paper No. T166-2.

Freeman, S. A., "Development and Use of Capacity Spectrum Method," *Proc. 6th U.S. NCEE*, Seattle, WA, 1998.

Hassiotis, S., and Jeong, G. D., "Assessment of Structural Damage from Natural Frequency Measurements," *Computers and Structures*, Vol. 49, 1993, pp.679-691.

ICBO, *1997 Uniform Building Code*, International Conference of Building Officials, Whittier, CA, 1997.

Jennings, P. C., Housner, G. W., and Tsai, N. C., "Simulated Earthquake Motions," *Technical Report*, Earthquake Engineering Research Laboratory, California Institute of Technology, CA, 1968.

Krawinkler, H., "Issues and Challenges in Performance Based Seismic Design," *Proc. SEWC 98*, San Francisco, CA, 1998, Paper No. T178-3.

Krawinkler, H., and Gupta, A., "Story Drift Demands for Steel Moment Frame Structures in Different Seismic Regions," *Proc. 6th U.S. NCEE*, Seattle, WA, 1998.

Krawinkler, H., and Zohrei, M., "Cumulative Damage in Steel Structures Subjected to Earthquake Ground Motions," *Computers and Structures*, Vol. 16, 1983, pp. 531-541.

Kunnath, S. K., Reinhorn, A. M., and Lobo, R. F., "IDARC Version 3.0: A Program for the Inelastic Damage Analysis of RC Structures," *Technical Report NCEER-92-22*, National Center for Earthquake Engineering Research, State University of New York, Buffalo, NY, 1992.

Lew, M., and Naeim, F., "Use of Design Spectrum-Compatible Time Histories in Analysis of Structures," *Proc. 11th WCEE*, Mexico City, Mexico, 1996, Paper No. 326.

Mainstone, R. J., "On the Stiffnesses and Strengths of Infilled Frames," *Current Paper CP 3/72*, Building Research Station, Garston, UK, 1971.

McCabe, S. L., and Hall, W. J., "Assessment of Seismic Structural Damage," *Journal of Structural Engineering*, ASCE, Vol. 115, No. 9, September 1989, pp. 2166-2183.

Park, Y. J., and Ang, A. H., "Mechanistic Seismic Damage Model for Reinforced Concrete," *Journal of Structural Engineering*, ASCE, Vol. 111, No. 4, April 1985, pp. 722-739.

Park, Y. J., and Ang, A. H., and Wen, Y. K., "Seismic Damage Analysis of Reinforced Concrete Buildings," *Journal of Structural Engineering*, ASCE, Vol. 111, No. 4, April 1985, pp. 740-757.

Polyakov, S. V., "On the Interaction Between Masonry Filler Walls and Enclosing Frame When Loaded in the Plane of the Wall," *Translations in Earthquake Engineering*, EERI, Oakland, CA, 1960, pp. 36-42.

Rodriguez, M., "An Energy and Displacement Approach for Evaluating Seismic Damage," *Proc. SEWC 98*, San Francisco, CA, 1998, Paper No. T227-2.

Saadeghvaziri, M. A., and Foutch, D. A., "Nonlinear Response of R/C Highway Bridges under the Combined Effect of Horizontal and Vertical Earthquake Motions," *Earthquake Engineering and Structural Dynamics*, Vol. 20, No. 6, June 1991.

Schiff, S. D., Hall, W. J., and Foutch, D. A., "Seismic Design Studies of Low-rise Steel Frames," *Structural Research Series No. 541*, University of Illinois at Urbana-Champaign, Urbana, IL, 1988.

SEAOC, *Performance Based Seismic Engineering of Buildings*, Structural Engineers Association of California, Sacramento, CA, 1995.

Shome, N., Cornell, C. A., Bazzurro, P., and Carballo, J. E., "Earthquakes, Records, and Nonlinear Responses," *Earthquake Spectra*, Vol. 14, No. 3, August 1998, pp. 469-500.

Sorace, S., "Seismic Damage Assessment of Steel Frames," *Journal of Structural Engineering*, ASCE, Vol. 124, No. 5, May 1998, pp. 531-540.

Teran-Gilmore, A., *Performance-Based Earthquake-Resistant Design of Framed Buildings Using Energy Concepts*, Ph.D. Thesis, Department of Civil Engineering, University of California, Berkeley, CA, 1996.

Whittaker, A., Constantinou, M., Tsopelas, P., "Displacement Estimates for Performance-Based Seismic Design," *Journal of Structural Engineering*, ASCE, Vol. 124, No. 8, August 1998, pp. 905-912.